

UNCLASSIFIED

AD NUMBER

AD819141

LIMITATION CHANGES

TO:

Approved for public release; distribution is unlimited.

FROM:

Distribution authorized to U.S. Gov't. agencies and their contractors;  
Administrative/Operational Use; JUN 1967. Other requests shall be referred to Rome Air Development Center, Griffiss AFB, NY.

AUTHORITY

RADC ltr 27 Aug 1973

THIS PAGE IS UNCLASSIFIED

RADC-TR-67-143  
Final Report



AD819141

**SINGLE CHANNEL MONOPULSE TECHNIQUES**

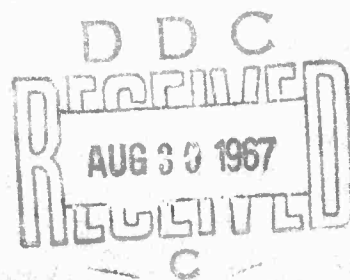
Samuel Boor  
Melvin Harvey  
Guy Pelchat  
et al

Radiation Incorporated

**TECHNICAL REPORT NO. RADC-TR-67-143**  
June 1967

This document is subject to special  
export controls and each transmittal  
to foreign governments, foreign na-  
tionals or representatives thereto may  
be made only with prior approval of  
RADC (EMLI), GAFB, N.Y. 13440

Rome Air Development Center  
Air Force Systems Command  
Griffiss Air Force Base, New York



When US Government drawings, specifications, or other data are used for any purpose other than a definitely related government procurement operation, the government thereby incurs no responsibility nor any obligation whatsoever, and the fact that the government may have formulated, furnished, or in any way supplied the said drawings, specifications, or other data is not to be regarded, by implication or otherwise, as in any manner licensing the holder or any other person or corporation, or conveying any rights or permission to manufacture, use, or sell any patented invention that may in any way be related thereto.

Do not return this copy. Retain or destroy.

## SINGLE CHANNEL MONOPULSE TECHNIQUES

Samuel Boor  
Melvin Harvey  
Guy Pelchat  
et al

Radiation Incorporated

This document is subject to special  
export controls and each transmittal  
to foreign governments, foreign na-  
tionals or representatives thereto may  
be made only with prior approval of  
RADC (EMLI), GAFB, N.Y. 13440



## FOREWORD


This final report was prepared by Radiation Incorporated, P. O. Box 37, Melbourne, Florida 32902 under Contract No. AF30(602)-4035, Project 4519, Task 451901, covering the period January 1966 to January 1967.


Lt E. Scheel, EMCRR, of the Rome Air Development Center, Griffiss Air Force Base, New York, was the RADC Project Engineer.

Significant contributions were made to this report by the following Radiation Incorporated personnel: D. F. Lehman, M. L. Livingston, A. R. Martin, H. G. Edwards, C. A. Catsimanes, and G. H. Smith.

This technical report has been reviewed by the Foreign Disclosure Policy Office (EMLI). It is not releasable to the Clearinghouse for Federal Scientific and Technical Information because this document contains information embargoed from release to Sino-Soviet Bloc Countries by AFR 400-10, "Strategic Trade Control Program."

This technical report has been reviewed and is approved.

Approved:   
ERIC E. SCHEEL, 1st Lt, USAF  
Project Officer

Approved:   
RICHARD M. COSEL  
Colonel, USAF  
Chief, Communications Division

FOR THE COMMANDER

  
IRVING D. GABELMAN  
Chief, Advanced Studies Group

## ABSTRACT

This report is the Final Technical Report for Contract Number AF 30(602)-4035, "Single Channel Monopulse Techniques." It describes the results of a study and investigation to obtain a technique for processing both the communications and tracking signals in a single receiver in a satellite communications system. Various techniques were studied, with emphasis on Pseudo-Monopulse, Frequency Division Multiplexing, Time Division Multiplexing, and the Automatic Manual Simulator (AMS), a mechanical scanning method. All systems were analyzed to determine basic feasibility. Detailed analyses of the most promising techniques (Pseudo-Monopulse, AMS, FDM) were made. Major factors considered were: performance in the presence of thermal noise, errors due to phase and amplitude unbalance, normalization (dependence of pointing error on received signal strength), acquisition problems, and equipment complexity. A relative evaluation of all Single Channel Monopulse Tracking Receiver (SCMTR) techniques, including three channel monopulse for comparison, was made, and Pseudo-Monopulse was shown to offer the most advantages for the stipulated conditions. A complete Pseudo-Monopulse receiver design was accomplished and is included in this report. The AMS technique was shown to be useful when equipment simplicity is the prime goal, and this technique is also described in detail, including the results of a one-axis analog computer simulation.

## TABLE OF CONTENTS

I.	Introduction	1
II.	Basic System Study Task	5
III.	SCMTR Evaluation	29
IV.	Pseudo-Monopulse SCMTR Design	44
V.	AMS	88
VI.	An Analysis of Monopulse Antenna Characteristics	97
VII.	Amplitude and Phase Errors in Monopulse Systems	130
VIII.	Normalization	139
IX.	Monopulse Noise Analysis	143
X.	Time Division Multiplexing (TDM)	150
XI.	Frequency Division Multiplex (FDM)	157
XII.	Pseudo-Monopulse	173
XIII.	Amplitude and Phase Errors in a Two-Channel Phase Monopulse Antenna	198
XIV.	Conclusion and Recommendations	207
Appendix I	Basic Limitation on Efficiency of Passive Combiners	210
Appendix II	Pseudo-Monopulse Noise Analysis	214
Appendix III	X-Band Low Noise Receiver Survey	237
Appendix IV	Acquisition Considerations with Pseudo- Monopulse Tracking	240
References		243
Bibliography		246

## LIST OF ILLUSTRATIONS

<u>Figure</u>	<u>Title</u>	<u>Page</u>
1	Atmospheric Attenuation	10
2	Maximum Rain Path Length as a Function of Elevation Angle with Freezing Altitude as a Parameter	11
3	AMS System Block Diagram	30
4	Pseudo-Monopulse Block Diagram	32
5	Full Monopulse Block Diagram	33
6	Time Division Multiplex Block Diagram	34
7	Frequency Division Multiplex Block Diagram	36
8	Pseudo-Monopulse SCMTR Block Diagram	45
9	Scanner Network Operation	46
10	Beam Shape Near Boresight of a Fifteen Foot Diameter Paraboloid at 8 GHz	55
11	Schematic Diagram for SCMTR Feed System	57
12	Demodulator Block Diagram	62
13	Typical Receive Antenna Patterns	65
14	Ferrite Scanner Operation	66
15	Response of 7 Cavity Waveguide Filter	68
16	VSWR versus Frequency of 7 Cavity Waveguide Filter	69
17	Block Diagram of Low-Noise Parametric Amplifier	73
18	AMS System Block Diagram	89
19	Analog Computer Functional Block Diagram for One Axis AMS Simulation	92

## LIST OF ILLUSTRATIONS

(continued)

<u>Figure</u>	<u>Title</u>	<u>Page</u>
20	Antenna-Receiver Off-Axis Gain	93
21	Antenna Step Responses - One Axis Simulation	94
22	Amplitude Sensing Monopulse Antenna	98
23	Phase Sensing Monopulse Antenna	98
24	General Coordinate System	99
25	Distribution Functions	99
26	Unnormalized Patterns of a Uniform and a Uniform Odd Illuminated Circular Aperture	105
27	Unnormalized Patterns of a Uniform and a Sinusoidal Illuminated Circular Aperture	107
28	Unnormalized Patterns of a Uniform and a Sinusoidal Illuminated Circular Aperture	108
29	Unnormalized Patterns of a Uniform and a Sinusoidal Illuminated Circular Aperture	110
30	Unnormalized Patterns of a Uniform and a Sinusoidal Illuminated Circular Aperture	111
31	Normalized Patterns of a Uniform and a Uniform Odd Illuminated Circular Aperture	114
32	Normalized Patterns of a Uniform and a Sinusoidal Illuminated Circular Aperture	115
33	Normalized Patterns of a Uniform and a Sinusoidal Illuminated Circular Aperture	116

## LIST OF ILLUSTRATIONS

(continued)

<u>Figure</u>	<u>Title</u>	<u>Page</u>
34	Normalized Patterns of a Uniform and a Sinusoidal Illuminated Circular Aperture	117
35	Normalized Patterns of a Uniform and a Sinusoidal Illuminated Circular Aperture	118
36	Comparison of Normalized and Unnormalized Functions	119
37	Phase Sensing Arrays	121
38	Calculated Sum and Difference Patterns for the Diamond Array	125
39	Calculated Sum and Difference Patterns for the Square Array	126
40	Basic Monopulse Model	131
41	Simplified Block Diagram of Tracking System	140
42	System Gain Factor versus Signal-to-Noise Ratio in the Reference or Sum Channel	141
43	Monopulse Receiver Simplified Block Diagram	144
44	Signal and Noise Spectra	147
45	Basic TDM System	151
46	Time Division Multiplex Block Diagram	156
47	FDM (Frequency Division Multiplex Block Diagram)	158
48	Basic SCAMP Processor	160
49	System Utilizing SCAMP	161

## LIST OF ILLUSTRATIONS

(continued)

<u>Figure</u>	<u>Title</u>	<u>Page</u>
50	SCAMP Processor Performance in the Presence of Noise	163
51	Ratio of Output Signal-to-Signal Power Ratio to Input Signal-to-Signal Power Ratio versus Larger Input SNR	164
52	Ratio of Output Signal-to-Signal Power Ratio to Input Signal-to-Signal Power Ratio versus Larger Input SNR	166
53	Ratio of Output SNR to Input SNR versus Input SNR	167
54	Power Ratio of Strongest Intermodulation Product to Weakest Output Signal versus Large Input SNR	168
55	Illustration of Symmetrical Channel Orientation	169
56	Illustration of Asymmetrical Channel Orientation	169
57	System Configuration Utilizing SCAMP Technique	171
58	Block Diagram of Pseudo-Monopulse Tracking Receiver	174
59	Q-Function Examples	179
60	Basic System Components and Properties	180
61	Full Monopulse Configuration	185
62	Pseudo-Monopulse with Three Preamplifiers	186
63	Pseudo-Monopulse with One Preamplifier	187
64	Pseudo-Monopulse with Three Preamplifiers	188
65	Pseudo-Monopulse with Two Preamplifiers	189
66	Pseudo-Monopulse with One Preamplifier	190
67	Pseudo-Monopulse with Two Preamplifiers	191

## LIST OF ILLUSTRATIONS

(continued)

<u>Figure</u>	<u>Title</u>	<u>Page</u>
68	Coordinate System	200
69	Two-Channel Monopulse Comparator	202



## LIST OF TABLES

<u>Table Number</u>		<u>Page</u>
1	Some Numerical Values of AZ-EL Dynamics Occurring during Passes of Medium Altitude and Near-Synchronous Communication Satellites	13
2	System Design Criteria Summary	24
3	Weighting Factors Used in SCMTR Evaluation	37
4	System Comparison Matrix	39
5	Typical Synchronous Satellite Link Budget	52
6	Ferrite Scanner Operational Characteristics	70
7	Parametric Amplifier Operational Characteristics	74
8	Oscillator Operational Characteristics	78
9	X64 Multiplier Operational Characteristics	80
10	Mixer-Preamplifier Characteristics	82
11	TDM Filter, Switch, and Bandwidth Requirements	155

## EVALUATION

The objective of this study was to investigate all possible single channel monopulse tracking techniques which would reduce equipment complexity in the tracking system of a satellite communications terminal, and to develop a design which could be reduced to practice using the best technique.

In this program, a literature search was conducted and several techniques were evaluated. As a result of this evaluation, it was concluded that the Pseudo Monopulse technique offered the most advantages for the stipulated conditions. The block diagram of a design which is currently in use on satellite terminals is presented.

*Eric E. Scheel*

ERIC E. SCHEEL, 1st Lt, USAF  
Project Engineer  
RADC, Griffiss AFB, NY

## SECTION I

### INTRODUCTION

#### 1. OBJECTIVE

The objective of this study program was to develop a single channel receiver technique which could be used in the design of ground terminal receivers in a communications satellite system. The Single Channel Monopulse Tracking Receiver (SCMTR) technique was developed to satisfy design requirements which are discussed in detail in Section II. A synopsis of the basic design criteria follows:

a. The SCMTR must be capable of processing both tracking and communications signals in a single receiver.

b. The basic technique must result in a design which minimizes overall equipment complexity.

c. The communications link shall be degraded by a maximum of 2 dB, with a design goal of 1 dB, over that achieved with a conventional three channel monopulse system.

d. An adequate tracking capability shall be provided, but there is no requirement for tracking above that necessary to meet the link degradation specification.

In short, the objective of this study program was to devise a technique for combining the tracking and communications information on a single channel such that a net saving in equipment would result (as compared with a three channel monopulse receiver system) and at the expense of only a slight performance degradation. That such a concept is feasible can be seen by noting that a major difference exists between a tracking system (e.g., radar) and a communications system. In the former, tracking per se is the desired result, whereas, in the latter tracking is used only as needed to maintain communications. In many satellite communications applications, basic monopulse tracking capability can be degraded by one or two orders of magnitude without greatly reducing the communications capability. When the tracking requirements are reduced, it is reasonable to assume that some savings in equipment can be effected. This fundamental tradeoff between

hardware complexity and degradation of the communications link, with tracking capability as a variable, was the basis for the study program.

## 2. APPROACH

The program was divided into six tasks, not including the preparation of reports. The first task was to perform a literature search. The search was concentrated in four general areas - general monopulse theory and practice, single channel tracking techniques, relevant microwave (including feeds and comparator) theory and techniques, and relevant receiver theory and hardware. The bibliography to this report is largely the result of the literature search.

The second task was the Basic System Study task. The purpose of this effort was to develop the basic ground rules for the remainder of the study. Basic terminology, fundamental considerations involving the satellite, antenna mount, environmental conditions and other factors which determine tracking dynamics, the basic scope of work, signal characteristics, and the communications link characteristics were defined as a part of this task. In addition, those factors which would be used to compare the various SCMTR techniques were delineated. In short, this task served to define the problem, place reasonable limitations on the scope of work, and indicate specific areas of endeavor.

The SCMTR Systems task included the definition and analysis of specific techniques. A generic breakdown included Time Division Multiplexing (TDM), Frequency Division Multiplexing (FDM), and hybrid techniques (including pseudo-monopulse and lobing). Initially, basic advantages and limitations of each technique were determined. Next, the most promising techniques were evaluated in detail.

The fourth task, performed concurrent with the SCMTR Systems task, was an equipment limitation study. The purpose of this task was to determine the state-of-the art equipment limitations for each of the SCMTR techniques and to supply the information necessary to perform a tradeoff evaluation between equipment complexity and performance characteristics.

The fifth task was an evaluation of the various techniques on a relative basis. As a part of this evaluation, a presentation of the results of the program to date was made at Rome Air Development Center on 28 November 1966. A summary of the evaluation is found in Section III. Results of the evaluation were used to determine the techniques to be used in the SCMTR System Design.

The final task, the SCMTR System Design, was the design of an SCMTR utilizing the best technique, as determined in the SCMTR evaluation

task. A detailed design, including block diagrams and, as applicable, circuit diagrams which can be reduced to practice was accomplished for the pseudo-monopulse technique. This design is presented in Section IV. In addition, a less detailed design was accomplished for the Automatic Manual Simulator (AMS), a technique which appears advantageous under some circumstances. The AMS is described in Section V.

### 3. SUMMARY OF RESULTS

The principal result of this program might appear to be the SCMTR design described in Section IV. The real value of the study, however, is in the analyses found in Sections VI through XIII and in the Appendices. The analyses can be used, as appropriate, for a wide choice of systems. For example, the different requirements of large, fixed site terminals, of very small terminals, of airborne terminals, and of telemetry systems or other non-related data gathering-tracking systems can be used in conjunction with the analyses to determine the feasibility of using a SCMTR. For the present problem - a fifteen foot antenna, 8 GHZ frequency, elevation-over-azimuth mount, transportable ground station operating with synchronous, near-synchronous, and 6000 n.m. orbit satellites - the pseudo-monopulse technique appeared to offer the greatest advantage. The AMS was also a desirable technique, particularly in the case when hardware simplicity is of utmost importance.

The results of the study program can perhaps be best summarized by describing the contents of this report. Section II defines the SCMTR requirements, develops specifications, defines the scope of the program, and discusses briefly the types of single channel techniques. Section III is a summary of the comparative evaluation of all SCMTR techniques. The results of the evaluation led to the design of a pseudo-monopulse system, which is the subject of Section IV. A further result of the evaluation was that the AMS technique should be investigated further, and the results of the AMS analysis - design are found in Section V.

Section VI contains an analysis of antenna and feed characteristics for both amplitude sensing and phase sensing monopulse systems. Section VII analyzes the effects of pre-comparator and post-comparator unbalances, both in amplitude and phase. Section VIII considers the normalization problem; i. e., the problem of obtaining an error signal which is independent of received signal strength. Section IX is an analysis of a monopulse system operating in the presence of thermal noise.

The TDM technique is described in Section X, and FDM methods, including SCAMP, are described in Section XI. Pseudo-monopulse is analyzed in Section XII, although a rigorous analysis of the operation in the presence of thermal noise is reserved for Appendix II. Two-channel

monopulse (where the error signals are in phase quadrature) amplitude and phase errors are discussed in Section XIII. The conclusions and recommendations are found in Section XIV.

Appendix I derives a significant limitation on the efficiency of passive (both reciprocal and non-reciprocal) three-ports. Appendix II contains a noise analysis of pseudo-monopulse. Appendix III contains a survey of X-band low noise receivers. Appendix IV discusses the satellite acquisition problem in a pseudo-monopulse receiving system.

## SECTION II

### BASIC SYSTEM STUDY TASK

#### 1. INTRODUCTION

The purpose of this section is to define the single channel monopulse tracking receiver (SCMTR) requirements. This program definition encompasses the specific contractual requirements, additional requirements derived from these specifications, a plan for meeting these requirements, and a method for evaluating the results of the program.

The objective of the overall program was to develop a technique which would allow a single channel receiver to be used simultaneously for both tracking and communications signals. This SCMTR would minimize equipment complexity without appreciably degrading the system performance compared with a conventional three channel receiver. Thus, a premium was placed on system simplicity and there was no need for tracking accuracies in excess of those required for good communications; i.e., an increase in tracking accuracy per se was of no benefit to the system. However, a tracking accuracy sufficient to maintain high sum channel gain was mandatory.

The scope of the program is discussed in detail in this section. Specific techniques which were studied are described, and tradeoff analyses which were to be made are tabulated. The results from this task were used in the remaining program tasks. The most important output from this task was a measure of the "goodness" of the various techniques; i.e., the criteria for selecting the "best" SCMTR techniques. Other significant outputs included limits on the scope of work, fundamental performance equations, and identification of the requirements for several specific analyses.

#### 2. COMMUNICATIONS TERMINAL

The SCMTR design is intended for use in ground terminals of a satellite communications system. The following paragraphs discuss the ground terminal characteristics and their impact on the SCMTR design. Ground terminal requirements are typical of satellite communications terminals. Furthermore, the basic requirements do not significantly restrict the generality of the expected results, as will be shown in later paragraphs.

The antenna being primarily considered is a 15-foot diameter

parabola. Of secondary consideration is a 60-foot parabolic antenna as well as sizes in between, when applicable. The antenna size is of major importance when considering initial acquisition, particularly the larger dishes, since the resultant narrow beamwidths aggravate the acquisition problem. The overall size, mass, moments of inertia, structural rigidity, characteristic frequencies, etc., are extremely important in the servo system design, but these mechanical characteristics are not of first order importance in determining the SCMTR configuration. The main limitation which results from a given structure and its drive system is a maximum value for servo bandwidth. It will be shown in this section that the dynamic requirements are such that a very wide servo bandwidth is not necessary. As a result, the mechanical characteristics and limitations are of minimum impact to the SCMTR design and were not given detailed attention during the study program. The antenna parameters which are of most significance to this study are beam width and gain, and these parameters are discussed in Paragraph 3. of this section.

The antenna will be mounted in an elevation-over-azimuth (Az-El) configuration. This type of mount is conventional and has several operational advantages. It also exhibits a major disadvantage - namely, a "keyhole" at the zenith position. This is easily illustrated by considering a zenith pass, which is characterized by a constant azimuth angle and an increasing elevation angle. At the zenith point, the elevation angle starts to decrease and the azimuth angle is required to instantaneously shift by 180 degrees. In the case of near-zenith passes a similar situation occurs, but the azimuth dynamic requirements are finite. In all cases, whether a  $90^\circ$  maximum elevation angle or a non-restricted elevation angle is used, the keyhole effect is present. Solutions to this problem are available by using some form of computed trajectory and slewing the antenna accordingly.

Use of an Az-El mount implies the need for protective circuitry. A typical mount would, for example, contain a mechanical stop, an electrical limit, a servo limit and a rate limit. The mechanical stop is a final, structural limit which prevents the antenna from exceeding some elevation angle. Stops would typically occur above zenith ( $95^\circ$  to  $100^\circ$ ) and below the horizon ( $-5^\circ$  to  $-10^\circ$ ). The mechanical stops are the final limit and, unless failures occur in the other protective circuitry, these stops would never be used. The electrical stops are typically limit switches set to prevent the antenna from reaching the mechanical stops. The servo limit is a mechanism which does not allow servo errors to be generated which would cause the mechanical stops to be reached. This servo limit is more restrictive than the electrical limit switches. A rate limit may also be incorporated to limit



the angular rate toward zenith (when near zenith) and toward the horizon (when near the horizon). These and other protective devices are typically a part of the Az-El mount and servo system design and are not peculiar to a SCMTR system. Further consideration of protective circuitry which is conventional to Az-El mounts has not been made, since it falls outside of the scope of the present program.

The frequency of operation is nominally 8 GHZ with an accuracy and stability of one part in  $10^8$ . The frequency, which is compatible with present and anticipated communications satellites, is extremely pertinent to the SCMTR design. Equipment limitations, such as noise temperature and gain as a function of hardware complexity, are dependent on operating frequency. Link considerations, including antenna gains, beamwidths, path losses, rain losses, etc. are also highly frequency dependent.

Frequency accuracy can affect the SCMTR design, and the specified value of 1 part in  $10^8$  will provide sufficient accuracy and stability for any SCMTR techniques presently visualized. The net frequency uncertainty due to doppler, satellite translators, and short term effects will generally be much greater than 1 part in  $10^8$ . The modulation will, in general, impose bandwidth requirements significantly greater than the frequency uncertainty due to stability limitations. As a result, frequency accuracy and stability are not restrictive and will not be an important consideration in most SCMTR systems.

Preamplifiers used with the SCMTR must be compatible with highly transportable terminals. A survey of low-noise receivers has been made as a part of this program to allow the proper system tradeoffs to be made. The survey is included as Appendix III of this report. Preamplifiers are extremely important in this study since the equipment complexity and system performance are directly affected, and in conflicting ways. The use of one or more preamplifiers in pseudo-monopulse is discussed in detail in Paragraph 3 of Section XII.

Operation with active satellites with orbits ranging from 6000 nautical miles, to near-synchronous, to synchronous is required. These conditions include both IDCSP and ADCSP satellites, and are, therefore, of both immediate and long-range importance. The orbits affect basic link parameters, frequency uncertainty, and the overall servo system. In general, the lowest altitude orbit determines the dynamic tracking requirements and the acquisition problem, whereas, the maximum altitude orbit is most significant in the communications link budget (received power level, required transmit power level).

The received signal may be either a CW signal or an angle modulated

signal. The satellite beacon signal may be used for tracking and thus the need for CW operation. The communications channel may be frequency modulated with analog or digital information. A maximum analog baseband of 8 kHz with a maximum modulation index of 10 is stipulated. Thus, a maximum RF bandwidth of 160 kHz is needed. The minimum baseband frequency will be approximately 300 Hz, assuming conventional voice and FDM operational characteristics.

A maximum data rate of 4800 bits per second has been stipulated for the digital signal. The maximum bandwidth anticipated for the digital mode is less than for the analog mode, since a relatively low modulation index can be used to obtain very low bit error rates. Thus, the maximum bandwidth to be considered is 160 kHz, as established by the analog channel. Various combinations of voice and teletype can be accomplished within this bandwidth.

The signal bandwidths are very important in most SCMTR systems. For example, the maximum bandwidth is important in FDM (for channel separation and crosstalk considerations) and TDM (for sampling rate and single channel bandwidth). The minimum baseband frequency is important in pseudo-monopulse and sequential lobing (for switching rates). Although the minimum information rate, 300 Hz, and the maximum bandwidth, 160 kHz, will be of prime importance, the impact of different modems on a given SCMTR technique will be considered as applicable.

### 3. SCMTR SPECIFICATIONS

The basic ground terminal characteristics were discussed in the previous section, and resulted in some general SCMTR performance requirements. Several additional specific requirements were imposed by the Statement of Work (PR C-6-2059) and still others were derived from the system requirements. These requirements have been discussed, derived (as appropriate), and tabulated to form the SCMTR Design Criteria.

Several general subjects, such as the communications link, will be discussed briefly since they affect the overall system requirements. The antenna, servo system, and basic structural components and the interrelations between these units must be defined to accomplish an overall terminal design. However, these units specifically are not within the scope of the present work. As a result, several key parameters will not be specifically discussed, although their effect on the SCMTR design will be estimated. For example, the antenna system inertias, frictions, wind load, backlash, and environmental requirements are of vital importance in determining the servo design and the resultant servo bandwidth. However, the system is not sufficiently well defined to determine all of the above

characteristics, and these details should not affect the basic SCMTR requirements. The approximate range of servo bandwidths will be determined from target dynamics and past experience on similar designs. In short, the problem will not be constrained any further than necessary in order that the resultant SCMTR design be as versatile as possible.

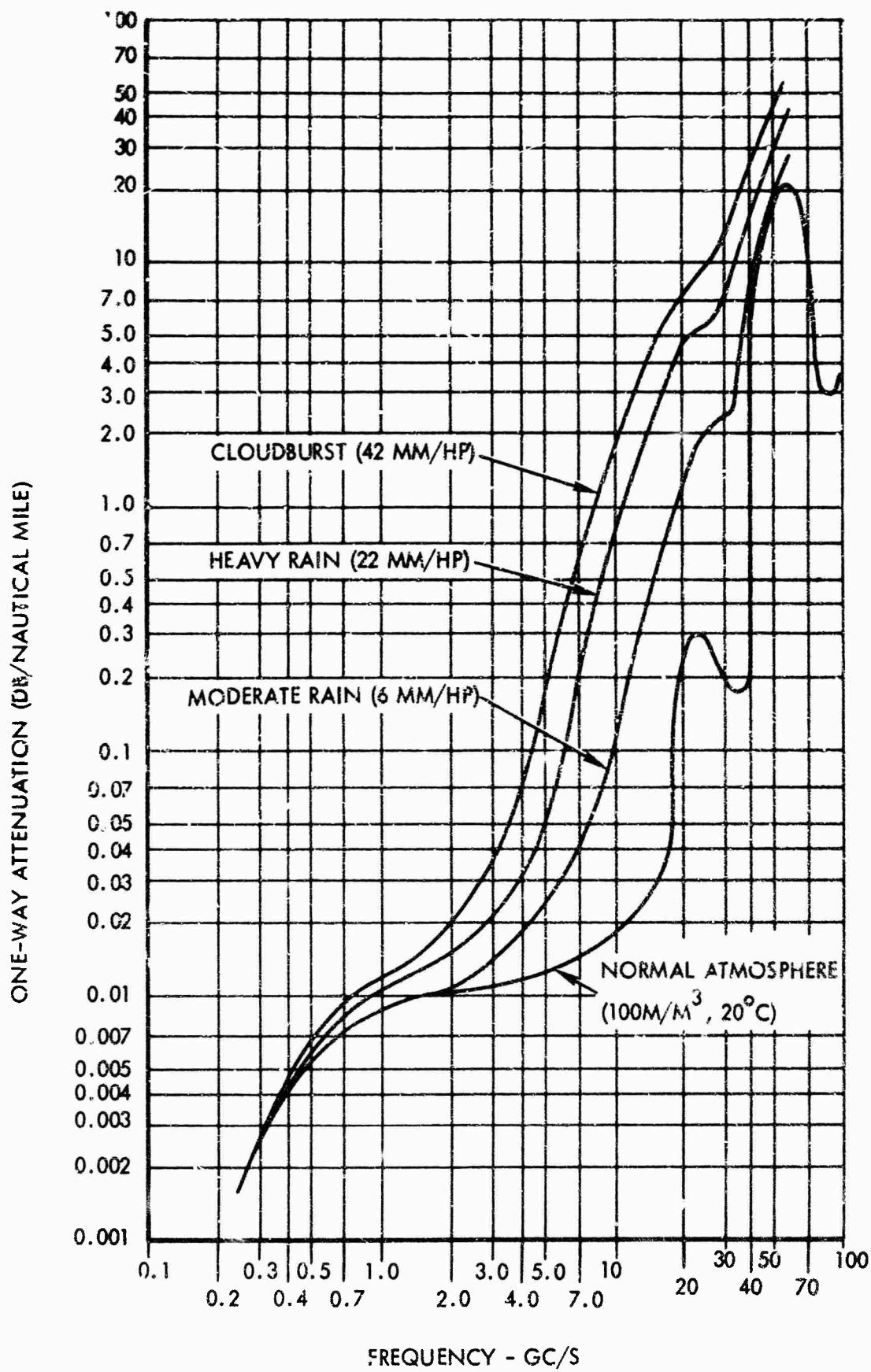
#### a. Satellite/Link Considerations

This paragraph will discuss the communications link as it affects the SCMTR design. The up-link, ground station transmitter to satellite receiver, will not be considered since it does not materially affect the design. A sufficient transmitter power to address the satellite is assumed, and with enough margin to tolerate minor pointing errors (small fractions of a beamwidth). The down-link is important to the SCMTR design in a relative rather than absolute sense; i.e., the absolute value of average received power would affect the channel capacity (and this is discussed in later sections), but variations in received power are of most importance at present. For example, variations due to rain, satellite antenna pointing errors, or ground antenna pointing errors are very important to some SCMTR techniques.

It will be assumed that the down-link signal power will be used with only a small margin for variations and, therefore, antenna losses due to pointing errors are of greatest importance. The absolute power levels, such as satellite ERP, "free space loss", polarization losses, and miscellaneous filter and line losses are, therefore, not important individually. The receiver antenna gain is not of great importance, for the same reasons, but the beamwidth is a critical item. Similarly, time variable losses such as satellite spin (resulting in satellite antenna gain variations), atmospheric absorption, and tracking error loss (allowable) are important in the SCMTR design.

The antenna gain, for a 15-foot parabola operating at 8 GHz will be 49 to 50 dB, depending upon the efficiency (efficiencies from 55% to 75% can be obtained). The half-power beamwidth ranges from 0.54 to 0.6 degrees in the H- and E-planes, respectively. A nominal beamwidth of 0.58 degrees will be used in succeeding paragraphs to determine tracking dynamics. If the antenna size were increased to a 60-foot diameter, the gain would increase by approximately 12 dB and the beamwidth would be reduced by a factor of 4 to approximately 0.145 degrees.

Signal variations caused by the satellite are principally due to power division in the limiter and spin axis effects. Power division occurs in the limiter when the number of users is greater than one. Changes in the number of users causes changes in the output power in a given channel.



47742

Figure 1. Atmospheric Attenuation

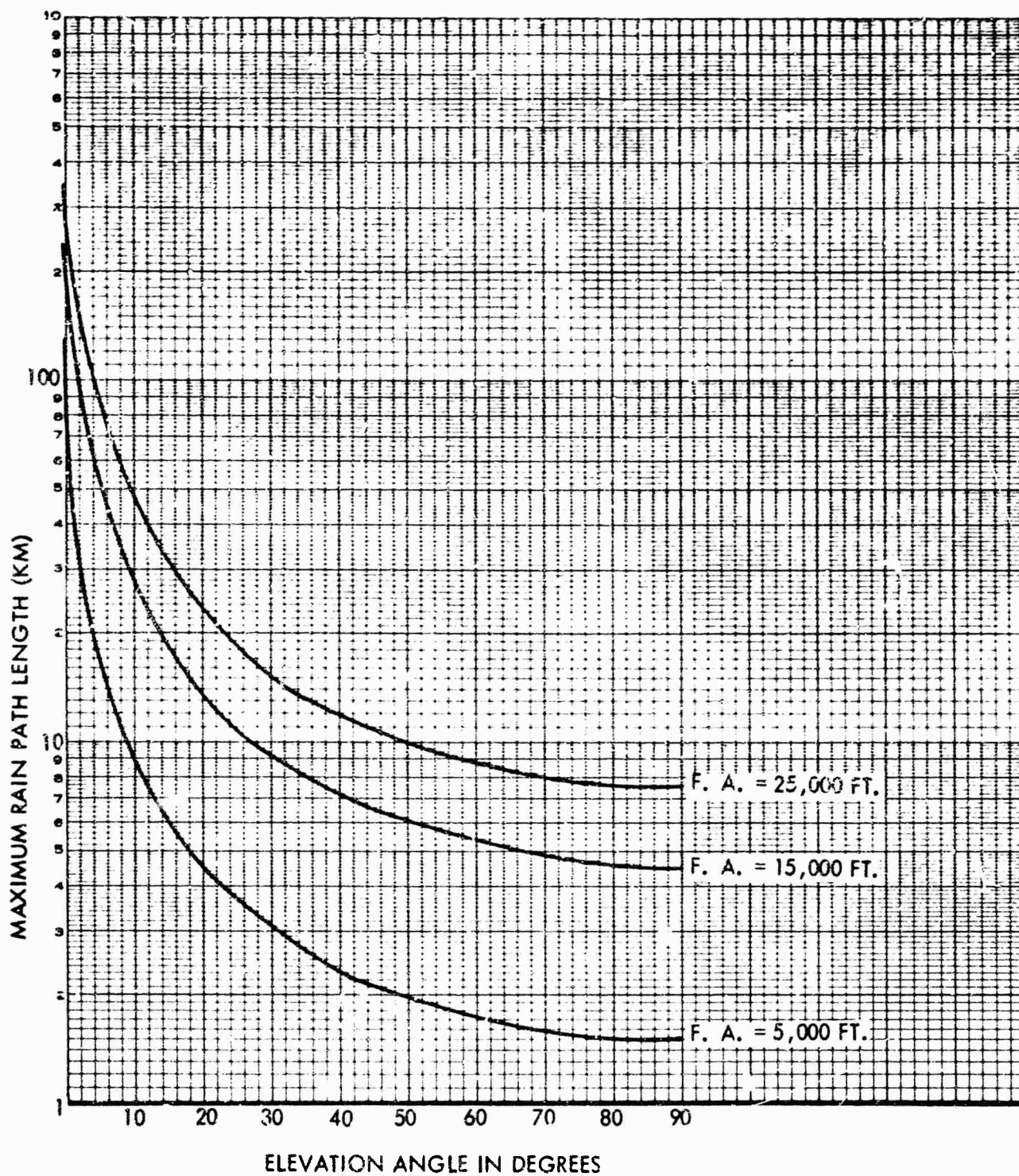


Figure 2. Maximum Rain Path Length as a Function of Elevation Angle With Freezing Altitude as a Parameter

It should be noted at this point, that there is a nonlinear relationship between the sensitivity of link degradation and azimuth axis error. The elevation error relationship is linear. This situation has the effect of making the link more sensitive to elevation than to azimuth errors at all elevation angles above the horizon. The basis for this statement can be tested quite simply by considering the extreme special case at zenith where error in the azimuth axis merely rotates the beam about the line of sight and causes no link degradation whatsoever, no matter how large the azimuth error may be. As a result of this variation in link sensitivity to azimuth axis errors, any meaningful assessment of tracking performance must be made on a beam-radial rather than a per axis basis.

The relationship between the beam-radial error that is of importance to the communications link and the error in the individual servo axes is as follows:

$$E_{BR} = \sqrt{E_{EL}^2 + (E_{AZ} \cos EL)^2} \quad (1)$$

where

$E_{BR}$  is the beam radial error  
 $E_{EL}$  is the elevation axis error  
 $E_{AZ}$  is the azimuth axis error  
 $EL$  is the elevation angle

The above expression was derived using simple trigonometric relationships. Clearly, at high elevation angles the importance of an azimuth axis error is much reduced compared with its importance at the horizon. This reduction of link sensitivity to azimuth error at high elevation angles compensates to some degree for the magnification in azimuth axis dynamics which occurs near zenith. A relatively crude, but useful, indication of the extent of this compensation can be found as shown immediately below.

Consider an idealized servo system for which the dynamic tracking error in each axis is directly proportional to the angular acceleration of the target satellite as seen by that axis. The same constant of proportionality is hypothesized for each axis, and this constant is normalized to unity for simplicity. (In an actual servo, the angular velocity of the target and the successive angular derivatives beyond acceleration will also contribute to the tracking error. However, the latter are negligible and the former can be made small in a relatively high  $K_V$ , Type 1 servo). Equation 1 can then be modified in this special case as follows:

$$E_{BR} \sim \sqrt{\ddot{EL}^2 + (\ddot{AZ} \cos EL)^2} \quad (2)$$

	Pass A: h=5000 Statute Miles, EL <sub>max</sub> =56°	Pass B: h=5000 Statute Miles, EL <sub>max</sub> =79°	Pass C: h=5000 Statute Miles, EL <sub>max</sub> =89°	Pass D: h=19000 Statute Miles, EL <sub>max</sub> =89°
Maximum Angular Rate (°/sec)				
AZ axis	0.063	0.19	2.2	0.064
EL axis	0.024	0.034	0.038	0.0011
Maximum Angular Acceleration (°/sec <sup>2</sup> )				
AZ axis	0.000043	0.00044	0.056	0.000046
EL axis	0.000036	0.00013	0.0015	0.0000012
Elevation Angle at time of AZ <sub>max</sub> (°)	51.0	77.1	88.9	89.8
$\ddot{EL}$ at time of AZ <sub>max</sub> (°/sec <sup>2</sup> )	0.000021	0.000081	0.00095	0.00000078
$\dot{AZ}$ at time of AZ <sub>max</sub> (°/sec)	0.047	0.15	1.8	0.044
$\dot{EL}$ at time AZ <sub>max</sub> (°/sec)	0.017	0.018	0.017	0.00062

Table 1. Some Numerical Values of AZ-EL Dynamics Occurring during Passes of Medium-Altitude and Near-Synchronous Communication Satellites.



where  $\ddot{E}L$  and  $\ddot{A}Z$  are angular accelerations in elevation and azimuth respectively. Values of  $\ddot{A}Z$ ,  $\ddot{E}L$ , and  $E\dot{L}$  at the points of maximum  $AZ$  for passes of the medium-altitude satellite reaching seventy-nine and eighty-nine degrees can be read from Table 1 and substituted into this equation to find the beam-radial following error in those two cases. The ratio of this beam radial error in the eighty-nine degree case to that in the seventy-nine degree case is 11.3. The ratio of azimuth-axis errors (azimuth axis angular acceleration for this idealized servo) in the two cases is 127, a figure that is an order of magnitude larger. Although this calculation has been performed at a single point in the pass and for an idealized servo, the result that it demonstrates is generally valid throughout the pass and for any actual servo. Failure to consider the markedly reduced sensitivity of the links to azimuth axis errors near zenith leads to an overstatement of azimuth servo performance requirements by more than an order of magnitude at elevation angles of eighty nine degrees and above, and by significant amounts at somewhat lower elevation angles. Such overstatement leads in turn to the design of servo systems with unnecessarily wide noise bandwidth - causing degradation in tracking performance at low S/N ratios due to increased tracking jitter error.

It should also be mentioned at this point that generally, if not always, the error signals generated at the antenna terminals are basically beam-radial; i.e., orthogonal signals are generated which are a function of the beam pointing error. Thus, it is in the signal processing, and more specifically, in any coordinate conversion processes, that the non-linear error signals become important.

Error expressions due to noise, amplitude unbalance, or phase unbalance for example, which are referred to the antenna beam can, therefore, be used directly and linearly to determine system performance. When the signals have been transformed to Az-El coordinates, the beam radial effect must be evaluated with the use of equation (1).

The zenith pass conditions can be evaluated for the worse case orbit of 6000 miles by noting that the angular velocity is approximately 0.029 degrees per second. One method for maintaining some communications during zenith or near-zenith passes would be to provide a programmed tracking mode which would slew the antenna in azimuth at a predetermined rate when the elevation angle exceeded a prescribed value (approximately one beamwidth from zenith). The important characteristics of this method are that a maximum error of 0.4 beamwidth results, yielding a communications signal loss of approximately 2 dB maximum. Another important parameter, in terms of the servo system, is the maximum azimuth slew rate required, 4.5 degrees per second. A tradeoff can be made between



the pointing error and slew rate, but these values are relatively close to optimum for the present case.

A more serious problem exists when operation with a 60-foot antenna is considered. Although the target dynamics are unchanged, the antenna beamwidth is much more narrow. As a result, the zenith pass poses a more difficult situation. For example, to maintain a pointing error corresponding to a 2 dB loss in gain, the azimuth rate must be increased by a factor of 4, resulting in approximately 18 degrees per second. Of course, several tradeoffs are available, including a much greater signal loss or a complete loss of signal for several seconds. A rate of 4.5 degrees per second, as required in the previous example, would result in a signal loss for less than 40 seconds.

The important points to note concerning azimuth and elevation rates are that the azimuth dynamics are much greater than the elevation requirements. Furthermore, the slewing rates necessary for near-zenith passes (and also for acquisition) are much greater than the tracking requirements. The greatest impact on the servo system will probably result from the "dynamic range" requirements -- the ratio of the maximum azimuth rate to the minimum angular step. The latter is of greatest significance when considering near-synchronous orbits and is a measure of the granularity of the system. Although the ratio is not dimensionless, it serves as a useful measure of the system requirements. For example, a granularity of 0.1 beamwidth (about  $0.06^\circ$ ) and an angular rate of  $4.5^\circ$  per second is expressed as a dynamic range requirement of 75, or about 19 dB. Additional servo system requirements will be discussed further in the following section.

#### c. Servo Bandwidth

The servo bandwidth requirements and limitations cannot be accurately determined within the scope of the present work. However, estimates based on similar operational conditions will serve to provide bounds on the performance. Fortunately, the precise value of servo bandwidth is not required to evaluate the various SCMTR techniques. An order of magnitude estimate is necessary to simplify the SCMTR analyses and this estimate will be made in the following paragraphs.

The dynamic requirements and structural components, including the dish itself, are of prime importance in the servo design. Typical parameters which must be known, determined, and/or evaluated include:

- (1) Inertia with respect to the azimuth and elevation axis.
- (2) Compliance and damping factor between the gear box and reflector.
- (3) Friction in the gear box, both static and coulomb, and backlash.
- (4) Maximum wind load torque.
- (5) Maximum and minimum angular velocities.
- (6) Maximum angular acceleration.
- (7) Allowable dynamic lag error.
- (8) The servo gain required as a function of frequency, which is further dependent upon the type of mount.
- (9) Acquisition requirements, such as static error from gear box to position readout and required scan patterns.
- (10) Input signal characteristics including antenna beamwidth, SCMTR gain, AGC characteristics, SCMTR peculiarities (such as scan or lobing rates) and any unusual filtering requirements.
- (11) Unusual environmental conditions, power limitations, or other applicable system specifications.

It is apparent that a detailed evaluation of the preceeding parameters is neither desired nor necessary. The basic SCMTR design should, if at all possible, be independent of most of the above parameters. The basic tracking requirements, as discussed in above section, indicate that a relatively low performance servo system would be adequate. The requirements are orders of magnitude less severe than for tracking radars with conventional aircraft or missiles as targets.

The requirements of "typical" satellite communications terminals operating with similar ground rules have been evaluated at Radiation Incorporated. The most severe requirements are satisfied with servo bandwidths of much less than 1 Hz. Quite often it is desirable to further limit the bandwidth to reduce tracking jitter. It appears conservative to assume that a maximum bandwidth of 0.1 to 0.2 Hz would be more than adequate for the stipulated conditions. This bandwidth is entirely

compatible with the structural resonances which can be achieved, assuming conventional military environmental requirements. The bandwidth could be reduced with no adverse consequences as far as the servo system itself is concerned. Therefore, a nominal 0.2 Hz servo bandwidth will be assumed, with a reduction by an order of magnitude possibly desired in some situations. Considering a type 2 servo, the equivalent two-sided noise bandwidth would then be approximately 1 Hz maximum. It is relatively easy to obtain a selection of servo bandwidths on a single terminal, and this eventuality should be considered as applicable.

#### d. Communications Bandwidths

Characteristics of the communications channel were generally outlined in section 2. The most important signal characteristics were that CW and angle modulation signals were being considered, with a maximum bandwidth of 160 kHz and a baseband range of 300 Hz to 8 kHz. Operation with teletype signals, both separately and multiplexed, was also assumed.

The widest communications bandwidth need be only 160 kHz plus an amount to allow for frequency uncertainties. If AFC or sweeping techniques are used, it is possible to circumvent the adverse effects of Doppler shift, transmitter drifts, satellite drifts, and local oscillator drifts. Expected drifts are discussed in later paragraphs, and the net result is that a maximum communications bandwidth of 200 kHz should be adequate. In the event larger drifts or Doppler shifts occur, some form of AFC would be mandatory to avoid serious degradation of the communications channel.

The minimum communications bandwidth is of interest, particularly its relation to the servo bandwidth, since this will determine the severity of the tracking noise problem. A reasonable minimum communications capacity would be a single 100 word per minute teletype channel with an error rate of  $1 \times 10^{-4}$ . Possibly a truncated voice channel would represent an operational minimum, but the teletype will be assumed since it represents a worst case.

A 100 word per minute teletype channel, with a bit error rate of  $1 \times 10^{-4}$ , requires a minimum theoretical signal-to-noise ratio of (2): a) +8.4 dB when antipodal (e.g., bi-phase modulation of the prime carrier) binary signaling is used; b) +11.4 dB when binary orthogonal signaling is used.

A degradation of 1 to 2 dB is typical of practical techniques. A signal-to-noise ratio of +13 dB (minimum) would be required using

PCM/FM (conventional frequency-shift keying, for example). Equivalent noise bandwidths of approximately 150 Hz would typically be obtained using FSK with  $\pm 42.5$  Hz shifts on a subcarrier. Under these conditions, then, 100 words per minute and  $1 \times 10^{-4}$  bit error rate, a signal-to-noise ratio of +13 dB in a 150 Hz bandwidth is required. This implies an input carrier to noise density (per Hertz of bandwidth) of

$$\frac{C}{n} = +13 + 10 \log_{10} 150 = +35 \text{ dB} \quad (3)$$

This value is particularly important when considered with respect to the tracking channel requirements. Since a maximum tracking noise bandwidth of approximately 1 Hz has been determined appropriate, the signal-to-noise ratio in the tracking bandwidth would be +35 dB under minimum communications conditions, (and assuming equivalent noise temperatures in the communications and tracking receivers). This relatively high value of potential tracking channel sensitivity can be utilized to simplify the SCMTR design. For example, a high effective noise figure in the tracking receiver would not seriously degrade the tracking performance. Quantitative results will be obtained for each SCMTR using the above signal levels. More detailed results cannot be stated at this point, since the tracking error due to noise is highly dependent on the particular SCMTR design.

#### e. Signal Characteristics

Several basic signal characteristics other than those previously determined can affect the SCMTR configuration. The basic modulation (angle modulation) techniques and minimum signal levels have been discussed in preceding sections. Other pertinent signal characteristics, including dynamic range, Doppler shifts, and extraneous modulations will be discussed in the following paragraphs.

Satellite induced modulations are expected to be relatively small, considering the present state-of-the-art. However, some modulation due to satellite motion is possible. For example, an "earth coverage" antenna mounted on a precessing vehicle could cause an AM and/or FM component on the received signal. Similar effects could be caused by atmospheric perturbations (e.g., cloud motion) and incidental AM or FM in the satellite translator or ground transmitter. The expected signal variations would be very small and should not significantly affect the SCMTR design. In the unlikely event that a signal variation occurred at a rate which would interfere with the receiver (e.g., an AM component at the scan frequency in a pseudo-monopulse system), the receiver design could be slightly altered to avoid the interference.

Additional signal modulations will be present, such as residual FM, (short-term oscillator instabilities), incidental AM, and possibly variations due to multipath. All of these effects are expected to be insignificant as far as the SCMTR design is concerned. In general, the undesired modulations will be far more detrimental to the communications channel than to the tracking channel.

The input signal levels can be considerably greater than the minimum channel capacity signal evaluated in section 3.4. For example, input signals which would produce a predetection signal-to-noise ratio of 20 dB or more in the widest signal bandwidth are very likely. The resultant carrier to noise density would be

$$\frac{C}{n} = +20 + 10 \log_{10} 2 \times 10^5 = +73 \text{ dB}$$

This is an increase of 38 dB over the minimum C/n previously calculated. This value is also compatible with anticipated satellite communications links. Thus, a 40 dB range of communications signal levels is likely, and the tracking channel dynamic range requirements are therefore at least 40 dB. Even greater variations are probable when the satellite type is changed; i.e., ERP, range, basic capabilities are varied.

The signal losses due to rain, as discussed in an earlier section, can result in a significant change in signal strength. The path losses and local area losses (due to reflection and local obstructions) can also cause signal variations. The total dynamic range should not greatly exceed the postulated values, however. Lower level signals would result in loss of communications and very much higher level signals would represent an unforeseen satellite capability and a significant waste of communications capability (it could be better utilized by serving more terminals, for example). Thus, a dynamic range specification of about 50 dB would be a conservative value, and it should not unduly restrict the SCMTR design.

Doppler shifts on the incoming signal are greatest for the lowest altitude satellites. The major impact of Doppler on the SCMTR design is in the acquisition mode. This is due to the extremely slow rate of change of frequency. Thus, the initial signal frequency uncertainty may be large, but it will not change rapidly and can easily be tracked with a slow AFC system. The maximum expected Doppler shift for a 6000 mile orbit is approximately  $\pm 100$  kHz on an 8 GHz signal. When near-synchronous and synchronous orbits are considered, the Doppler shift is essentially zero.

#### f. Acquisition Parameters

The exact acquisition problem depends upon a number of variables, both in satellite characteristics and ground terminal characteristics. The general problem is one of locating a signal which has an initial uncertainty in both position and frequency. Thus, a two-dimensional search is necessary to find the satellite.

The frequency uncertainty is due to transmitter frequency drifts (beacon signal drifts), receiver frequency uncertainties (local oscillator drifts), and Doppler shifts. The frequency drifts in transmitter and receiver are relatively small, ranging from 1 part in  $10^6$  to 1 part in  $10^8$  typically, which corresponds to 8 kHz to 80 Hz with an 8 GHz signal. Doppler shifts can be greater than 100 kHz, in general. Therefore, if no other information is available, a frequency uncertainty in the range of the Doppler shift is present. Alternately, a relatively inaccurate "guess" based on ephemeris information would reduce the Doppler uncertainty by an order of magnitude. Note that this ephemeris data is necessary to place reasonable bounds on the space uncertainty. Two "worst case" values are therefore suggested for the frequency uncertainty:

A frequency range of less than  $\pm 150$  kHz would be required under the most adverse conditions.

A frequency range of  $\pm 15$  kHz would be required under normal conditions.

The spacial uncertainty is due to three major factors; ephemeris inaccuracies, unknown locality, and unknown local orientation. The first factor is due to measurements on the satellite and, except for the first few orbits, contributes very little to the overall problem. The second factor, lack of precise knowledge of the terminal location can be significant, particularly in initial acquisition (the first operation in a given location). The third factor is probably most significant in transportable terminals, since an inaccurate knowledge of direction (true North) and local vertical are directly added to the other uncertainties. A detailed analysis of this problem has been accomplished for a terminal with capabilities similar to those in the present case (assuming antenna size, frequency stability, communications capability, and mobility can be used to equate terminal complexity). The results of this analysis are simply that, for the lowest altitude satellites, a maximum spacial uncertainty of 2 degrees in each direction is probable. A total sweep of  $\pm 3$  degrees in each direction would be a conservative value, and should not impose unduly harsh requirements on the antenna drive system of servo system.

These changes are relatively long term variations (occurring at intervals ranging from minutes to hours) and will not be of great importance to the SCMTR. These changes are not vastly different from the variations in signal level due to range; i.e., changes in free space attenuation. Spin axis ripple, on the other hand, can occur at rates in the order of a cycle per second and with a magnitude in the order of 0.5 to 1.0 dB. This variation must be considered in some SCMTR designs.

The most severe potential signal variation is that due to rain, particularly at low elevation angles. At frequencies above a few GHz the atmospheric attenuation increases rapidly with frequency. This effect is shown in Figure 1, which is a graph of atmospheric attenuation versus frequency for four conditions of rain. Expected path lengths through rain, as a function of satellite elevation angle and for several freezing altitudes are shown in Figure 2. A conclusion which can be drawn from these curves is that large losses can be expected due to rain when low elevation angles are used. The impact of this on the SCMTR design is simply that a communications bandwidth reduction is probable under these conditions, so a worst case analysis based on minimum communications bandwidths should be made. The rate of change of attenuation due to rain is, in general, relatively low, so the principal effect is long term and is reflected in the channel capacity.

#### b. Tracking Dynamics

The SCMTR is required to operate with satellites in orbits ranging from 6000 nautical miles, to near-synchronous, to synchronous. Since a large amount of data<sup>(1)</sup> is available for 5000 mile orbits, a separate calculation for 6000 mile orbits was not deemed necessary. The 5000 mile orbit has slightly greater dynamic requirements than the 6000 mile orbit, so it can be used in a worst case design. Of perhaps greater significance is the fact that these dynamic requirements are not limiting parameters in the SCMTR design. There are two reasons for this: first, the acquisition mode generally imposes greater dynamic requirements since a spacial search must be made to locate the satellite in a reasonable length of time; secondly, the zenith pass represents a worst case problem and this is considered separately.

Target dynamics for low orbits are plotted in detail in reference (1). Selected values from these curves are tabulated in Table 1. Also listed in this table are the dynamics for a 19,000 mile orbit, which is representative of a "near-synchronous" satellite. The ideal synchronous orbit imposes no dynamic requirements, and a practical "synchronous" orbit exhibits very low dynamics compared to the "near-synchronous" case. As a result, the 5000 mile parameters will be used as worst case conditions to determine the SCMTR requirements.

The variable which has not yet been discussed is the time allowed for acquisition. Time is a parameter which varies with the tactical usage of the equipment and is particularly important in handover, and this is most significant when lower altitude satellites are being used. Acquisition times of a few minutes, for the worst case frequency and spacial uncertainties are not unreasonable. If an extremely fast acquisition time is needed, it could impose additional requirements on the SCMTR.

It is also enlightening to view the acquisition problem from a different point. Consider first the dynamics required of the tracking system simply to follow the satellite after acquisition. It is apparent that the dynamics required to acquire the satellite are no less than, and are in fact greater than, the tracking dynamics. Thus, the acquisition mode imposes the most severe dynamic requirements. For this reason, mode switching may be required. For example, a wide band condition may be needed for acquisition, and would result in a relatively large tracking error due to noise. However, once acquisition was accomplished, a narrower bandwidth could be used to reduce the noise errors.

g. Additional Performance Requirements

One performance requirement imposed directly by the Statement of Work, Exhibit "A" of PR C-6-2059, is that the SCMTR shall not degrade the predetection signal-to-noise (S/N) ratio more than 2 dB, with a design goal of 1 dB. In order that the communications channel be affected only slightly by the SCMTR, every effort should be made to meet the 1 dB design goal. It is worth noting, at this time, that the other SCMTR specifications discussed in this section are compatible with this requirement, and that the predetection S/N degradation is the single, most important measure of SCMTR performance.

Another performance characteristic which is important to the tracking is crosstalk. Crosstalk in this sense refers to elevation tracking errors which would cause signals to appear in the azimuth error channel and vice-versa. A further characteristic which should be evaluated is the bias error problem; i.e., amplitude or phase unbalance in the system which would result in a constant boresight error.

The crosstalk and bias error problem can be evaluated for the cases of "amplitude" monopulse and "phase" monopulse, since one of these two antenna techniques is typically used to obtain tracking information. A detailed analysis is not generally possible without further specifying the method for combining the various feed signals to obtain the sum and difference signals. However, some general characteristics can be found.



These characteristics are derived in Section VII. A summary of the general factors which are pertinent to this program follows:

The microwave-antenna system is assumed to consist of a number of feeds, or elementary elements. The outputs from these feeds enter a device called a comparator. The output of the comparator consists of three separate signals; the sum channel, elevation error channel, and azimuth error channel. It should be noted that the azimuth error channel represents a beam radial component and is actually an error channel orthogonal to the elevation error channel, not the azimuth axis mount error. Ideally, the sum channel is maximum and the difference channels are zero when the antenna is pointed at the satellite. In practice, however, pointing errors occur as a result of pre-comparator errors; i.e., amplitude and phase unbalances prior to the output of the comparator. The nature of these errors are that amplitude unbalances cause boresight shifts in an amplitude monopulse system and phase unbalances cause boresight errors in a phase sensing monopulse feed (the errors being described with respect to the feed terminals). "Opposite" errors (i.e., phase errors in an amplitude monopulse) result in imperfect nulls on boresight. Thus, a signal appears in the error channel(s) at boresight, but it represents a minimum; i.e., moving the antenna in any direction would increase the error signal. This boresight signal, with respect to the sum channel signal at boresight, is often referred to as the null depth of the system. A specification on the null depth would therefore place specific requirements on the "opposite" unbalances.

It has been assumed for this program that boresight errors must be controlled such that the pointing error would cause a relatively small sum channel loss; i.e., any boresight losses must be included in the overall sum channel degradation specification. An important point, however, is that most, if not all, of the SCMTR techniques being evaluated utilize the same feeds and comparators as a full monopulse system. Therefore, pre-comparator errors will, for the most part, cause identical degradation in all SCMTR methods and in full monopulse. Techniques which do not conform to this general statement should be analyzed to assure that realistic pre-comparator errors do not cause significant performance degradation.

Post-comparator errors will, in most cases, result in cross-talk in SCMTR's and cause a loss in gain in nearly all systems. The gain loss phenomenon is usually found in the correlation detector (in the case of phase unbalance) or as a direct gain change (in the case of amplitude unbalance). The major impact of this change in gain is to place more stringent gain margin requirements on the servo system. Thus, relatively large post-comparator variations can usually be tolerated without significant

system degradation when the pre-comparator errors are small. The combination of pre- and post-comparator errors will result in crosstalk. A small amount of crosstalk will cause the antenna to "spiral" towards a target rather than be moved in the true direction of pointing error. Of course, when the crosstalk becomes very large, the antenna inward spiral becomes a circle and finally an outward spiral, so a reasonable limit must be imposed on crosstalk. The impact of post-comparator errors has been analyzed for the various SCMTR techniques as appropriate.

#### h. SCMTR Requirements - Summary

The most important SCMTR system design requirements are tabulated in Table 2.

TABLE 2

#### System Design Criteria Summary

Antenna:	15-foot diameter; $0.58^\circ$ beamwidth.
Mount:	Elevation-over-azimuth.
Tracking Dynamics:	See Table 1.
Servo Noise Bandwidth:	1 Hz maximum; 0.1 Hz minimum.
Acquisition:	Frequency Uncertainty: $\pm 150$ kHz worst case. $\pm 15$ kHz typical.
	Spatial Uncertainty: $\pm 3^\circ$ typical.
Frequency:	8 GHz nominal. $\pm 1$ part in $10^8$ accuracy and stability.
Modulation:	CW or FM
RF Bandwidth:	160 kHz maximum. 150 Hz minimum
Receiver Signal Level:	C/n of +35 dB to +65 dB.
Sum Channel Degradation:	2 dB maximum. 1 dB design goal.

#### 4. BASIC SCOPE OF WORK

The purpose of this paragraph is to describe the overall scope of the study program. This scope resulted from both the requirements of the Statement of Work, PR C-6-2059 and the requirements discussed above. The basic purpose of this program has been to develop a design for a Single Channel Monopulse Tracking Receiver (SCMTR).

The SCMTR must process signals received by an antenna to provide azimuth and elevation error signals for use in the antenna servo system and must demodulate an angle modulated signal to obtain the baseband information. The SCMTR consists of the necessary receive feeds, the comparator which forms sum and difference channels, one or more low-noise preamplifiers, mixers, amplifiers, a single IF amplifier, detectors necessary to obtain the azimuth and elevation error signals, and demodulators necessary to obtain the baseband information.

The objectives of this program are to reduce the complexity of conventional monopulse tracking systems while preserving their angular tracking accuracy and to incorporate the communications demodulators into the SCMTR without degrading the pre-detection S/N more than 1 dB (design goal). In order to best obtain the objectives of this program, some aspects of the problem must be emphasized while others are given only cursory examination. Following paragraphs will discuss the factors which have been emphasized in this study.

Techniques which can minimize the feed-comparator-microwave circuit components have been investigated, but feed design per se was not emphasized. Ample work has been done in this area, as evidenced in the literature search. Furthermore, the feed and comparator components are usually common to the different SCMTRs. An analysis of monopulse antenna characteristics is found in Section VI.

The pre-amplifier, mixer, and IF amplifier areas have been of prime importance in this program. It is here that the major system complexity tradeoffs have been made. For example, use of multiple, complex pre-amplifier systems will result in improved performance, but a significant reduction in complexity is possible with (potentially) a small performance degradation. In some SCMTR techniques unduly harsh requirements may be placed on mixer and amplifiers. Thus, particular emphasis was placed on these elements when the various SCMTRs were evaluated.

Detector characteristics can be significant, particularly when threshold performance is being considered. Thus, any peculiar detector requirements imposed by a particular SCMTR have been evaluated. Detector parameters are most important when evaluating the tracking errors due to

noise, but, as shown earlier, the tracking noise bandwidth is much less than the communications bandwidth. Therefore, detector performance is important in only a few SCMTR techniques.

Although the servo system design is not within the present scope of work, servo design parameters have been considered as they interact with the SCMTR. This effect was evidenced by requirements on signal processing which might affect the servo system (e. g. , AGC requirements can affect servo gain and bandwidth). Limitations imposed by azimuth and elevation drive systems were considered as they affected SCMTR concepts.

An additional case which was considered was the acquisition problem. As discussed earlier, acquisition of the satellite imposes requirements more stringent than tracking dynamics. The situation is most acute when larger antennas are used. Specifically, the feasibility of extending the SCMTR techniques to tracking antennas as large as 60-feet in diameter was considered.

A requirement imposed by the Statement of Work was that two SCMTR approaches be considered: 1) a SCMTR which incorporated communication signal demodulation in addition to forming the error signals and 2) a SCMTR which only forms the error signals. Since it became apparent that a SCMTR technique which combines the communications and tracking signals was feasible, the latter approach was not considered.

Several specific analyses were performed to aid in the design and evaluation of the SCMTRs. Parameters which were evaluated for each SCMTR technique include the following:

- a. Equipment complexity - a vital parameter which includes not only the size, weight, and other physical characteristics but also the difficulty of alignment and the ability to maintain calibration.
- b. Cost - the economics may be a significant measure of the value of a technique; design and alignment costs are considered as well as component costs.
- c. Angular tracking accuracy - tracking accuracy is an important parameter, but tracking accuracy beyond that necessary to maintain sum channel gain does not improve the overall terminal capability.
- d. Sum Channel Degradation - the most important single performance parameter; it incorporates the effects of all aspects of the problem into a single factor -- how well can the basic communications channel function.

- e. Carrier to noise density requirements - an evaluation of the minimum  $C/n$  necessary to track the satellite.
- f. Dynamic Range - any peculiar dynamic range requirements due to the different multiplexing techniques.
- g. Bandwidth Requirements - significant bandwidth requirements peculiar to the various SCMTR techniques.
- h. Pre- and Post-comparator requirements - the amplitude and phase linearity necessary to avoid boresight errors and crosstalk.

The above list is not exhaustive, and other pertinent parameters were evaluated as well (see Section III).

The basic philosophy which was adopted in evaluating the various techniques was one of comparison; i.e., relative merits rather than absolute values were used in the evaluation. In particular, the SCMTR techniques were compared with each other and with a conventional, three-channel monopulse receiver system. In most respects the three-channel receiver offers the ultimate in performance, whereas the SCMTRs were typically less complex. The basic tradeoff, then, was performance versus equipment complexity. In this sense, an optimum tradeoff occurs when the performance is compromised by a negligibly small amount and the hardware requirements are greatly reduced. A tabulation of the characteristics of each SCMTR, as well as full monopulse receivers is found in Section III.

## 5. SCMTR TECHNIQUES

This section will describe briefly specific SCMTR techniques, which have been analyzed. These techniques were coarsely evaluated to determine their potential usefulness. Techniques which appeared most promising were then evaluated in detail. Finally, the most promising methods were designed in detail (see Section IV and V).

### a. Full Monopulse

Three channel monopulse receivers were studied for two important reasons. First, the performance characteristics of full monopulse was used as a baseline in evaluating all SCMTRs. Secondly, the basic analysis (of full monopulse) was directly applicable to several SCMTR techniques. Therefore, full monopulse receiver evaluation was a necessary part of the overall program.

b. Frequency Division Multiplexing

Frequency Division Multiplexing (FDM) is a basis for a family of SCMTRs. In addition to the basic FDM analysis, an important modification was evaluated, the SCAMP technique<sup>(3)</sup>. SCAMP is an FDM system which utilizes hard limiting to achieve normalization with respect to the received signal strength.

c. Time Division Multiplexing

Time division multiplexing (TDM) is another basic technique which was investigated. Pure TDM was analyzed for high sampling rates with respect to the communications bandwidth. A detailed analysis of slow TDM was not deemed worthwhile, since the technique has a serious shortcoming; when a sampling rate slower than twice the basic information bandwidth is used, an irrecoverable loss of information occurs. This loss cannot be measured meaningfully in terms of dB of degradation, but must rather be described in terms of down time. Since such a shortcoming is generally undesirable, and certainly intolerable in tactical situations, the technique was not investigated further.

d. Hybrid Techniques

Methods which cannot be classified as either FDM or TDM were arbitrarily called hybrid techniques. It is in this general area that the most potentially useful techniques were found. At least three basic hybrid techniques appeared promising and were investigated in some detail. The first of these, called pseudo-monopulse, is a technique for adding a small portion of the error signals to the sum signal. Different types of pseudo-monopulse were investigated, including both square wave and sine wave modulation (or sampling) methods. The basic technique called lobing was investigated. Both sequential lobing and conical scan have been examined, and the techniques are electrically identical to pseudo-monopulse. Finally, the Automatic Manual Simulator (AMS) was examined. The AMS is similar, in concept, to an extremely slow lobing system, with the exception that the entire antenna is moved rather than just the feed. Again, the signal characteristics are identical with pseudo-monopulse.

## SECTION III

### SCMTR EVALUATION

#### 1. INTRODUCTION

The relative evaluation of Single Channel Monopulse Tracking Receivers (SCMTR) analyzed during the program is accomplished in this Section. The evaluation necessarily involves tradeoffs in performance versus complexity, and is made on a relative basis rather than an absolute one. The basic technique used in the evaluation consists of assigning weights to each of eleven different factors, and then grading each system relatively, for each factor. The three channel full monopulse approach is included for comparison purposes only. The overall system characteristics of importance to this evaluation were described in Section II.

The various SCMTR techniques, as well as Full Monopulse, are briefly described in the next paragraphs. The descriptions are followed by an explanation of the weighting factors used in the evaluation. This is followed by the evaluation itself, with an explanation of the factors and the relative grades. Finally, the results of the evaluation are summarized.

#### 2. SCMTR TECHNIQUES

##### a. AMS (Automatic Manual Simulator)

A basic block diagram illustrating the AMS technique is shown in Figure 3. The technique is essentially a conical scan or lobing type system with the scanning accomplished by mechanically rotating the entire antenna. The rotation is accomplished by driving the antenna drive and servo system from a low frequency generator.

The system requires only a single feed (not a monopulse feed) which drives a receiver utilizing either a manual gain control or an extremely slow AGC. The receiver output is detected in an envelope detector. This detected signal is then compared with the two orthogonal generator signals. This comparison, done in a phase-sensitive detector circuit, provides the two error signals to drive the servo.

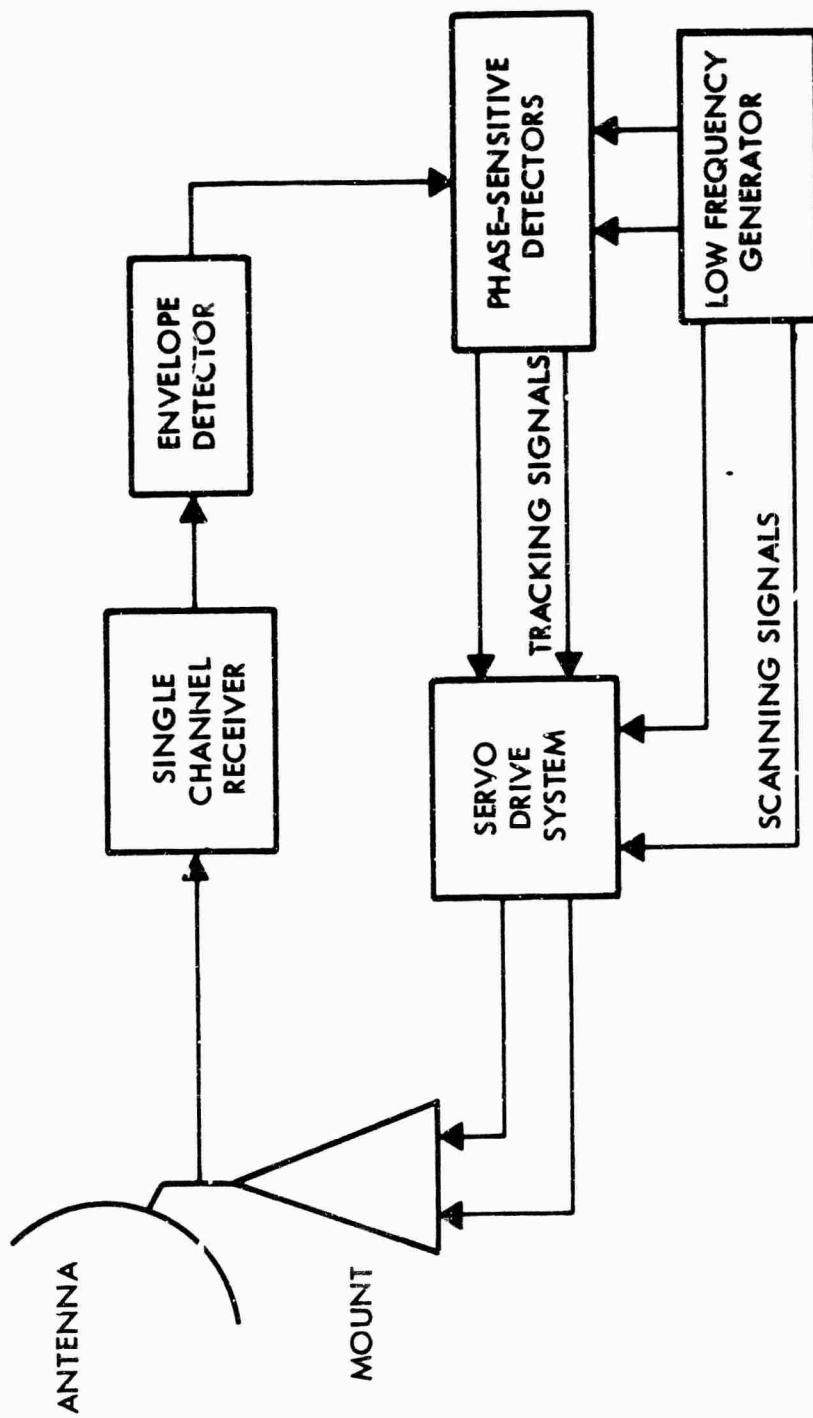


Figure 3. AMS System Block Diagram



b. Lobing or PM (Pseudo-Monopulse)

A block diagram of the Pseudo-Monopulse technique is shown in Figure 4. Conical scan and sequential lobing are very similar in principle and will be included in this discussion. The input from each of four feeds is used in the comparator to form the sum  $\Sigma$ , and two difference signals  $\Delta_{AZ}$  and  $\Delta_{EL}$ . The difference, or error signals, are combined in the scanner at a relatively low rate (less than 100 Hz), and added in-phase to the sum signal in the coupler to form an AM output signal. The signals may also be added in quadrature (phase modulation) when the basic communications information on the RF carrier is a few hundred Hz minimum (lower rates would cause crosstalk with the scanning signal).

The AM signal is processed through a single channel down to some IF, where the signal is divided and supplied to the error detectors and the data demodulator. By proper choice of the switching, or Q functions, the output of the detectors after low pass filtering is the desired normalized DC voltage containing both magnitude and phase information. Conical scan forms the AM signal by physically rotating the single feed, or electronically scanning the single beam. As a result, the comparator and coupler are replaced with the beam scanning circuitry, and the remaining circuitry is identical to PM.

c. FM (Full Monopulse)

Figure 5 shows the basic block diagram of the Full Monopulse technique. Three complete receivers or channels are used, and the normalization is accomplished using an AGC voltage derived from the  $\Sigma$  channel and applied to all three channels. This technique requires that each channel be matched in phase and amplitude over its entire dynamic range. RF amplifiers are shown in the error channels but are not always necessary. The  $\Sigma$  channel output is used as a phase reference in the error detectors. The detector outputs are proportional to the error signal amplitudes for small errors and preserve the sign information.

d. TDM (Time Division Multiplex)

Shown in Figure 6 is a block diagram of the basic TDM, Time Division Multiplex technique. The system is identical to Full Monopulse down to the first IF. At this point, narrow filters are used to band limit the signal before sampling. This prevents degradation due to high frequency noise or extraneous signals present in the IF. The required switching rate is at least  $2W$ , where  $W$  is the highest frequency component in the signal. This switching rate will require an IF bandwidth at least  $6W$ , in order that

Figure 4 Pseudo-Monopulse Block Diagram

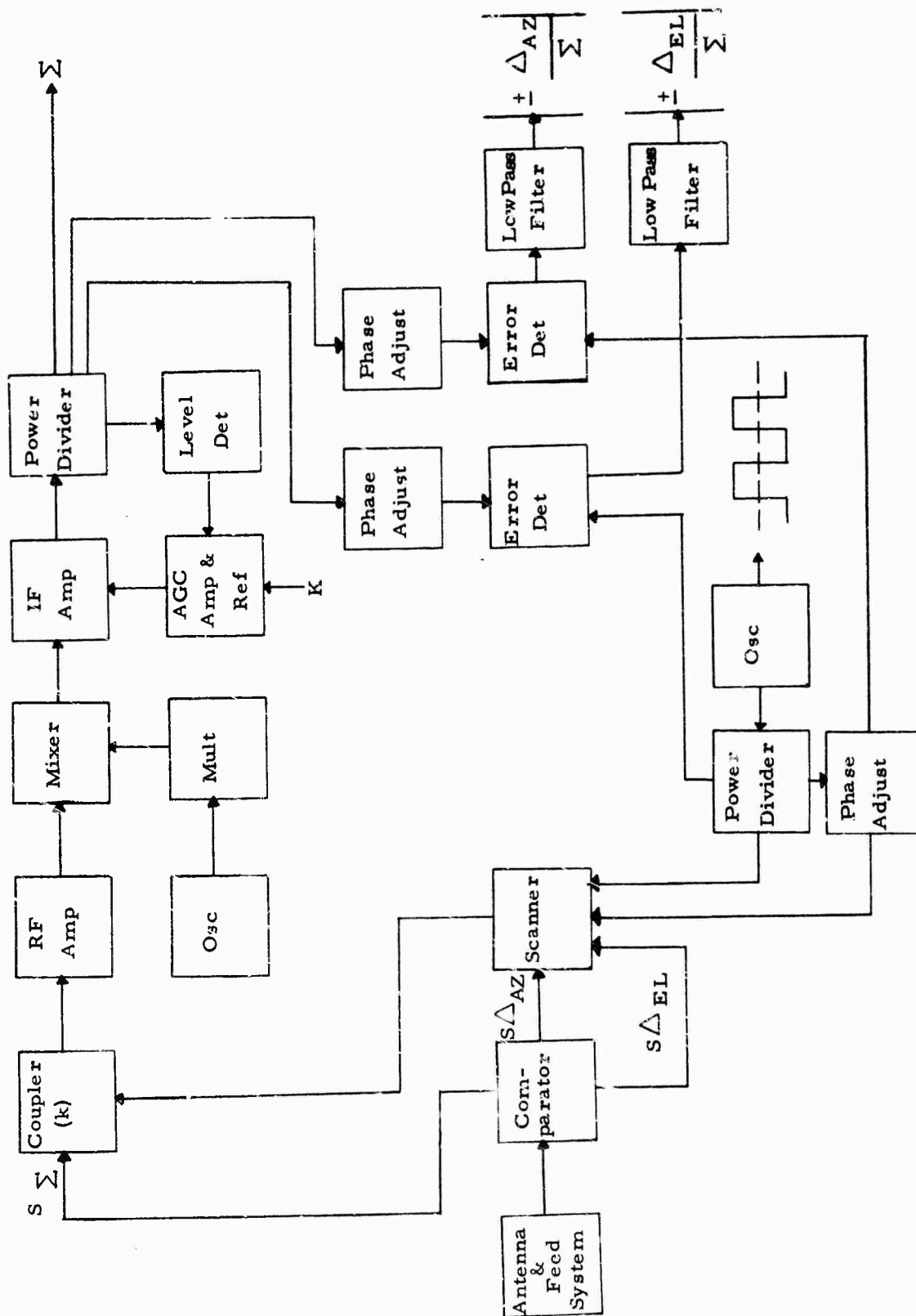
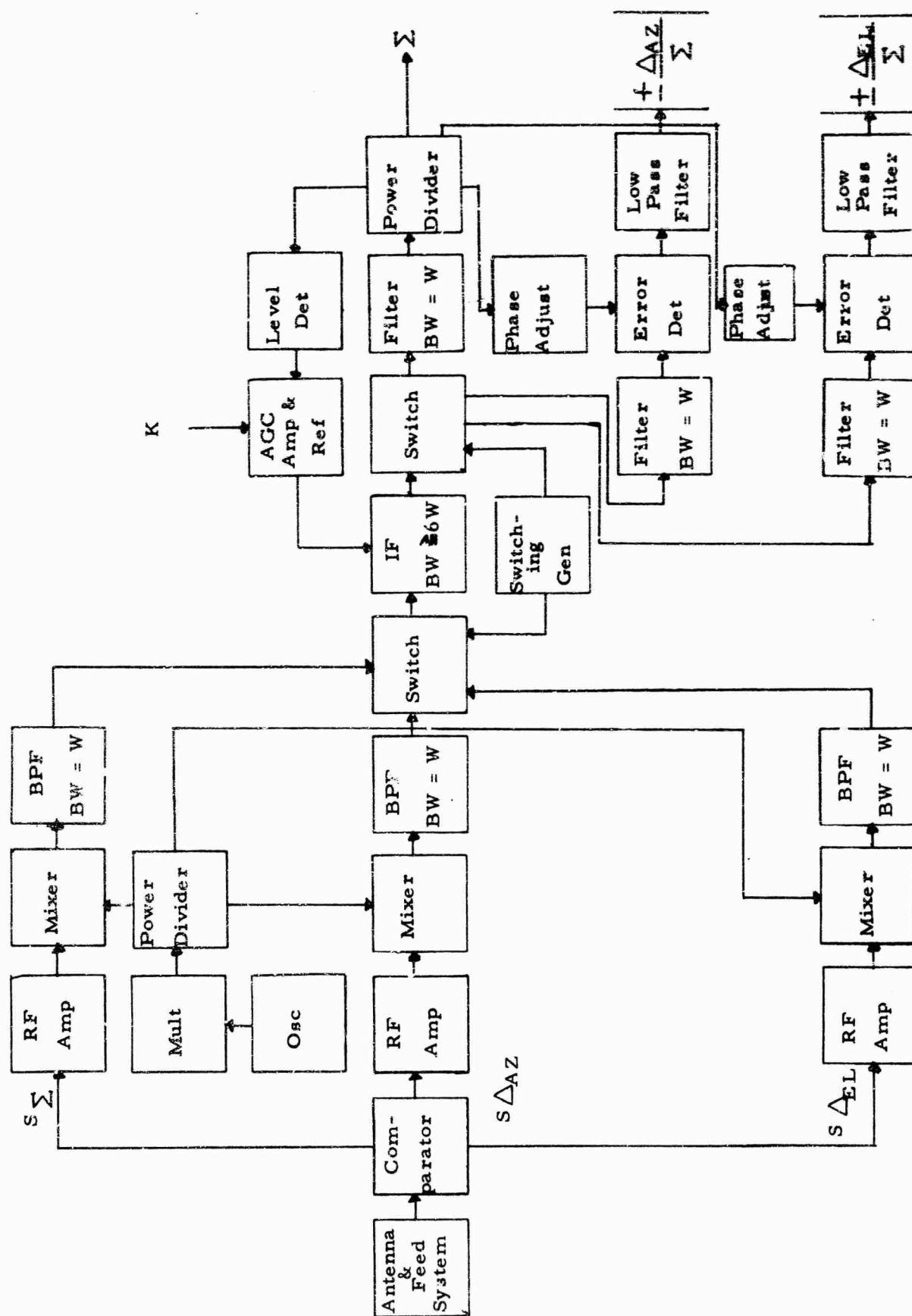




Figure 6 Time Division Multiplex Block Diagram



the output of the IF be essentially zero before the next sample arrives. The IF output is supplied to a second switch operated in time sync (lagging by the IF delay) with the first switch.

The post IF switch output is supplied to three filter identical to the filters used prior to sampling. AGC is developed using the  $\Sigma$  channel filter output and is applied to the IF amplifier to achieve normalization. The error detectors and remaining circuitry are identical to the FM technique.

e. FDM (Frequency Division Multiplex)

Shown in Figure 7 is a block diagram illustrating the FDM (Frequency Division Multiplex) technique. The RF Amplifier outputs are mixed to three separate center frequencies such that their individual spectra do not overlap. The difference frequencies  $f_2-f_1$  and  $f_2-f_3$  are formed and applied to separate mixers. The  $\Sigma$  and  $\Delta$  signals are summed linearly and amplified in the broadband IF. Again, AGC is developed from the  $\Sigma$  channel output and applied to the IF for normalization. The  $\Sigma$  signal is mixed with the signal  $f_2-f_1$  and the mixer sum output at center frequency  $f_2$  is used as the reference in the error detectors. The  $\Delta$  signal at center frequency  $f_3$  is mixed with the signal  $f_2-f_3$  and the mixer sum output is applied to the error detector. In SCAMP (Single Channel Monopulse Processor) the AGC circuitry is replaced by a symmetrical bandpass limiter used to achieve normalization. Otherwise, the block diagram and above discussion here is equally applicable to SCAMP.

### 3. WEIGHTING FACTORS

The factors considered most important when evaluating the techniques discussed in the preceding paragraphs are itemized below. Also, relative weights assigned to each factor are listed opposite the factors. It should be emphasized that the relative weights are arbitrary. When considering the techniques for a specific application the weighting could change. The values listed in Table 3 are felt to most nearly reflect the goals and results of the present study in an unbiased manner. The maximum weight assigned is 10, and it appears opposite the factor(s) that are felt to be of greatest importance.

Sum channel degradation and equipment complexity are given the maximum value of 10. Equipment complexity may in many cases be of lesser importance, but one of the major design goals in this program was to develop an SCMTR technique with less stringent equipment requirements than full monopulse. Sum channel degradation is unquestionably important and is weighted at maximum value. Normalization and tracking error are assigned weights of nine, since both directly affect sum channel degradation.

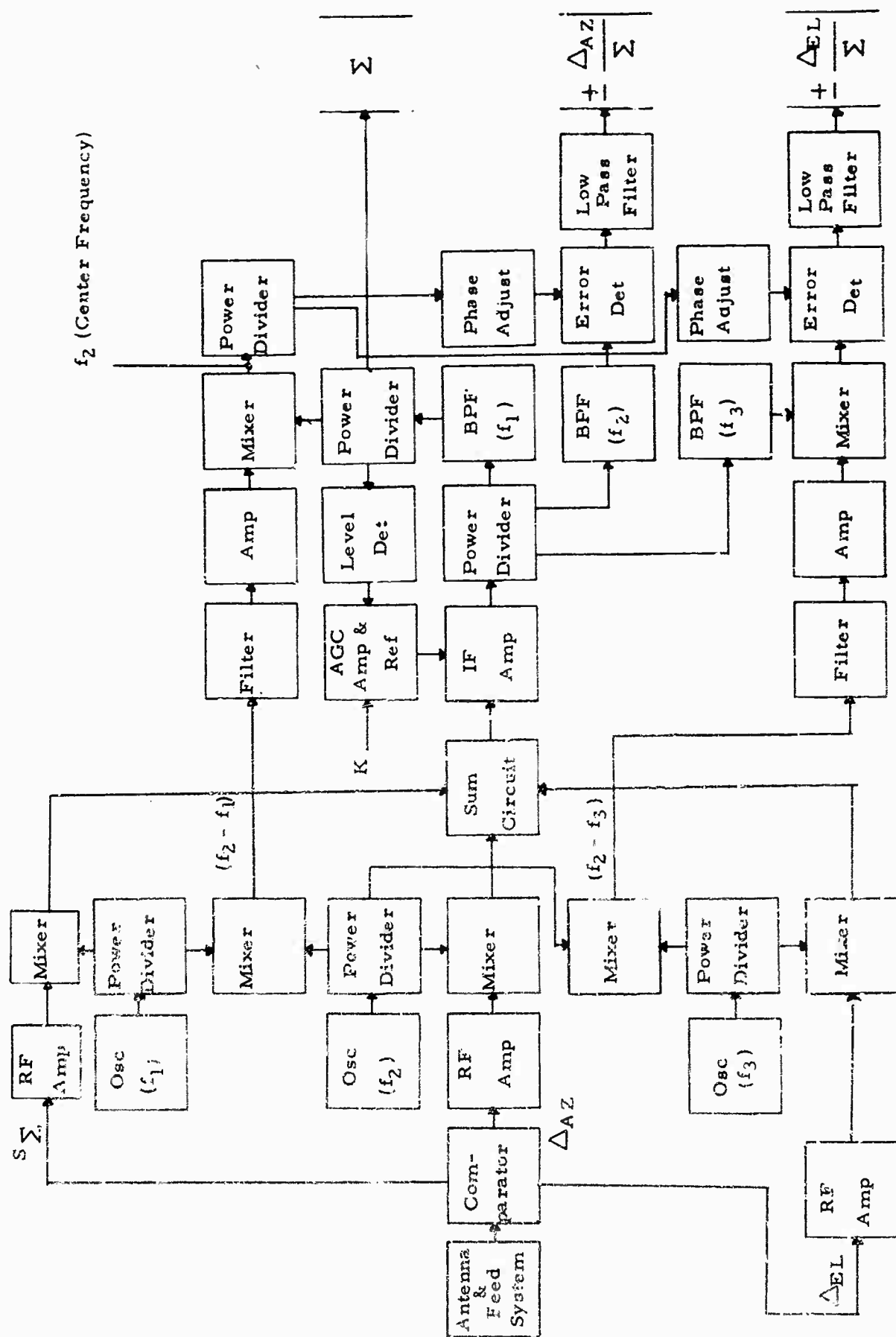


Figure 7 Frequency Division Multiplex Block Diagram

TABLE 3  
WEIGHTING FACTORS USED IN SCMTB EVALUATION

<u>Factor</u>	<u>Relative Weight</u>
Degradation	10
Normalization	9
Equipment Complexity	10
Cost	7
Dynamic Range	5
Tracking Error	
Pre-and Post Comparator Errors	9
Noise Errors	9
Bandwidth Requirements	5
Synchronization	6
Amplitude and Phase Response	6
Crosstalk	8
Reliability	8

Tracking errors result from two distinct causes, noise and pre-post comparator errors, so two separate weighting factors have been used. Crosstalk and reliability are both assigned 8, since these factors may directly contribute to sum channel degradation. Reliability, or lack thereof, can result in complete equipment failure with significant down time and costly repairs, whereas, crosstalk will result in tracking errors and extraneous signals in the sum channel.

Cost is the most arbitrary factor in this case, and is given a 7. In many cases, it is directly related to equipment complexity. Synchronization, amplitude and phase response, are each weighted 6. Examples of synchronization are time sync of the sampling switches in TDM, which can cause gain loss and crosstalk, and filter bandwidth alignments in FDM. Amplitude and phase response is important from the viewpoint of distortion in the  $\Sigma$  channel. Loss of normalization and tracking errors are also introduced if amplitude and phase is not linear. Finally, dynamic range and bandwidth are interrelated, and both can cause distortion and crosstalk.

#### 4. SYSTEM GRADING

Shown in Table 4 is the System Comparison Matrix. Each of the basic systems, or techniques, appear in a separate column opposite the weighting factors. The first column lists the items used to evaluate the different techniques. Some of the reasons for each relative grading are discussed below. Again, it is emphasized that the numbers are somewhat arbitrary and may be changed considerably when applied to a specific mission.

##### a. Sum Channel Degradation

FM, with no sum channel degradation, receives the maximum value of 10, and multiplication by the weighting factor results in a total of 100 as shown in the second column under FM. FDM has relatively small sum channel loss, but is given a 9 since it requires a summing circuit and broad IF bandwidth. PM and lobing have similar degradation due to coupler and crossover loss, respectively, and are assigned a grade of 7. AMS is similar to PM or Lobing in that sum channel signal loss is the mechanism whereby pointing error is measured and corrected. TDM has switching losses, and is assigned a 5.

##### b. Normalization

All techniques studied have normalization problems for low SNRs (10 or less). However, PM and Lobing with single IFs and square law detectors exhibit the best overall normalization characteristics and are given a 9. Coherent AGC will improve normalization further, but at



Item	Weighting Factor	AMS			Lobing			FM			PM			TDM			FDM		
Degradation (1 dB design goal)	10	7	70	7	7	70	10	100	7	70	5	50	9	90					
Normalization	9	4	36	9	81	4	36	9	81	7	63	8*	72						
Equipment Complexity	10	10	100	8	80	6	60	9	90	2	20	4	40						
Cost	7	10	70	7	49	5	35	8	56	1	7	3	21						
Dynamic Range	5	8	40	9	45	7	35	9	45	4	20	10*	50						
Tracking Error	9	2	18	2	18	5	45	2	18	4	36	5	45						
Noise	9	5	45	5	45	3	27	5	45	4	36	4	36						
Pre-Comparator and Post-Comparator	5	10	50	10	50	9	45	10	50	5	25	5	25						
Bandwidth Requirements	6	9	54	9	54	10	60	9	54	3	18	6	36						
Synchronization	6	10	60	10	60	3	18	10	60	6	36	9	54						
Amplitude and Response	8	9	72	10	80	8	64	10	80	5	40	4	32						
Crosstalk	8	7	56	10	80	5	40	10	80	4	32	3	24						
Reliability	8	7	56	10	80	5	40	10	80	4	32	3	24						
Totals			671		712		565		729		383		525*						
*SCAMP													506						

TABLE 4

SYSTEM COMPARISON MATRIX

the possible expense of equipment complexity. The "SCAMP" technique is graded 8, since it is inferior to PM or Lobing. FDM and TDM are rated 7, since both require a relatively wide IF bandwidth. FM and AMS require that the AGC characteristics be known, and FM must have the AGC curve in its three channels matched over the system dynamic range, so both techniques are graded 4.

c. Equipment Complexity

Equipment complexity is meant to include such things as size, weight, and quantity of equipment. The AMS technique requires a low frequency generator and detector electronics, but a simple feed. Its main feature is its simplicity, and it is graded 10. PM requires a Q generator and scanner, while the Lobing technique requires a Q generator and either a mechanical feed nutator or scanning electronics. PM is thus given a 9 and Lobing an 8. TDM requires extremely wideband IFs, narrow filters and fast switches and is graded 2. Since FDM requires a broadband IF, seven mixers, and three extra oscillators, it is given a 4. FM is relatively less complex than FDM and more so than Lobing, and is graded 6.

d. Cost

In general, cost is related directly to equipment complexity and is graded accordingly. The weighting factor can be adjusted, for any particular application, to either increase or decrease its relative importance as desired.

e. Dynamic Range

The "SCAMP" technique, due to its limiting, has a 10 for dynamic range. PM and Lobing are then graded 9, based on a single receiver and relatively narrow band IF. AMS is given an 8, since it requires that the IF gain be normalized or manual gain used. The wide bandwidth and switching loss in the TDM technique requires more RF gain relative to the other techniques, so it is rated 4. FM requires three matched IFs and is given a 7, compared to the 8 for FDM, which requires one relatively wide IF amplifier.

f. Tracking Error

As mentioned earlier, this item is composed of two categories, noise and pre-comparator, post-comparator errors. Each carries a maximum value of 5 in grading, making 100 the maximum total points for tracking error.

g. Noise Error

AMS, Lobing and PM have similar tracking errors due to noise as a result of their crossover loss, and are rated 2 each. FM and FDM have no equivalent losses and get the maximum value of 5. Although no direct crossover loss is experienced in TDM, there are similar problems with switching loss in the error channels which results in loss of normalization, so TDM is rated a 4.

h. Pre-Comparator and Post-Comparator Errors

Lobing and PM exhibit similar pre-comparator errors and no significant post-comparator errors. AMS has no comparator and has very low equivalent losses, so each of the three techniques are rated 5. FM has three receivers to contribute both pre- and post-comparator errors, and is rated 3. TDM has potential problems with matching the switches and FDM with mixers and filters, and they are graded 4.

i. Bandwidth Requirements

AMS, Lobing and PM require no increase in bandwidth to accommodate the tracking feature, and are all rated at the maximum value of 10. FM, which uses three matched IF's, is rated 9. The two techniques TDM and FDM require wide IF bandwidths compared to the information bandwidth and both are rated 5.

j. Synchronization

FM has no synchronization problems and receives the maximum value of 10. AMS, Lobing and PM require synchronization between the lober and detector, so each are rated 9. Possibly the most difficult technique, insofar as synchronization is concerned, is TDM due to the high speed switches, so it is graded 3. FDM has a bandpass alignment problem in the filters, essentially a "synchronization" problem, and is rated 6.

k. Amplitude and Phase Response

Linear Amplitude and Phase Response are more easily achieved with wide bandwidths compared to the information bandwidth, and, of course, with fewer components. AMS, Lobing, and PM have a single IF which may be optimized in bandwidth to produce flat amplitude and linear phase response over the information band and is rated 10. FDM or TDM with their increased IF bandwidths pose more severe problems. FDM is given 9, because of the increased number of components required, and resultant alignment problems. TDM is rated 6 due to the requirement for narrow band filtering before and

after the sampling switches. FM is rated 3 since it requires that the RF and IF components have matched amplitude and phase characteristics over the operating dynamic range.

#### 1. Crosstalk

Crosstalk includes tracking errors from one axis, azimuth for instance, affecting the elevation channel and vice versa. Also, crosstalk includes spurious type signals caused by LO leakage from one channel to another.

Lobing and PM are rated 10 because of the single receiver and LO requirements. This assumes that synchronization is such as to not introduce significant crosstalk between the error channels. FM requires three receivers and three LO's with the isolation (LO) problem and is given an 8. TDM has an isolation problem in the switches as well as LO leakage between channels and is rated 5. FDM has a frequency separation problem, together with LO isolation between channels, and is rated at 4. "SCAMP" is no better than FDM due to its hard limiter and associated intermodulation products. AMS is rated 9 because errors in one axis can slightly affect the other. This is due to mechanical pointing Vs. readout discrepancies, but is otherwise similar to lobing and PM.

#### m. Reliability

PM and Lobing require a scanner and nutating feed, respectively, with a single receiver and both are rated a 10 for reliability. AMS requires that the antenna drive motor be cycled while tracking and is therefore rated 7. The other techniques, FM, TDM and FDM, are rated 5, 4, and 3 in that order. FM requires three complete receivers, but FM is considered more reliable than TDM with a single IF, high speed switches, and narrow band filters. FDM has several oscillators and mixers in addition to the single IF and narrow filters, and appears to be less reliable than the other approaches.

#### 5. SUMMARY

The preceding discussion, as shown by the totals in the evaluation, indicate that PM and Lobing will each provide a practical approach to a Single Channel Monopulse Tracking Receiver design. Either approach can be adaptable to mobile stations, and provide a communication signal (sum channel) for data demodulation in a separate receiver with less than 1 DB degradation. Also, the evaluation indicates that TDM is the least desirable design approach when all the tradeoffs are considered. AMS, when considered largely from the equipment complexity and communication degradation standpoint, will provide equal, if not superior, performance as a SCMTR for the orbital dynamics of interest in this study.

The two basic techniques, PM and AMS, were of sufficient interest to warrant further investigation. PM is useful in not only the present situation, but also in those cases where tracking dynamics pose more of a problem. AMS, on the other hand, is attractive as a "stand by" mode, which would replace (or augment) a manual mode. Since each technique exhibited significant advantages, two SCMTR designs were accomplished. The major SCMTR design, found in Section IV, is a pseudo-monopulse system. The less complex technique, AMS, is described in Section V.

## SECTION IV

### PSEUDO-MONOPULSE SCMTR DESIGN

#### 1. INTRODUCTION

The complete design of a SCMTR utilizing the pseudo-monopulse technique is described in this section. The basic system block diagram is described, including acquisition and tracking error considerations. Next, the subsystem design considerations are discussed. Following this is the equipment description, which illustrates the feasibility of implementing the basic concept. Finally, the basic characteristics of the design are summarized.

#### 2. THE PSEUDO-MONOPULSE SYSTEM CONCEPT

The basic pseudo-monopulse SCMTR is illustrated in Figure 8. The antenna-feed system selected is an amplitude-comparison monopulse type. The sum and two difference beams are formed in the comparator (a series of hybrid tees) and, up to this point, the system is identical to a conventional three-channel amplitude monopulse tracking system.

The system from the comparator to the receiver is the heart of the pseudo-monopulse receiver and is termed the "scanner network". This scanner network takes the two difference channels and time shares them at the output of the "scanner" for error modulation of the sum channel. This concept is illustrated in Figure 9 (although a 12 dB coupler is illustrated, a 10 dB coupler is used in the present system). The phasing of the three channels from the feed aperture to the output of the scanner network is important, but not critical. For broad band operation, the phase lengths should be equal in order to accomplish proper phasing. The separate lines are carefully designed to be the same phase length, and phase length adjustments are built into two of the lines to account for any small design or fabrication errors. Considerable attention is given to VSWR at each component interface to minimize the effects on amplitude and phase response in the comparator.

The basic system design is based on concepts developed in Section XII; e.g., the use of a single preamplifier following the directional coupler is shown to be optimum in a practical situation. The sum and

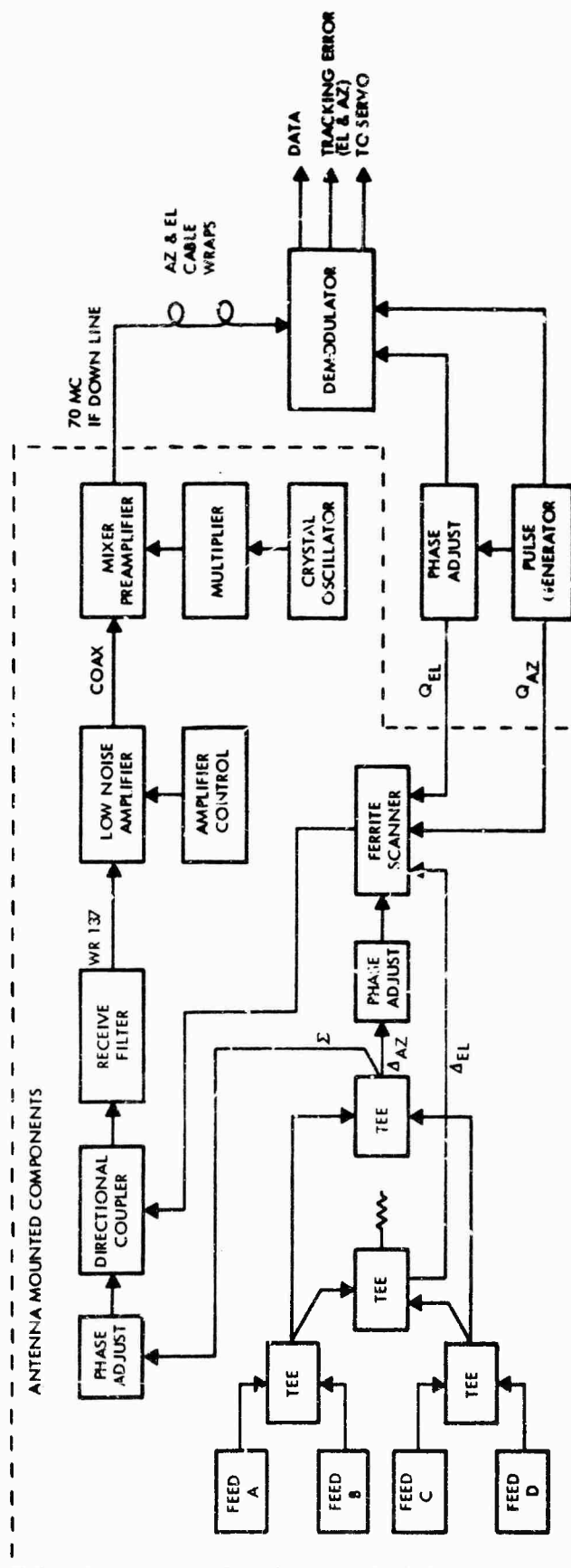


Figure 8. Pseudo-Monopulse SCMTR Block Diagram

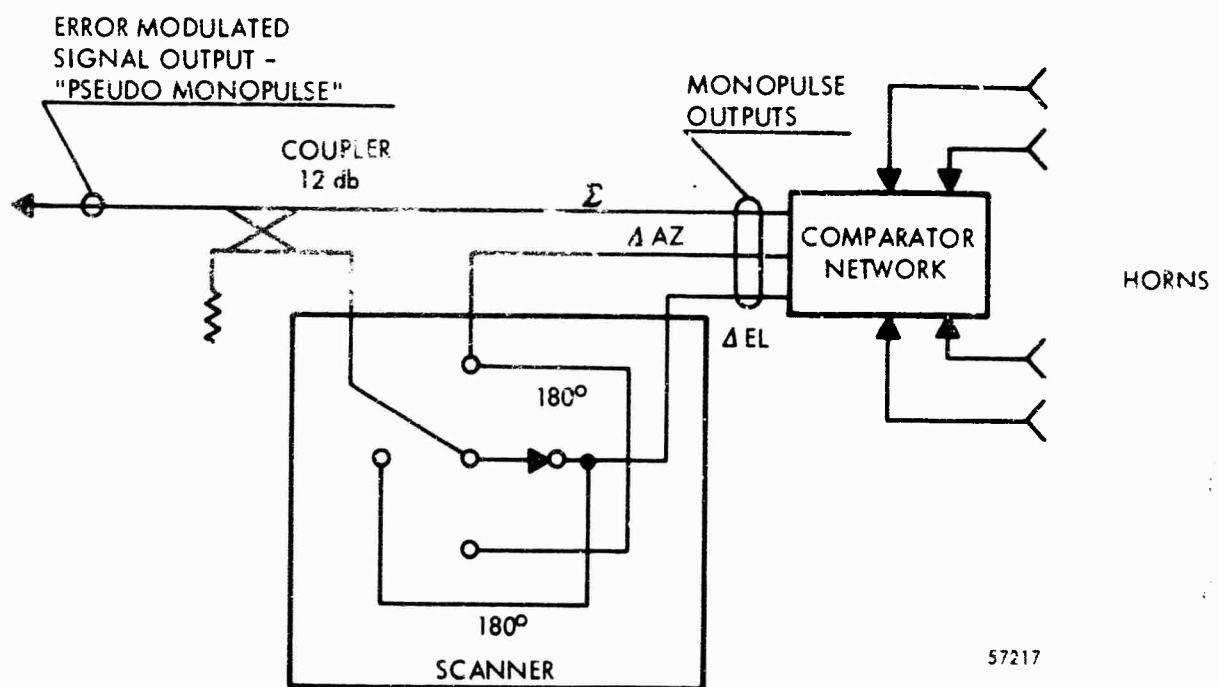


Figure 9. Scanner Network Operation



difference channel degradation caused by the pseudo-monopulse technique is also described in Section XII as well as criteria for the selection of the scanning signals.

The scanner and coupler are followed by a low noise amplifier. The amplifier gain is sufficient to establish the receiver noise temperature as approximately that of the amplifier itself. The contribution from the following mixer is due to its 8 dB input noise figure modified by a small cable loss between the amplifier output and the mixer input. The total second stage contribution does not exceed 2°K at the highest operating temperature.

#### a. Acquisition Considerations

Generally, there are no conflicts between the requirements of the receiving subsystem for data acquisition and the requirements for antenna servo tracking. However, normal receiver design often does not adequately consider the receiving subsystem as part of the antenna servo dynamics. Studies have been conducted which show that the AGC loop bandwidth should be at least as wide as the antenna servo bandwidth, and preferably much wider. In addition, the AGC loop should introduce very little phase shift at the frequency of the AC tracking error signal. If the pseudo-monopulse switching frequencies can be high enough, the above AGC loop bandwidth requirements can very easily be met. If the switching speeds cannot be increased far enough to meet the above requirements using normal AGC filter techniques, it may be necessary to use a notch in the AGC feedback at the frequency of AC servo error signal. Using this technique the AGC bandwidth can be made as high as one third of the AC servo error signal frequency.

Another requirement for the AGC loop is that it maintains a constant gain at the AC servo error signal frequency over the full dynamic range of the RF input levels. This requirement can be easily met from plus 10 dB signal-to-noise ratio in the IF bandwidth to maximum RF signal input by using an integrator in the AGC feedback. With an integrator in the feedback the scale factor at the output of the envelope detector in volts per degree off target will be down one dB at +10 dB signal-to-noise ratio, down 6 dB at zero dB signal-to-noise ratio, and decreases 2 dB per each dB of degradation of signal-to-noise ratio, as shown in Section VIII. This can be improved somewhat by using coherent AGC. However, the use of coherent AGC complicates the receiver design. In some cases, when a phase-lock detector is employed for demodulation, the use of a quadrature detector provides coherent AGC at little additional expense.

The mission requirements for an automatic tracking antenna system often place additional requirements on the receiving subsystem. The data bandwidth, the frequency uncertainties, the uncertainty of the location of the target, the RF beamwidth and the servo dynamics should all be considered in selecting the antenna search pattern and the method of frequency acquisition to be used in the receiving subsystem to optimize the probability of acquisition.

In typical satellite communications links the angular uncertainties and frequency uncertainties require that the receiver automatically sweep through the frequency uncertainties and automatically acquire the signal frequency. Since the receiver would be sweeping in frequency at the same time the antenna is performing an angular search pattern, an additional requirement on the receiving subsystem is that its automatic frequency acquisition capabilities be sufficient to allow the antenna to search the angular uncertainty with a high probability of acquiring the signal. When the signal is detected by the receiving subsystem, a signal to the antenna position memory circuit must be sent from the servo while the target is still within the antenna beamwidth. The receiver frequency search and acquisition system must also allow for the probability that the antenna servo system will allow the antenna to overshoot sufficiently to move the antenna beam past the source before the position memory can return the antenna to the position it occupied at the instant it was switched to position memory; i.e., a period of signal loss may occur due to mechanical overshoot, since the antenna cannot be stopped instantaneously.

Analyses have been made which relate the receiving subsystem frequency acquisition technique, the other system capabilities and mission requirements to the probability of detection. The results of these analyses for the particular mission requirements must be incorporated into the receiver design in order to achieve the desired probability of detection. This subject is discussed in detail in Appendix IV and reference (4).

#### b. Angular Tracking Error Analysis

The angular tracking error analysis is concerned with small errors near boresight only, since large pointing errors would result in significant sum channel signal loss. Also, since the system produces two error channels that are orthogonal, the errors can be treated independently.

Two basic types of systems, amplitude and phase sensing,

are of the most interest\*. The amplitude-sensing system has each feed radiation pattern displaced from the antenna system boresight axis. Thus, for all signals within the antenna beamwidth, except those on boresight, unequal signal amplitudes are induced in the feeds. When the two signals are subtracted, a null is produced only for those signals arriving along the boresight axis. The phase-sensing system has each feed radiation pattern symmetrical about its individual boresight axes. All feed patterns have parallel boresight axes, and the far field radiation patterns are overlapping, resulting in equal amplitude signals in each feed for any source within the feed beamwidth. There is a time or phase delay between the signals arriving at each feed due to the physical spacing between them for all signals arriving off boresight. The phase characteristics result in a well defined boresight axis which is midway between and parallel to the individual feed boresight axes. In Section VII it is shown that, in the phase sensing system, precomparator phase errors cause proportional boresight errors and precomparator amplitude errors cause null depth variations. The inverse is true for the amplitude sensing system (precomparator amplitude unbalance results directly in boresight shifts while precomparator phase errors cause null depth variations). In a pseudo-monopulse system design, post-comparator errors can be made negligibly small. In addition to the phase and amplitude errors, there also exists a pointing error due to noise.

In the system configuration of interest here, the amplitude sensing approach is applicable, since the feed arrangement used has a single aperture with four closely spaced feeds. The tracking error is a result of many factors, including

- Multipath/Fading
- Servo Lag (dynamic)
- Wind Loading
- Noise
- Precomparator and Postcomparator errors
- Normalization errors

However, for SNR's (Signal-to-noise ratios) of interest, and since high pointing accuracy with respect to the antenna beamwidth is not required, only noise and comparator errors will be considered in detail. The remaining factors are system parameters which are essentially independent of the SCMTR technique.

The expected values of SNR in the sum channel, and the

---

\* Although "pure" amplitude or phase sensing systems are not realizable, it is convenient to analyze the systems based on the predominant characteristics.

phase and gain differentials between the sum and difference channels, will be used independently to determine the single axis tracking error. The beam radial error will be determined for low elevations, and the expected sum channel degradation due to tracking error estimated.

#### (1) Tracking Error Due To Noise

The exact expression for pseudo-monopulse noise error is found in Appendix II. The expression is

$$\left(\frac{S}{N}\right)_{\text{out}} = \frac{P_{EL/2}}{\left[\sigma_{ER}^2 + \frac{\sigma_s^2}{K}\right] \left[1 + \frac{\sigma_s^2}{2P_s} + K \left(\frac{3}{4} \frac{P_{EL}}{P_s} + \frac{1}{4} \frac{P_{AZ}}{P_s} + \frac{\sigma_{ER}^2}{2P_s}\right)\right]} \cdot \frac{W}{\beta} \quad (4)$$

where the P's are signal powers,  $\sigma^2$  are noise powers, W and  $\beta$  are pre-and post-detection bandwidths, and  $K = \frac{k^2}{1 - k^2}$  where  $k^2$  is the coupling factor.

Equation (4) can be simplified considerably in most practical cases of interest. When relatively small coupling is used and the noise power in each channel is equal, the expression for small pointing errors reduces to

$$\left(\frac{S}{N}\right)_{\text{out}} \doteq \frac{k^2}{2} \cdot \frac{W}{\beta} \cdot \frac{P_{EL}}{\sigma^2} \cdot \frac{1}{\left[1 + \frac{1}{2(S/N)_s}\right]} \quad (5)$$

$$\left(\frac{S}{N}\right)_{\text{out}} \doteq \frac{k^2}{2} \cdot \frac{W}{\beta} \cdot \frac{P_{EL}}{\sigma^2} \quad (6)$$

when the sum channel signal-to-noise ratio is greater than 6 dB

The pointing error can be determined from equation (6) and by knowing the antenna difference channel pattern. The feed design will produce a difference channel slope,  $M_T(o)$ , of

$$M_T(o) = \frac{S_{\Delta}'(o)}{S_{\Sigma}(o)} \quad (7)$$

which is the slope of the difference channel divided by the sum channel gain, both evaluated at boresight. The difference channel signal,  $P_{EL}$ , is then given by

$$P_{EL} = M_r^2(o) \cdot \overline{\theta^2} \cdot P_s \quad (8)$$

where  $\overline{\theta^2}$  is the mean square pointing error. When a high gain servo is used, the pointing error is determined by equating the output signal to the output noise; i.e., let the output signal-to-noise ratio be unity. Then

$$1 = \frac{k^2}{2} \cdot \frac{W}{\beta} \cdot \frac{M_r^2(o)}{\sigma^2} \cdot \overline{\theta^2} P_s \quad (9)$$

$$\overline{\theta^2} = \frac{2\beta\sigma^2}{k^2 W M_r^2 P_s} = \frac{2\beta}{k^2 M_r^2 (C/N)} \quad (10)$$

where  $C/N$  is the carrier to noise density in the sum channel.

It is apparent from equation (10) that the mean square angular error due to noise is directly proportional to  $\beta$ , the servo bandwidth. Therefore, smoother tracking results when the servo bandwidth is held to the minimum value necessary to follow target dynamics, overcome wind loading, and provide an operating margin of safety.

The expected  $C/N$  in a typical synchronous satellite system is found from the link budget of Table 5. System parameters, defined in following paragraphs, are:

$$M_r^2 = 3.14 \text{ per degree}^2$$

$$k^2 = 0.1 \text{ (10 dB coupler)}$$

$$\beta = 1 \text{ Hz}$$

The resultant pointing error due to noise is then

$$\overline{\theta^2} = \frac{2 \times 1}{0.1 \times 3.14 \times 0.89 \times 10^6} = 0.715 \times 10^{-6} \quad (11)$$

or  $\overline{\theta}_{rms} = 0.847 \times 10^{-3} \text{ degrees}$

TABLE 5  
TYPICAL SYNCHRONOUS SATELLITE LINK BUDGET

Satellite (synchronous) effective radiated power:	(+) 50 dBm
Free space attenuation (synchronous):	(-) 201.9 dB
Atmospheric Absorption:	(-) 0.4 dB
Receiving Antenna Gain:	(+) 50 dB
Margin for Power Control Error:	(-) 1.0 dB
Feed and Line Loss (comparator included):	(-) 1.2 dB
Receiver Signal Power:	(-) 104.5 dBm
Receiving System Noise Density*:	(-) 175 dBm/cps
Receiver Carrier to Noise Density:	69.5 dB

\* The receiver noise density is based on an antenna noise temperature of 40°K at 10° elevation, parametric amplifier input temperature of 120°K and a line loss of 1 dB at 350°K ambient temperature.

This shift results in a negligible loss in gain due to pointing error. It is apparent that the system is capable of operation at significantly lower signal levels without degrading the gain as a result of pointing angle noise.

## (2) Precomparator and Postcomparator Errors

The errors caused by both pre- and postcomparator amplitude and phase unbalance are derived in Section VII. Since, in a pseudo-monopulse system, the postcomparator errors can be made negligibly small, only the precomparator errors are of interest. Furthermore, since a time-orthogonal Q function is used in the scanner, the null depth does not cause a boresight shift (as would occur in a two-channel monopulse system for example). Therefore, the most important error, for this amplitude sensing system, is the boresight shift caused by precomparator amplitude unbalance.

It is shown in Section VII that for an amplitude sensing system, the condition

$$K G(u) = 1 \quad (12)$$

determines boresight. Then,

$$\frac{G_A - G_B}{G_A + G_B} = M_T \cdot \theta \quad (13)$$

where  $G_A$  and  $G_B$  are the equivalent gains of the two elevation sensing feeds. Then,

$$1 - \frac{G_B}{G_A} = \left[ M_T \cdot \theta \right] \frac{G_A + G_B}{G_A} \quad (14)$$

Near boresight,

$$\frac{G_A + G_B}{G_A} \doteq 2 \quad (15)$$

assuming identical individual feed patterns, so that

$$\frac{G_B}{G_A} \doteq 1 - 2 \left[ M_T \cdot \theta \right] \quad (16)$$

From this,

$$\theta = \frac{1 - G_B/G_A}{2 M_T} \text{ degrees} \quad (17)$$

where  $G_B/G_A$  is the precomparator amplitude unbalance. The system can be designed to obtain an amplitude unbalance of less than 0.1 dB over the frequency band of interest. This would result in a boresight shift of

$$\theta = \frac{1 - 1.0233}{2 \times 1.77} = 6.6 \times 10^{-3} \text{ degrees} \quad (18)$$

Again, a negligible sum channel loss occurs due to pointing error.

The overall rms system pointing error due to both noise and amplitude unbalance in both azimuth and elevation is found by combining the errors as independent random variables. The resultant error is

$$\begin{aligned} \theta_e &= 10^{-3} \cdot \sqrt{2 \cdot (6.6)^2 + 2 \cdot (0.847)^2} \\ &= 9.42 \times 10^{-3} \text{ degrees} \end{aligned} \quad (19)$$

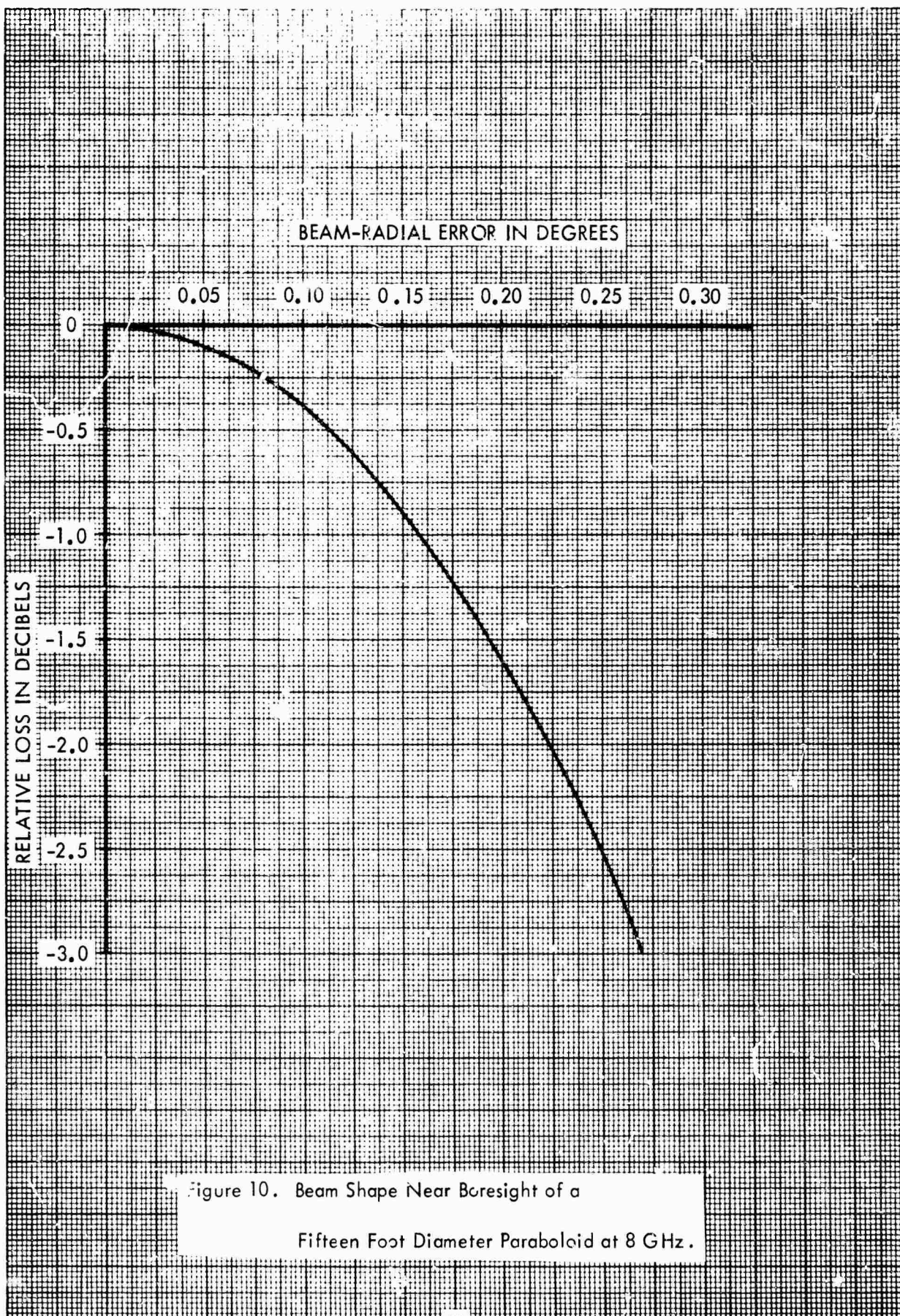
The composite error, then, is less than 2% of the beamwidth, and the resultant loss in gain will be well below 0.1 dB, as seen from Figure 10, the approximate antenna beam pattern near boresight.

### 3. SYSTEM DESIGN CONSIDERATIONS

The basic factors to be considered in the realization of the SCMTR illustrated in Figure 8 are discussed in this section. These requirements are based on the general system requirements of Section II and the detailed characteristics of the pseudo-monopulse technique described in Section XII. The detail design/characteristics of the elements considered in this paragraph will be described in paragraph 4 of this Section.

As shown in Figure 8, the signals from each of four separate feeds are combined in the comparator. Hybrid tees are used to form the sum and the two difference signals. The comparator outputs are combined in the scanner and coupler before entering the receiver. The coupler output drives the receive filter and low noise amplifier. After filtering and amplification, the signals are mixed with the local oscillator and translated to the IF band for demodulation. The data signal is demodulated in an angle demodulator (phase-lock loop or discriminator) and the composite tracking signal is detected in an AM detector. The two axis tracking error signals are then separated in synchronous detectors, utilizing the same signals which combined the two channels in the scanner.





a. Feeds and Comparator

The amplitude monopulse feed consists of four closely spaced horns which illuminate a dish or Cassegrain subreflector. At X-band these feeds are generally used in conjunction with the Cassegrain configuration because the corporate feed is large and/or an apex feed would present a weight or structural problem and perhaps an electrical problem through aperture blockage. The schematic diagram for the single channel monopulse feed system is shown in Figure 11. This system is capable of both transmitting and receiving a signal through the same feed. The feed consists of 4 horns, 4 diplexers, 4 magic tees, a ferrite scanner, coupler, and polarizer.

An elevation error signal  $\Delta_E$  and an azimuth error signal  $\Delta_A$  are given by the vector combination

$$\Delta_A = (A + C) - (B + D)$$

$$\Delta_E = (A + B) - (C + D)$$

where A, B, C, and D are the signals at feeds A, B, etc. Two magic tees adjacent to the feeds take the sum and differences of signals received from the feeds with the sum going out the shunt tee and the difference out the series tee. The series arms of these two magic tees are then fed to another magic tee from which an azimuth error signal is obtained. The shunt arms from the first two magic tees are likewise fed to another magic tee which produces an elevation error (in the shunt arm) and a sum signal (the total sum received from the four feeds is obtained from the series arm). The two error signals are fed to the scanner, and the sum channel is fed to a directional coupler.

b. Scanner

The scanner is a device for combining the two error channels on a single channel in an optimum manner, as described in Section XII. Early techniques for sampling the channels included diode switching (in the UHF range) and various mechanical devices. The former exhibits excessive losses at X-band and the latter is not as reliable as electronic techniques. The most suitable technique at present utilizes ferrite phase shifters to obtain the necessary switching-phase shifting functions. These devices are reliable, capable of high speed operation, and can be easily operated with a wide range of switching rates.

c. Directional Coupler

The basic tradeoff between sum channel degradation and difference channel sensitivity determines the selection of the coupling

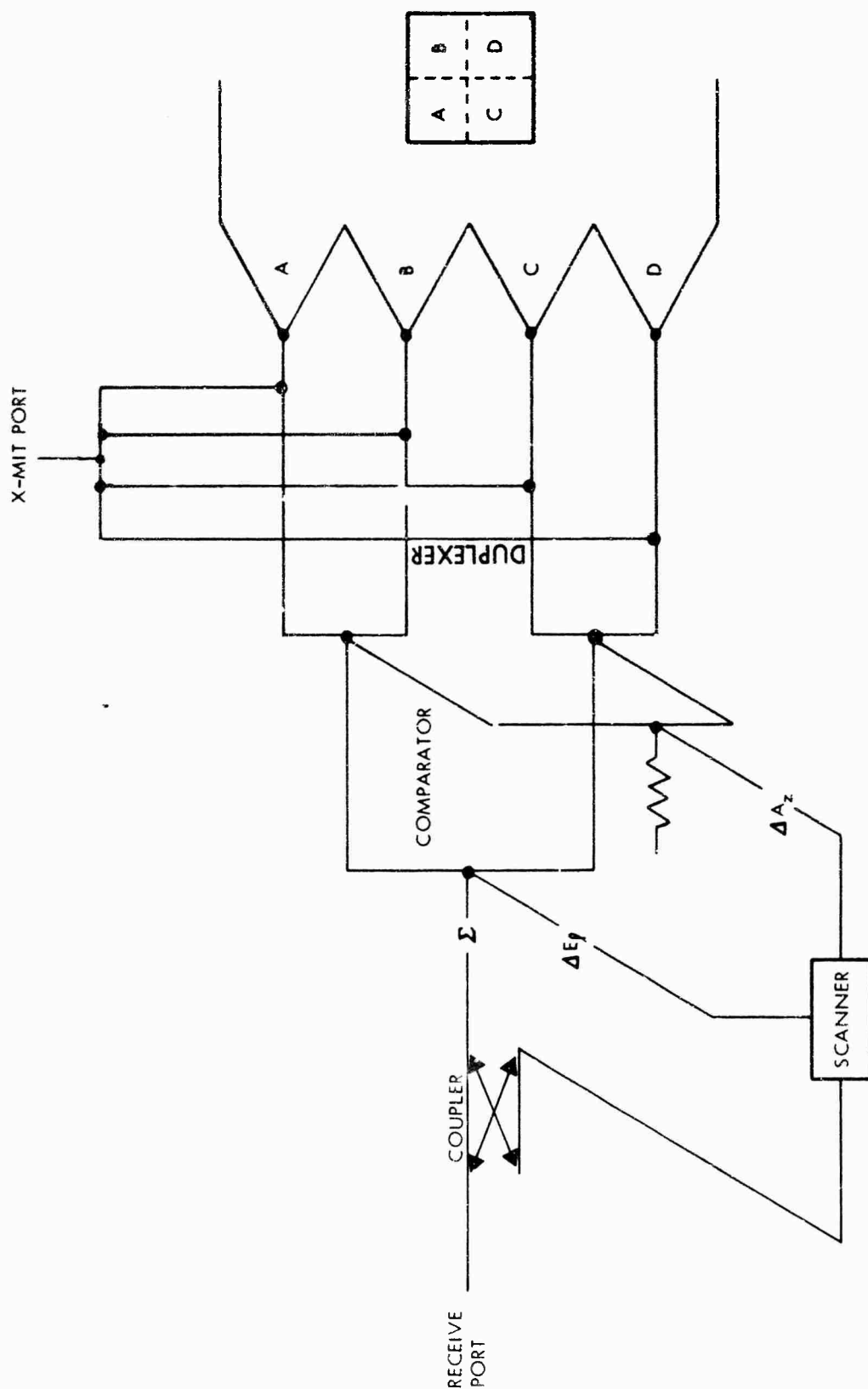


Figure 11. Schematic Diagram for SCMR Feed System

factor in the directional coupler. When the scanner itself is lossy, the difference pattern gain must be reduced by this amount, thus requiring tighter coupling (more sum channel degradation) for a given tracking sensitivity. A 10 dB coupler is chosen for this system, resulting in a 0.46 dB loss of communication signal power and approximately 13 dB overall loss in tracking sensitivity. The overall loss is the sum of the scanner, coupler, and line (insertion) losses. The output of the coupler is an envelope modulated signal whenever there is a system pointing error. This signal is supplied to the receive filter.

d. Receive Filter

The Receiver filter is required to provide most (60 dB) of the image rejection for the system. The filter is a bandstop unit in WR 137 guide, providing over 60 dB rejection to frequencies in the band  $7.86 \text{ Gc} \pm 25 \text{ Mc}$ . The insertion loss in the receive band of  $8 \text{ Gc} \pm 25 \text{ Mc}$  is less than 0.3 dB with input and output VSWR less than 1.3:1.

e. Low Noise Preamplifiers

Low noise amplification of the 8 GHz signal may be accomplished by several types of devices. The device characteristics, capabilities, and limitations were surveyed during this program, and the results are found in Appendix III. It appears that a suitable compromise between system complexity (compatible with highly transportable terminals) and system sensitivity would be best achieved by using uncooled parametric amplifiers.

An uncooled two stage amplifier would provide a minimum of 30 dB gain, a noise temperature (including second stage contributions) in the order of  $110^\circ\text{K}$ , and a fixed tuned 1 dB bandwidth in excess of 50 MHz. The amplifier would also provide high isolation (100 dB) to any signals at its output terminals, such as the local oscillator energy used for the first frequency down converter. The maximum in-band signal level for 0.5 dB gain compression is -50 dBm, and -20 dBm for 500 Mc out-of-band signals.

f. Local Oscillator

Signal sources for the mixer having the required stability of  $10^{-8}$  over the operating temperature range can be provided using either X-band source locked to a stable reference, or by multiplying the output of crystal controlled oscillator. The X-band source, when locked to a stable reference will provide the required stability with a wide tuning range. This approach obviously requires some sort of stable reference, such as Hewlett-Packard 5100A/5110A Synthesizer, that is tunable with the required frequency stability, and a method of developing the AFC signal, such as the

Hewlett-Packard (Dymec) Synchronizer Model 2654A-M1. This technique provides tunability and frequency stability at the expense of size, weight, cost, reliability, and does not lend itself to transportable type systems.

The oscillator-multiplier technique appears more attractive for transportable systems due to the reduction in equipment required, size, weight, increased reliability, and reduced costs. The multiplier can be designed for 10-15 percent bandwidth at X-band, and tunability can be accomplished by replacing the oscillator unit itself to provide the desired output frequency.

The selection of the LO frequency is based upon several factors. For this design, a single conversion will be used prior to the demodulator input. This will allow the signal to be routed from the antenna through the azimuth and elevation cable wraps (or rotary joints) at a relatively low frequency to avoid excessive transmission line loss and subsequent system noise degradation.

The exact IF frequency is not critical, but should be based upon a spurious analysis, together with hardware compatibility. The latter suggests an IF somewhere below 100 Mc/s, and, since a spurious analysis indicates that the lowest order spurious near 100 Mc is of the form  $2(F_{in} - F_{LO})$ , 70 Mc/s IF is chosen. The fourth order spurious is then located at 140 Mc/s center frequency, and is not in-band.

Next, the choice of the basic oscillator frequency is made, again considering spurious and hardware compatibility. Since the multiplication process will result in all harmonics of the basic frequency at the multiplier output, it is wise to choose the basic frequency such that whenever there is mixing between the desired multiplier output and any undesired signal (harmonic) at the multiplier output, the sum or difference does not equal the IF frequency. Therefore, the basic frequency should not be near 70 Mc/s, and a frequency near 124 Mc/s is selected. This will require a X64 multiplication factor to provide an LO frequency at 7930 Mc/s using low side injection to produce the 70 Mc IF.

The first frequency translation signal is derived from a crystal controlled oscillator and multiplier. The multiplier is a solid state X64 unit capable of +10 dBm minimum output power over the band 7.930 Gc  $\pm$  25 Mc at all operating temperatures. The multiplier accepts an input level of +10 dBm, in the frequency range 123-125 Mc.

The basic frequency is provided by a crystal-controlled oscillator in a dual proportional-control oven. Frequency stability is  $1(10^8)/24$  hours, and  $1(10^9)/15$  minutes. Warmup time is less than 30 minutes at the lowest operating temperature. The output power is +13

dBm minimum at a frequency of approximately 124 Mc.

g. Mixer-Preamplifier

The mixer-preamplifier design must result in a device which will simultaneously translate the incoming RF energy at 8 GHz to an IF where suitable demodulators are available, and provide a noise temperature that will not significantly degrade the system noise performance. Recent work in microwave diodes<sup>(5)</sup> have resulted in lower noise characteristics, and mixers utilizing Schottky barrier gallium arsenide diodes, when properly optimized, display near minimum theoretical mixer noise figures.

Tests on single-ended X-band mixers have indicated noise figures as low as 4.8 dB, including a 1.5 dB IF noise figure. Use of low noise mixer-preamplifiers eliminates the need for low noise amplifiers preceding the mixer such as TDA's (Tunnel Diode Amplifiers) or TWT's (Traveling Wave Tubes), as single side band noise figures of 6-9 dB are available using preamplifiers with noise figures of 2.0 dB or less.

A balanced mixer configuration is preferred for several reasons:

(1) Efficient use of LO power. All the LO power (and the signal power) ultimately reach the diodes. This results in an overall improvement in conversion efficiency, requiring less LO power than the single diode configuration.

(2) Low VSWR's over wide frequency ranges. Reflections at the diodes, where a 3 dB coupler is used as the coupling mechanism are propagated out the other input arm. This will result in relatively poor isolation between input arms, and impedance match at each diode is important to insure high isolation (20-30 dB) plus low VSWR.

(3) Local Oscillator Noise Suppression. The use of 90 degree differential phase shift hybrids and reverse polarity of one diode with respect to the other allows suppression of LO noise components at the IF output, while the IF components add in-phase. Additionally, strip line couplers and short slot hybrids in waveguide lend themselves to very compact balanced mixer assemblies.

The parametric amplifier output is supplied to a low-noise mixer/preamplifier combination and mixed with a local oscillator frequency to produce a 70 MHz center frequency output. The RF to IF gain is 50 dB  $\pm$  3 dB, and the input noise figure (single side-band) is less than 8 dB, using no low noise amplification prior to the mixer. The input

passband is in excess of 50 MHz at 8 GHz, with a 20 MHz (1 dB) passband at the 70 MHz output terminals.

The saturated output power is +10 dBm minimum, resulting in a -70 dBm in-band saturation level for the overall system. Local oscillator power required is +3 dBm, in the frequency range 7.93 GHz  $\pm$  25 MHz. The 50 MHz LO and RF bandwidth will allow any 20 MHz in the RF passband to be translated to a center frequency of 70 MHz by changing the LO frequency. Amplitude variations are less than  $\pm$  0.3 dB over the 20 MHz output bandpass and all internally generated spurious signals at the output are at least 60 dB below the desired output signal level.

#### h. Demodulator Subsystem

The Single Channel Monopulse Tracking Receiver demodulator operates on the incoming RF carrier at 70 MHz center frequency and delivers baseband or multiplexed information plus elevation and azimuth error signals to the terminal equipment and servos, respectively. Figure 12 shows the basic operation of the demodulator.

The demodulator accepts the 70 MHz signal, converts it down to 21.4 MHz using a mixer with a local oscillator injection signal from a Voltage Controlled Oscillator (VCO). The 21.4 MHz signal is then amplified and filtered in a filter whose passband is tailored to the information bandwidth. The signal is centered in the filter passband by the AFC circuitry, which controls the frequency of the 43.6 MHz VCO. The filter output is fed to a post amplifier that provides four outputs, all at approximately 1 millivolt into 50 ohms.

One output is supplied to an AM detector for envelope detection of the 21.4 MHz IF signal. The detected AM is supplied to the AGC amplifier. The amplifier compares the DC value of detector output with a preset voltage K, and any difference is amplified and used as a means to control the gain of the 21.4 MHz IF amplifier to maintain the detector output at a constant value. The loop time constant is set to approximately 1 second.

Another output is supplied to a 21.4 MHz discriminator. The discriminator output is a DC voltage that is integrated, amplified, and then used to control the frequency of the VCO.

The remaining two outputs drive two phase detectors, one in the phase lock loop, and another that develops the error modulation signals and a coherent DC voltage that is used to indicate a locked condition in the demodulator. The upper phase detector output drives a DC



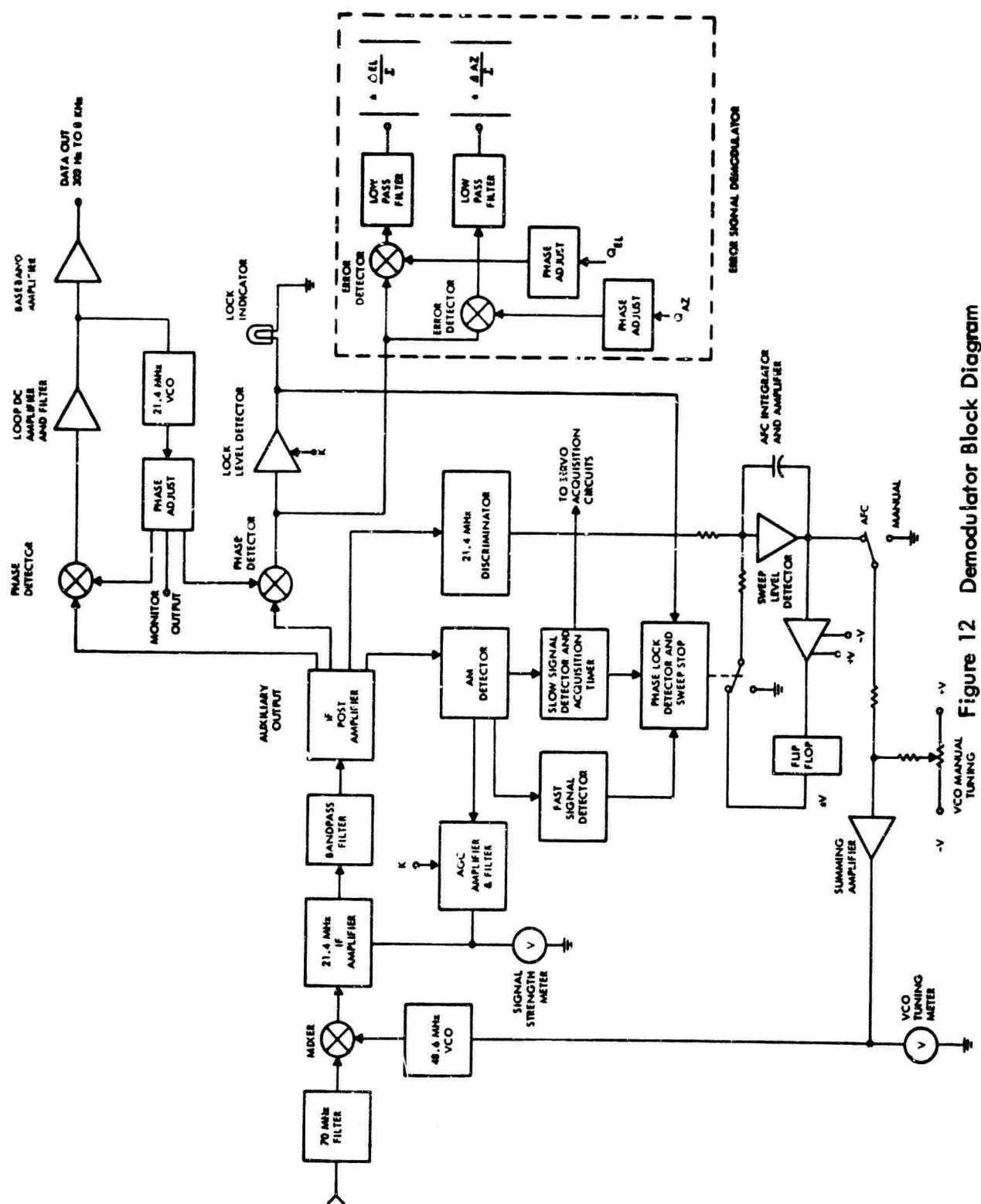


Figure 12 Demodulator Block Diagram



amplifier and filter whose output is used to control the 21.4 MHz VCO. The filter output is proportional to the frequency deviation of the 21.4 MHz carrier and, therefore, provides the FM data output to the baseband amplifier. The lower phase (synchronous) detector is driven in quadrature with the upper phase detector and acts as an amplitude detector when the loop is locked. The synchronous detector output is supplied to four different locations:

One output of the synchronous, or coherent detector, is supplied to a DC amplifier where the DC component is compared to a preset voltage K, and the difference amplified and used to drive the lock indicator.

Another output is fed to the phase lock detect and sweep stop circuitry, to disable the AFC sweep circuitry whenever the loop is locked. The sweep remains disabled for a period of about four seconds after lock is lost, due to an input from the signal detector circuitry. This technique allows for momentary loss of signal without the AFC sweep being activated.

The remaining two outputs from the synchronous detector are fed to the pointing error detectors. These detectors are also fed from the Q function generating equipment that drives the scanner. Whenever the proper synchronization is achieved, one error detector output, after low pass filtering, is the normalized elevation error signal and the other detector output provides the azimuth error signal to the servo equipment.

The AGC loop is basically defined by its time constant and dynamic range. Since the principal variation in signal level is caused by a non-synchronous satellite from horizon to horizon, a wide dynamic range is not required. A 40 dB AGC range will suffice for the wide range of signal levels which may ultimately be expected. A fast AGC is not required to avoid saturation and since a slow AGC is available to aid acquisition, an AGC time constant in excess of 0.5 seconds is needed.

#### i. Q-Function Generator

The Q-Function generator is required to develop orthogonal sampling signals. The sampling signals are used to drive the ferrite scanner, where the multiplexing is accomplished, and to drive error detectors, where the final demodulation is accomplished. In the present case, the generator is required to develop four pulsed waveforms, equally spaced from each other. The basic repetition rate can be set somewhat arbitrarily. In the present system, a 25 to 30 Hz rate is selected. The rate must be much greater than the servo bandwidth (1 Hz) and less than the lowest information rate (300 Hz) to avoid potential crosstalk problems.

One final consideration is to avoid, when possible, subharmonics of power line frequencies, since hum would cause error signals to be generated in a power line coherent system. The Q-function generator should also incorporate a timing or phase adjustment to compensate for the propagation delays through the scanner and receiver. This variable, a one-time adjustment, insures that orthogonal demodulation is accomplished, thereby avoiding crosstalk between azimuth and elevation channels.

#### 4. EQUIPMENT DESIGN

a. Satellite Communication terminals are generally required to transmit and receive circular polarization. To obtain this polarization, a device called a polarizer is inserted between the duplexer and the feed horn. A four polarizer combination, one for each feed, is needed in the present case. An axial ratio of less than 1 dB across the receive band can be achieved with the polarizer. The duplexing and polarizing functions can be combined for systems having two way capability (transmission as well as reception). The transmit port should be isolated at least 30 dB from the receiver port. If one way capability is desired, the duplexer may be omitted and the comparator is attached directly to the polarizer.

The comparator and feed horn are connected to the duplexer-polarizer combination to form the complete feed assembly. The VSWR can be maintained less than 1.1 at both transmit and receive ports across the band.

Typical sum and difference patterns for a 15 foot parabolic dish at 8 GHz is shown in Figure 13. The 3 dB beamwidth is approximately 0.57 degrees, and the gain is 50 dB relative to isotropic. The null, or boresight will shift for any unbalance in the precomparator arms but this unbalance can be specified and calibrated to be less than 0.1 dB across the receive band. The sum and difference patterns are both plotted on the same ordinate scale. The relative on-axis difference slope can be computed from Figure 13, and is approximately given by

$$M_T(0) = \frac{S_{\Delta}(0)}{S_{\Sigma}(0)} = \frac{0.1}{0.0565 \text{ deg}} = 1.77 \text{ per degree} \quad (20)$$

#### b. Scanner

The scanner, shown schematically in Figure 14, uses two folded magic tees with the parallel arms connected by two identical  $0^\circ$  to  $180^\circ$  differential digital latching ferrite phase shifters. The two difference

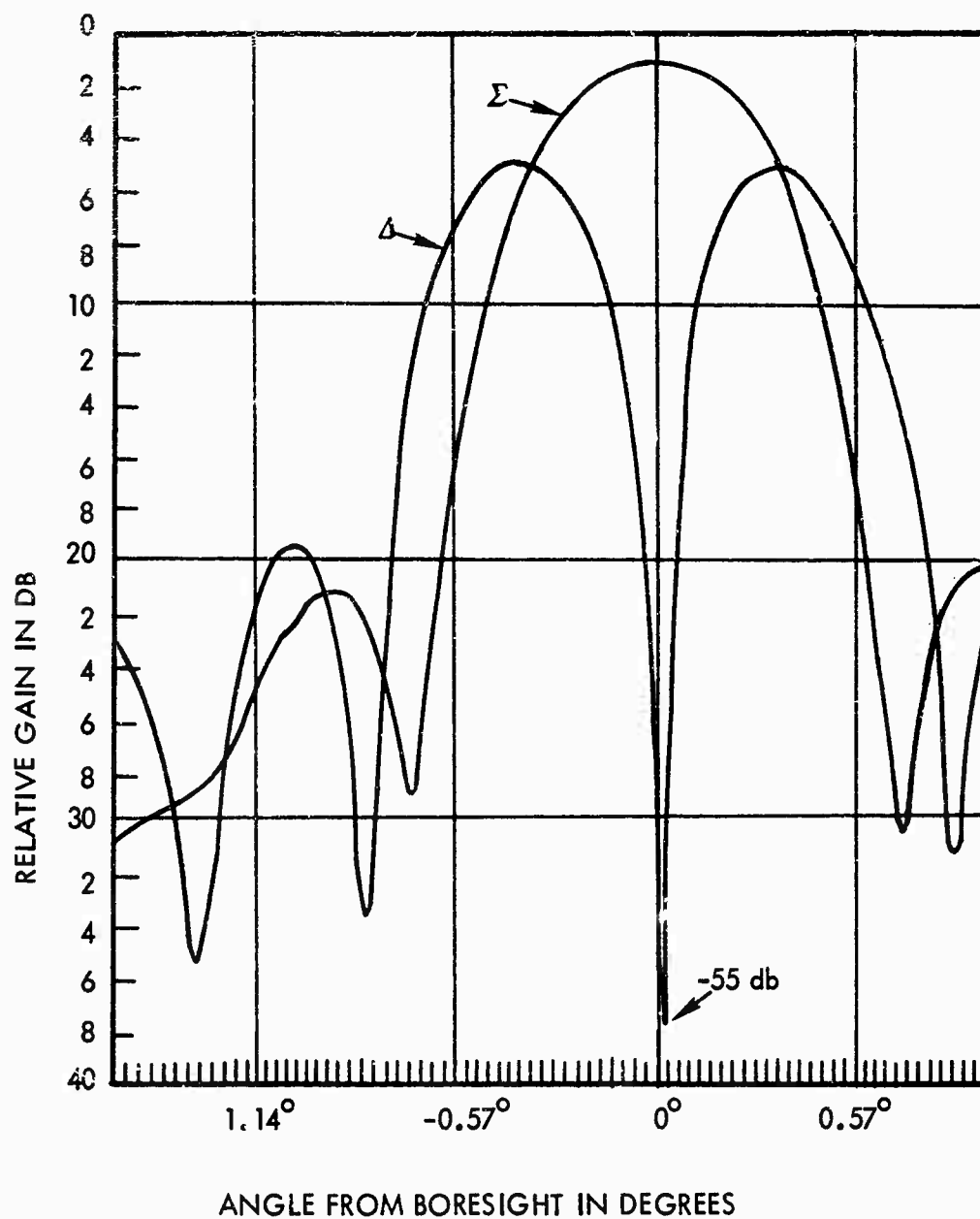
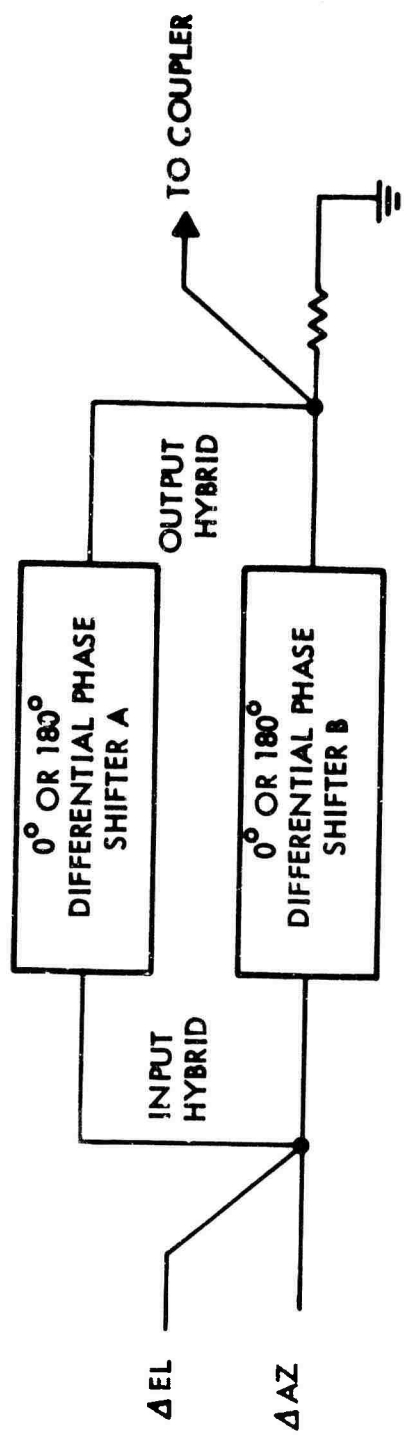


Figure 13. Typical Receive Antenna Patterns



PHASE SHIFT STATES	PHASE SHIFTER A	PHASE SHIFTER B	OUTPUT TO COUPLER
1	0°	0°	$\Delta EL @ 0^\circ$
2	180°	0°	$\Delta AZ @ 0^\circ$
3	180°	180°	$\Delta EL @ 180^\circ$
4	0°	180°	$\Delta AZ @ 180^\circ$

Figure 14. Ferrite Scanner Operation

signals are fed to the E and H arms of the first hybrid and switched sequentially by the phase shifters to the output arm of the second hybrid. The output signal is a square wave sampling of the two difference signals providing sequential lobing of the antenna beam.

A Ferrite Scanner developed for a similar terminal uses +28 V DC for the driver power and four trigger pulse inputs, one for each state of each phase shifter. Since ferrites are temperature sensitive and the unit would be used over a typical temperature range of  $-25^{\circ}\text{F}$  to  $+150^{\circ}\text{F}$ , the ferrite portion of the scanner is thermally insulated from the hybrid tees and temperature controlled at  $+150^{\circ}\text{F} \pm 5^{\circ}\text{F}$ . The power used to temperature control the scanner is 120 V 400 cycle AC, but the unit also operates with 60 cycle power. The scanner is completely militarized and has a calculated MTBF of 500,000 hours. Operation characteristics are given in Table 6.

#### c. Directional Coupler

A standard waveguide directional coupler with 10 dB coupling and 20 dB directivity can be used. Connecting lines in the system are WR 137 waveguide using CPR 137 flanges. Lines should be capable of pressurization with 1 psig of dry air. The coupler should be compatible with these interface requirements.

#### d. Receive Filter

As discussed earlier, the receive filter is used to provide the receiver with adequate image rejection. For a passband at  $8\text{ GHz} \pm 25\text{ MHz}$  and using low side injection with a 70 MHz IF, the image band is  $7.86\text{ GHz} \pm 25\text{ MHz}$ . Thus, the filter must pass frequencies in the range 7975-8025 MHz with as low insertion loss as possible, and reject frequencies in the band 7835-7885 MHz at least 60 dB. The low insertion loss is required to avoid system noise degradation, since each 0.1 dB loss will add approximately  $7^{\circ}\text{K}$  to the overall system noise temperature. The filter is a 7 cavity direct coupled 0.02 dB ripple Chebyshev filter. The unit is electroformed out of copper with all inside surfaces gold flashed to reduce loss.

The measured rolloff characteristic of a breadboard 7 cavity filter suitable for use in this design is shown in Figure 15, and the VSWR in Figure 15. The actual filter stopband in this case extends below 7835 MHz and the rejection exceeds 60 dB at 7885 MHz. As shown in Figure 16, the VSWR is less than 1.05 in-band. The insertion loss is approximately 0.2 dB at 8.0 GHz and less than 0.4 dB at the lower band edge. Further optimization of this unit would allow the maximum in-band loss to be less than 0.2 dB.

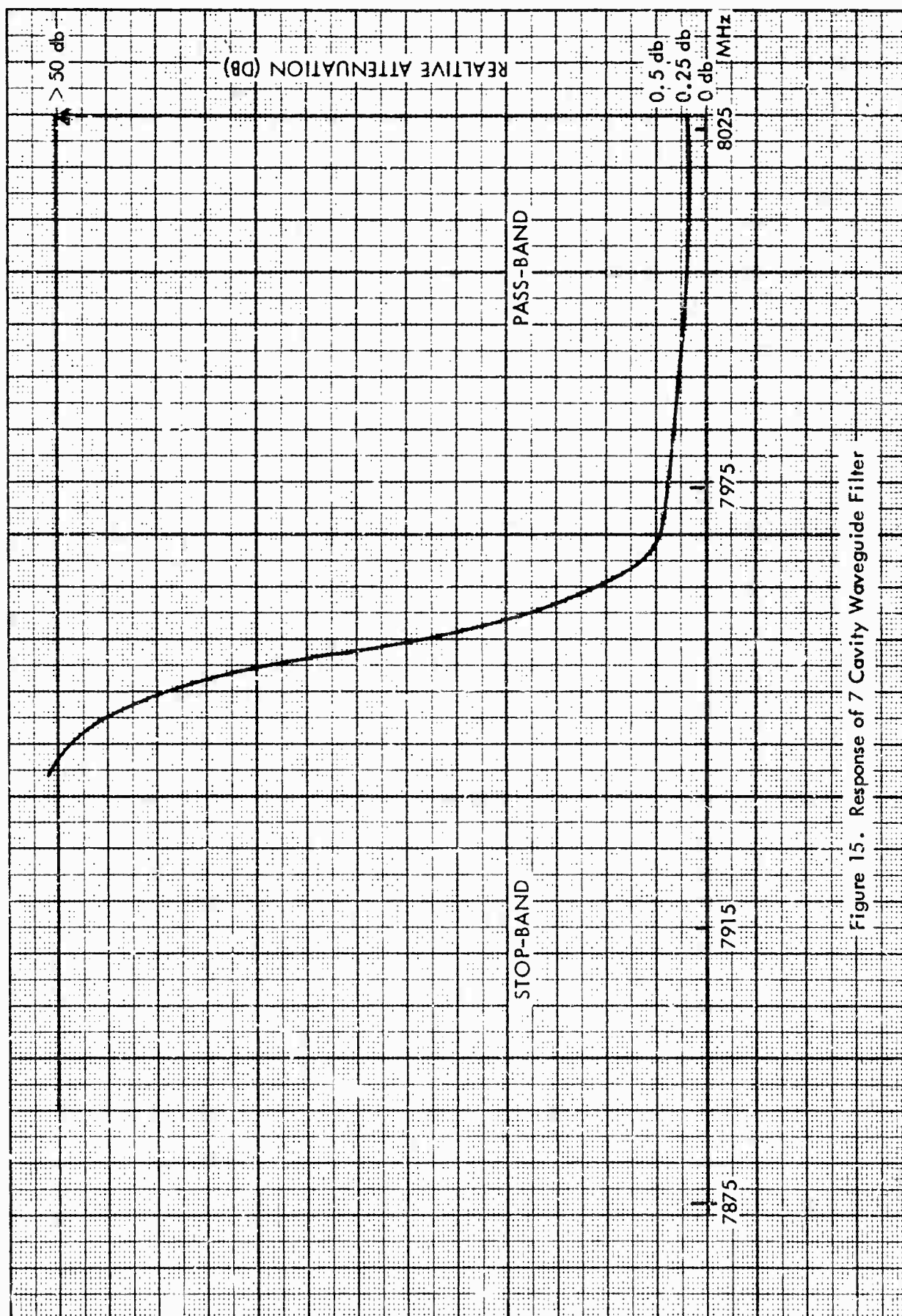


Figure 15. Response of 7 Cavity Waveguide Filter



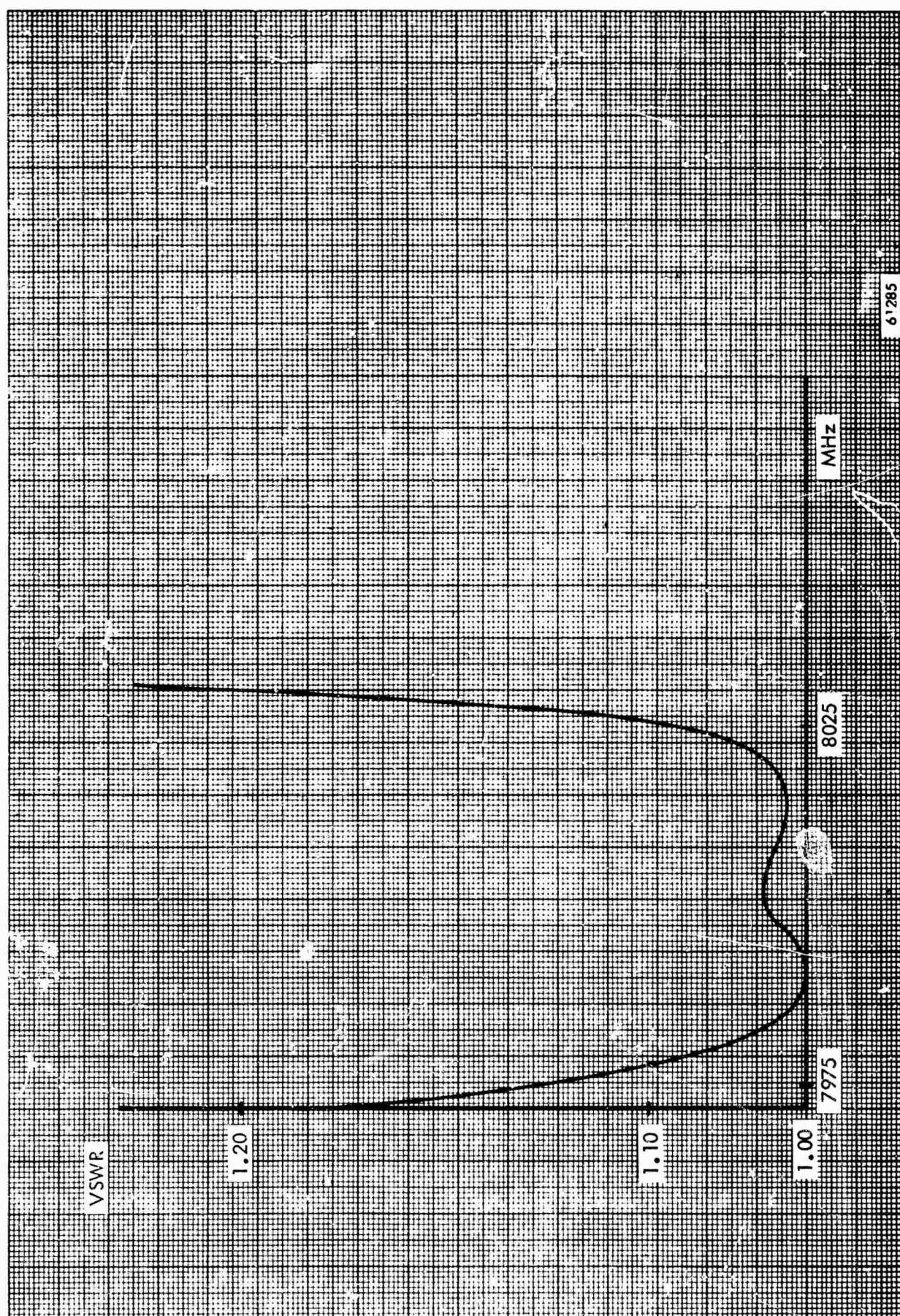


Figure 16. VSWR vs Frequency of 7 Cavity Waveguide Filter

TABLE 6

## FERRITE SCANNER OPERATING CHARACTERISTICS

Frequency Range:	8 GHz $\pm$ 25 MHz
Insertion Loss:	less than 1.0 dB
Phase Shift:	0° to 180° latching per phase shifter
Isolation:	Input to output, 20 dB minimum, for the undesired signal input
Variation in Overall Phase Shift Between Assemblies:	$\pm$ 20° maximum
Input Power:	28 V DC, $\pm$ 0.028 V, 1 watt maximum
Hybrid Characteristics:	Folded H plane VSWR, E-arm: 1.10 maximum VSWR, H-arm: 1.10 maximum Isolation, E and H arms: 40 dB, minimum Isolation, Parallel arms: 25 dB, minimum
Unbalance:	0.10 dB maximum
Drive Requirements:	Each phase shifter is two wire, with a 0 to +12 $\pm$ 3 volt pulse of 10 microsecond duration to switch from one state to another. One line for 0° state, and one line for 180° state.

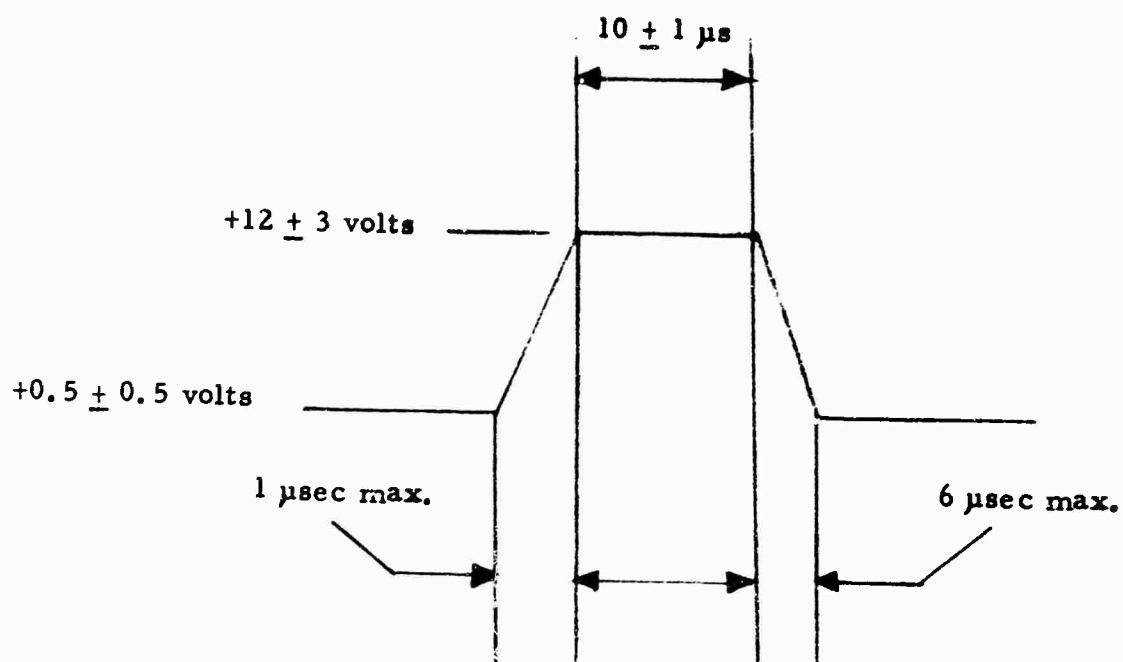
The drive pulse has the following characteristics:

(See Page 2 of Table 6)



TABLE 6

(Page 2)



Repetition Period is  $40 \pm 4$  ms

#### e. Preamplifier

The basic approach selected for the preamplifier is a single-ended one-port difference frequency amplifier. The single-ended approach is chosen to meet the low-noise requirement at lower pump powers and provide a fixed tuned bandwidth. Figure 17 shows the block diagram of the amplifier and remote controls. The amplifier consists of two cascaded amplifier modules each integrated with three circulators, pump circuitry components, and remote controls. Bias to each amplifier is injected separately through tees in the RF line after each amplifier module to permit individual and independent adjustment of each stage. A DC blocking capacitor isolates the individual stages, while a low pass filter is used between stages to provide additional filtering to the idler and pump frequencies. Pump power is sampled, detected and compared to a DC reference voltage K. The difference, or error, is amplified in a DC amplifier and used to control the attenuation in the pump line. Thus, constant pump power is supplied to each diode. The leveling circuitry is provided in one integrated module.

Temperature stabilization is used to insure stability over the entire temperature range using heaters and thermostats. The thermostats are set to maintain the enclosure at a temperature ( $120^{\circ}\text{F}$ ) near the upper end of the operating range. For ambient temperatures above  $120^{\circ}\text{F}$  the heating circuitry is disabled. Air is circulated in the enclosure by a blower. Air circulation is disabled at low temperatures (below  $30^{\circ}\text{F}$ ) to avoid unnecessary losses through the enclosure walls. Temperature stabilization is used mainly to prevent changes in varactor contact potential, pump power, and frequency. A summary of the amplifier performance requirements is listed in Table 7.

#### f. Local Oscillator

The local oscillator consists of a low frequency crystal controlled oscillator followed by a multiplier. These components will be described separately in following paragraphs.

(1) Oscillator Design. The oscillator design approach uses a dual proportional control oven to provide frequency stability over the temperature range, and solid state circuitry to multiply the oscillator output to the desired frequency. The outer oven operates at  $70^{\circ}\text{C}$  and the inner oven at  $75^{\circ}\text{C}$  to provide heat transfer from inside to outside at the highest ambient operating temperature. The ovens require 15 watts of DC power at turn-on and the warmup time is approximately 20-25 minutes at the lowest operating temperatures. Power required after the warmup period is about 5 watts. The oscillator itself uses a basic 25 MHz fifth overtone crystal. The crystal drive is chosen to optimize stability and noise characteristics.

Figure 17 Block Diagram of Low-Noise Parametric Amplifier

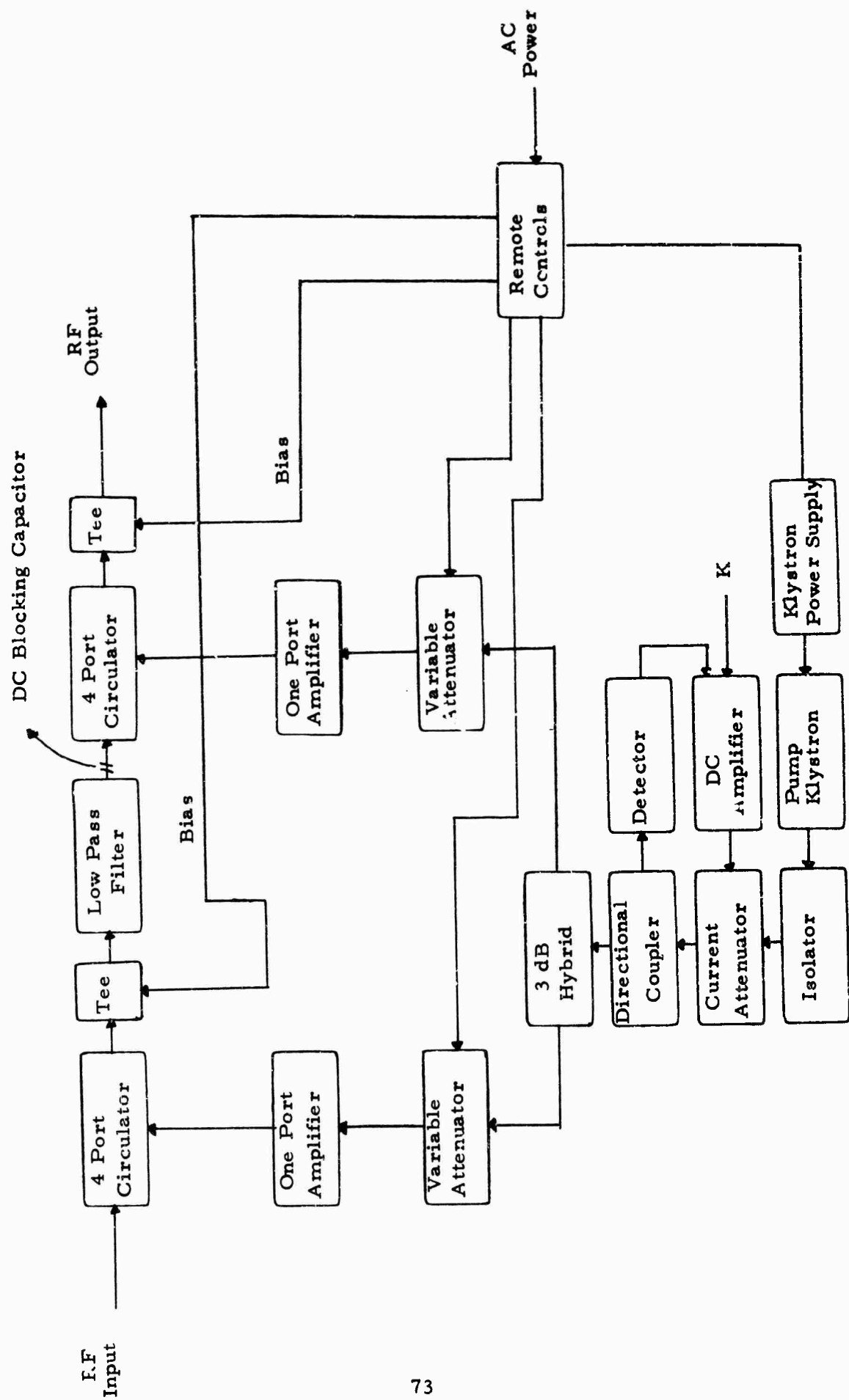


TABLE 7

## PARAMETRIC AMPLIFIER OPERATIONAL CHARACTERISTICS

Input Frequencies:	8 GHz $\pm$ 25 MHz
Passband:	50 MHz minimum at 1 dB points
Overall Gain:	30 dB minimum, 35 dB maximum
Tunability:	Fixed Tuned
Noise Temperature:	100°K at 290°K ambient temperature. The noise temperature will degrade to 117°K at 339°K ambient. These temperatures are in the presence of a source VSWR of 2.0:1 and at any phase
Dynamic Range:	-40 dBm in-band at 0.5 dB gain compression or less
Susceptibility to Out-of-Band Frequencies:	The amplifier is unaffected by -20 dBm signals 500 MHz out-of-band
Amplitude Response:	The amplitude variation is less than $\pm 0.2$ dB/10 MHz over the passband. The response does not vary more than $\pm 0.5$ dB over the entire passband.
VSWR:	Input and Output, 1.5:1 maximum. All performance requirements are met when the amplifier is driven from a source with VSWR = 2.0:1 in WR 137 waveguide, and driving a 50 ohms (VSWR = 2.0:1 load in coax (RG 214/U).

(See Page 2 of Table 7)

TABLE 7

(Page 2)

Primary Power:	208 volts $\pm$ 5%, 3 phase 400 $\pm$ 12 Hz 4 wire 200 watts maximum at a power factor of 0.85 or higher
Reliability:	The equipment has a MTBF (Mean Time Between Failure) of 10,000 hours
Air Leakage:	Less than 1 cc/hr under 1 lb. psig at input, output or both. The amplifier will withstand 10 psig
Operating Temperature:	Air temperature from $-30^{\circ}\text{F}$ for periods of 3 days, to $+150^{\circ}\text{F}$ for four (4) hour periods daily
Non-Operating Temperature:	Continuous exposure, air temperature from $-80^{\circ}\text{F}$ for 24 hour periods, to $+155^{\circ}\text{F}$ for 24 hour periods
RFI:	MIL-I-11748 for Class I equipment
Relative Humidity:	5% at air temperatures of $+150^{\circ}\text{F}$ 97% at temperatures of $85^{\circ}\text{F}$ with condensation below $85^{\circ}\text{F}$
Elevation:	
Operating:	Up to 10,000 feet above sea level
Non-operating:	Up to 40,000 feet above sea level
Vibration:	5-55 Hz 0.03 inch double amplitude 55-500 Hz $\pm$ 5 G
Remote Controls and Indicators:	Run time monitor, pump power monitor, beam and repeller voltage test points, gain and frequency adjust. ON-OFF switch, bias voltage and attenuator current test points, and system voltage meter with test selector switch

(See Page 3 of Table 7)

**TABLE 7**

**(Page 3)**

**Connectors:**

Input, CPR 137 waveguide  
Output, Type "N" female coax

**Size and Weight:**

The antenna mounted enclosure is  
16" x 16" x 7" and weighs 45 pounds.  
The control panel is 14" x 14" x 12"  
and weighs 25 pounds.

The oscillator output is multiplied in a X5 multiplier with the circuitry outside the oven, and the multiplier output is supplied to a narrowband crystal filter centered at the output frequency. Sufficient interstage filtering is used to suppress the nearest harmonic at least 80 dB below the desired output level. The oscillator unit has the operational characteristics listed in Table 8.

## (2) Multiplier

The X64 multiplier requires an input signal in the range 123-125 MHz, approximately, and provides a CW signal in the frequency range  $7.930 \text{ GHz} \pm 25 \text{ MHz}$  at a level of +10 dBm, minimum over the operating temperature range  $-30^{\circ}\text{F}$  to  $150^{\circ}\text{F}$ . The design uses two doublers in a transistor-amplifier-multiplier module, and two step recovery diodes, each providing X4 multiplication, in a diode multiplier module. Successive interstage filtering is used to provide at least 80 dB rejection to the nearest harmonic. The multiplier has the operational characteristics listed in Table 9.

## g. Mixer-Preamplifier

The mixer design utilizes a balanced configuration with the signal input and LO inputs on opposite sides and orthogonal to each other. The configuration is normally referred to as "crossbar", and its main advantage is in size and weight.

The crossbar configuration performs much as a magic tee, with the LO and signal inputs isolated from each other similar to the E- and H-plane arms on the tee. The diodes are mounted in the parallel arms of the tee in their respective holders. Both signal and LO ports are coaxial (type "N" female) and the IF output is coax to the preamplifier input. The mixer uses two matched Schottky barrier gallium arsenide diodes.

The IF amplifier utilizes 6 stages of amplification each providing approximately 8 dB of gain. Each stage has predictable variations with temperature using highly reliable planar epitaxial silicon transistors. Also, the overall unit is temperature compensated to provide stable operation from  $-30^{\circ}\text{F}$  to  $150^{\circ}\text{F}$ . The mixer-preamplifier performance characteristics are listed in Table 10.

## h. Demodulator Subsystem

(1) Input Filter. The input filter is used to reject out-of-band signals present at the demodulator input and prohibit the 48.6 MHz VCO from leaking out the input terminals. For a filter 3 dB bandwidth of 4 MHz, a 3 section Butterworth filter will reject the 48.6 MHz signal

TABLE 8

OSCILLATOR OPERATIONAL CHARACTERISTICS

Frequency:	123-125 MHz
Frequency Stability:	$1/10^8$ per 24 hours and $1/10^9$ per 15 minutes. This stability is provided at any temperature within the operating temperature range. The temperature may change to any other temperature within the operating temperature range and the stability shall not exceed that specified above.
Residual FM:	The FM noise in the output is less than 15 Hz rms in a 300 Hz to 10 kHz band each side of the carrier when the oscillator output frequency is multiplied to 10 GHz and measured there.
Output Level:	+13 dBm, -0 dB, +2 dB into 50 ohms (VSWR:1.5:1 over operating temperature range.
Spurious and Harmonics:	All spurious output frequencies are at least 80 dB below the signal output level (a spurious is any frequency other than the output frequency and its harmonics). Harmonics of the output frequency are at least 40 dB below the output signal level.
Connectors:	Type "TPS" female Power, Cannon DEH-9P-20-1
Power Required:	+28 V DC, 1% regulation and 1 millivolt rms ripple.
Warmup Time:	The output frequency stability is within specification within 30 minutes after oven and oscillator circuitry are activated simultaneously at any operating temperature in the temperature range.

(See Page 2 of Table 8)



TABLE 8

(Page 2)

Frequency Adjustment:	The output frequency is adjustable to compensate for drift over a 5 year period.
Reliability:	130,000 hours, MTBF
Operating Temperature Range:	-30°F to +150°F
Shock:	5 G's in three perpendicular planes for 11 ms.
Non-Operating Vibration:	5-55 Hz, 0.03" double amplitude 55-500 Hz, 5 G's

TABLE 9

## X64 MULTIPLIER OPERATIONAL CHARACTERISTICS

Output Frequency Range:	7.93 GHz $\pm$ 25 MHz
Multiplication Factor:	X64
Input Level:	+10 dBm $\pm$ 3 dB
Output Level:	The output level is adjustable from 0 to +10 dBm at any output frequency in the range 7.930 GHz $\pm$ 50 MHz and at any temperature in the operating temperature range for a constant input signal level.
Input and Output Impedance:	50 ohms, VSWR less than 1.3:1
Output Level Variation:	$\pm$ 2 dB, maximum, as the input frequency at a constant level is tuned to cover the output frequency range at a constant temperature.
Load Characteristics:	The multiplier delivers the output level into 50 ohms with a maximum VSWR of 1.5:1.
Output Attenuator:	An uncalibrated attenuator with a minimum range of 10 dB continuously adjustable is provided to set the output level.
Spurious and Harmonics:	All spurious signals in the output frequency range are 80 dB or more below the desired output level. All spurious signals outside the output frequency range are 60 dB or more below the desired output level. Harmonics of the output frequency are 40 dB or more below the desired output level. (A spurious is any frequency other than the output frequency or its harmonics).

(See Page 2 of Table 9)

TABLE 9

(Page 2)

Noise:	<p>AM noise in the output is 70 dB or more below the output signal level in a 20 kHz band centered on the output frequency <math>F_0</math>, excluding the band <math>F_0 \pm 300</math> Hz.</p> <p>FM noise in the output is less than 4 Hz rms in a 300 Hz to 10 kHz band each side of <math>F_0</math>.</p>
Stability:	The multiplier is unconditionally stable for any source or load VSWR at all frequencies.
Power:	+28 V DC, 10 watts 1 mv rms ripple, 1% no load to full load regulation.
Operating Temperature:	-30°F to 150°F
Reliability:	75,000 hours MTBF
Connectors:	<p>Input: TPS female</p> <p>Output: Type "N" female</p> <p>Power: Cannon Dem-9P</p>

TABLE 10

## MIXER-PREAMPLIFIER CHARACTERISTICS

Noise Figure:	8 dB, maximum, including a 2.0 dB IF noise figure
Input Frequency:	8 GHz $\pm$ 25 MHz
LO Frequency:	7.93 GHz $\pm$ 25 MHz
LO Power:	+3 dBm, +5, -3 dB
LO Isolation:	20 dB, minimum, at input and output ports
RF to IF Gain:	50 $\pm$ 2 dB
Gain Variation:	+ 3 dB, over temperature range -30°F to 150°F
RF BW:	20 MHz, minimum, at 1 dB points 80 MHz, maximum, at 60 dB points
Dynamic Range:	+10 dBm at the output for less than 0.5 dB gain compression
VSWR:	Input: 1.2/1 maximum, 50 ohms Output: 1.2/1 maximum, 50 ohms LO: 1.5/1 maximum, 50 ohms
Spurious Response:	All internally generated intermodulation and spurious responses in the output bandpass 70 $\pm$ 10 MHz are 60 dB or more below the desired output level, when the input unmodulated CW signal level is -50 dBm or less
Operating Temperature Range:	-30°F to 150°F
Shock:	25 G's in three perpendicular planes for 11 ms

(See Page 2 of Table 10)

TABLE 10

(Page 2)

Non-operating Vibration:	5-55 Hz, 0.03" double amplitude 55-500 Hz, 5 G
Connectors:	Input: Type "N" female Output: TPS female LO: Type "N" female
Reliability:	40,000 hrs. MTBF
Power Requirements:	400 mw at 28 V DC 10 mv ripple (rms) 1% regulation no load to full load

approximately 100 dB. Third order components at frequencies 27.2 and 91.4 MHz generated in the mixer are attenuated at least 90 dB. The filter has an impedance level of 50 ohms, and uses high Q inductors and capacitors to provide near optimum response. The insertion loss is less than 3 dB.

(2) Mixer. The mixer uses a 70 MHz input amplifier, a 48.6 MHz buffer amplifier, a balanced mixer, and a 21.4 MHz output buffer amplifier. Each amplifier is a single common emitter stage. The input 70 MHz amplifier is matched to 50 ohms over a wide frequency range to preserve the input filter response. The balanced mixer uses diodes in a "ring" configuration to provide large signal handling capability with a linear response. The mixer has a conversion loss of 10 dB. The total overall gain of the mixer is 0 dB, as the amplifier gains compensate for the mixer conversion loss. The 48.6 MHz buffer amplifier has 10 dB gain to supply +10 dBm LO power for the mixer drive.

(3) 48.6 MHz VCO. The 48.6 MHz VCO is controlled in the manual mode, from a front panel control, or by the sum of the manual input and voltage out of the AFC/Sweep integrator in the AFC mode. The oscillator uses a Colpitts circuit with a varactor as the tuning element. The tuning sensitivity is 50 kHz/volt  $\pm$  5%. Thus, a sawtooth of + 3 volts will provide  $\pm$  150 kHz sweep. The frequency stability is  $\pm$  1( $10^{-5}$ )/ $^{\circ}$ C. Low temperature coefficient components are used, together with temperature compensation.

(4) 21.4 MHz IF Preamplifier. The 21.4 MHz IF pre-amplifier provides the gain control in the SCMTR, and has a minimum of 40 dB AGC range. The amplifier has 50 dB of available gain and a 3 dB bandwidth of 4 MHz. The AGC is set to provide 0 dBm at the amplifier output on noise alone, and is linear for a signal-plus-noise output level up to 0 dBm. The amplifier uses 6 stages of gain, with the first five gain-controlled to provide a linear gain versus bias characteristic. The last stage operates as a linear amplifier with fixed gain to drive the IF filter. The linear characteristic allows the signal strength meter to be calibrated in dB, and makes the loop dynamics independent of initial conditions.

(5) 21.4 MHz IF Filter. The IF bandpass filter provides the function of setting the SCMTR predetection bandwidth. To accommodate an 8 kHz baseband signal with modulation index of 10, at least 175 kHz of IF bandwidth is required. To provide margin, and optimum amplitude and phase characteristics over the information spectrum, a 500 kHz IF bandwidth is provided. The filter bandwidth will reduce the noise level 9 dB at its output to a value of -9 dBm (with a 0 dBm output from the 21.4 MHz IF preamplifier). The filter is a 4 pole linear-phase filter.

(6) 21.4 MHz IF Post-Amplifier and AM Detector. The primary function of the IF post-amplifier is to provide sufficient level at each of its outputs to drive the various circuits which follow. Each output is at a level of 0 dBm, requiring approximately 25 dB of active gain. Three stages of gain supply +14 dBm into a resistive power divider using emitter degeneration to provide stable operation over the temperature range. The transistors used in the amplifier are all VHF-UHF silicon epitaxial types with low inter-electrode capacitances. The auxiliary output may be used for checking the gain of the demodulator or counting frequency. The AM detector is a diode followed by a simple RC filter to provide linear envelope detection. The impedance level is 200 ohms, and the DC output is approximately 1 volt. The AM detector output is divided and supplied to the AGC filter/amplifier, and the signal detect circuitry.

(7) 21.4 MHz Discriminator. The 21.4 MHz discriminator is a temperature-compensated LC unit with a peak-to-peak bandwidth of 2 MHz. Extra care is required in the design to provide a symmetrical transfer characteristic at its crossover frequency of 21.4 MHz. This is necessary to avoid an output at low SNR which would cause the VCO to shift frequency. An offset would introduce distortion if it were sufficient to cause the signal sidebands to suffer unsymmetrical attenuation in the IF filter. The temperature stability of the zero-crossover is  $\pm 250$  Hz/ $^{\circ}$ C or less, and the sensitivity is 5 mv/kHz.

(8) AGC Amplifier. A high gain integrator with capacitive feedback is used for the AGC amplifier. The feedback is used to establish the 0.5 sec time constant, and the high gain assures that the IF output voltage remains constant over the 40 dB AGC range. The AGC amplifier drives the AGC line of the 21.4 MHz IF preamplifier and the signal strength meter.

(9) 21.4 MHz Phase Detectors. Two 21.4 MHz phase detectors are provided. One is used to operate the phase-lock loop, and the other to provide a coherent DC output and error signals for tracking. The phase detector circuit is a full wave diode bridge with current limiting resistors in series with each diode. Both signal and VCO, or reference signal, is amplified in a buffer amplifier before entering the phase detectors. The sensitivity is approximately 1.0 volts/radian, and the inherent balance is adjusted to less than 10 mv.

(10) 21.4 MHz Voltage-Controlled Oscillator (VCO). An LC VCO is used for the 21.4 MHz oscillator to provide a wide tuning range of  $\pm 150$  kHz. The design is practically the same as that used in the 48.6 MHz VCO. The output is divided in a resistive power divider to supply the loop phase detector, coherent detector, and an auxiliary rear panel connector for monitoring purposes. The VCO output is +10 dBm,

and each output of the power divider is 0 dBm. The tuning sensitivity is 200 kHz/volt. One output of the relative power divider employs a quarter wavelength subminiature coaxial line to introduce 90° of phase shift. This output is supplied to the coherent AM detector.

(11) 21.4 MHz Loop DC Amplifier and Filter. The loop amplifier/filter combination is an operational amplifier with an RC network which controls the feedback around the amplifier. The amplifier has a DC gain in excess of 5000, a gain-bandwidth product of 20 MHz, and an input drift less than 20  $\mu\text{V}/^{\circ}\text{C}$ . The design provides a modified type 2 loop with a noise bandwidth of approximately 300 kHz.

(12) Loop Lock Indicator. The output of the coherent detector is applied to a level detector. The level detector is actually a high gain operational amplifier connected as an integrator. The reference for the level detector is + 0.5 volt. Whenever there is a voltage above + 0.5 volt at the detector output, a relay is closed and the lock indicator light is energized indicating a locked condition. Also, the level detector supplies an input voltage to the phase lock detect and sweep stop circuitry to stop the sweep in the AFC loop.

#### i. Error Signal Detector

The error signal detectors are simply two phase-sensitive detectors, driven with quadrature signals. The detectors operate in the same manner as the phase detectors described in the previous section. The operating frequency is approximately 25 Hz and rectangular waves, rather than sine waves, are used as the reference signals.

### 5. SUMMARY

The previous paragraphs have described the pseudo-monopulse technique in sufficient detail to assure its feasibility. The basic errors were analyzed and shown to be relatively small in an operational environment.

The alignment required is relatively simple, with the major alignment functions accomplished in the basic design. The precomparator amplitude and phase alignment is identical with that of a full monopulse system. The key to a wide band matched system design is to maintain both electrical and mechanical symmetry. A simple post comparator alignment is necessary to obtain pure AM, with no FM, at the scanner output. This adjustment is non-critical and can be accomplished by nulling the FM component, monitored by the data demodulator, when a CW input is used with a fixed antenna pointing error. The remaining adjustment is a timing or phase adjustment of the 25 Hz signal to prevent



crosstalk. Again, the adjustment is easily accomplished by nulling the azimuth error channel when only an elevation pointing error exists and vice-versa. In practice, this error can be made negligible by simply adjusting the timing while monitoring the waveforms on an oscilloscope. All alignments are one-time (factory) adjustments; periodic calibration is not required.

The basic SCMTR can be used equally well with a larger antenna, such as a 60-foot dish. The servo gain constants would be changed, of course, and the acquisition problem would be made worse (although a compensating effect occurs due to the increased system sensitivity). The errors due to noise and system unbalances would be reduced approximately in proportion to the antenna beamwidth reduction.

The pseudo-monopulse technique, then, is feasible, requires no particularly difficult alignment procedures, is capable of maintaining calibration for long periods of time, and can be used on antennas of much larger (or small) size. In short, pseudo-monopulse is a practical, generally applicable, SCMTR technique.

## SECTION V

### AMS

#### 1. INTRODUCTION

The AMS (Automatic Manual Simulator) technique evolved as a method for simulating the actions of a well-trained, untiring, human operator in a manual track situation. The underlying principles are, therefore, centered on the details of the manual track operation. Manual track of a target is generally accomplished by monitoring the receiver signal strength while manually positioning the antenna. The antenna is moved in each axis, but one axis at a time, in such a manner as to maximize the received signal strength.

In order to obtain maximum sensitivity, the operator would use a linear receiver, rather than one with AGC. The typical "scanning" operation is one of slewing the antenna back and forth and noting the position of peak signal strength. The scanning operation performed by the operator is of paramount importance! Initial investigations did not recognize the importance of the scanning operation, and a technique was theorized which did not require scanning. Such a system is not practical, although the technique of using known or measurable antenna perturbations (e. g., caused by wind, drifts, or noise) is theoretically possible.

A human operator can efficiently scan in only one axis at a time, but an automated system can simultaneously scan both axes, using orthogonal scanning signals. The next step, then, is to postulate a two-axis "back-and-forth" type of scan, and recognize that a mechanical conical scan has been defined. Although various orthogonal waveforms could be utilized, sine waves (used to generate a conical scan) are optimum in terms of mechanical stress for a given sampling rate.

#### 2. AMS SYSTEM

A block diagram of the AMS system is shown in Figure 18. The basic scanning is controlled by the signal generator. Two outputs from the signal generator, a sine and cosine wave, are fed to the basic servo circuitry. This servo, in general, is the antenna driving mechanism which would normally be required for a manual track or full monopulse autotrack system. The servo, through an appropriate geartrain, drives

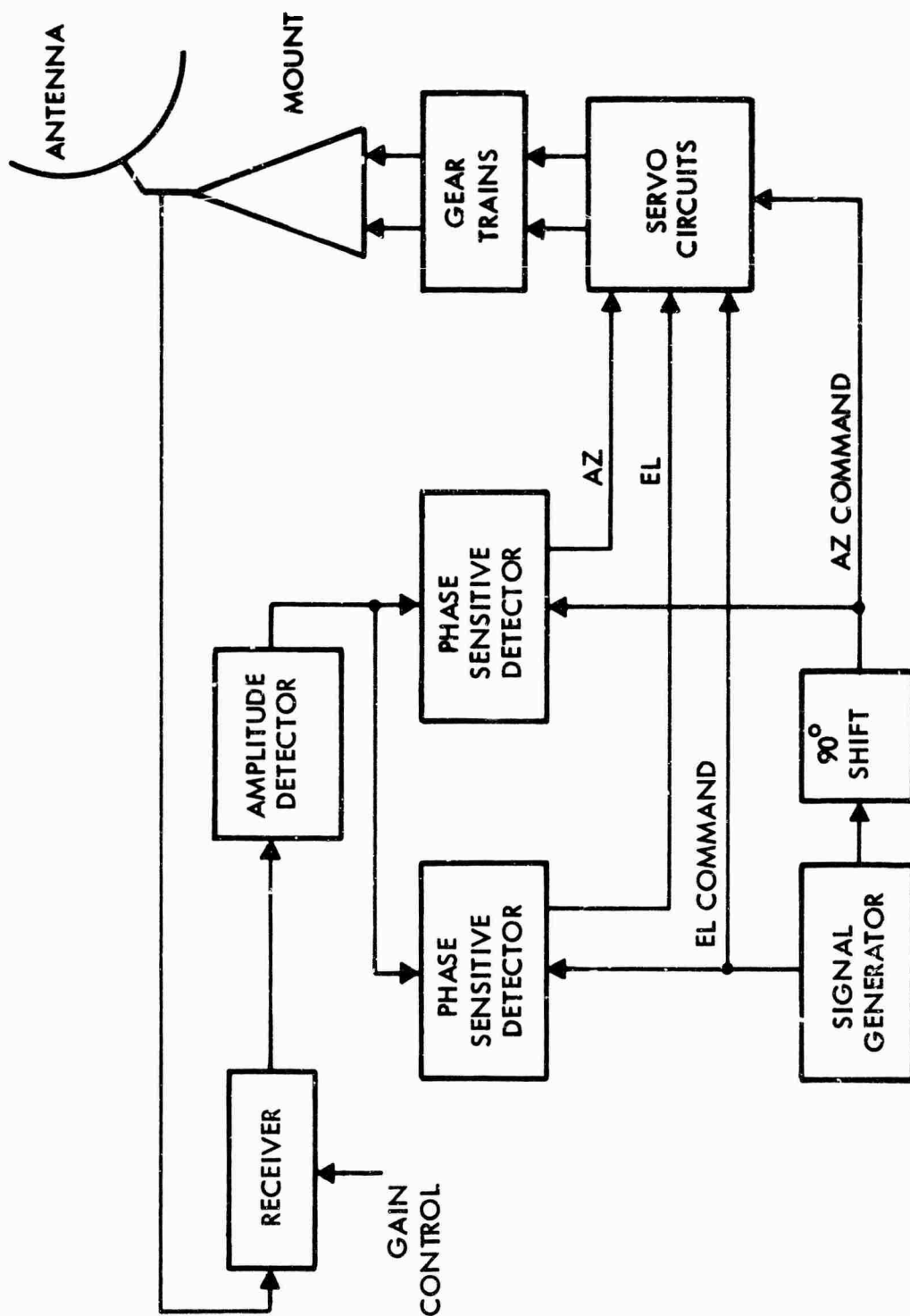


Figure 18. AMS System Block Diagram

the antenna in a manner controlled by the commands from the signal generator; i.e., it performs a conical scan at a rate determined by the sine wave frequency and of an amount (squint or crossover angle) controlled by the sine wave amplitude.

The antenna requires only a single feed (or the sum channel may be used when a tracking feed is already on the antenna) and generates the pointing error signal by virtue of the scanning operation on the mount. When the antenna is pointed off-bore-sight the received signal is amplitude modulated at the scan frequency, by an amount dependent upon the pointing error, and with a phase (with respect to the scan signal) determined by the direction of error. Thus, the information required for tracking is completely contained in the amplitude modulation of the carrier.

The signal enters the receiver and IF amplifier and is separated into two outputs. One output drives the communications demodulator and the other drives an amplitude detector. The communications information is recovered in the former and the tracking information in the latter. The output from the amplitude detector drives quadrature phase sensitive detectors. These detectors can be implemented in the same manner as in pseudo-monopulse. Alternatively, a nearly optimum compromise would utilize solid state relays to accomplish the demodulation. The solid state relay technique may be more desirable from a hardware standpoint due to the very low frequencies involved. The basic principle is to use gating pulses, synchronous with the zero crossings of the scanning signals, as the reference signals in the phase sensitive detectors. Careful balance of the detectors is necessary to alleviate the low pass filtering problem; i.e., to simplify the removal of the scanning frequency and its harmonics from the servo drive signals. The two signals developed in the quadrature phase demodulators are the pointing error signals, which are used to drive the servo circuitry.

The hardware requirements of the AMS system, in addition to the basic single channel feed-antenna-receiver and servo system, are simply to provide the signal generator, AM detector, and quadrature phase demodulator. These circuits are of conventional design and do not require particularly stringent balance, alignment, or other unusual care in construction. The servo circuits must be suitably modified, of course, to accept the scanning signals and the error signals. In most cases, this requires only the addition of summing resistors (on already existent operational amplifiers) and modification of time constants by changing resistor and/or capacitor values.

### 3. SYSTEM LIMITATIONS

In order to determine the practical system limitations, it was necessary to investigate the scan frequency limitations. This investigation culminated in a one-axis simulation of the system on an analog computer. A single mass model of a typical antenna system including servo electronics was used in the simulation. A functional block diagram of the system is shown in Figure 19. The antenna pattern, near bore-sight, was approximate with a cosine function as shown in Figure 20. This corresponds to a normalized half-power beamwidth of 90 degrees.

The antenna step response was investigated for various values of scan frequency,  $f_s$ , to servo bandwidth, BW. This was accomplished by holding the servo bandwidth and the amplitude of the scan signal constant while varying the scan frequency. The antenna step response and error are shown for  $f_s/BW = 10$  and 5 in Figure 21. The servo system was found to be unstable when the ratio  $f_s/BW$  was reduced to 4. The scanning frequency which is superimposed on the analog computer response would not be seen on a two axis received signal; i.e., in a conical scan system with no angular error, the amplitude modulation is zero. The actual antenna position does, of course, exhibit the scan frequency characteristic shown in Figure 21 in both the one axis and two axis case.

Thus, a lower limit on the ratio  $f_s/BW$  is 4 to 5 in a practical situation. The theoretical or Shannon limit is a sampling rate of twice the signal bandwidth, for a "bandlimited" signal. In the present case, a non-bandlimited signal exists due to loop stability requirements. Therefore, an important limitation of the AMS technique is that a sampling rate of at least 4 to 5 times the servo bandwidth be used to obtain adequate phase and gain margin to support loop stability.

The maximum scanning rate is limited by the allowable wear on the antenna drive system. The best compromise in this regard is to select a scanning frequency below mount resonance by an amount sufficient to avoid the torque multiplication effects at resonance. Thus, a scan value of one-half the mount resonant frequency would generally be a conservative selection, and a value of 0.8 to 0.9 times mount resonant frequency could be used in well-damped systems.

The scan frequency-servo bandwidth values are thus limited in a practical case. A servo bandwidth in the order of one-tenth the mount resonance is indicated, with values as high as one-fifth representing an upper limit. In many situations this limit is not of vital consequence. For example, a servo-antenna system capable of tracking low altitude



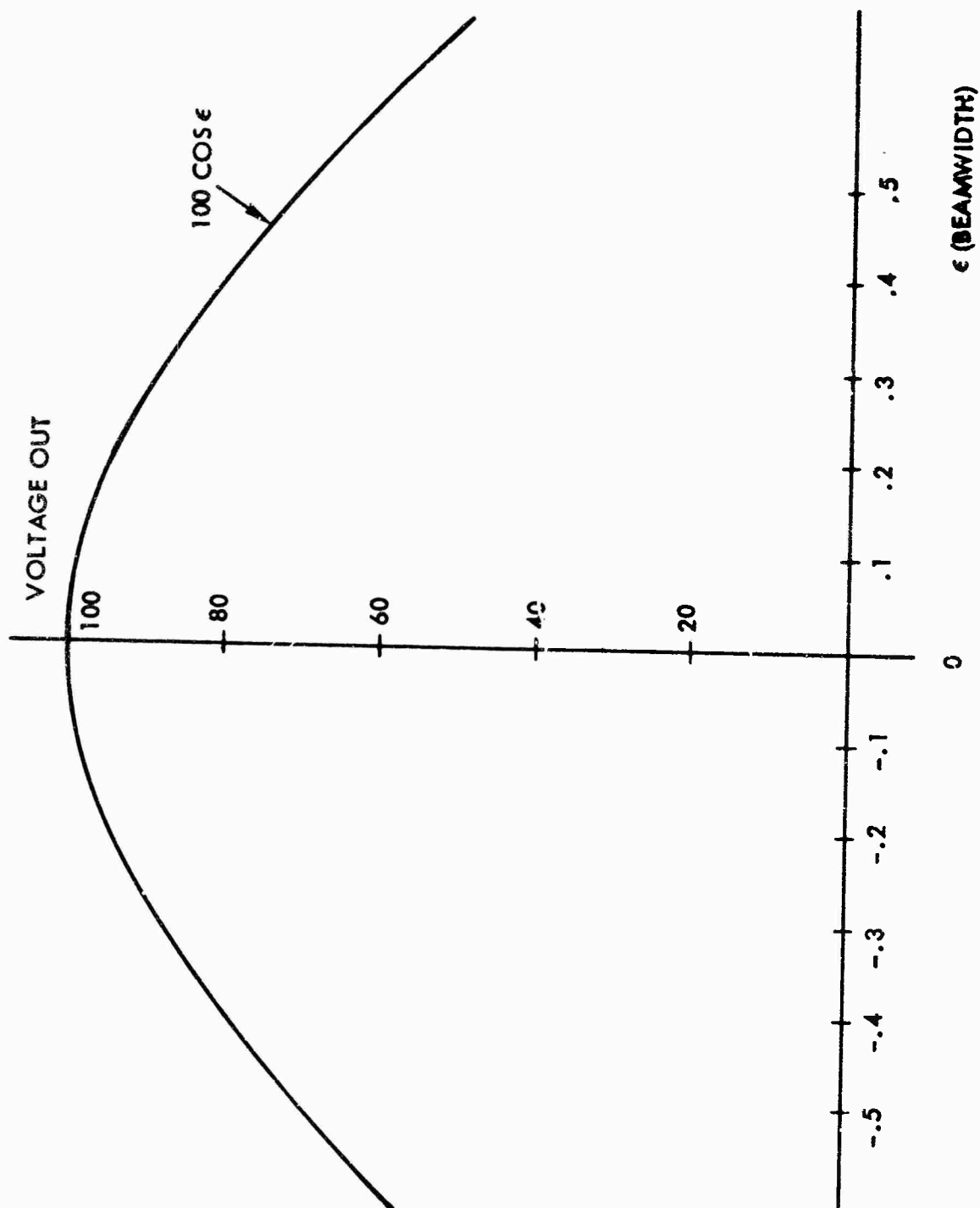


Figure 20. Antenna-Receiver Off-Axis Gain

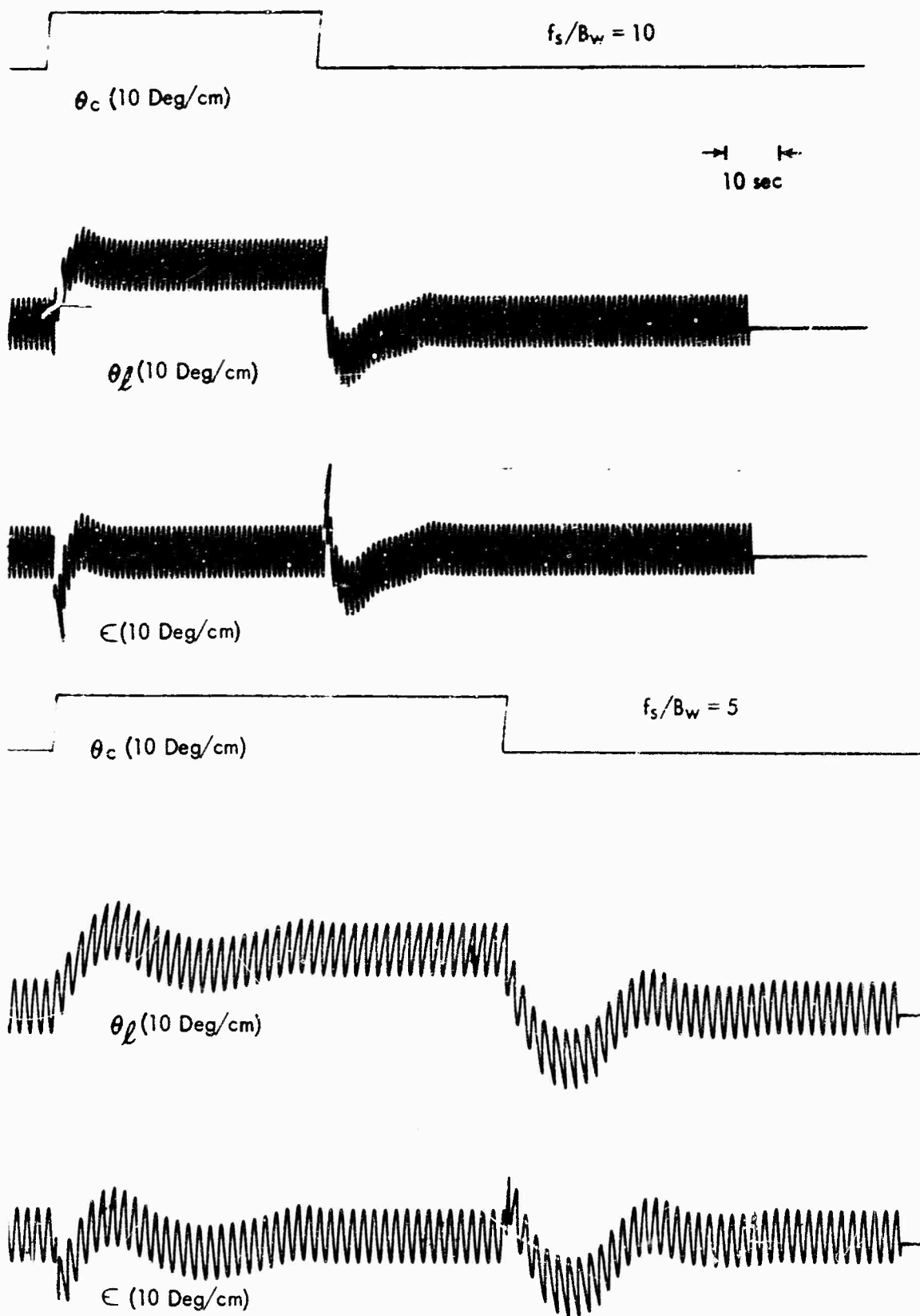


Figure 21. Antenna Step Responses - One Axis Simulation



(5000 miles or less) satellites would easily be capable of operation with synchronous and near-synchronous satellites in the AMS mode.

One other limitation also exists in a practical case. The basic servo design was (probably) based on maximum torque requirements due to wind, ice, and other factors. Since the scanning signal requires torque, the maximum torque limits could be exceeded were the AMS used under the worst case design conditions. Also, the torque required for scanning increases in proportion to the scan frequency, a further motivation for placing an upper limit on the scan rate. It appears, then, that as long as the AMS is not used under absolute worst case antenna loading conditions, the system reliability will not be appreciably reduced.

#### 4. SUMMARY

The AMS technique can be easily implemented and is a significant improvement over a manual track system. A prime need for this technique is foreseen as a back-up system. That is, the addition of the AMS to existing auto-track systems would be easily accomplished and would offer an additional tracking mode useful for nearly all situations which the original system was designed to handle.

The AMS could also be used as the prime tracking system when equipment simplification is desired. The implementation is again relatively simple, with basic limitations being determined by the servo and antenna drive systems. The receiver characteristic should be linear (not AGC) or an AGC with a time constant much longer than the scanning period. This would result in maximum sensitivity, and is the recommended design, but an AGC receiver could be used by an appropriate selection of the AM pickoff point. The latter is not recommended without a detailed analysis of the effects of the AGC system upon the overall tracking system stability and sensitivity.

The AMS should be particularly useful on lightweight, transportable terminals. The technique is directly applicable for example, as an additional mode on terminals now in production (the AN/TSC-54). Modifications to the basic technique which would improve system reliability under certain operating conditions are possible. For example, when target dynamics are slow (e.g., synchronous or near-synchronous satellites) the AMS can be timed to track for a short period of time (perhaps one minute) and be disabled for a longer period of time (ten to fifteen minutes). A more sophisticated modification would store the signal strength at the time tracking was disabled and automatically enable the AMS when the signal strength decreased by a prescribed amount. An obvious limitation to the latter modification, and to the basic technique for that matter, is in the normal fluctuations in received signal strength. The basic AMS can be

used only when the signal fluctuations are different from the scanning signals. Rapid fluctuations are no more degrading than slow fluctuations, but only the latter (if due to pointing errors) can be corrected with the tracking system. Since the normal signal characteristics in a satellite communications link vary at a slow rate, the AMS is particularly well suited to this application. The technique is recommended both as a prime tracking system, when equipment complexity is at a premium, and as a back-up system in more sophisticated terminals.

## SECTION VI

### AN ANALYSIS OF MONOPULSE ANTENNA CHARACTERISTICS

#### 1. INTRODUCTION

An analysis of amplitude and phase sensing monopulse system is made in the following sections in order to compare their system performance. Figures 22 and 23 show the general configurations of these systems. Of primary interest is a comparison of the maximum angular sensitivity (difference mode slope at boresight) of the two types of systems each having approximately the same gain; i.e., equivalent aperture areas. This is perhaps the most significant measure of monopulse system performance since the slope at the center of the difference pattern is a prime factor in the ability of a monopulse antenna to accurately track a target. Also of interest is the gain at the peaks of the difference pattern since it may affect the ability of a monopulse antenna to achieve angle lock-on of a distant target.

The amplitude sensing monopulse system is considered first and followed by an analysis of two practical phase sensing monopulse systems. Comparison of the results of these analyses is then made.

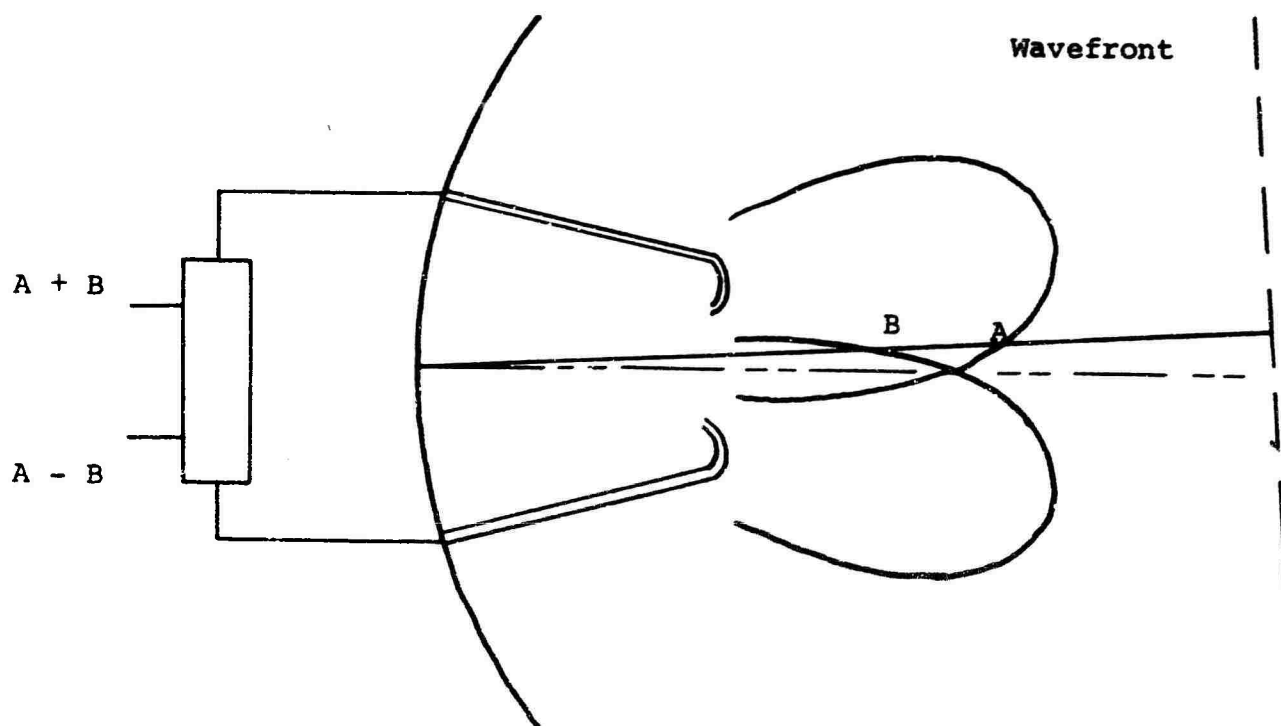
#### 2. AMPLITUDE SENSING MONOPULSE

In order to analyze the amplitude monopulse system, the relationship between the far-field difference patterns and their corresponding aperture distributions are investigated. In the following analysis only circular apertures of finite size are considered. Also, the phase of the patterns and distribution functions will be considered to remain constant except for 180 degree phase reversals.

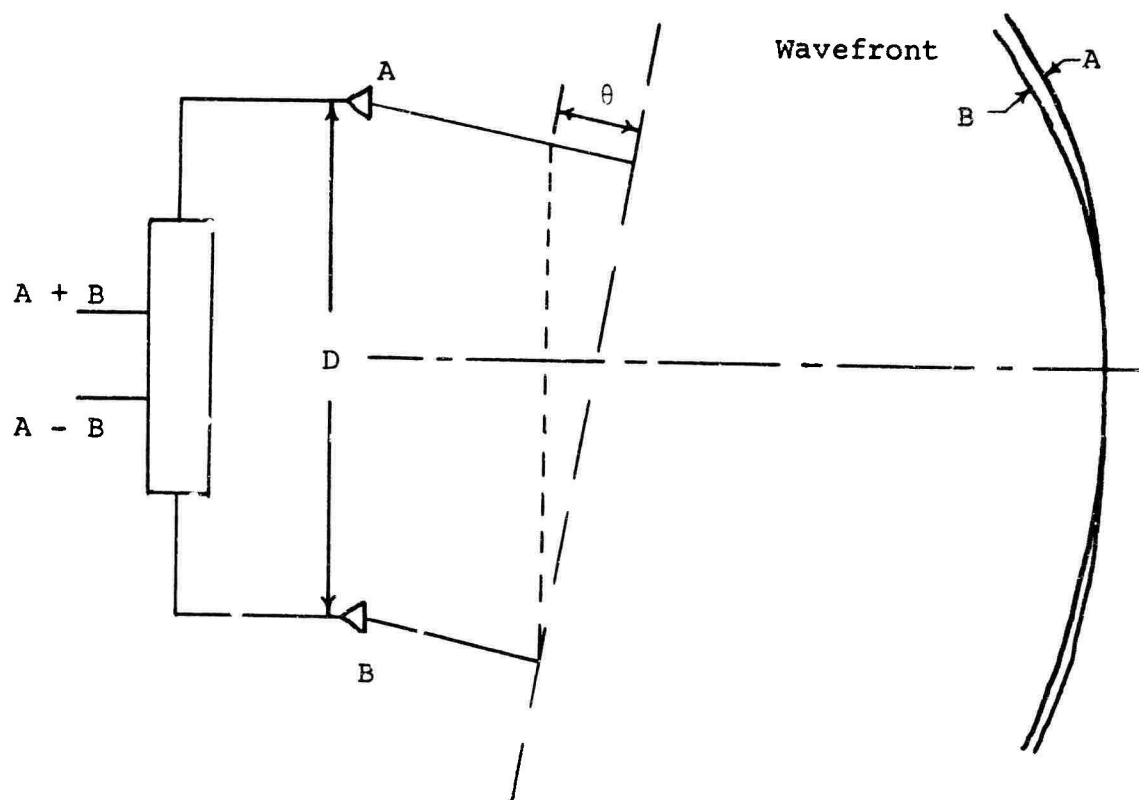
To calculate the radiation pattern in the Fraunhofer region, the following general expression is used (6).

$$g(\theta, \phi) = \iint F(\zeta, \eta) e^{jks \sin \theta (\zeta \cos \phi + \eta \sin \phi)} d\eta d\zeta \quad (21)$$

where  $F(\zeta, \eta)$  is the aperture distribution normalized to a maximum value of unity. Figure 24 shows the coordinate system corresponding to the above equation. In considering the special problem of a circular aperture of radius  $a$ , it is convenient to introduce the following variables.



Amplitude Sensing Monopulse Antenna  
Figure 22



Phase Sensing Monopulse Antenna  
Figure 23

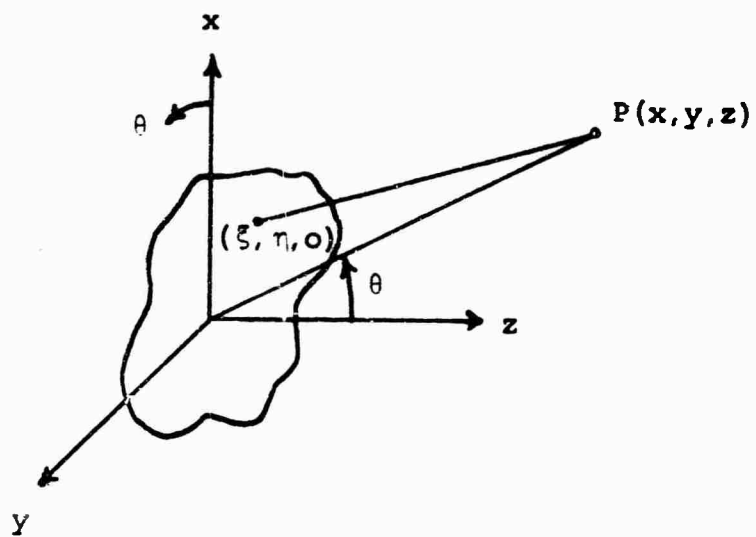


Figure 24 General Coordinate System

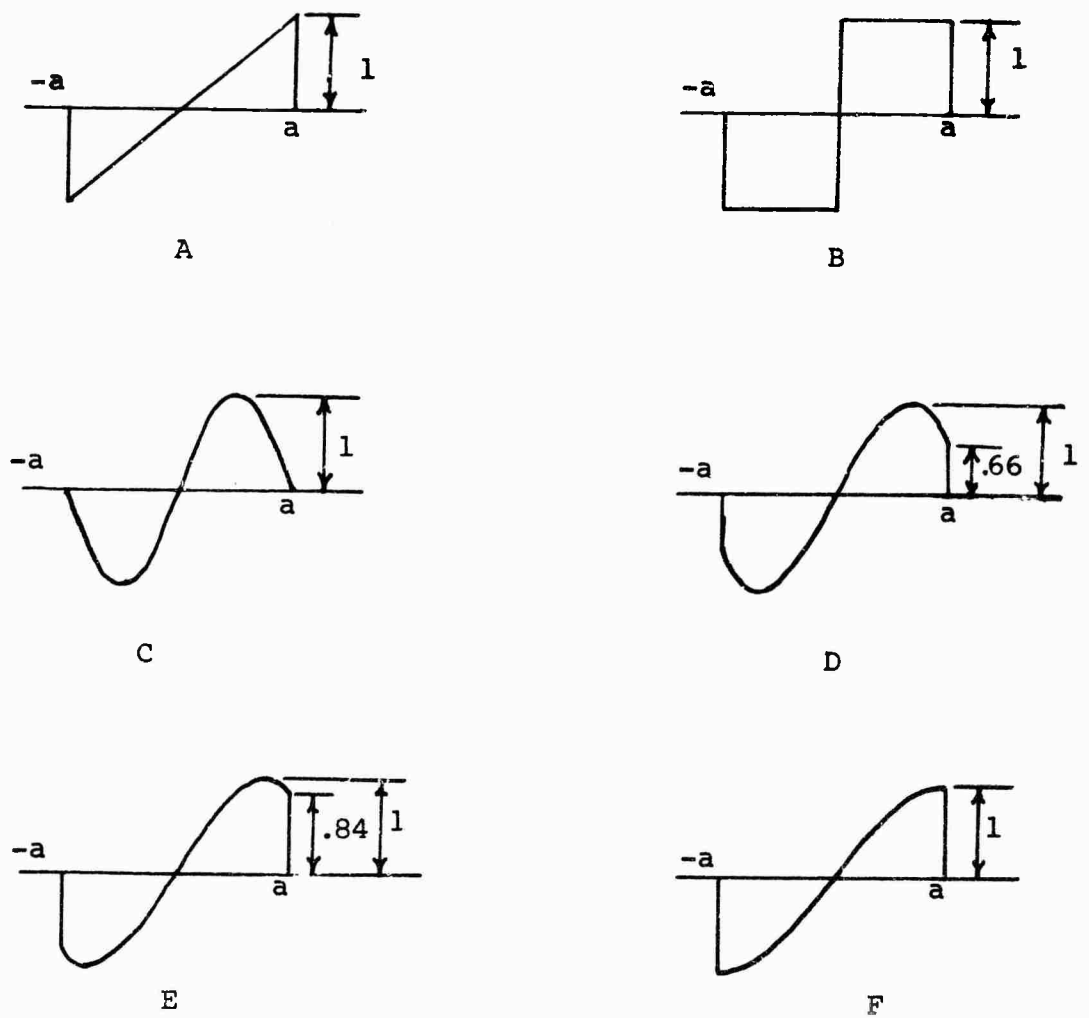


Figure 25 Distribution Functions

$$\zeta = \zeta/a$$

$$\eta = \eta/a$$

$$u = ka \sin \theta$$

With these variables,  $g(\theta, \phi)$  transforms to  $g(u, \phi)$  and  $F(\zeta, \eta)$  transforms to  $f(\zeta, \eta)$ . Using these variables and the proper limits of integration for a circular aperture, the diffraction integral becomes:

$$g(u, \phi) = a^2 \int_{-1}^1 \int_{-\sqrt{1-\zeta^2}}^{\sqrt{1-\zeta^2}} f(\zeta, \eta) e^{ju(\zeta \cos \phi + \eta \sin \phi)} d\eta d\zeta \quad (22)$$

Only those distributions which are independent of  $\eta$  will be considered. In addition, only the far-field pattern in the principle plane of  $\phi = 0$  degrees will be discussed. With these constraints the diffraction integral may be written as:

$$g(u) = 2a^2 \int_{-1}^1 \sqrt{1-\zeta^2} f(\zeta) e^{ju\zeta} d\zeta \quad (23)$$

In order to simplify the relationship, only those distribution functions which are even or odd functions will be considered. The far-field patterns resulting from even distribution functions,  $f_e(\zeta)$ , and odd distribution functions,  $f_o(\zeta)$ , will be denoted by  $S_\Sigma(u)$  and  $S_\Delta(u)$ , respectively. For these two cases, the diffraction integral becomes:

$$\begin{aligned} S_\Sigma(u) &= 2a^2 \int_{-1}^1 \sqrt{1-\zeta^2} f_e(\zeta) e^{ju\zeta} d\zeta \\ S_\Delta(u) &= 2a^2 \int_{-1}^1 \sqrt{1-\zeta^2} f_o(\zeta) e^{ju\zeta} d\zeta \end{aligned} \quad (24)$$

These integral relationships will now be simplified. Separating the integrals into the sum of two integral terms:

$$S_{\Sigma}(u) = 2a^2 \left\{ \int_0^1 \sqrt{1-\zeta^2} f_e(\zeta) e^{ju\zeta} d\zeta + \int_{-1}^0 \sqrt{1-\zeta^2} f_e(\zeta) e^{ju\zeta} d\zeta \right\}$$

$$S_{\Delta}(u) = 2a^2 \left\{ \int_0^1 \sqrt{1-\zeta^2} f_o(\zeta) e^{ju\zeta} d\zeta + \int_{-1}^0 \sqrt{1-\zeta^2} f_o(\zeta) e^{ju\zeta} d\zeta \right\}$$

Introducing the following change of variable in the second integral terms,

$$\zeta = -\zeta$$

$$d\zeta = -d\zeta$$

the expressions become:

$$S_{\Sigma}(u) = 2a^2 \left\{ \int_0^1 \sqrt{1-\zeta^2} f_e(\zeta) e^{ju\zeta} d\zeta + \int_0^1 \sqrt{1-\zeta^2} f_e(-\zeta) e^{-ju\zeta} d\zeta \right\}$$

$$S_{\Delta}(u) = 2a^2 \left\{ \int_0^1 \sqrt{1-\zeta^2} f_o(\zeta) e^{ju\zeta} d\zeta + \int_0^1 \sqrt{1-\zeta^2} f_o(-\zeta) e^{-ju\zeta} d\zeta \right\}$$

Making use of the fact that,

$$f_e(\zeta) = f_e(-\zeta)$$

$$f_o(\zeta) = -f_o(-\zeta)$$

the above relationships become:

$$S_{\Sigma}(u) = 2a^2 \int_0^1 \sqrt{1-\zeta^2} f_e(\zeta) [e^{ju\zeta} + e^{-ju\zeta}] d\zeta$$

$$S_{\Delta}(u) = 2a^2 \int_0^1 \sqrt{1-\zeta^2} f_o(\zeta) [e^{ju\zeta} - e^{-ju\zeta}] d\zeta .$$

These expressions may now be written as:

$$S_{\Sigma}(u) = 4a^2 \int_0^1 \sqrt{1-\zeta^2} f_e(\zeta) \cos(u\zeta) d\zeta$$

$$S_{\Delta}(u) = j4a^2 \int_0^1 \sqrt{1-\zeta^2} f_o(\zeta) \sin(u\zeta) d\zeta$$
(28)

In order to make a valid comparison of different aperture illuminations, the distribution functions,  $f_e(\zeta)$  and  $f_o(\zeta)$ , must be subject to some constraint such as constant power(7). Initially, the far-field patterns of various distribution functions will be calculated by means of the above relationships. Finally, these results will be normalized to the constraint of constant power radiated. The process of normalizing will be discussed further at that time.

It is well known that the maximum theoretical gain of a circular aperture antenna is obtained with uniform illumination with no spillover. This even distribution gives a secondary pattern characteristic of a sum channel pattern. This will be calculated to provide a representative sum pattern to which difference patterns can be compared. For the uniform amplitude distribution,  $f_e(\zeta) = 1$ , the above diffraction integral is easily evaluated. The secondary amplitude sum pattern is given by:

$$S_{\Sigma}(u) = \pi a^2 \Lambda_1(u)$$
(29)

where  $\Lambda_1(u)$  is the first order lambda function.

The main concern here is the difference patterns which are obtainable with odd aperture distribution functions. Only those odd distributions which result in real analytic functions for the secondary amplitude pattern will be considered. In order to compare the slope of the difference pattern for two types of monopulse sensing systems, it is desirable to have a suitable reference standard. It has been stated that the maximum theoretical angular sensitivity (difference mode slope at boresight) is obtained with a linear odd antenna aperture illumination having no spillover(8). This maximum sensitivity provides a suitable reference standard for rating difference slopes of monopulse antennas. Thus, a circular aperture with a normalized linear odd illumination is used as a difference mode standard.

The far-field difference patterns of a circular aperture with several different odd distribution functions have been calculated and are



presented in the following paragraphs. These will be normalized to constant power later.

One odd distribution function which would be of interest is the linear odd distribution as illustrated in Figure 25-A. However, the solution of the diffraction integral with  $f_0(\zeta) = \zeta$  is not a straightforward procedure. This integral will be solved later with a distribution function that very closely approximates the linear odd distribution function. Of primary concern is the boresight slope of the difference pattern rather than the actual amplitude pattern. This can be found rather easily by using the following technique. Reviewing, for an odd distribution  $f_0(\zeta)$  the difference pattern is given by:

$$S_{\Delta}(u) = j4a^2 \int_0^1 \sqrt{1-\zeta^2} f_0(\zeta) \sin(u\zeta) d\zeta \quad (30)$$

The slope of the difference pattern is given by:

$$M(u) = |d/du[S_{\Delta}(u)]|$$

$$M(u) = 4a^2 \int_0^1 \zeta \sqrt{1-\zeta^2} f_0(\zeta) \cos(u\zeta) d\zeta \quad (31)$$

The slope at boresight is given by the above expression with  $u = 0$ .

$$M(0) = 4a^2 \int_0^1 \zeta \sqrt{1-\zeta^2} f_0(\zeta) d\zeta \quad (32)$$

Thus, for  $f_0(\zeta) = \zeta$ , the unnormalized on-axis difference pattern slope becomes:

$$M_{un}(0) = 4a^2 \int_0^1 \zeta^2 \sqrt{1-\zeta^2} d\zeta \quad (33)$$

The evaluation of this integral is straightforward and the resulting boresight slope is:

$$M_{un}(0) = (\pi/4)a^2$$

$$M_{un}(0) = .787a^2 \quad (34)$$

This procedure for differentiating  $g(u)$  before it is integrated allows the evaluation of the on-axis difference slope without having to first evaluate the diffraction integral for the far-field pattern and then evaluating the slope of this function at  $u = 0$ .

Another distribution function investigated was the uniform odd distribution as illustrated in Figure 25-B. This distribution is given by:

$$\begin{aligned} f_o(\zeta) &= 1 & 0 < \zeta < 1 \\ f_c(\zeta) &= -1 & -1 < \zeta < 0 \end{aligned}$$

For this distribution, the diffraction integral for the far-field pattern can be evaluated. This gives the following analytic function for the secondary amplitude pattern.

$$S_{\Delta}(u) = j2\pi a^2 H_1(u)/u \quad (35)$$

where  $H_1(u)$  is the first order Struve function. A plot of this difference pattern is shown in Figure 26. To determine the on-axis slope of this difference pattern, the technique used above may be used or the expression for  $g(u)$  may be differentiated after it has been integrated. Both methods arrive at the same result. This latter method will be used.

$$\begin{aligned} M(0) &= |d/du[S_{\Delta}(u)]_{u=0}| \\ M_{un}(0) &= 2\pi a^2 d/du[H_1(u)/u]_{u=0} = 0 \end{aligned} \quad (36)$$

It can be shown that this reduces to:

$$\begin{aligned} M_{un}(0) &= (4/3)a^2 \\ M_{un}(0) &= 1.333a^2 \end{aligned} \quad (37)$$

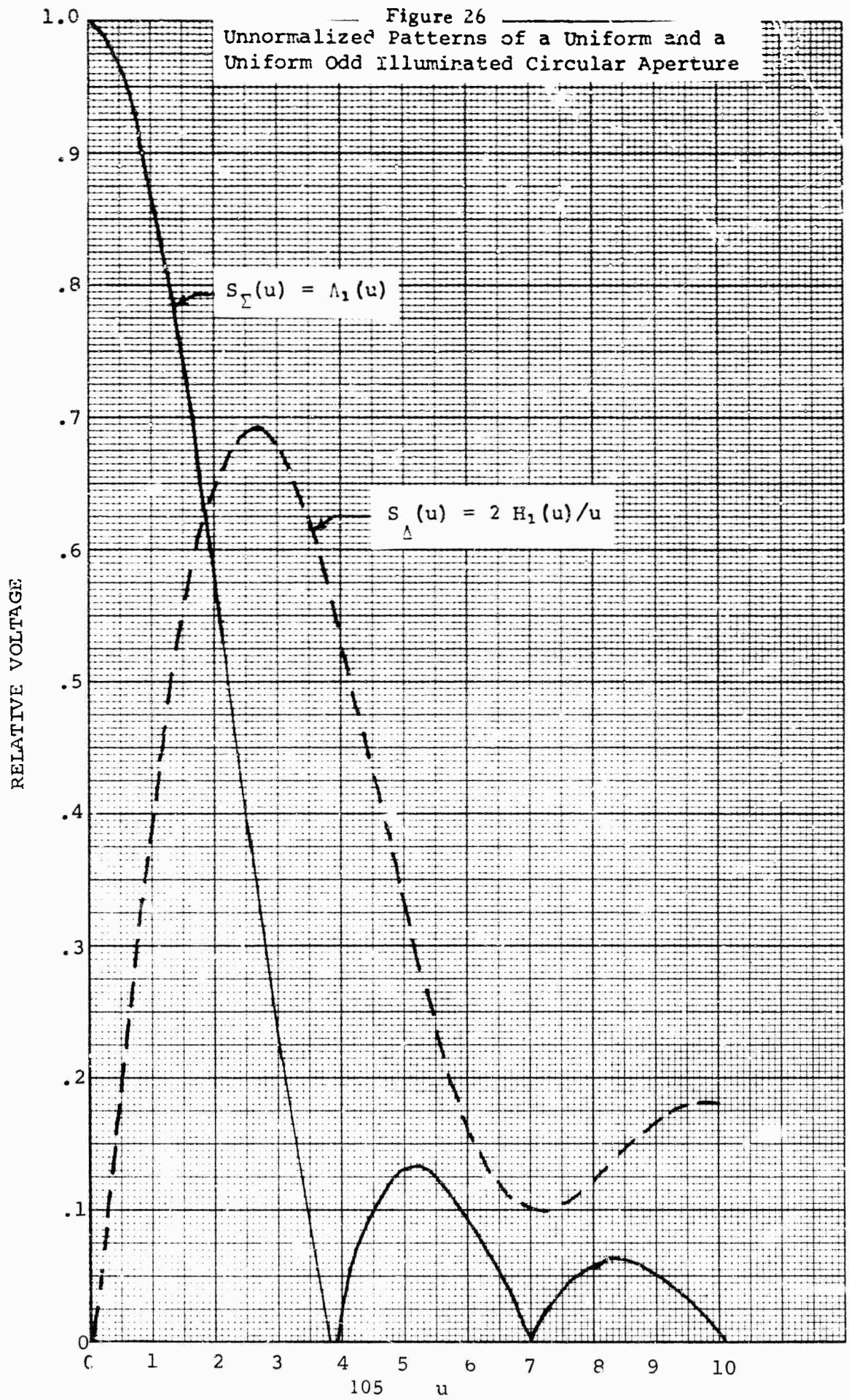
Also of interest is the far-field patterns resulting from sine curve distribution functions with no spillover. This distribution is given by:

$$f_o(\zeta) = \sin(u_1 \zeta) \quad -1 < \zeta < 1$$

With this distribution the diffraction integral can be evaluated. The resulting expression for the secondary amplitude pattern is given by:

$$S_{\Delta}(u) = j\pi a^2 [\Lambda_1(u-u_1) - \Lambda_1(u+u_1)]/2 \quad (38)$$

Figure 26  
Unnormalized Patterns of a Uniform and a  
Uniform Odd Illuminated Circular Aperture



A more detailed discussion of the evaluation of the integral is given in Paragraph 5. Carrying out the operation described above, the on-axis difference pattern slope is given by:

$$M_{un}(0) = (\pi/4)a^2 u_1 \Lambda_2(u_1) \quad (39)$$

The above two relationships will now be evaluated for different values of  $u_1$ . The first to be considered will be that of  $u_1 = \pi$ . Figure 27 shows the secondary pattern. The on-axis slope is given by:

$$M_{un}(0) = .9719a^2 \quad (40)$$

It is also of interest to determine the maximum on-axis slope that is obtainable with this type of distribution function. This is found by determining what value of  $u_1$  causes the slope of the on-axis slope function to vanish. That is:

$$d/du[M_{un}(0)] = 0 \quad (41)$$

Carrying out this operation, the following transcendental equation results:

$$J^2(u_1) = u_1 J_3(u_1) \quad (42)$$

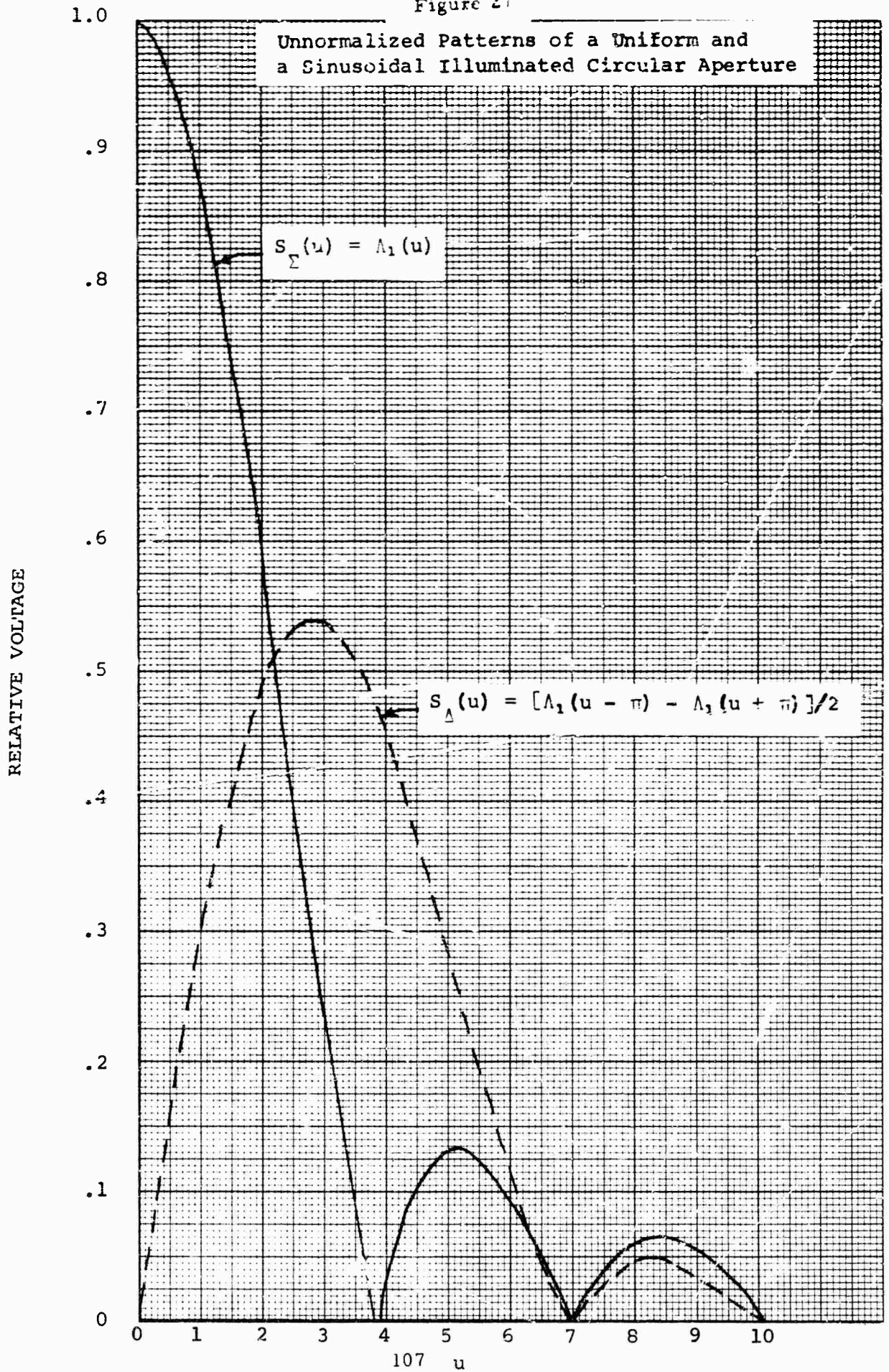
Solving this for  $u_1$  gives  $u_1 = 2.3$ . Using this value of  $u_1$  the resulting value of the boresight difference pattern slope is:

$$M_{un}(0) = 1.1308a^2 \quad (43)$$

Figure 28 shows the resulting far-field pattern with  $u_1 = 2.3$ . With this value of  $u_1$ , the illumination edge taper of the distribution function is found to be .666 or -3.53 dB, as shown in Figure 25-D.

Another case of interest is that value of  $u_1$  which gives the maximum difference gain for this type of distribution. It has been shown<sup>9)</sup> that the maximum peak difference gain is obtained with  $u_1 = 2.57$ . This distribution function is illustrated in Figure 25-E. The illumination edge taper for  $u_1 = 2.57$  is found to be .84 or -1.52 dB. With this value of  $u_1$ , the on-axis

Figure 27





1.0

Figure 28

Unnormalized Patterns of a Uniform and  
a Sinusoidal Illuminated Circular Aperture

RELATIVE VOLTAGE

.9

.8

.7

.6

.5

.4

.3

.2

.1

0

$$S_{\Sigma}(u) = \Lambda_1(u)$$

$$S_{\Delta}(u) = [\Lambda_1(u - 2.3) - \Lambda_1(u + 2.3)]/2$$

108 u

10

9

8

7

6

5

4

3

2

1

0

difference slope is given by:

$$M_{un}(0) = 1.1132a^2 \quad (44)$$

Figure 29 shows the far-field pattern obtained with this distribution.

The last special case of interest is that of  $u_1 = \pi/2$  which is illustrated in Figure 25-F. This approaches the linear odd distribution discussed earlier. The value of the boresight difference pattern slope is given by:

$$M_{un}(0) = .9991a^2 \quad (45)$$

and the secondary amplitude pattern is shown in Figure 30.

In the previous paragraphs, several far-field difference patterns have been calculated from various odd distribution functions. These patterns and distribution functions will now be normalized to the constant power radiated. The power radiated is proportional to:

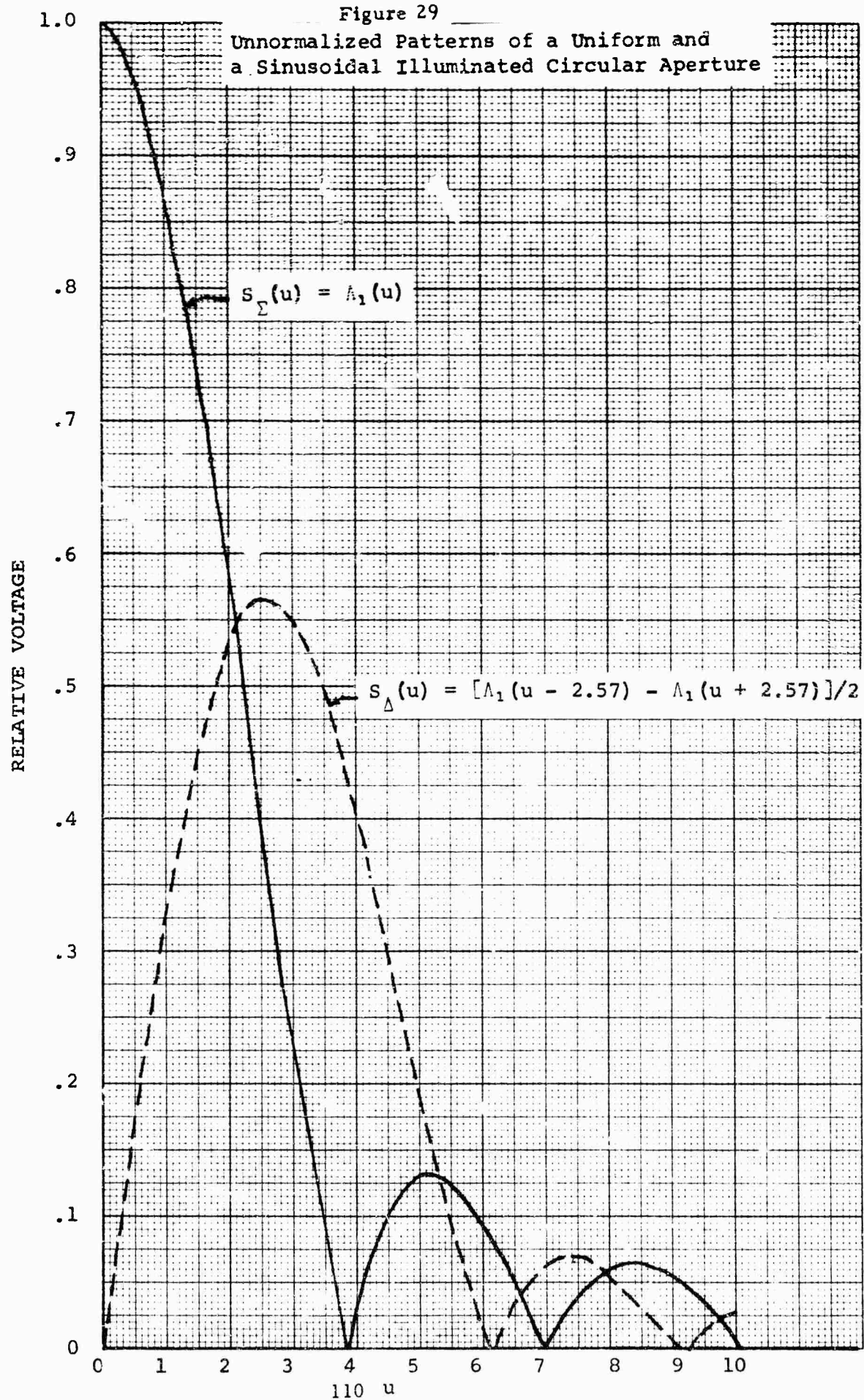
$$P_{rad} \propto a^2 \int_{-1}^1 \int_{-(1-\zeta^2)^{1/2}}^{(1-\zeta^2)^{1/2}} |f(\zeta, \eta)|^2 d\eta d\zeta \quad (46)$$

The unnormalized pattern and distribution functions are divided by a normalizing factor,  $\gamma$ . The normalized pattern and distribution functions are then given by:

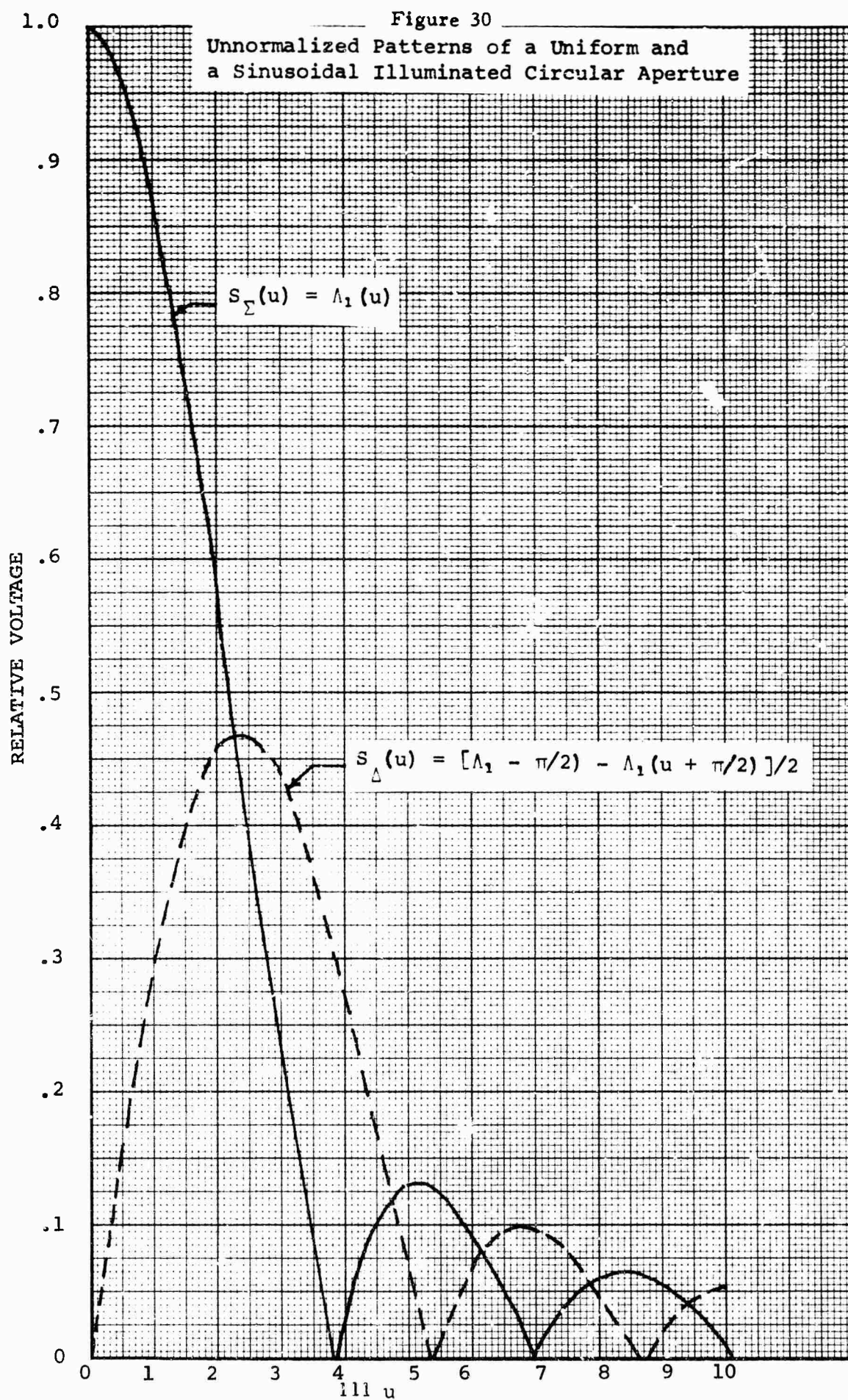
$$\begin{aligned} g_n(u) &= g_{un}(u)/\gamma \\ f_n(\zeta, \eta) &= f_{un}(\zeta, \eta)/\gamma \end{aligned} \quad (47)$$

It is now necessary to determine the normalizing factor,  $\gamma$ . The constant power radiated condition is satisfied if all the normalized distribution functions satisfy:

Figure 29







$$a^2 \int_{-1}^1 \int_{-(1-\zeta^2)^{1/2}}^{(1-\zeta^2)^{1/2}} |f_n(\zeta, \eta)|^2 d\eta d\zeta = k \quad (48)$$

where  $k$  is an arbitrary constant. Since  $k$  is arbitrary, it is convenient to assign it a value of  $\pi$ . It will be seen later that this has the effect of normalizing all the distributions to the uniform distributions case. The above equation becomes:

$$a^2 \int_{-1}^1 \int_{-(1-\zeta^2)^{1/2}}^{(1-\zeta^2)^{1/2}} |f_n(\zeta, \eta)|^2 d\eta d\zeta = \pi \quad (49)$$

Combining this with the expression for  $f_n(\zeta, \eta)$  results in:

$$\gamma^2 = a^2/\pi \int_{-1}^1 \int_{-(1-\zeta^2)^{1/2}}^{(1-\zeta^2)^{1/2}} |f_{un}(\zeta, \eta)|^2 d\eta d\zeta \quad (50)$$

Thus, to determine the normalizing factor, the above integral must be solved for each given distribution function. It is noticed that  $\gamma$  takes on different values for different distribution functions.

Since all of the distribution functions considered are independent of  $\eta$ , the expression for  $\gamma^2$  may be written:

$$\gamma^2 = 2a^2/\pi \int_{-1}^1 \sqrt{1-\zeta^2} |f_{un}(\zeta)|^2 d\zeta \quad (51)$$

Since  $|f_{un}(\zeta)|^2$  is always an even function, the integral may be reduced to:

$$\gamma^2 = 4a^2/\pi \int_0^1 \sqrt{1-\zeta^2} |f_{un}(\zeta)|^2 d\zeta \quad (52)$$

Due to the complexity of this integral, it was decided to evaluate the integral by graphical techniques. For each of the above distribution functions, the above expression  $\sqrt{1-\zeta^2} |f_{un}(\zeta)|^2$  was plotted for values of  $\zeta$  from zero to one. The area under the curve was found by means of a planimeter. With this, the value of  $\gamma$  can be determined for the various distributions functions.

Having determined the normalization factor, the normalized far-field pattern can now be found. Figures 31, 32, 33, 34, and 35 show the far-field patterns of the distribution functions discussed below, normalized to constant power radiated. Also, the boresight difference pattern slope must be normalized. The normalized on-axis difference slope is given by:

$$M(0) = M_{un}(0)/\gamma \quad (53)$$

Figure 36 gives the comparison of the normalization factors, and the unnormalized and normalized on-axis slopes for the various distributions discussed above. Also, presented is the relative on-axis difference slope  $M_r(0)$ . This is the on-axis difference slope relative to the maximum possible sum voltage. In this case, boresight voltage of the far-field pattern resulting from a uniformly illuminated circular aperture of radius  $a$  is used. Therefore,

$$M_r(0) = M(0)/S_\Sigma(0) \quad (54)$$

which for the distribution described above becomes:

$$M_r(0) = M(0)/\pi a^2 \quad (55)$$

In addition, the on-axis difference slope ratio,  $k_o$ , is presented. This is a ratio of the on-axis difference slope to the maximum possible difference slope (linear-odd distribution) and is expressed in decibels. Also, presented is the unnormalized and normalized difference mode peaks  $G_{un}$  and  $G$ , respectively. In addition, the normalized difference mode peaks are expressed in decibels,  $G_o$ , below the sum channel peak (uniform distribution).

Figure 31

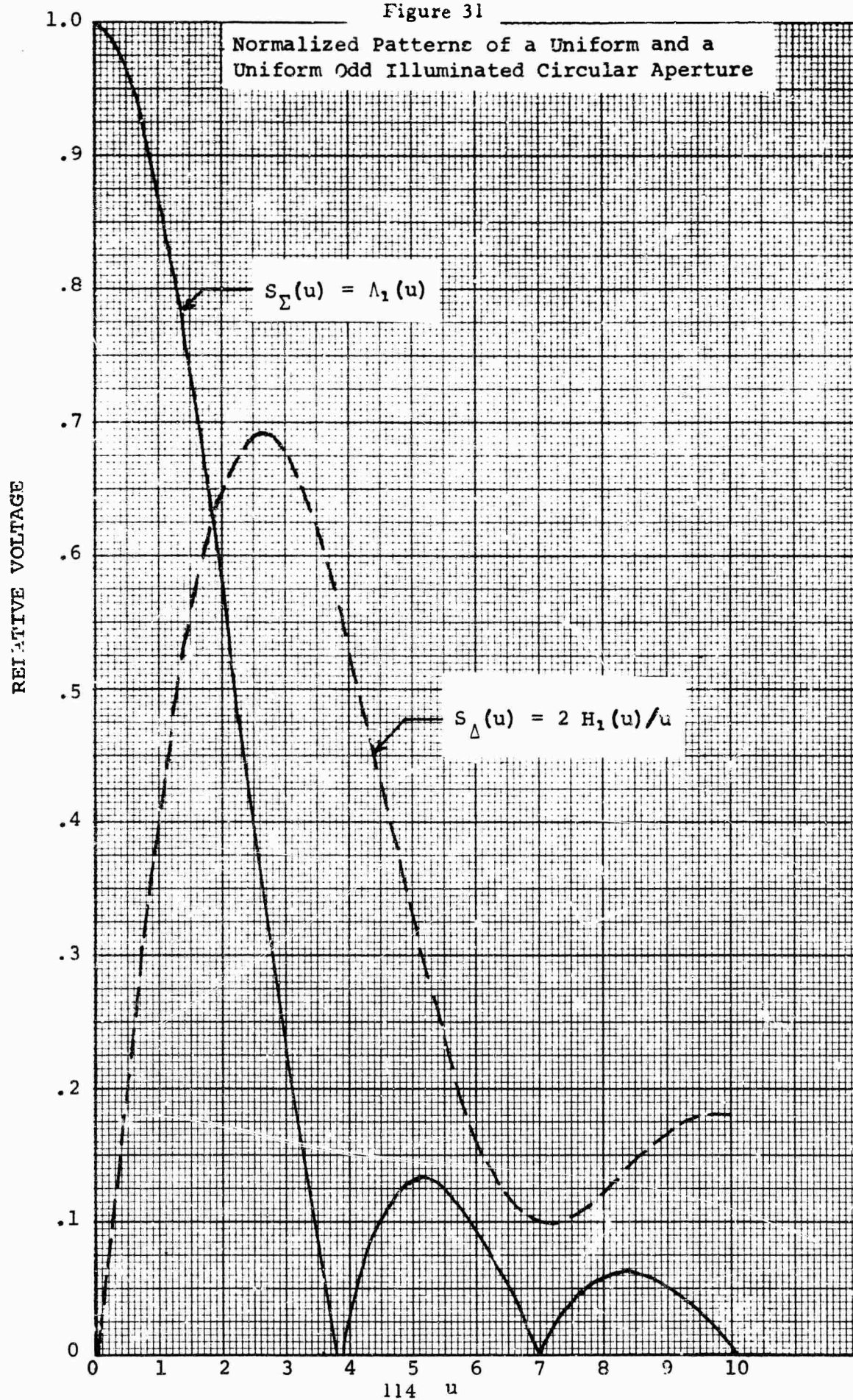




Figure 32

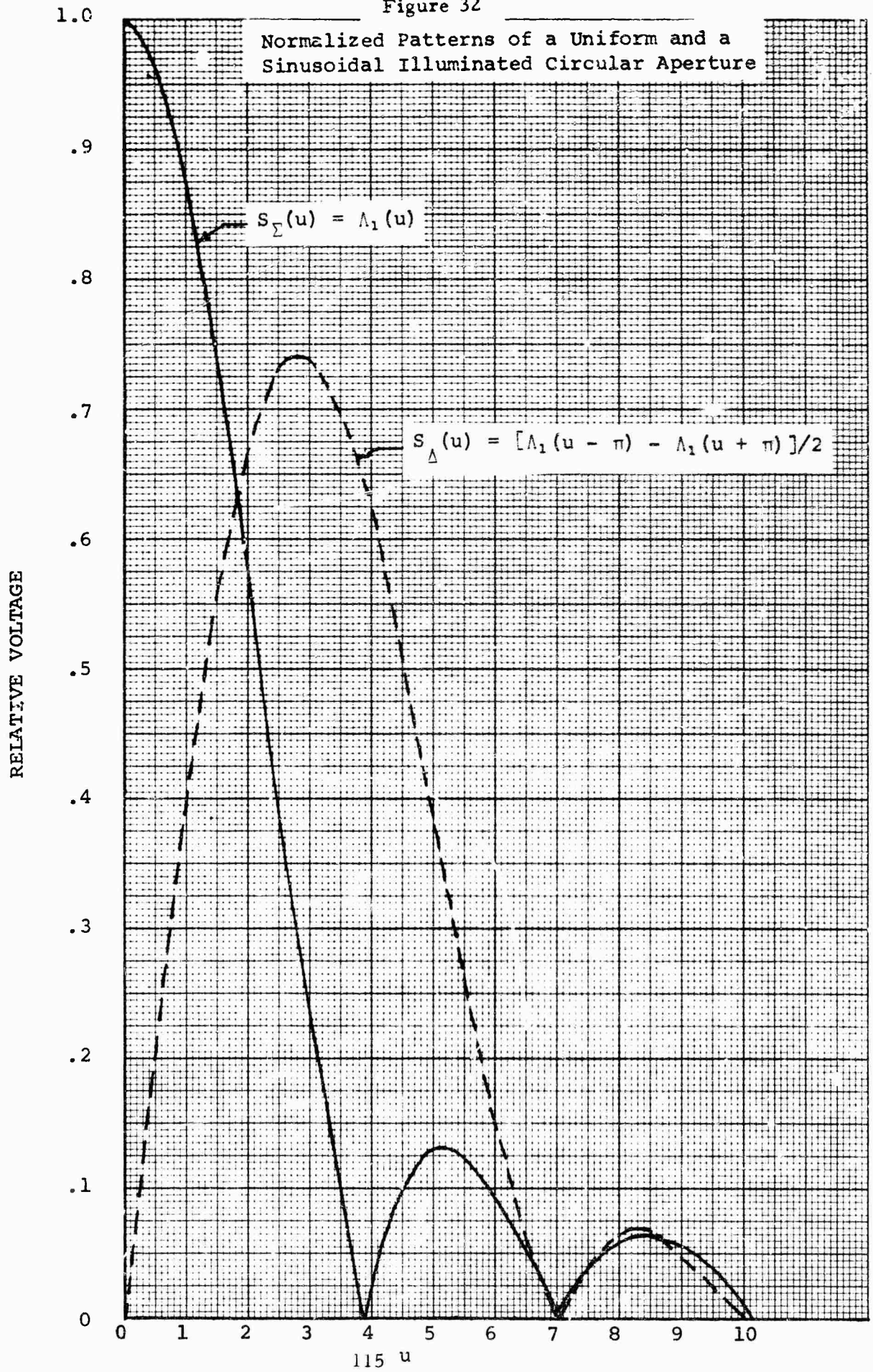
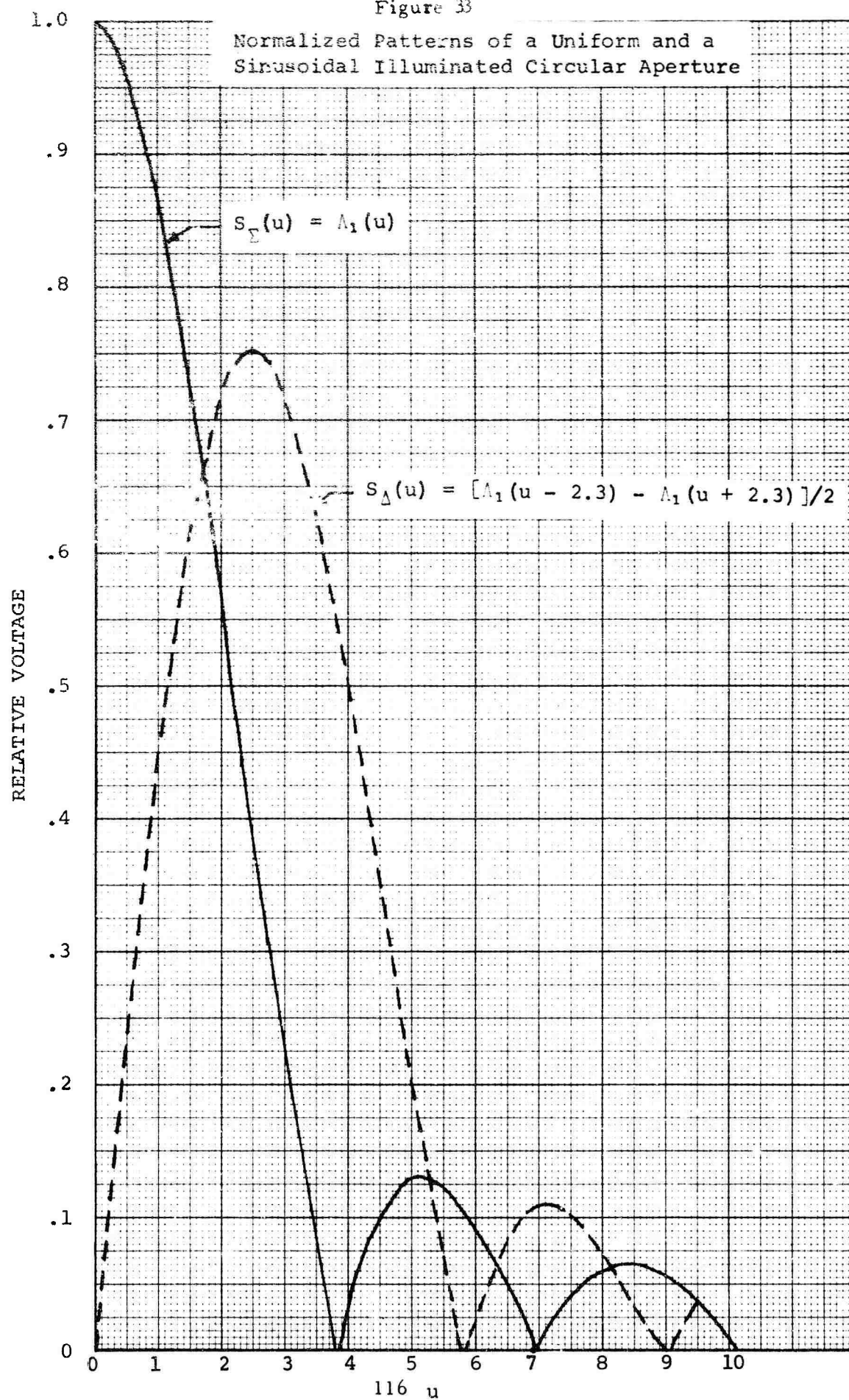


Figure 33



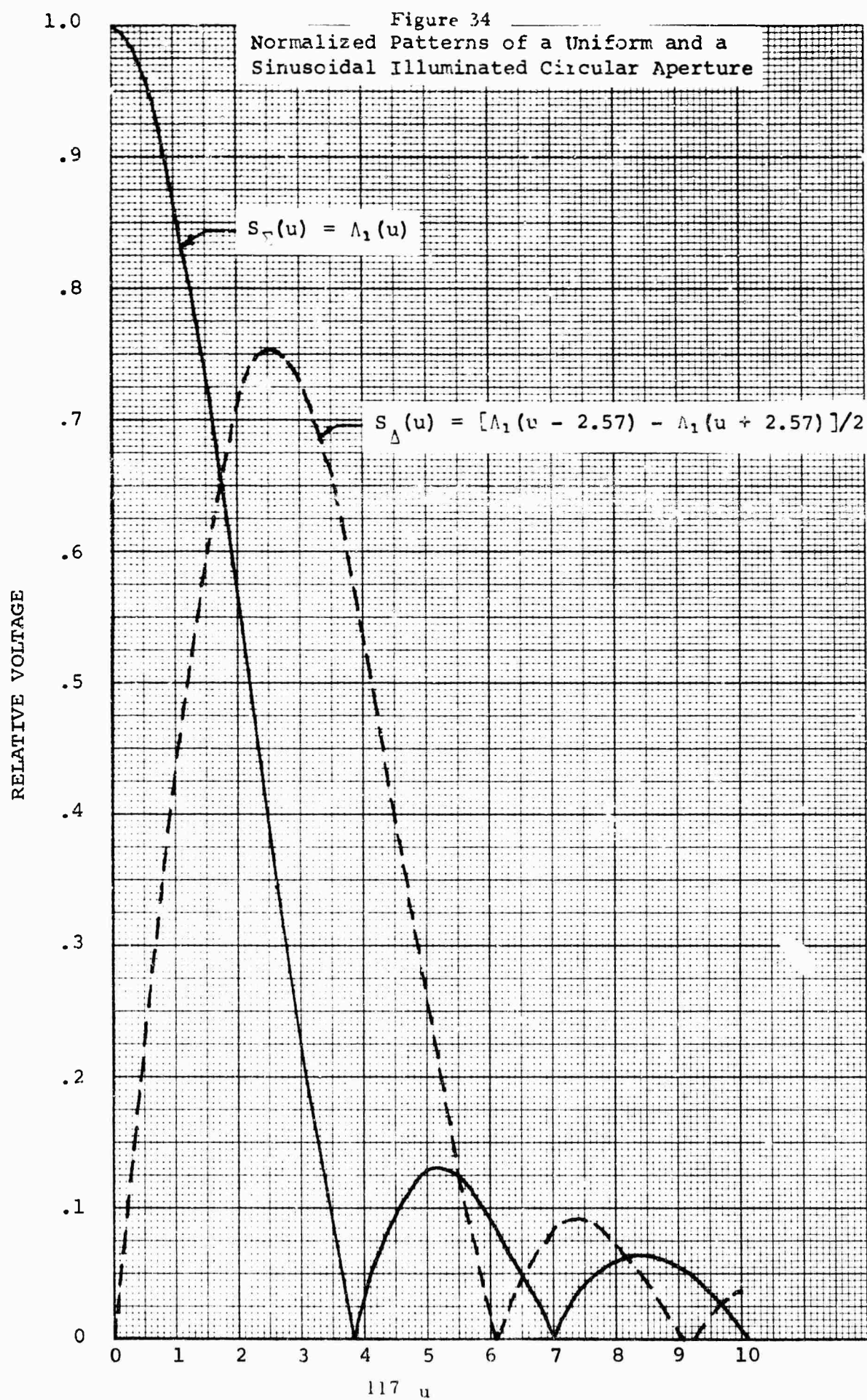




Figure 35

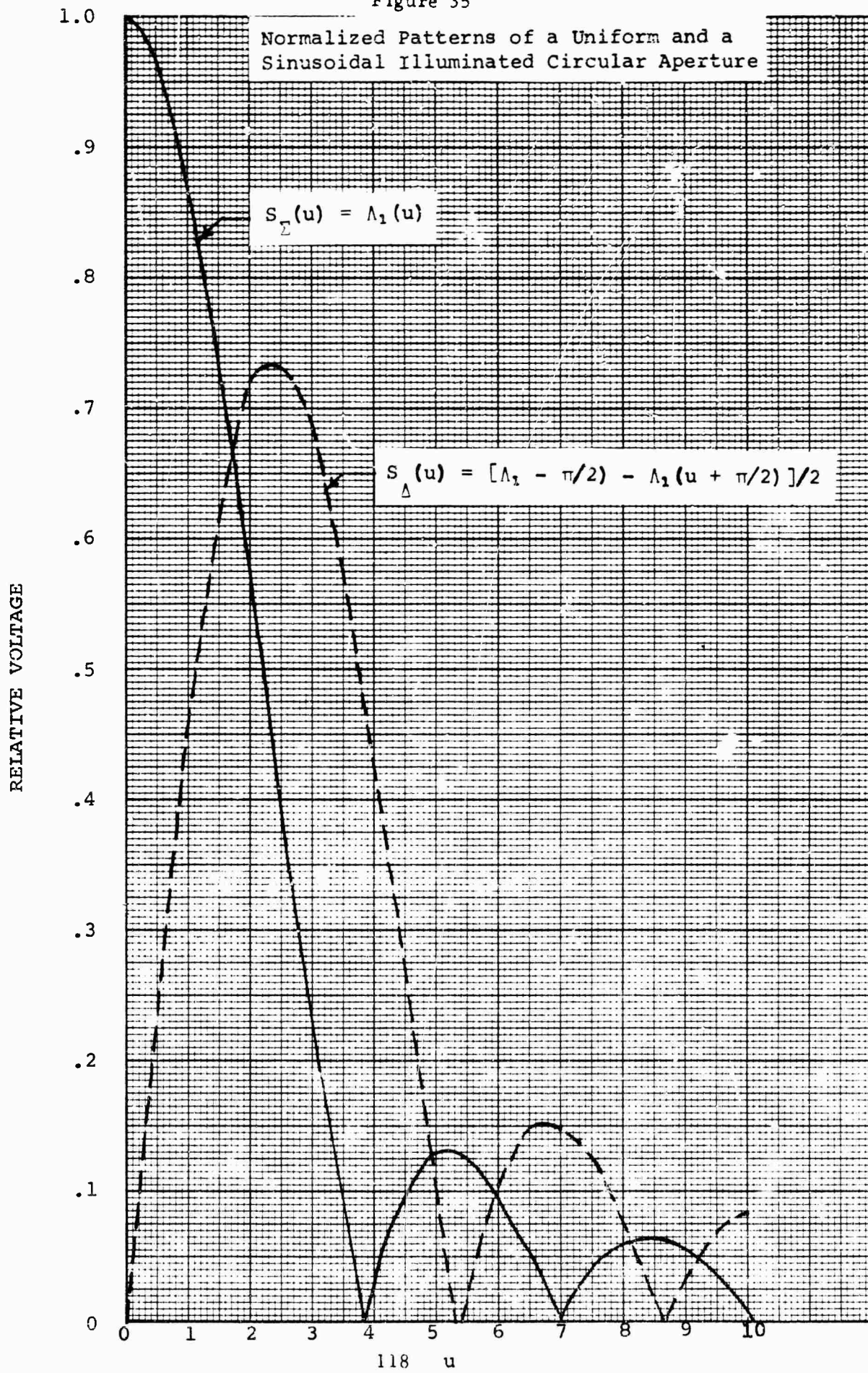

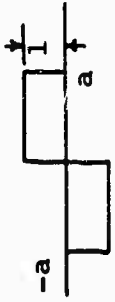








Figure 36 Comparison of Normalized and Unnormalized Functions

Distribution	$\frac{a}{\gamma}$	$M_{un}(0)$	$M_r(0)$	$M(0)$	$K_o$	$G_n$	$G$	$G_o$
	2.000	$.787a^2$	.501	1.574a	0.0 db			
	1.000	$1.333a^2$	.424	1.333a	-1.447 db	.692	.692	-3.35 db
	1.370	$.972a^2$	.424	1.332a	-1.452 db	.540	.740	-2.62 db
	1.344	$1.131a^2$	.484	1.520a	-.304 db	.560	.752	-2.48 db
	1.331	$1.132a^2$	.472	1.482a	-.523 db	.566	.753	-2.47 db
	1.571	$.999a^2$	.500	1.570a	-.022 db	.467	.734	-2.69 db

### 3. PHASE SENSING MONOPULSE

For the phase sensing monopulse system, two types of practical antenna configurations are considered. These are the square array and diamond array configurations of the "cloverleaf" antenna. A schematic representation of these two configurations is shown in Figure 37. For these configurations, the aperture shape will be normalized to an equivalent circular aperture. This is done in order that a true comparison can be made to the amplitude sensing monopulse system. In the following analysis, the element pattern of the array will be approximated by that obtained with a uniformly illuminated circular aperture which has an area equivalent to that of the element aperture. With this uniform illumination approximation, there is no problem of normalizing to constant power radiated since  $a/\gamma$  equals one for this case. The development of the relationships for the far-field radiation patterns and the on-axis difference pattern slope will be carried out simultaneously for the two types of array configurations.

Letting  $\Phi$  equal the phase delay due to the element separation we have

<u>Diamond Array</u>	<u>Square Array</u>	
$\Phi_{\Sigma} = (2\pi/\lambda) (D/2) \sin\theta$	$\Phi_{\Sigma} = (2\pi/\lambda) (D/\sqrt{2}) \sin\theta$	
$\Phi_{\Delta} = (2\pi/\lambda) D \sin\theta$	$\Phi_{\Delta} = (2\pi/\lambda) (D/\sqrt{2}) \sin\theta$	(56)

From array theory, the far-field radiation pattern of the array may be determined in terms of the element pattern,  $g(\theta)$ :

$$\begin{aligned}
 S_{\Sigma}(\theta) &= 4g(\theta) [(1 + \cos\Phi_{\Sigma})/2] & S_{\Sigma}(0) &= 4g(0) \cos(\Phi_{\Sigma}/2) \\
 S_{\Delta}(\theta) &= -2g(\theta) \sin(\Phi_{\Delta}/2) & S_{\Delta}(0) &= -4g(0) \sin(\Phi_{\Delta}/2)
 \end{aligned}
 \tag{57}$$

As seen from Figure 37, it is necessary to multiply the above voltage expressions by the appropriate value,  $1/2$  or  $\sqrt{2}/2$ , in order to conserve power through the antenna.

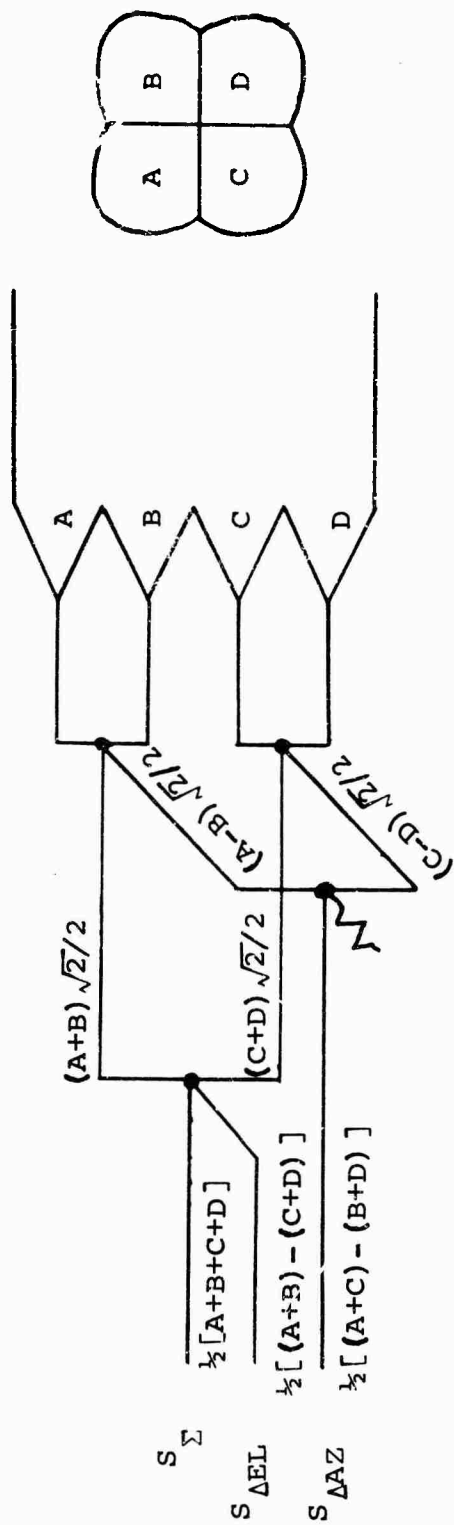


Figure 15-A. Square Array

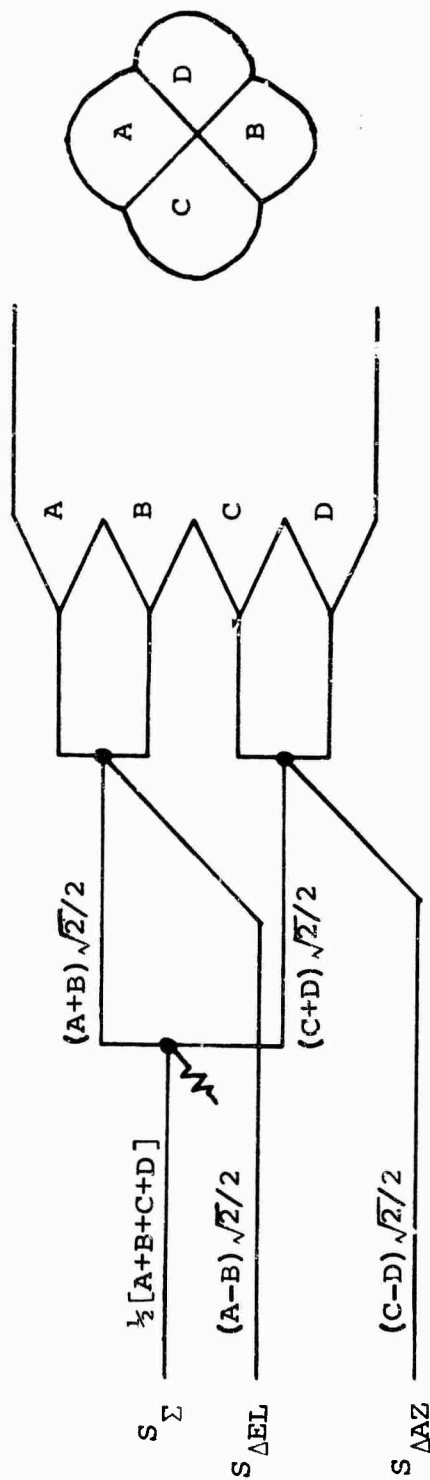


Figure 37 Diamond Array

<u>Diamond Array</u>	<u>Square Array</u>	
$S_{\Sigma}(\theta) = 2g(\theta) [(1 + \cos \theta_{\Sigma})/2]$	$S_{\Sigma}(\theta) = 2g(\theta) \cos(\theta_{\Sigma}/2)$	
$S_{\Delta}(\theta) = -\sqrt{2} g(\theta) \sin(\theta_{\Delta}/2)$	$S_{\Delta}(\theta) = -2g(\theta) \sin(\theta_{\Delta}/2)$	(58)

It is now desirable to make the following change in variable:

$$u' = (2\pi/\lambda) (D/2) \sin \theta \quad (59)$$

Also, the element far-field pattern will be approximated by that obtained with a circular aperture whose area is equivalent to that of the element. By simple geometry, it can be shown that the diameter of the equivalent circular aperture is given by .904D where D is the diameter of the main axis of the element aperture. With this approximation, the element pattern becomes:

$$g(u') = \pi (.904D/2)^2 \Lambda_1(u') \quad (60)$$

With these relationships, the equations for the far-field sum and difference patterns become:

<u>Diamond Array</u>	
$S_{\Sigma}(u') = \frac{1}{2} \pi (.904D)^2 \Lambda_1(u') [(1 + \cos u')/2]$	
$S_{\Delta}(u') = -(\sqrt{2}/4) \pi (.904D)^2 \Lambda_1(u') \sin u'$	(61)

<u>Square Array</u>	
$S_{\Sigma}(u') = \frac{1}{2} \pi (.904D)^2 \Lambda_1(u') \cos [(\sqrt{2}/2) u']$	
$S_{\Delta}(u') = -\frac{1}{2} \pi (.904D)^2 \Lambda_1(u') \sin [(\sqrt{2}/2) u']$	(62)

To normalize the "cloverleaf" antenna to an equivalent circular aperture, the following relationship is used:

$$D = 1.107a$$

where (a) is the radius of the equivalent circular aperture. Introducing the variable:

$$u = (2\pi/\lambda) a \sin \theta$$

results in:

$$u' = .553u$$

With this, the equations for the far-field sum and difference patterns are given by:

Diamond Array

$$S_{\Sigma}(u) = \frac{1}{2} \pi a^2 \Lambda_1(.553u) [(1 + \cos(.553u))/2] \quad (63)$$

$$S_{\Delta}(u) = -\frac{1}{2} \pi a^2 (\sqrt{2}/2) \Lambda_1(.553u) \sin(.553u)$$

Square Array

$$S_{\Sigma}(u) = \frac{1}{2} \pi a^2 \Lambda_1(.553u) \cos[(\sqrt{2}/2).553u] \quad (64)$$

$$S_{\Delta}(u) = -\frac{1}{2} \pi a^2 \Lambda_1(.553u) \sin[(\sqrt{2}/2).553u]$$

Simplifying the above equations, they become:

Diamond Array

$$S_{\Sigma}(u) = \frac{1}{2} \pi a^2 \Lambda_1(.553u) [(1 + \cos(.553u))/2] \quad (65)$$

$$S_{\Delta}(u) = -\frac{1}{2} \pi a^2 (\sqrt{2}/2) \Lambda_1(.553u) \sin(.553u)$$

Square Array

$$S_{\Sigma}(u) = \frac{1}{2} \pi a^2 \Lambda_1(.553u) \cos(.391u) \quad (66)$$

$$S_{\Delta}(u) = -\frac{1}{2} \pi a^2 \Lambda_1(.553u) \sin(.391u)$$

Using these relationships, the sum and difference patterns are calculated and shown in Figure 38 and 39 for the two antenna configurations. As seen by Figures 38 and 39, the peak of the difference patterns for the diamond and square arrays are -5.25 dB and -3.57 dB, respectively.

To determine the on-axis slope of the above difference patterns, the following relationship is used:

$$M(0) = \left| \frac{d}{du} [S_{\Delta}(u)]_{u=0} \right| \quad (67)$$

Carrying out this operation and utilizing the fact that  $\Lambda_1(.553u)$  is a maximum at  $u = 0$  which gives  $\Lambda_1'(0) = 0$ , the following results:

<u>Diamond Array</u>	<u>Square Array</u>	
$M(0) = \frac{1}{2}(1.228)a$	$M(0) = \frac{1}{2}(1.228)a$	
$M(0) = .614a$	$M(0) = .614a$	(68)

The relative on-axis difference slope, given by:

$$M_r(0) = \left| \frac{d}{du} [S_{\Delta}(u)]_{u=0} \right| / S_{\Sigma}(0) \quad (69)$$

can now be determined.

<u>Diamond Array</u>	<u>Square Array</u>	
$M_r(0) = .391$	$M_r(0) = .391$	(70)

It is interesting to note that the on-axis difference slope is the same for both configurations of the "cloverleaf" antenna.

The above relative boresight difference slopes can be compared directly to those found previously for the amplitude sensing monopulse system. However, in order to compare the actual on-axis difference slope values,  $M(0)$ , and the sum and difference patterns, the results found for the amplitude sensing monopulse must be modified.

Figure 38

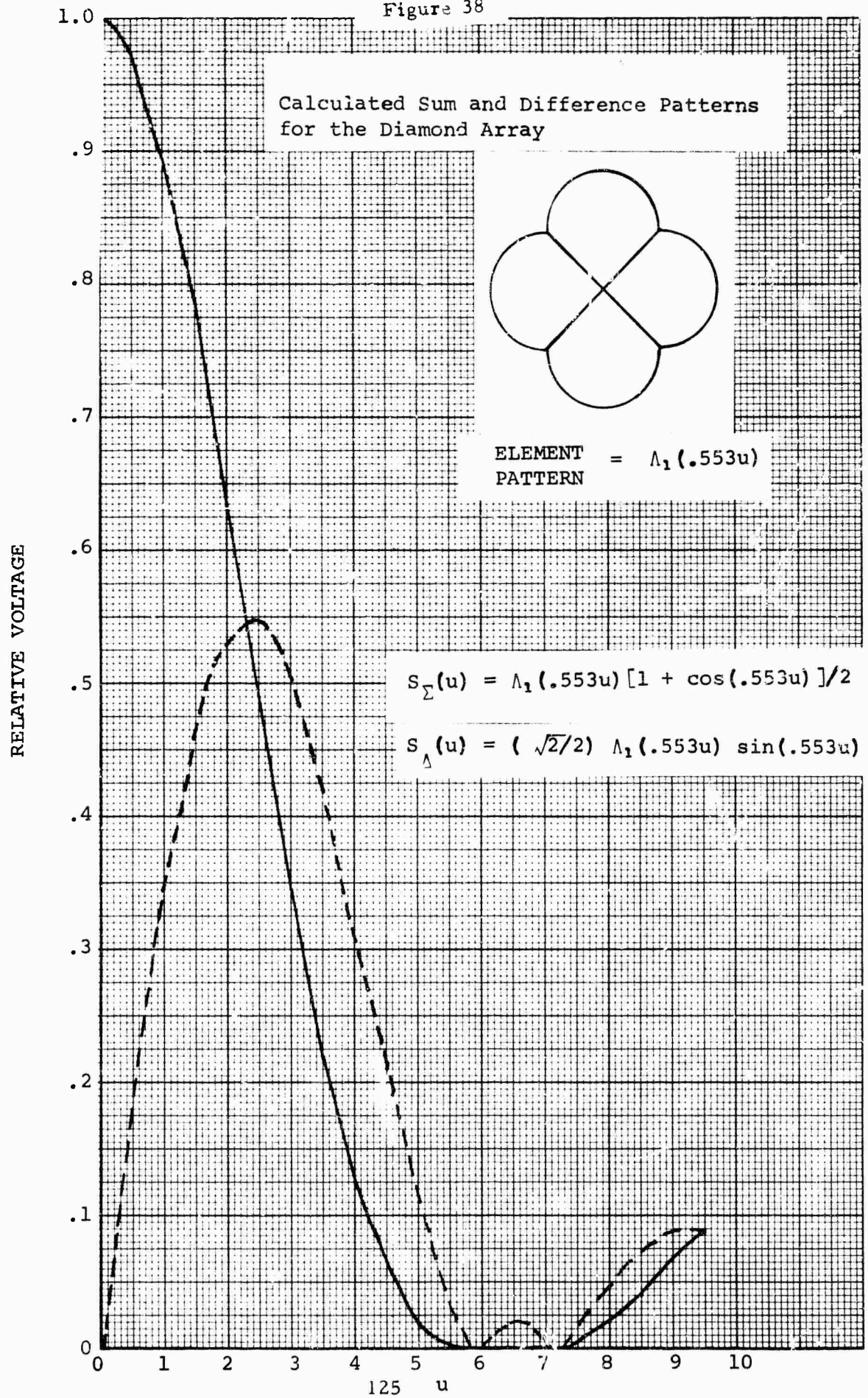
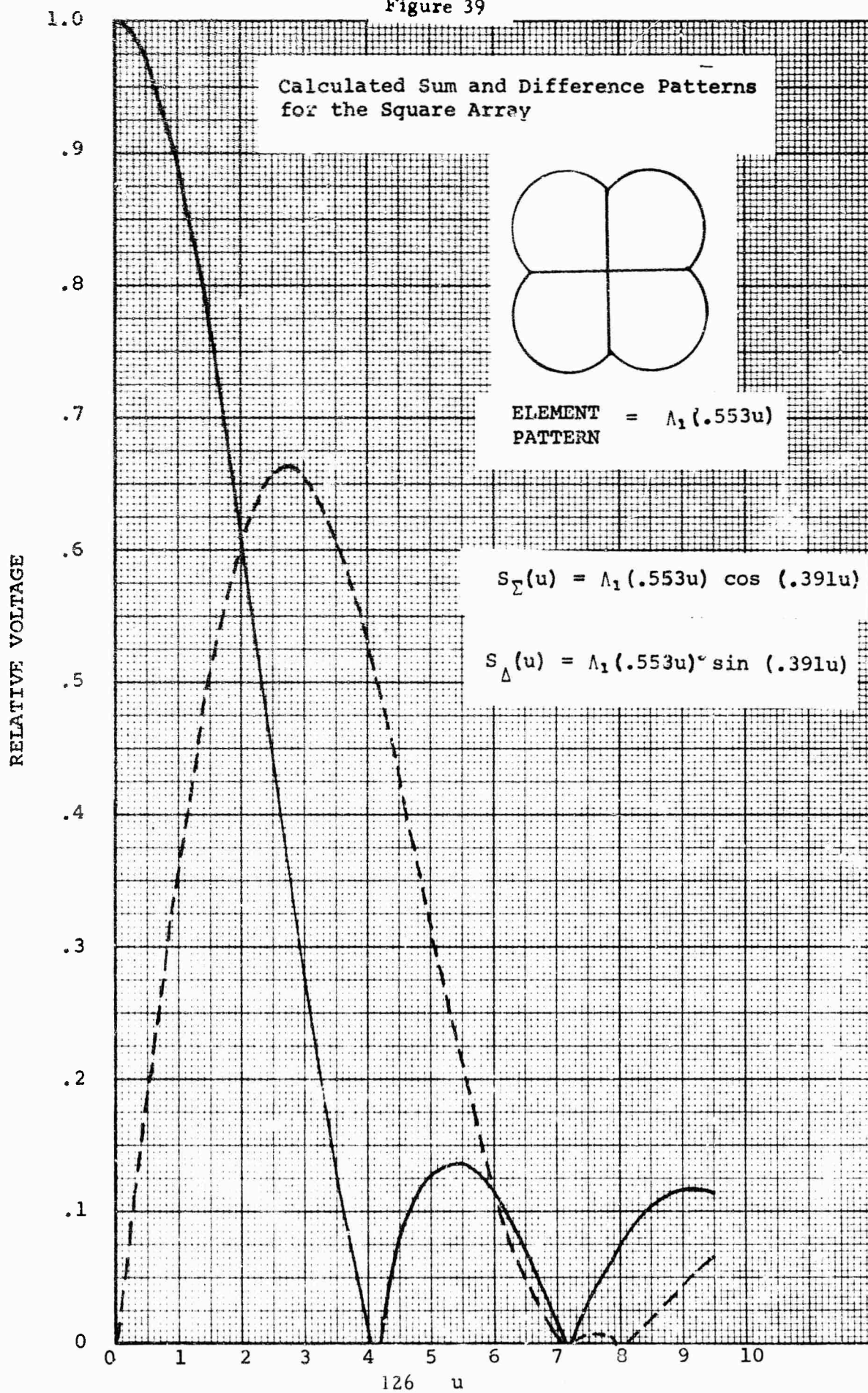


Figure 39





When calculating the far-field from the various aperture distributions, no stipulation was made on how these distributions were formed. In forming these distributions, a system of hybrids as shown in Figure 27 is used. As was done for the phase sensing monopulse, the sum and difference patterns and on-axis difference slopes of the amplitude sensing case must be multiplied by a factor of  $1/2$  to conserve power through the antenna.

## COMPARISON

With the amplitude sensing monopulse relationships found above multiplied by a factor of  $1/2$ , a direct comparison of the amplitude sensing and phase sensing monopulse systems discussed can be made. Of primary concern is the difference mode slope at boresight. As seen from the previous paragraphs, with the proper choice of ideal aperture distribution function the on-axis difference pattern slope of the amplitude monopulse system exceeds that obtained with the phase sensing monopulse systems discussed above. However, the only meaningful comparison that can be made is with the full sine curve illumination function. This is the only theoretical aperture distribution described above that can be related directly to a practical aperture illumination. All the other distribution functions could not be obtained in a practical system without a large amount of spillover. With this excess spillover the constant power radiated constraint applied above would be violated and on-axis slope and the difference peak gain obtained with the practical system would be less than the theoretical values obtained above. Thus, the full sine curve illumination is the only distribution function of those given above which gives a good theoretical representation of a practical amplitude monopulse system. With this, the on-axis difference pattern slope obtained with a practical amplitude monopulse sensing system ( $M(0) = .666a$ ) exceeds that of the practical phase sensing monopulse system ( $M(0) = .614a$ ) discussed above by a small amount.

Although the on-axis difference slope obtained with a practical amplitude monopulse sensing system (uniform and full sine curve distribution functions) exceeds that of a practical phase sensing monopulse system, it must be remembered that in an actual amplitude sensing monopulse system the sum and difference aperture distribution functions are formed by the same feed mechanism. When this is done there is usually a compromise between the sum channel gain and the on-axis difference pattern slope. Thus, the ability to form both the uniform amplitude distribution and the full sine curve distribution would be a difficult task without introducing some spillover which would lower the on-axis difference pattern slope. However, with the phase sensing monopulse system both the sum channel gain and the on-axis difference slope vary the same with regards to the element's aperture distribution.

The element distribution (uniform) which gives the maximum sum channel gain also gives the best on-axis difference slope and there is no need to compromise between the two as there is with the amplitude sensing monopulse system. Therefore, in an actual system one could normally expect to obtain a greater on-axis difference slope with the phase sensing monopulse system than with an amplitude sensing monopulse system.

## 5. EVALUATION OF FAR-FIELD PATTERN

To determine the far-field difference pattern in the principle plane ( $\phi = 0^\circ$ ) of a circular aperture antenna of radius  $a$ , the following relationship is used:

$$S_{\Delta}(u) = j4a \int_0^1 \sqrt{1-\zeta^2} f_o(\zeta) \sin(u\zeta) d\zeta \quad (71)$$

where  $u = (2\pi/\lambda)a \sin \theta$  and  $f_o(\zeta)$  is the odd aperture distribution function. For the case of  $f_o(\zeta) = \sin(u_1 \zeta)$ , the diffraction integral becomes:

$$S_{\Delta}(u) = j4a \int_0^1 \sqrt{1-\zeta^2} \sin(u_1 \zeta) \sin(u\zeta) d\zeta \quad (72)$$

Using the following trigonometric identity,

$$2 \sin x \sin y = \cos(x-y) - \cos(x+y) \quad (73)$$

the integral may be written as:

$$S_{\Delta}(u) = j2a^2 \left\{ \int_0^1 \sqrt{1-\zeta^2} \cos(u-u_1)\zeta d\zeta - \int_0^1 \sqrt{1-\zeta^2} \cos(u+u_1)\zeta d\zeta \right\} \quad (74)$$

Utilizing the following relationship:

$$J_1(z) = (2z/\pi) \int_0^1 \sqrt{1-t^2} \cos(zt) dt \quad (75)$$

the above integrals become:

$$g(u) = j\pi a^2 \left\{ \frac{J_1(u-u_1)}{(u-u_1)} - \frac{J_1(u+u_1)}{(u+u_1)} \right\} \quad (76)$$

This may be written as:

$$g(u) = j\pi a^2 [ \Lambda_1(u-u_1) - \Lambda_1(u+u_1) ] / 2 \quad (77)$$

The slope of  $g(u)$  at  $u = 0$  can now be determined

$$M = \frac{d}{du} [g(u)] \quad (78)$$

$$M = j\pi a^2 \left\{ \frac{d}{du} [(u-u_1)^{-1} J_1(u-u_1)] - \frac{d}{du} [(u+u_1)^{-1} J_1(u+u_1)] \right\}$$

Noting that,

$$\frac{d}{dx} [x^{-n} J_n(x)] = -x^{-n} J_{n+1}(x) \quad (79)$$

The above expression becomes:

$$M = j\pi a^2 \left\{ \frac{J_2(u+u_1)}{(u+u_1)} - \frac{J_2(u-u_1)}{(u-u_1)} \right\} \quad (80)$$

Evaluating this at  $u = 0$  and realizing that  $J_2(x) = J_2(-x)$ ,

$$M(0) = j2\pi a^2 \frac{J_2(u_1)}{u_1} \quad (81)$$

which may be written as:

$$M(0) = j(\pi/4) a^2 u_1 \Lambda_2(u_1) \quad (82)$$

## SECTION VII

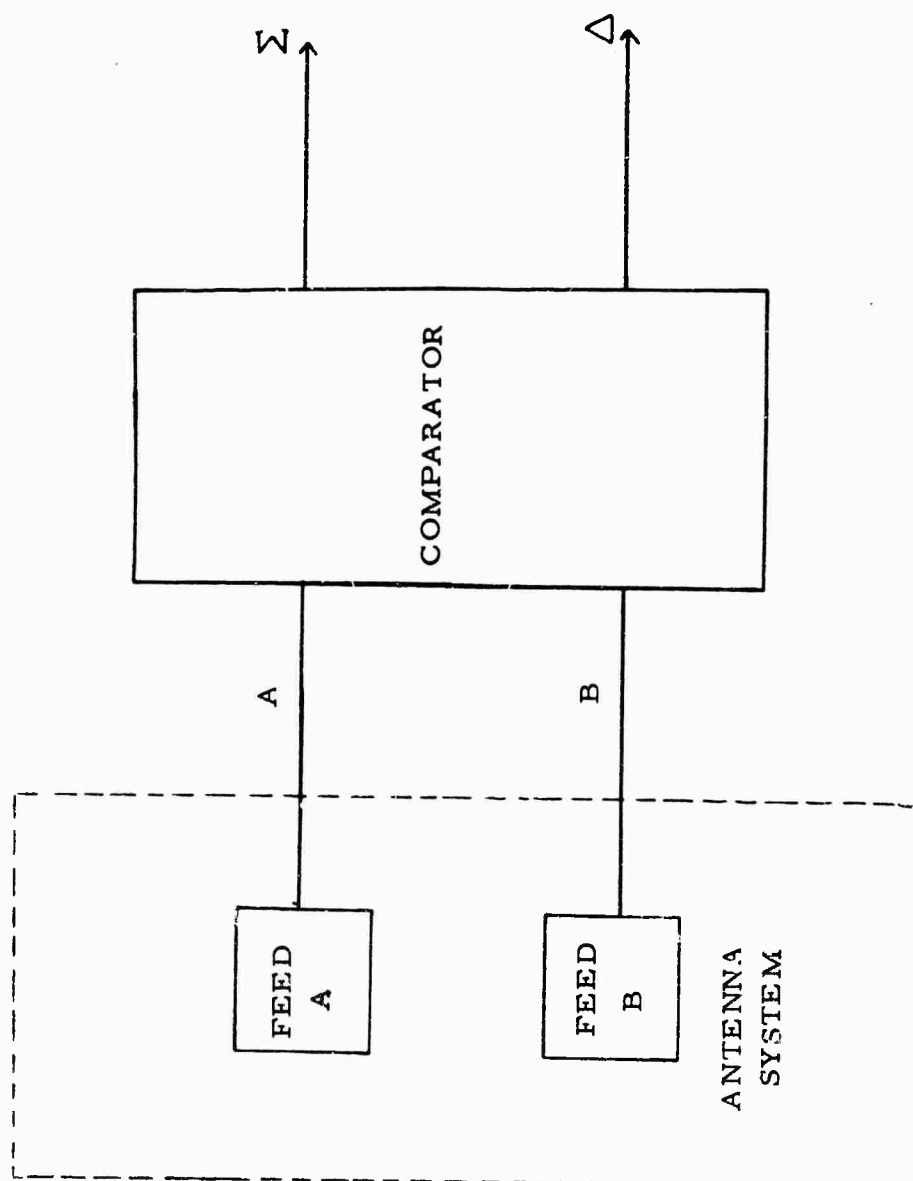
### AMPLITUDE AND PHASE ERRORS IN MONOPULSE SYSTEMS

Microwave monopulse antenna systems are generally characterized by a feed and reflector system followed by a comparator. The comparator outputs include main beam (sum channel) signals and error channel (difference channel) signals. The sum channel carries the basic communications information (or radar signal in the case of radar systems) and the difference channels are used to obtain antenna pointing information. Typical characteristics of monopulse systems, in particular amplitude sensing and phase sensing systems, are analyzed in detail in a two-part article by Cohen and Steinmetz, (10). Specific antenna characteristics were assumed, but the basic method of analysis is general and would be useful in determining the parameters of any monopulse system characterized by an antenna system and comparator.

The purpose of this section is to summarize the general effects of pre-comparator errors and post-comparator errors. A simplified model will be used to demonstrate the basic effects, but a rigorous analysis will not be made. The Cohen and Steinmetz article, for example, would furnish much more detail, including quantitative results. The pre- and post-comparator errors and their effects could be analyzed as required for specific configurations using the same techniques. The simplified model provides a degree of insight which is difficult to obtain from the more detailed exact model.

Throughout this section a one-dimensional monopulse system will be considered. In conventional systems, two orthogonal axes are used to obtain two-dimensional tracking signals. Since the two error channels are orthogonal, they can be treated individually without loss of generality. It will be further assumed that the feed-reflector system provides two outputs which enter the comparator. The comparator then supplies two outputs, namely the sum (representing the main beam of the antenna) and the difference (containing angular pointing information). When more than two feeds are considered, their combination errors can be evaluated in a similar manner. When a two-channel monopulse is considered (i.e., the two error channels are placed on a single channel by adding the signals in phase quadrature) the conclusions reached in this section are not valid. This problem is discussed in detail in Section XIII.

Consider the two feed outputs, as shown in Figure 40, to be given by:



BASIC MONOPULSE MODEL

Figure 40

$$\begin{aligned}
A &= \sqrt{2} G_A(u) \cos [\omega t + \phi_A(u)] \\
B &= \sqrt{2} G_B(u) \cos [\omega t + \phi_B(u)]
\end{aligned}
\tag{83}$$

where  $u$  is a normalized function of the angle between boresight and the signal source

$G_A, G_B$  are gain functions

$\phi_A, \phi_B$  are phase functions

$\omega$  is the operating frequency

All quantities are real, but not necessarily independent.

The feed signals are fed to the comparator, typically a hybrid (magic-tee) network. For the two cases of most general interest, amplitude monopulse and phase monopulse, the  $\Sigma$  output is the sum  $A + B$  and the  $\Delta$  output is the difference  $A - B$ , modified by a  $\sqrt{2}$  factor to conserve power. The problem of interest is the effect of gain and phase errors, so a gain factor  $K$  and a phase shift  $\theta$  will be associated with the comparator processing,

Then,

$$\begin{aligned}
\begin{matrix} \Sigma \\ \Delta \end{matrix} &= K_A G_A(u) \cos [\omega t + \phi_A(u) + \theta_A] \\
&\quad \pm K_B G_B(u) \cos [\omega t + \phi_B(u) + \theta_B]
\end{aligned}
\tag{84}$$

These equations can be rewritten as,

$$\begin{matrix} \Sigma \\ \Delta \end{matrix} = C \left[ \cos \omega t \pm K G(u) \cos [\omega t + \phi(u) + \theta] \right]
\tag{85}$$

Where  $C = K_A G_A(u)$  is a gain "constant", dependent upon  $u$

$\theta_A = -\phi_A(u)$  is an arbitrary phase constant

$\phi(u) = \phi_B(u) - \phi_A(u)$  is the phase difference between the signal received at the two feeds.

$\theta = \theta_B - \theta_A$  is the differential phase shift (error) in the comparator.

$K = K_B/K_A$  is the ratio of the pre-comparator gains in the two channels.

$G(u) = G_B(u)/G_A(u)$  is the ratio of the magnitudes of the two feed signals.

Using trigonometric identities, equation (85) can be rewritten as

$$\sum_{\Delta} = C \left[ \begin{aligned} &(1 \pm KG(u) \cos [\phi(u) + \theta]) \cos \omega t \\ &\pm (KG(u) \sin [\phi(u) + \theta]) \sin \omega t \end{aligned} \right] \quad (86)$$

It should be noted that equation (86) separated the amplitude functions, phase functions, and orthogonal time functions, so each effect can be independently determined. In practice, ideal amplitude monopulse systems do not exist, but they can be usefully approximated by considering  $G$  to carry the pointing information. Similarly, a pure phase monopulse system can be approximated by assuming  $G$  to be independent of  $u$ .

The case of most interest at present is operation near boresight. Under these conditions:

$$K \rightarrow 1$$

$$G(u) \rightarrow 1$$

$$\phi(u) \rightarrow 0$$

$$\theta \rightarrow 0$$

When all four quantities approach their respective design goals, the sum output is

$$\sum = 2 C \cos \omega t \quad (87)$$

Amplitude and phase variations would, of course, alter the sum channel output and the effects can be quantitatively evaluated using equation (86).

The difference channel is of much greater interest since its output varies rapidly as amplitude and phase variations are introduced. The conditions for zero output on the difference channel are

$$\begin{aligned} KG(u) \cos \left( \vartheta(u) + \theta \right) &= 1 \\ \text{and} \quad KG(u) \sin \left( \vartheta(u) + \theta \right) &= 0 \end{aligned} \quad (88)$$

Due to the orthogonality of the terms, local minima will occur when each term is "independently" minimized. These effects are more easily seen when a specific sensing system is considered. For example, in a phase-sensing monopulse,  $G$  is essentially independent of  $u$  and the pointing information is carried in  $\vartheta(u)$ , the relative phase of the incoming signal. Then, the second equation in (88) is the most important factor for small changes in pointing angle; i.e., to obtain a null we required that

$$\vartheta(u) + \theta = 0 \quad (89)$$

Thus, a small phase shift  $\theta$  prior to the comparator will result in a boresight shift, an amount such that equation (89) is satisfied.

Examining the first term of (88), we find that the output is an even function of the angle  $\vartheta(u) + \theta$ . Then, to a first approximation, the boresight shift does not alter this term. An amplitude shift, from the ideal value of  $KG = 1$  would cause a minimum rather than a null. Thus, a magnitude of

$$|\Delta| = |C(1 - KG)| \quad (90)$$

occurs due to amplitude errors, when the system is on boresight. The ratio of this boresight magnitude to the peak value of  $|\Delta|$ , as pointing angle  $u$  is varied, is the nulldepth of the system. Smaller values of null depth (better nulls) require better amplitude balance.

The phase-sensing system can be summarized as follows: pre-comparator phase errors cause boresight errors in direct proportion (as a function of normalized pointing angle  $u$ ); pre-comparator amplitude errors cause null depth variations (imperfect nulls). In this simple analysis, second-order effects have been ignored. This is normally a good assumption, since large pointing errors are not of general interest because they result in significant loss in sum channel gain.

Analagous results can be obtained for an amplitude-sensing system using equation (88). In an ideal amplitude system,  $\vartheta$  is independent of  $u$  and  $G(u)$  contains the pointing information. Then, the first equation (88) is the predominant function for determining boresight angle. The cosine



function changes very slowly for small arguments, so the boresight is essentially determined when

$$KG(u) = 1 \quad (91)$$

Thus, pre-comparator amplitude unbalance ( $K \neq 1$ ) results directly in boresight shift ( $G(u) \neq 1$ ).

The second equation of (88) varies most rapidly with the term  $\sin [\phi + \theta]$ . A null occurs when  $\phi + \theta = 0$ . Pre-comparator phase errors result in an imperfect null with a magnitude approximately given by

$$|\Delta| \doteq |CK G(u) \sin \theta| \doteq |\theta| \quad (92)$$

where  $\theta$  is in radians of phase error. As before, the ratio of minimum amplitude to maximum amplitude is known as the null depth. Better null depths are obtained with better pre-comparator phase matching.

The amplitude-sensing system can be summarized as follows: pre-comparator amplitude unbalance results directly in boresight shifts; pre-comparator phase errors cause null depth variations.

The boresight errors and null depths can be evaluated using the equations developed here when the antenna functions  $G(u)$  and  $\phi(u)$  are known. The qualitative effects have been discussed, and show the pre-comparator errors of a type like the sensor (i.e., amplitude unbalance in an amplitude-sensing monopulse) cause boresight pointing errors, whereas, pre-comparator errors of the opposite type from the sensor cause imperfect nulls at boresight. In the event a different sensor is used (dependent on both phase and amplitude), the effects of pre-comparator errors can be evaluated in an analogous manner. The two major effects will generally be boresight shifts and null-depth variations with magnitudes in proportion to the pre-comparator errors.

In the above derivation,  $\omega$  was treated as a constant. In general,  $\omega$  can be a function of time (e.g., an angle modulated signal). As long as the spectrum occupied by  $\omega$  is narrow compared to the average operating frequency, the results are unaltered. This notation will be maintained in the following discussion of post-detection effects.

The effects of post-detection errors are highly dependent upon the receiver technique and the mode of detection. The problem which will be considered here is a full monopulse (three channel receiver) with a cross-correlation detector (a multiplier). The results are identical when time quadrature sampling is used in a pseudo-monopulse system.

The sum and difference channel signals are given in equation (86). If the sum channel gain and phase are arbitrarily selected with respect to the difference channel, the sum channel can be rewritten as

$$\Sigma = C \left[ (1 + KG \cos \psi) \cos \omega t - KG \sin \psi \sin \omega t \right] \quad (93)$$

where

$$\psi = \vartheta(u) + \theta$$

and for brevity the  $u$  dependence of  $G$  is not written.

The difference channel is assumed to undergo a gain and phase shift with respect to the sum channel. Then,

$$\Delta = C' \left[ (1 - KG \cos \psi) \cos (\omega t + \gamma) + KG \sin \psi \sin (\omega t + \gamma) \right] \quad (94)$$

where  $C'/C$  is the difference channel gain with respect to the sum channel and  $\gamma$  is the phase shift of the difference channel with respect to the sum channel.

Using trigonometric identities, equation (94) can be rewritten as:

$$\Delta = C' \left\{ \left[ (1 - KG \cos \psi) \cos \gamma + KG \sin \psi \sin \gamma \right] \cos \omega t + \left[ - (1 - KG \cos \psi) \sin \gamma + KG \sin \psi \cos \gamma \right] \sin \omega t \right\} \quad (95)$$

The means for obtaining pointing information will now be specified as a correlation detection. Other kinds of detection would in general, result in different post-comparator error effects. The correlator is simply a multiplier followed by a low pass filter. The effect of the filter is to remove double frequency components (and, in practice, to remove leakage of the fundamental). The action of the correlator can be easily seen by noting that the multiplication of sum and difference channels results in three kinds of terms  $\cos^2 \omega t$ ,  $\sin^2 \omega t$ , and  $\cos \omega t \sin \omega t$ .

Using the identities:

$$\begin{aligned} 2 \cos^2 \omega t &= 1 + \cos 2\omega t \\ 2 \sin^2 \omega t &= 1 - \cos 2\omega t \\ 2 \sin \omega t \cos \omega t &= \sin 2\omega t \end{aligned} \quad (96)$$

it is apparent that only the constants are of importance, since the  $2\omega t$  terms are removed by the low-pass filter. The resultant pointing angle output,  $e_A$ , in an amplitude monopulse system is given by:

$$e_A = \frac{CC'}{2} \left\{ \left[ 1 - (KG)^2 \right] \cos \gamma + 2 KG \sin \psi \sin \gamma \right\} \quad (97)$$

In the absence of pre-comparator phase shifts,  $\psi = 0$  and

$$e_A = \frac{CC'}{2} \left[ 1 - (KG)^2 \right] \cos \gamma \quad (98)$$

Thus, the gain (slope of the error signal as a function of pointing angle) is modified by  $C'$ , the gain factor in the error channel, and is reduced by  $\cos \gamma$ , where  $\gamma$  is the post-comparator phase error.

Referring back to equation (97), the effect of pre-comparator and post-comparator phase shifts is seen to be of second order. It can be important near boresight, however, since a pointing error results. Bore-sight occurs when,

$$\left[ 1 - (KG)^2 \right] \cos \gamma + 2 KG \sin \psi \sin \gamma = 0 \quad (99)$$

It is apparent that the gain loss is relatively small for rather large phase errors, since the two sine factors are multiplied together. This term is generally of importance only when high pointing accuracy is required (e.g., in the radar case).

The pointing angle output,  $e_p$ , in a phase sensing system is found in a similar manner. A  $90^\circ$  phase shift is introduced in the difference channel with respect to the sum channel prior to the correlator, but otherwise the operation is identical. The filtered output is

$$e_p = \frac{CC'}{2} \left\{ \left[ (KG)^2 - 1 \right] \sin \gamma + 2 KG \sin \psi \cos \gamma \right\} \quad (100)$$

In this case the second term is the basic pointing signal, and the first term is a (second order) error signal. Thus, when the pre-comparator amplitude errors are zero ( $KG = 1$ ), the expression reduces to:

$$e_p = CC' \sin \psi \cos \gamma \quad (101)$$

As in the amplitude monopulse case, the gain (slope) is modified by  $C'$  and by  $\cos \gamma$ .

Boresight occurs when,

$$\left[ (KG)^2 - 1 \right] \sin \gamma + 2 KG \sin \psi \cos \gamma = 0 \quad (102)$$

Again, a second order effect is present since  $\sin \gamma$  is a small value for moderately small phase shifts and  $(KG)^2$  is nominally equal to unity. The net effect caused by pre-comparator amplitude errors and post-comparator phase errors is a small boresight error.

In summary, two basic effects are seen when post-comparator errors are present. First, a gain variation is caused by both amplitude and phase errors. This gain change will result in changes of the servo system gain. Second, a boresight shift is present when both pre-comparator errors (of the opposite kind from the type of monopulse system) and post comparator phase shifts are present. The boresight shift is a second order effect and will not generally be a significant source of sum channel gain reduction. The amount of sum channel gain change can be determined from these equations when the antenna gain and phase functions are known.

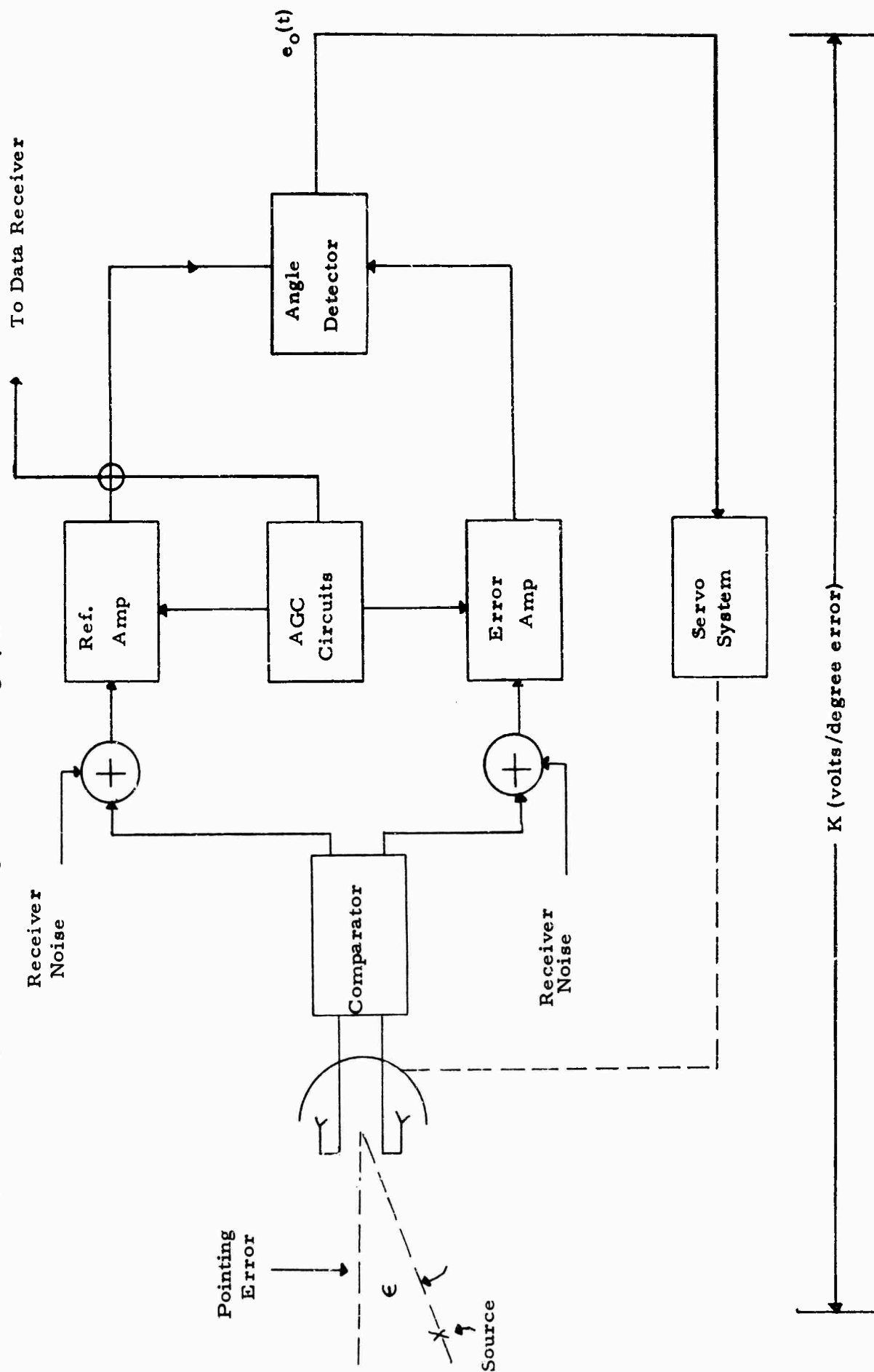
## SECTION VIII

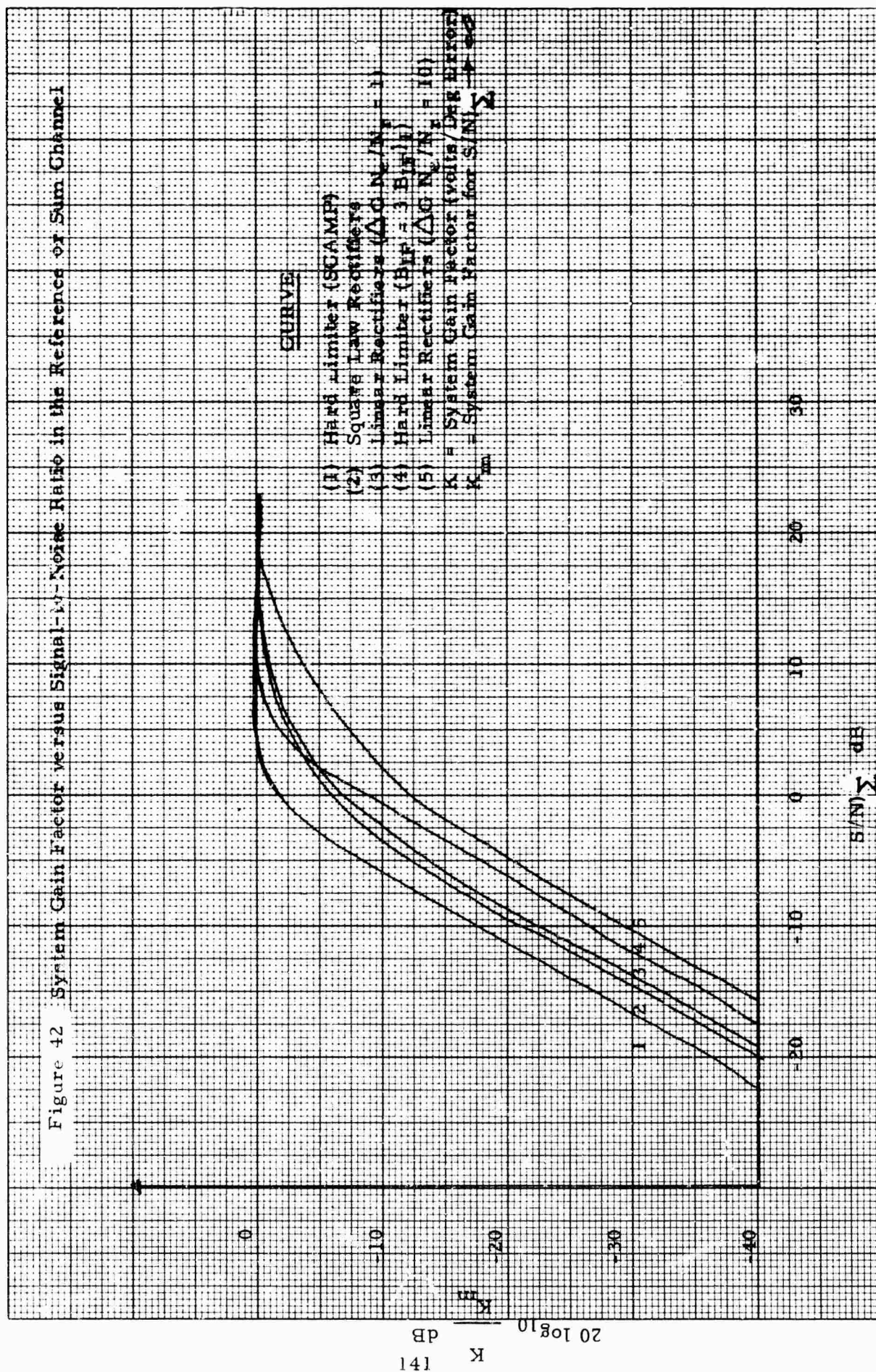
### NORMALIZATION

An optimum receiver would provide an angular pointing error which is independent of the received signal strength. The antenna and receiver noise causes the tracking system gain to change below that value at high signal strength, and the system performance is accordingly degraded. The tracking system is said to be normalized when its gain is dependent only on pointing error and not on signal strength. Figure 41 shows a simplified tracking system beginning with a source or transmitter and ending with an error voltage  $e_o(t)$  into the servo system. Only one channel (one axis) tracking circuitry is shown. The system gain factor  $K$  is in units of volts per degree pointing error and it is desired that  $K$  (average value) not change when the distance between source and antenna changes (for a constant pointing error  $\epsilon$ ).

Figure 42 shows the effect of noise on  $K$  for systems using different schemes to achieve normalization. Curves 2, 3 and 5 are from Pelchat (11). Curve 2 assumes that the angle detector is a perfect multiplier and the AGC or signal level detector is a square law rectifier. The  $S/N$   $\sum$  ratio is measured at the output of the sum channel amplifier. Curve 3 assumes that linear rectifiers are used in the level and angle detectors and that the ratio,  $\Delta G N_e/N_r$ , of noise powers in the sum and error channels measured at the input to the angle detector is unity. Curve 5 again uses linear rectifiers, but the ratio  $\Delta G N_e/N_r$  is 10. Here,  $\Delta G$  is the ratio of error to sum channel gain,  $N_e$  and  $N_r$  are the noise powers in the error and reference channels referred to the antenna terminals. Curve 1 is for the case of a hard limiter used to provide normalization similar to the system configuration described by Rubin and Kamen<sup>(12)</sup>. This curve was compiled from data given in Davenport<sup>(13)</sup> (Figure 4), and Jones<sup>(14)</sup> (Figure 3). The IF bandwidth is equal to that used in the systems having AGC circuitry, and the same received signal power will then result in identical signal-to-noise ratios at the IF output. However, in a practical case, the limiter or SCAMP approach will require at least three times the IF bandwidth as used in the AGC type systems, since the error signals have the same information bandwidth as the sum channel, and must not overlap in the frequency spectrum at the limiter input. Curve 4 is plotted for the minimum required IF bandwidth, and same received signal strength as the AGC type systems.

Figure 41 Simplified Block Diagram of Tracking System





For identical  $S/N)_{\Sigma}$  at the IF output, the limiter approach provides superior normalization characteristics at values of  $S/N)_{\Sigma}$  equal to 10 or less. When the different systems are compared for the case of equal signal strengths at the antenna terminals, the hard limiter, due to its increased IF bandwidth, is inferior to the square law or linear rectifier AGC systems ( $\Delta G N_e / N_r = 1$ ). It is noted that coherent or synchronous AGC would normally provide normalization to values of  $S/N)_{\Sigma}$  out of the IF less than 0 dB, depending upon the ratio of the IF to loop or reference filter bandwidths. Thus, as long as the system is locked and tracking,  $K$  is essentially constant at the value  $K_m$ . The use of a coherent system can impose additional problems, particularly during acquisition.

In a typical communications situation at least a +6 dB  $S/N$  would be anticipated, resulting in a normalization change of less than 3 dB for square law or linear detectors (curves 2 and 3). Therefore, when the signal strength is sufficient for good communications, the normalization problem is not severe. In other situations, however, the servo loop gain change at low values of  $S/N$  could impose severe design problems.



## SECTION IX

### MONOPULSE NOISE ANALYSIS

The purpose of this section is to analyze the noise characteristics of a monopulse system. The system includes three receivers of bandwidth,  $W$ , two cross correlation detectors, and two low pass filters, as shown in Figure 43. The signal-to-noise ratio (SNR) on the error channels is derived as a function of the signals and noise densities at the inputs. Since the operations performed on the two error channels are identical, only one channel will be analyzed.

The input signals are angle modulated (e.g., FM or PM) and are assumed to be identical except for a gain factor. Input noise is assumed to be white, gaussian noise, independent and with different (in general) density in each channel. The inputs are passed through ideal bandlimiting filters of bandwidth  $W$  and centered at a frequency of  $f_c$ . Then,

$$\begin{aligned} y_s(t) &= A g(t) + n_s(t) \\ y_{el}(t) &= B g(t) + n_e(t) \end{aligned} \tag{103}$$

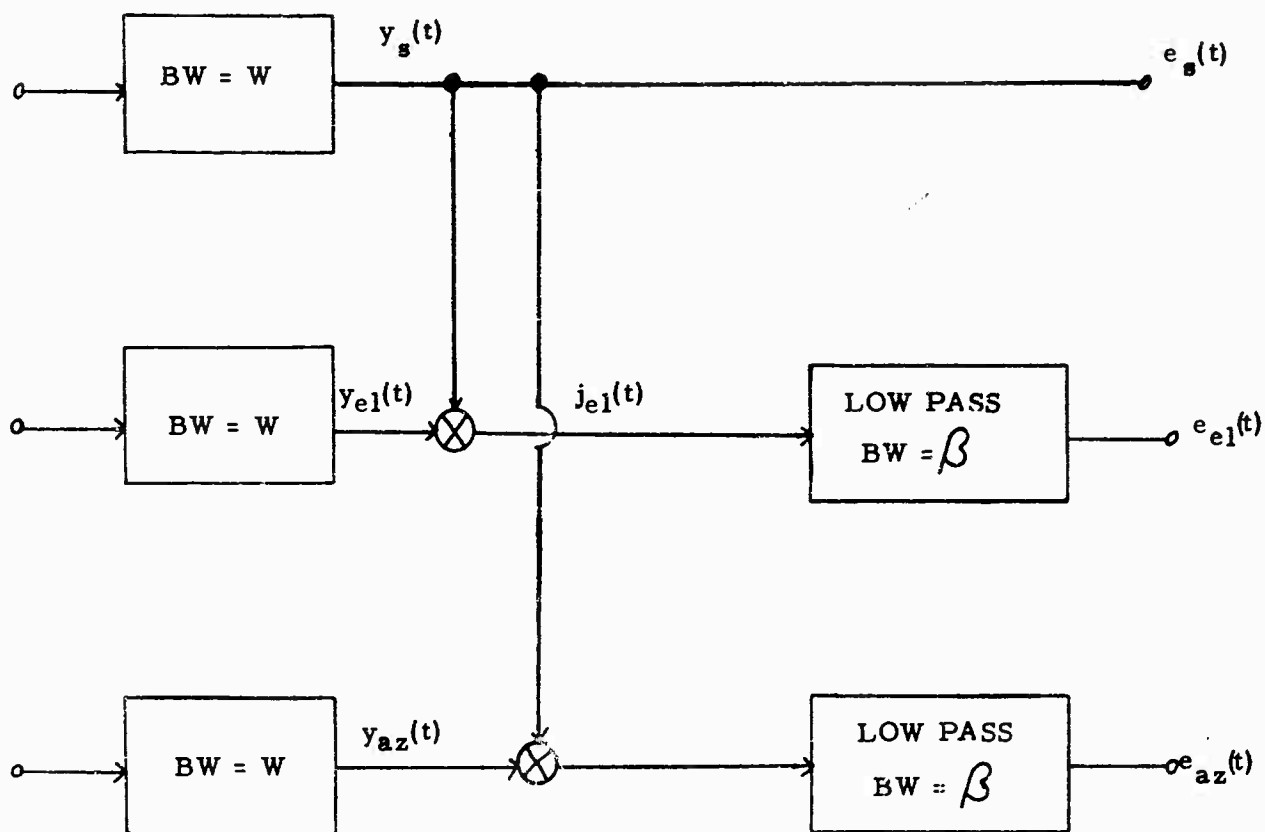
where  $E(g^2(t)) = 1$

to normalize the power levels.

The spectrum of  $g(t)$  is zero outside of the frequency interval of bandwidth  $B$  centered at  $f_c$ . The noise spectra can be similarly described as

$$\left. \begin{aligned} S_{ns}(f) &= \frac{N_s}{2} \\ S_{ne}(f) &= \frac{N_e}{2} \end{aligned} \right\} f_c - \frac{W}{2} \leq f \leq f_c + \frac{W}{2} \tag{104}$$

Then, the SNR on the sum channel can be found as follows:



### Monopulse Receiver

Simplified Block Diagram - Figure 43

$$\text{Signal power} = A^2$$

$$\text{Noise power} = N_s W$$

$$\therefore \text{SNR}_s = \frac{A^2}{N_s W} \quad (105)$$

The remaining problem, then is to find the SNR on the elevation channel. The general procedure to be used in this analysis is as follows: the autocorrelation function of output of the multiplier is found; the Fourier transform of the autocorrelation function is obtained, which is the power spectral density. The appropriate low pass portion of the spectrum is retained as the output of the filters.

The multiplier output is given by,

$$\begin{aligned} j_{el}(t) &= (y_s(t)) \cdot (y_{el}(t)) \\ &= ABg^2(t) + Ag(t) n_e(t) + Bg(t) n_s(t) + n_s(t) n_e(t) \end{aligned} \quad (106)$$

The characteristic of the angle modulated signal is described as follows:

$$g(t) = \sqrt{2} \cos \vartheta(t) \therefore E [g^2(t)] = 1 \quad (107)$$

where  $\vartheta(t)$  represents the modulated carrier frequency.

The autocorrelation function of the multiplier output is

$$\begin{aligned} R_{j_{el}}(\tau) &= E [j_{el}(t) j_{el}(t+\tau)] \\ &= E \left\{ \left[ ABg^2(t) + Ag(t) n_e(t) + Bg(t) n_s(t) + n_s(t) n_e(t) \right] \cdot \left[ ABg^2(t+\tau) \right. \right. \\ &\quad \left. \left. + Ag(t+\tau) n_e(t+\tau) + Bg(t+\tau) n_s(t+\tau) + n_s(t+\tau) n_e(t+\tau) \right] \right\} \end{aligned} \quad (108)$$

Noting that the expected value of the noise functions is zero, the only non-zero terms will be signal terms and autocorrelation noise terms (not cross-correlation noise terms). Then, defining  $R_x(\tau)$  as the autocorrelation function for the time function  $x$ , equation (108) can be rewritten as,

$$\begin{aligned}
 R_{j_{el}}(\tau) = & A^2 B^2 R_g^2(\tau) + A^2 R_g(\tau) R_{n_e}(\tau) \\
 & + B^2 R_g(\tau) R_{n_s}(\tau) + R_{n_s}(\tau) R_{n_e}(\tau)
 \end{aligned}
 \tag{109}$$

The Fourier transform of equation (109) yields the spectrum of  $j_{el}(\tau)$  as follows:

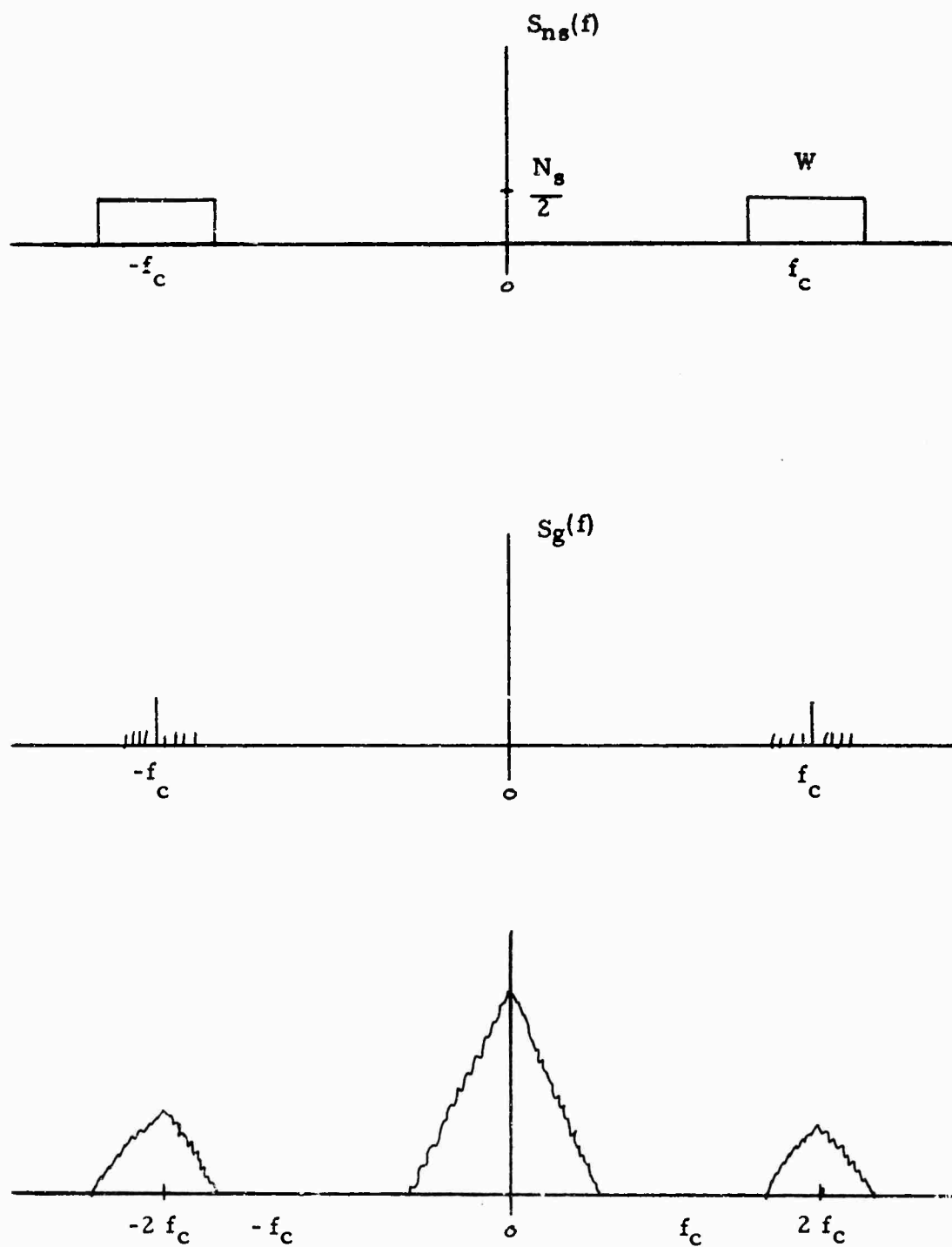
$$\begin{aligned}
 S_{j_{el}}(f) = & A^2 B^2 S_{g^2}(f) + A^2 S_g(f) * S_{n_e}(f) \\
 & + B^2 S_g(f) * S_{n_s}(f) + S_{n_s}(f) * S_{n_e}(f)
 \end{aligned}
 \tag{110}$$

where the symbol  $*$  denotes convolution; i.e.,

$$S_g(f) * S_{n_e}(f) = \int_{-\infty}^{\infty} S_g(x) S_{n_e}(f - x) dx$$

Equation (110) can be most easily evaluated by referring to the spectra shown in Figure 44. In addition, the case of interest in the monopulse situation occurs when the low pass bandwidth  $\beta$  is very small compared to  $W$ , the bandwidth of the incoming signal. Under these conditions, the outputs of interest occur very near to zero frequency and can be considered as having flat spectra of width  $\beta$  and magnitude equal to the DC value of the unfiltered function. An evaluation of each term in (110) follows:

$$\begin{aligned}
 S_{g^2}(0) &= \text{DC signal power in } g^2(t) \\
 g(t) &= \sqrt{2} \cos \phi(t) \\
 g^2(t) &= 2 \cos^2 \phi(t) = 1 + \cos 2\phi(t) \\
 \therefore S_{g^2}(0) &= 1 \quad f_c + \frac{W}{2}
 \end{aligned}
 \tag{111}$$



# SIGNAL AND NOISE SPECTRA

Figure 44

$$\begin{aligned}
 S_g(f) * S_{n_e}(f) &= 2 \int_{f_c - \frac{W}{2}}^{f_c + \frac{W}{2}} \frac{N_e}{2} S_g(x) dx \\
 &= \frac{N_e}{2} \left[ \text{total signal power} \right] = \frac{N_e}{2}
 \end{aligned} \tag{112}$$

similary,  $S_g(f) * S_{n_s}(f) = \frac{N_s}{2}$  (113)

$$\begin{aligned}
 S_{n_e}(f) * S_{n_s}(f) &= \frac{N_e N_s}{4} \times 2 \int_{f_c - \frac{W}{2}}^{f_c + \frac{W}{2}} dx \\
 &= \frac{N_e N_s W}{2}
 \end{aligned} \tag{114}$$

The elevation channel output can now be written,

$$S_{el}(o) = A^2 B^2 + \frac{A^2 N_e}{2} + \frac{B^2 N_s}{2} + \frac{N_e N_s W}{2} \tag{115}$$

The desired (noise free) signal output is the term  $A^2 B^2$ . The noise power is then determined by the low pass filter of two sided bandwidth  $2\beta$ . The total noise power out is

$$N_{out} = \beta (A^2 N_e + B^2 N_s + N_e N_s W) \tag{116}$$

Then, the output signal-to-noise ratio is,

$$SNR_{el \text{ out}} = \frac{A^2 B^2}{\beta (A^2 N_e + B^2 N_s + N_e N_s W)} \tag{117}$$

Equation (117) is the desired result. An identical expression can be derived for the azimuth channel, when  $N_e$  is replaced by  $N_a$ , the noise density on the azimuth input. Equation (117) can be written in a more illuminating manner by making the following identifications:

$$\frac{A^2}{N_s W} = \text{SNR}_s \text{ is the sum channel input SNR in a bandwidth } W \quad (118)$$

$$\frac{B^2}{N_e W} = \text{SNR}_e \text{ is the elevation channel input SNR in a bandwidth } W$$

Then,

$$\text{SNR}_{el \text{ out}} = \frac{W}{\beta} \left[ \frac{\text{SNR}_e}{1 + \frac{\text{SNR}_e}{\text{SNR}_s} + \frac{1}{\text{SNR}_s}} \right] \quad (119)$$

Equation (119) defines the output SNR on the elevation error channel in terms of input bandwidth, video bandwidth, and input SNR's. In many cases, the equation can be further simplified. When tracking, the sum channel signal is much stronger than the error signal,  $\text{SNR}_e \ll \text{SNR}_s$ . Furthermore, when the system is operating well above threshold, a large input  $\text{SNR}_s$  is expected.

$$\text{SNR}_{el \text{ out}} \approx \frac{W}{\beta} \cdot \text{SNR}_e \quad (120)$$

Thus, under high signal conditions and when tracking, the output SNR is equal to the input SNR when measured in the same bandwidth. Under rather marginal communications conditions, when  $\text{SNR}_s = 1$ , the output SNR is degraded by an additional 3 dB.

SECTION X  
TIME DIVISION MULTIPLEXING  
(TDM)

One technique for combining the three input signals (one sum and two difference channels) of a monopulse system onto a single channel is time sharing, or TDM. One type of TDM which could be considered would be a "slow" switching between the three channels, where "slow" means that the switching period is very long compared to the reciprocal of the bandwidth of the incoming signal. This method results in an irrecoverable loss of sum channel information during those times when the difference channels are being passed. As a result, the method is not generally usable in a communications terminal. The "slow" switching technique will not be considered further.

The alternate TDM technique, "fast" sampling, will be discussed in this section. Basic limitations exist in the switching rate, bandwidth, and crosstalk in this type of system. Fortunately, some fundamental sampling theorems can be applied to obtain limits on this problem.

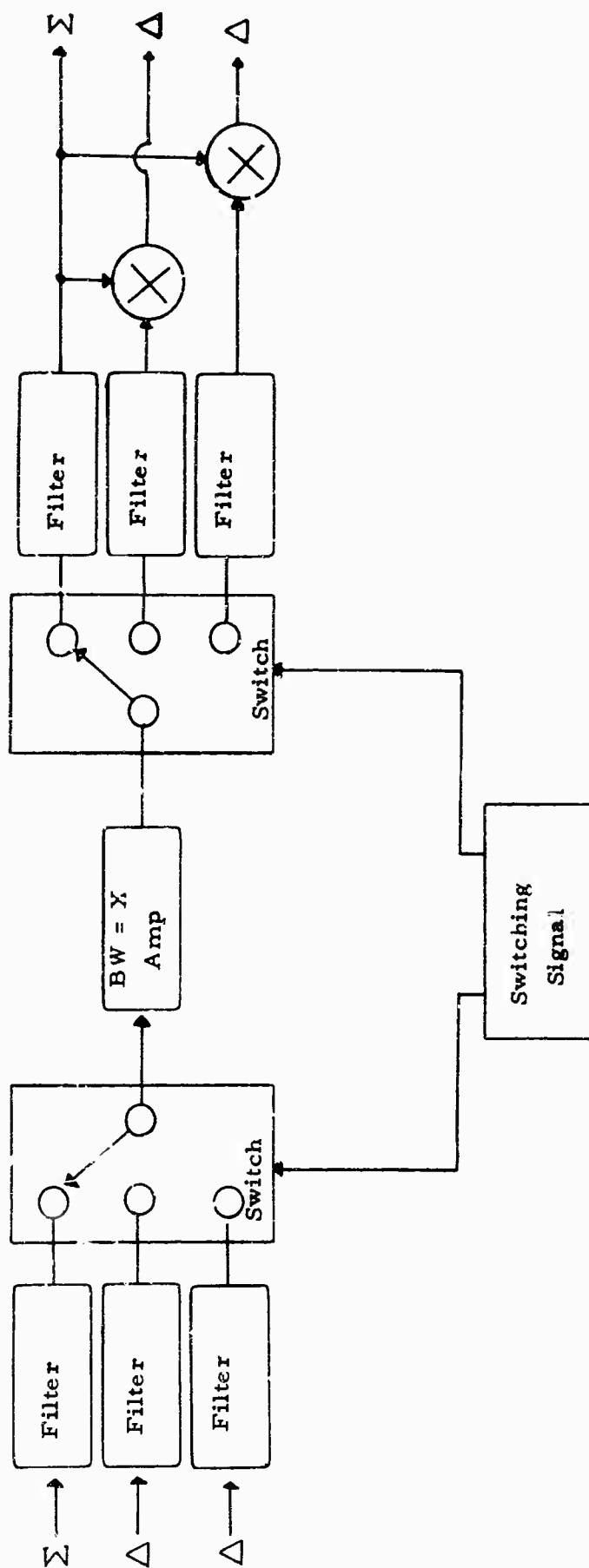
A general TDM system can be represented by the simplified block diagram of Figure 45. The three input signals pass through bandlimiting filters prior to the first switch. The filters will be considered to be ideal (non-realizable) filters which pass without loss all signals in a bandwidth  $B$  centered at the carrier frequency and provide infinite rejection at all other frequencies. Realizable filters will be considered later, but the use of ideal filters is necessary at this point to allow sampling theorems to be used.

Sampling theorems for bandpass functions have been presented by several authors (15, 16, 17, 18) and are essentially bandpass versions of Shannon's<sup>(19)</sup> classical sampling theorem. The bandpass sampling theorem requires that a minimum sampling rate  $f_R$  of

$$f_R = 2\omega \left(1 + \frac{k}{m}\right) \quad (121)$$

be used to allow recovery of the initial signal.





Basic TDM System Figure 45

where  $\omega$  is bandwidth of the signal

$f_2$  is highest frequency in band

$m$  is largest integer not exceeding  $f_2/\omega$

$$k = \frac{f_2}{\omega} - m$$

Thus, the required rate varies between  $2\omega$  and  $4\omega$  and, for high center frequencies with respect to bandwidth, is nearly equal to  $2\omega$ . This expression is based on an ideal impulse sampling, but is equally valid (18) for finite width samples. The sample width becomes very important when the switching is done prior to the high gain amplifiers in the receiver. In that case, the sample width determines the gain and can significantly degrade the noise figure in a practical system. The amount of degradation depends upon the bandwidth and noise figure of following stages as well as preamplifier gain.

The amplifier following the sampler must have a wide bandwidth or crosstalk will result. This is shown in the following paragraphs by considering ideal filters and impulse sampling. The single channel amplifier bandwidth is denoted by  $X$ . The impulse response of an ideal filter of width  $X$  is proportional to

$$h(t) = \frac{\sin \pi tX}{\pi tX} \quad (122)$$

the familiar "sine  $X$  over  $X$ " characteristic. The function is maximum at  $t = 0$  and exhibits zeros at integer values of  $(tX)$ . Therefore, an appropriate choice of  $X$  would be one which makes the response due to all past samples identically zero at the instant of sampling.

For example, consider the case when three input channels of bandwidth  $B$  are to be sampled. The minimum sampling rate for each channel is  $2B$ . Thus, a total of  $6B$  samples per second are required to characterize all three channels. If these samples are equally spaced in time and used to drive the ideal filter of bandwidth  $X$ , then the filter output due to all past samples can be made zero by choosing  $X = 6B$ ; i. e., when  $t = N/6B$  is the time of sampling ( $N$  an integer), the product  $tX = N$  is always an integer. In summary, for the case of impulse sampling, using equally spaced sampled samples and an ideal bandwidth precisely 6 times the inverse of the sampling rate, there is no crosstalk. This system is obviously unrealizable, but it does illustrate the lower limit on bandwidth required.

It is also possible, of course, to use nonuniform and/or non-identical sampling methods. Any change from uniform, identical sampling would result in an increased amplifier bandwidth requirement. It might be desirable, for example, to sample the sum channel many times for each sample of the difference channel. Since it is always necessary to sample the difference channels at a rate  $2B$  or higher, the overall sampling rate requirement would increase and the bandwidth of the amplifier would increase accordingly. In the event the samples were not evenly spaced, crosstalk becomes a problem which can be alleviated only by increasing the amplifier bandwidth.

In a more practical situation, finite width samples would be used and realizable filters would be required. Under these conditions, the sampling pulse shape and the amplifier filter shape can be selected to minimize overshoot<sup>(15)</sup>, which is equivalent to reducing crosstalk. The present problem is quite severe, however, since one channel (sum) is normally much larger than the others. As a result, the signal in the amplifier due to the sum channel must be made extremely small when the difference channels are being passed.

The signals in the bandpass amplifier are sampled in a switch which is synchronous with the input sampler. The three switch outputs are filtered, to recover the initial signal, and then correlated to obtain the pointing error signals. The switching design problem is directly related to the input filter bandwidth. Impulse sampling would require that the switching time (the time required to switch off input 1 and switch on input 2) be negligible compared to  $1/6B$ . In a finite sampling system, a switching time which is short compared to  $1/6B$  would be desirable, with a switching time of one-half the sampling time representing an upper limit in a practical system.

Since the input filter bandwidth is a key element in the TDM system, the practical limitations on this filter must be considered. Minimum duplication of circuitry and, therefore, maximum benefit from the single channel technique is obtained by placing the filters and switches as close (electrically) to the antenna as possible. If the filters precede preamplification, then insertion loss is of prime importance, since it contributes directly to sum channel degradation. An X-band limitation, considering realizable unloaded  $Q$  (resonator quality factor) to be in the order of 10 to 20,000 in a practical size, would then be a minimum bandwidth of 10 to 20 MHz. Even a simple filter (and thus a very poor approximation to the necessary bandlimiting filter) would exhibit several tenths of a dB insertion loss. Considering this optimistic condition, a 10 MHz bandlimited signal, the switching time must be much less than 16 nanoseconds and the amplifier bandwidth must be much greater than 60 MHz. It appears, then,

that X-band switching is not practical, considering the present state-of-the-art (note that the insertion loss of the switch must also be very low to prevent sum channel degradation).

More reasonable parameters are available when switching is done at an intermediate frequency. In the limit, the filter bandwidth is restricted by the signal bandwidth (when AFC is used) or by the frequency uncertainty (oscillator stabilities and Doppler shifts) plus the signal bandwidth. In the present case, the minimum bandwidth is approximately 200 kHz, as limited by signal characteristics. The resultant switching required is a time less than 0.8 microseconds. The amplifier bandwidth must be much greater than 1.2 MHz. When AFC is not used, the bandwidth must be nearly 400 kHz, due principally to Doppler shifts. In this case, the switching time must be much less than 0.4 microseconds and the amplifier bandwidth must be greater than 2.4 MHz. A summary of the three cases, X-band switching, IF switching with AFC, and IF switching without AFC is shown in Table 11.

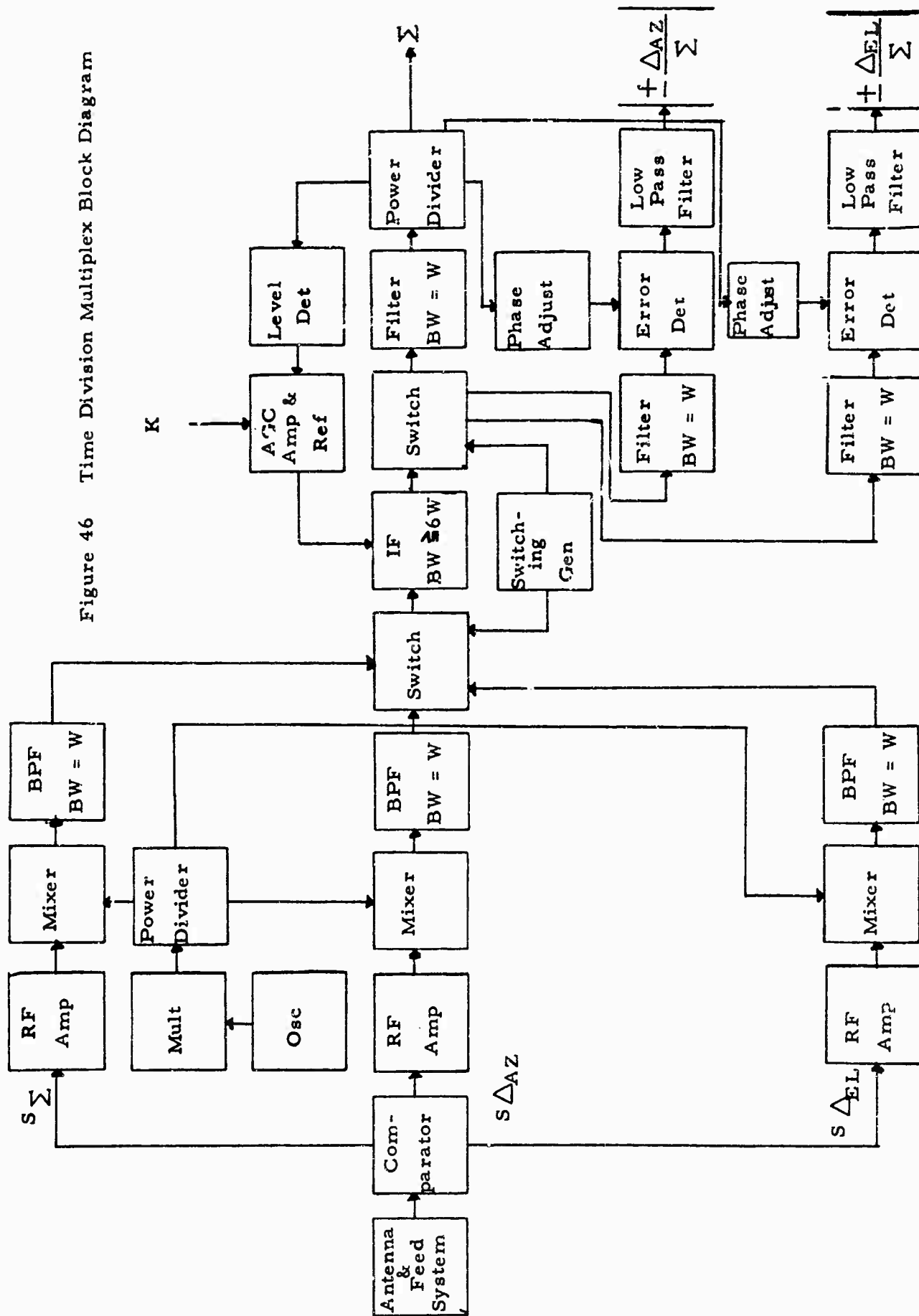
The block diagram of a practical TDM SCMTR is shown in Figure 46. This system uses three RF amplifiers and mixers and does the switching at an intermediate frequency. It is apparent from the block diagram that the implementation is relatively complex. The basic technique is inferior to other techniques in both performance and equipment complexity. In short, the use of TDM is not recommended in the design of a single channel monopulse tracking receiver.

TABLE 11

## TDM FILTER, SWITCH, and BANDWIDTH REQUIREMENTS

	X-Band Switching	IF Switching with AFC	IF Switching w/o AFC
Realizable Filter Bandwidth	10 MHz	200 kHz	400 kHz
Switching Time	$\gg 16$ nsec	$\gg 0.8$ u sec	$\gg 0.4$ u sec
Amplifier Bandwidth	$> 60$ MHz	$> 1.2$ MHz	$> 2.4$ MHz

Figure 46 Time Division Multiplex Block Diagram



## SECTION XI

### FDM (FREQUENCY DIVISION MULTIPLEX)

#### 1. BASIC SYSTEM

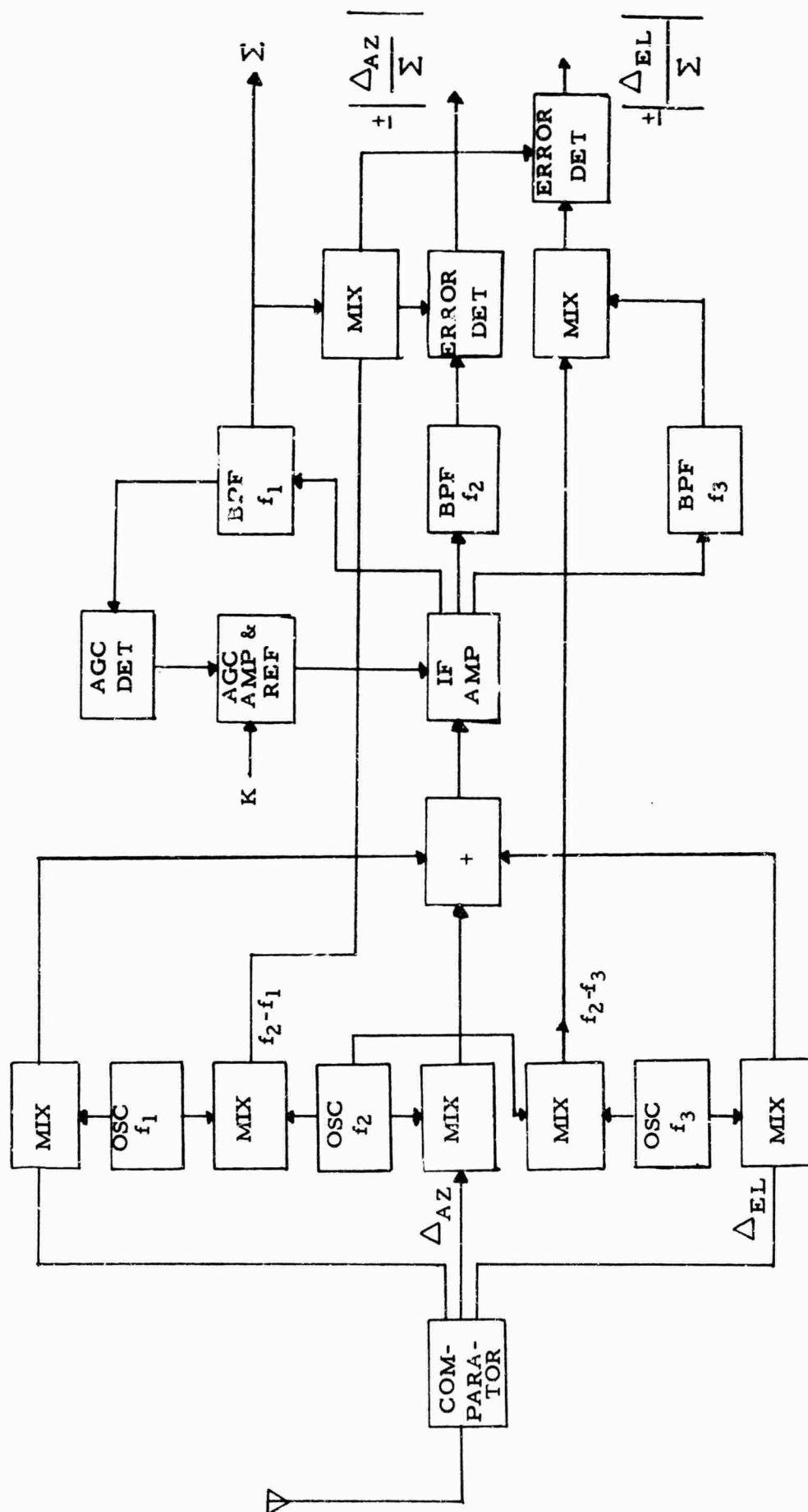
The basic FDM (Frequency Division Multiplex) technique is illustrated in block diagram form in Figure 47. The sum and difference signals are mixed with the frequencies  $f_1$ ,  $f_2$ , and  $f_3$  such that their individual spectra do not overlap. Actually, intermodulation requirements dictate the exact frequencies as will be discussed later. The signals are added in a linear summing circuit and fed to a single IF amplifier. The IF output is supplied to three bandpass filters with center frequencies  $f_1$ ,  $f_2$ , and  $f_3$ . The sum channel is applied to a detector and AGC amplifier with a reference DC voltage to develop AGC for the IF amplifier. The desired effect is one of normalization, such that the output from the error detector is independent of the received signal level.

The sum channel is mixed to the center frequency  $f_2$  and used as a reference in the phase sensitive error detectors. The input signals for each detector are centered at  $f_2$ , where the output from the bandpass filter  $f_3$  is mixed with the frequency  $(f_2 - f_3)$  before the detector. The normalization process, using the sum channel for the AGC, will depend upon the performance of the detector in the AGC loop in the presence of low SNR's in the sum channel. Some of the more common detection schemes have been compared in Section VIII.

The basic FDM method will provide a single channel system with potentially equivalent performance to three channel monopulse. The equipment requirements are quite severe, however. A particularly interesting problem, common to all monopulse systems, is one of normalization (see Section VIII). The combination of the normalization problem and the FDM technique led to consideration of the SCAMP technique, a special case of the general FDM method.

#### 2. SCAMP

A technique which utilizes the normalization phenomena which occurs when two or more signals of unequal amplitude are passed through



**Figure 47** **FDM (Frequency Division Multiplex Block Diagram**



a common hard limiter has been proposed<sup>(12)</sup>. This technique has been named SCAMP - Single Channel Monopulse Processor, and is shown in basic form in Figure 48. There are characteristics of this basic system which appear directly applicable to monopulse radar systems. Monopulse radar systems incorporate methods for precision direction finding by simultaneously comparing the energy incident on two or more antennas (or patterns). If these signals are compared by taking the ratio of one signal to another, problems of amplitude and phase variations are minimized. Under certain conditions, the SCAMP system provides this function on an instantaneous basis using rather unsophisticated equipments.

The basic SCAMP system consists of a linear summing circuit followed by a hard limiter which is in turn followed by bandpass filters. The summing circuit allows the signals, which are far enough separated that their significant sidebands do not overlap, to be linearly added prior to processing through a single channel. After limiting the composite signal is routed to bandpass filters. The filters, one for each signal, must be pre-selected to match the center frequency and bandwidth requirements of a particular signal.

A monopulse system which incorporated the SCAMP processor is shown in Figure 49. Since the three signals are to be processed in a single channel they must be converted to center frequencies which differ by at least twice the information bandwidth of the signals. The outputs of these mixers are at "IF" frequencies. At this point, the signals are linearly summed (equivalent to the summing point in the "Basic SCAMP Processor" of Figure 48), and passed through the SCAMP processor to the section which converts the three signals back to their mutually coherent state. After this point, the signals are detected and the information routed to the tracking logic.

As will be noted from Figure 48, the forms of the output signals from the SCAMP processor are:

$$S'_1 \approx K_1 \sin(\omega_1 t + \phi_1(t))$$

$$S'_2 \approx K_2 \left[ \frac{A_2(t)}{A_1(t)} \right] \sin(\omega_2 t + \phi_2 t) \quad (123)$$

The signal  $S'_1$  corresponds to the sum channel signal of Figure 49, and it is assumed that its amplitude,  $A_1(t)$  is larger than either of the amplitudes ( $A_2$  and  $A_3$ ) of the signals which correspond to the difference channel signals; i.e.,  $S'_2$  and  $S'_3$ . The factors  $K_1$  and  $K_2$  are parameters dependent upon the limiter characteristic.

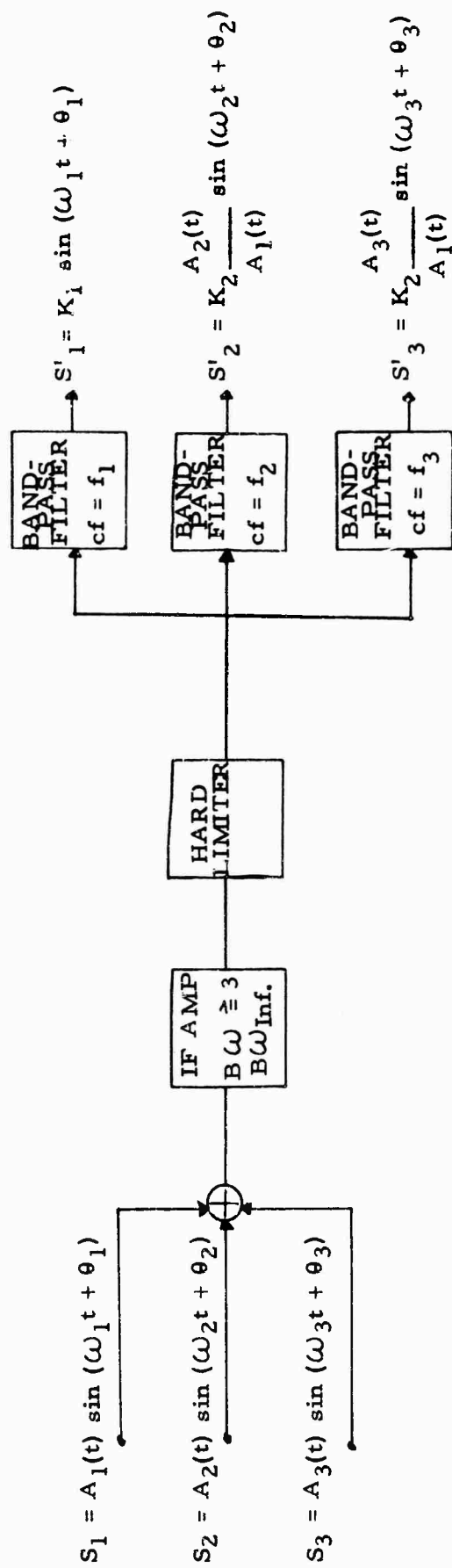


Figure 48 Basic SCAMP Processor



These approximations for the SCAMP processor outputs are valid for  $A_2/A_1$  (which corresponds to the ratio of a difference signals' amplitude to the sum signals' amplitude in Figure 49) less than about 0.5 and for the condition of the sum channel being at least 4 or 5 dB above the noise level.

Although the SCAMP processor seems to offer a significantly improved technique, it has several characteristics which could, dependent upon the proposed utilization, cause problems. The reasoning which accounts for the normalization indicated by equation (123) and for several other pertinent characteristics has been given in varying degrees in the references (3, 12-14 and 20-25). Based on these, consideration of each of the characteristics relevant to the FDM system of Figure 49 follows.

The normalization phenomenon, the key to the utilization of a limiter-bandpass filter scheme, has clearly defined, but non-critical limitations (See Figure 50). Figure 50 shows that as the SSR\* approaches unity, the normalized output signal starts increasing and the other output signal starts decreasing. Considering the effect on the system of Figure 49, this phenomena would cause a negligible shift in the antenna pointing angle. No problem areas are encountered as the SSR approaches zero.

Figure 50 also shows the effect of input SNR on the normalization. For cases in which the input SNR is greater than unity, the normalization is essentially independent of the SNR. The variation noted for SNRs less than unity may be neglected since one is not generally interested in slight angular errors (which would result from this variation) in situations of negative SNR.

Consideration of weaker signal suppression (the amount that the weaker signal is suppressed below the stronger signal) effects leads to an analysis of the variation of this phenomena as a function of input signal-to-signal ratio (SSR) and input signal-(larger)-to-noise ratio (SNR).

Jones (14) has studied the effects of two sinusoids in narrowband Gaussian noise. Figure 51 shows the relative suppression of one signal by the other in the presence of noise, and it is noted that for signals buried in noise, little or no suppression of one signal by another takes place. Whenever the large input SNR is 10 dB or more the maximum suppression is 6 dB when the relative signal levels at the input ( $S_2/S_1$ ) is equal to or less than  $10^{-2}$ . For larger values of  $S_2/S_1$ , approaching

---

\* SSR is to be interpreted as weaker signal-to-stronger signal ratio.

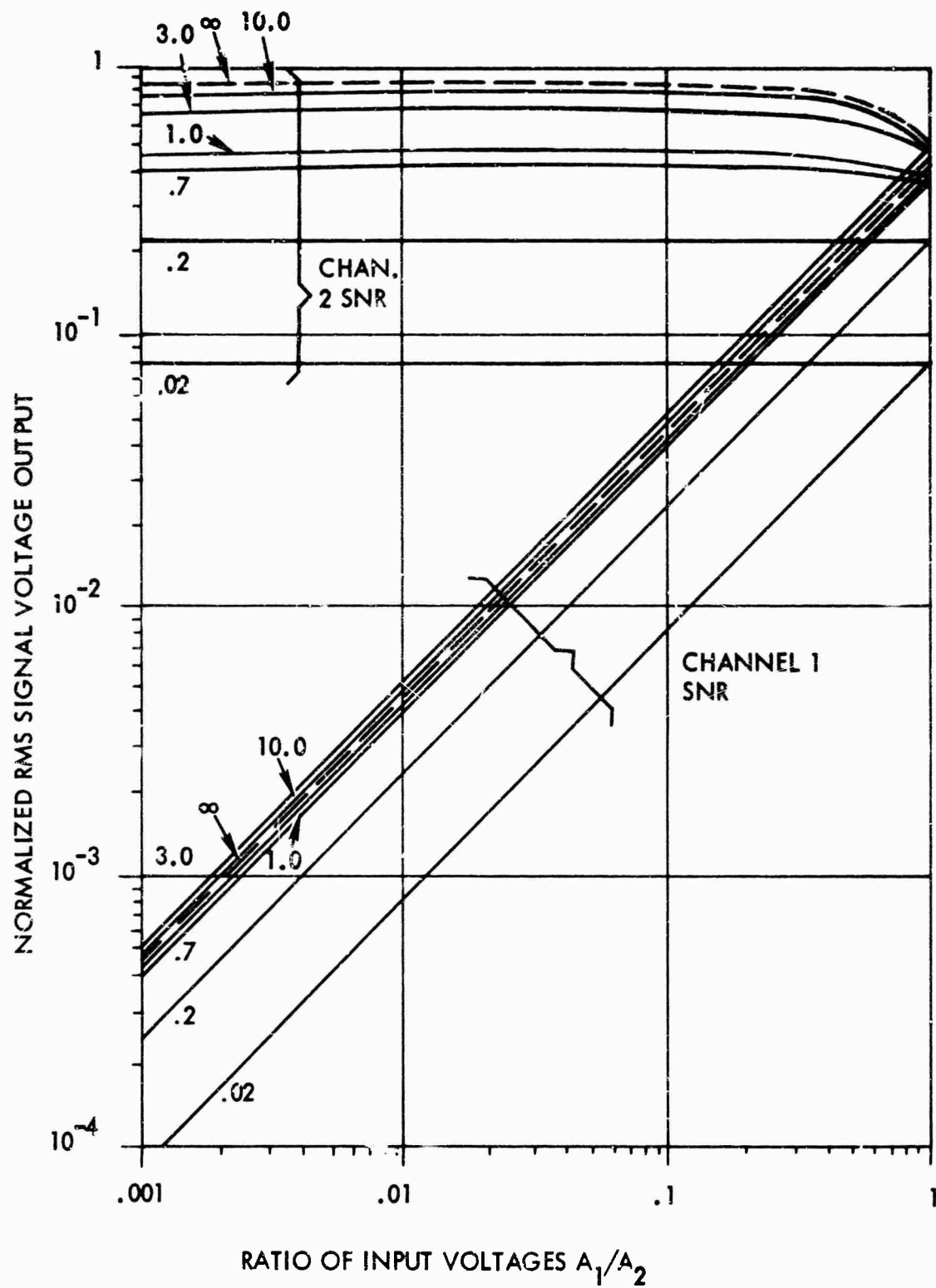


Figure 50. SCAMP Processor Performance in the Presence of Noise

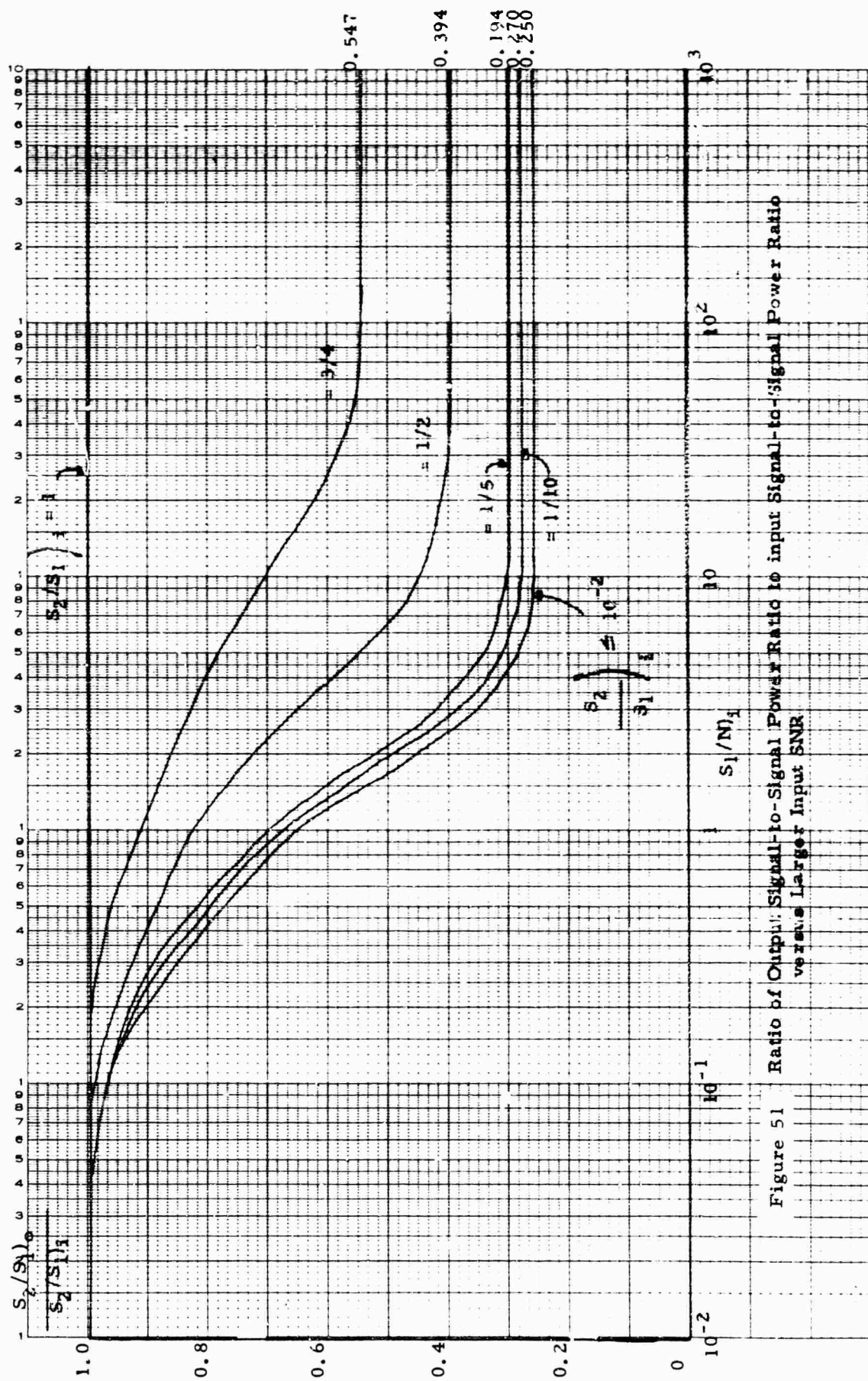


Figure 51 Ratio of Output Signal-to-Input Power Ratio to Input Signal-to-Input SNR versus Larger Input SNR

unity, less suppression is observed, with none at all for  $S_2/S_1 = 1$ .

Shaft<sup>(24)</sup> has analyzed the situation for the case where three signals are processed through the limiter in the presence of noise. Figure 52 shows the suppression when there are one strong and two weak signals and was plotted from data obtained by Shaft. The signal suppression approaches 5-1/2 dB for high signal-to-noise ratios in the large input signal channel. Also, it is noted that the weaker signal is enhanced at low SNR's in the large signal channel for  $S_3/S_1$  less than  $10^{-2}$ .

When considering the limiting effect on SNR produced by the ideal bandpass limiter, it should be noted that the SNR for the weak signal can be degraded below that at the limiter input. Figure 53 shows the ratio of the output SNR to the input SNR as a function of the larger input SNR, with the input signal-to-signal power ratio ( $S_2/S_1$ ) as a parameter. From this figure, the output SNR to input SNR lies in the range 0 to 2 for two signals in noise as compared to the range  $\pi/4$  to 2, for one signal input SNR's equal to or greater than one. When strong noise is dominating the limiter, the SNR's of both input signals is decreased by a factor of  $\pi/4$  (about 1 dB). When one signal is much stronger than the other and noise, the SNR of the strong signal increases by a factor of 2, whereas, the SNR of the weak signal decreases by the factor 1/2. This fact can be obtained from Figure 53 directly by noting that the product of  $S_1/N_i$  and  $S_2/S_1$  gives  $S_2/N_i$ . Then, the intersection of this value (on the abscissa) of Figure 53 with the reciprocal of  $S_2/S_1$  gives  $S_2/N_c$  ( $S_2/N_i$ ). It is noted that when the two signals are of equal strength ( $S_2/S_1 = 1$ ) and much stronger than the noise, the normalized SNR tends to zero for both signals. The equal output SNR's are large compared to unity, but are much smaller than the large and equal input SNR's.

Another important aspect of limiting as utilized in a SCAMP system is that of intermodulation. Figure 54 expresses in power the relationship of the strongest intermodulation product ( $2f_1 - f_2$ ) to the weakest output signal level. When the input signal strengths are equal and much stronger than the noise, the strongest intermodulation ( $2f_1 - f_2$ ) is 9.5 dB below either of the two output signal powers. However, when one signal is much stronger than the other and noise, the largest intermodulation product is about equal to the weakest output signal level. The strengths of all intermodulation products fall off rapidly with decreasing SNR, and for the larger input SNR equal to unity, the strongest intermodulation product is 12 dB or more below the weakest signal.

Channel orientation has a significant effect upon the amount of intermodulation present. This process has been analyzed and evaluated experimentally<sup>(20)</sup>. The symmetrical configuration of Figure 55 produces



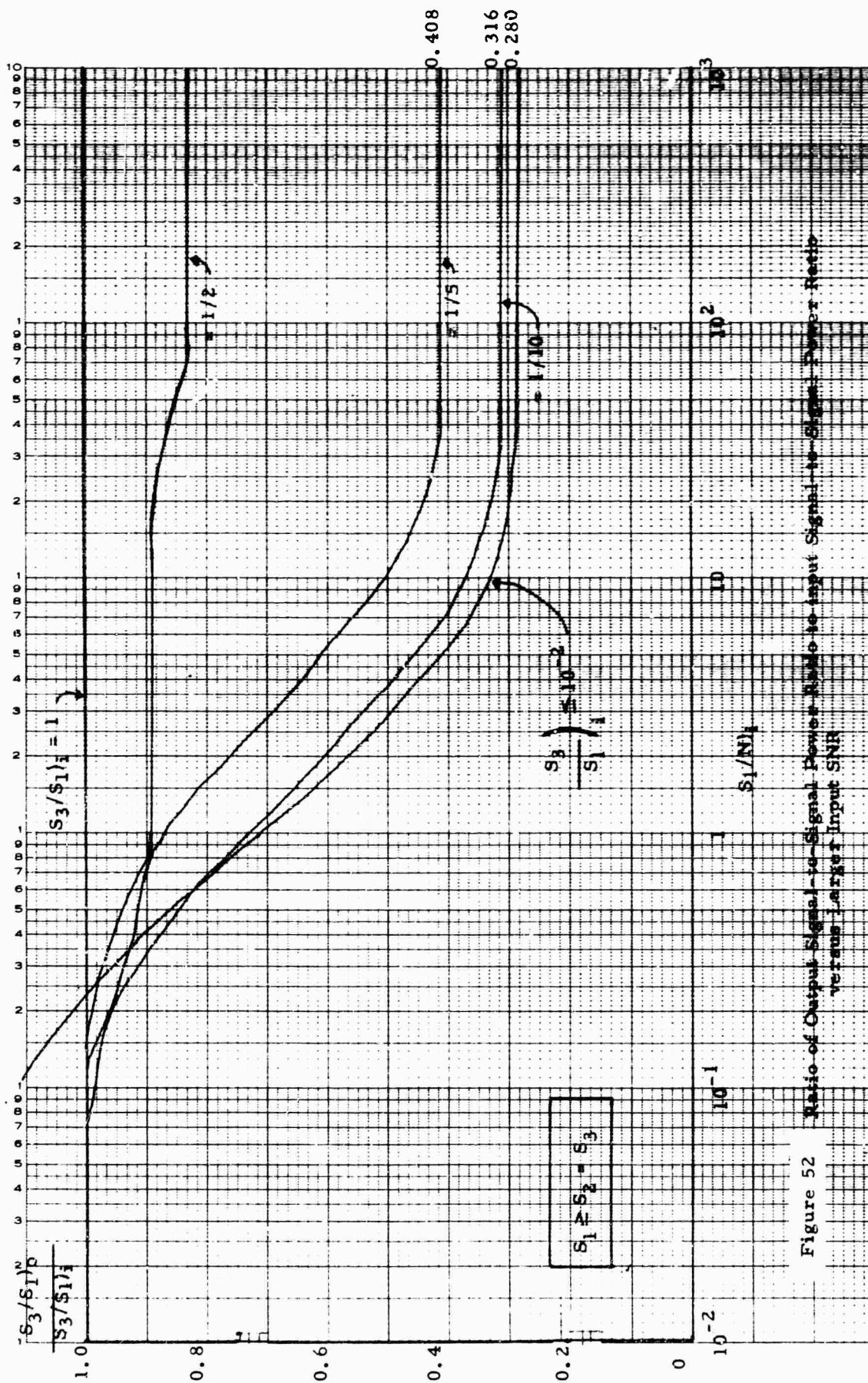


Figure 52 Ratio of Output Signal-to-Signal Power Ratio to Input Signal-to-Signal Power Ratio versus Larger Input SNR



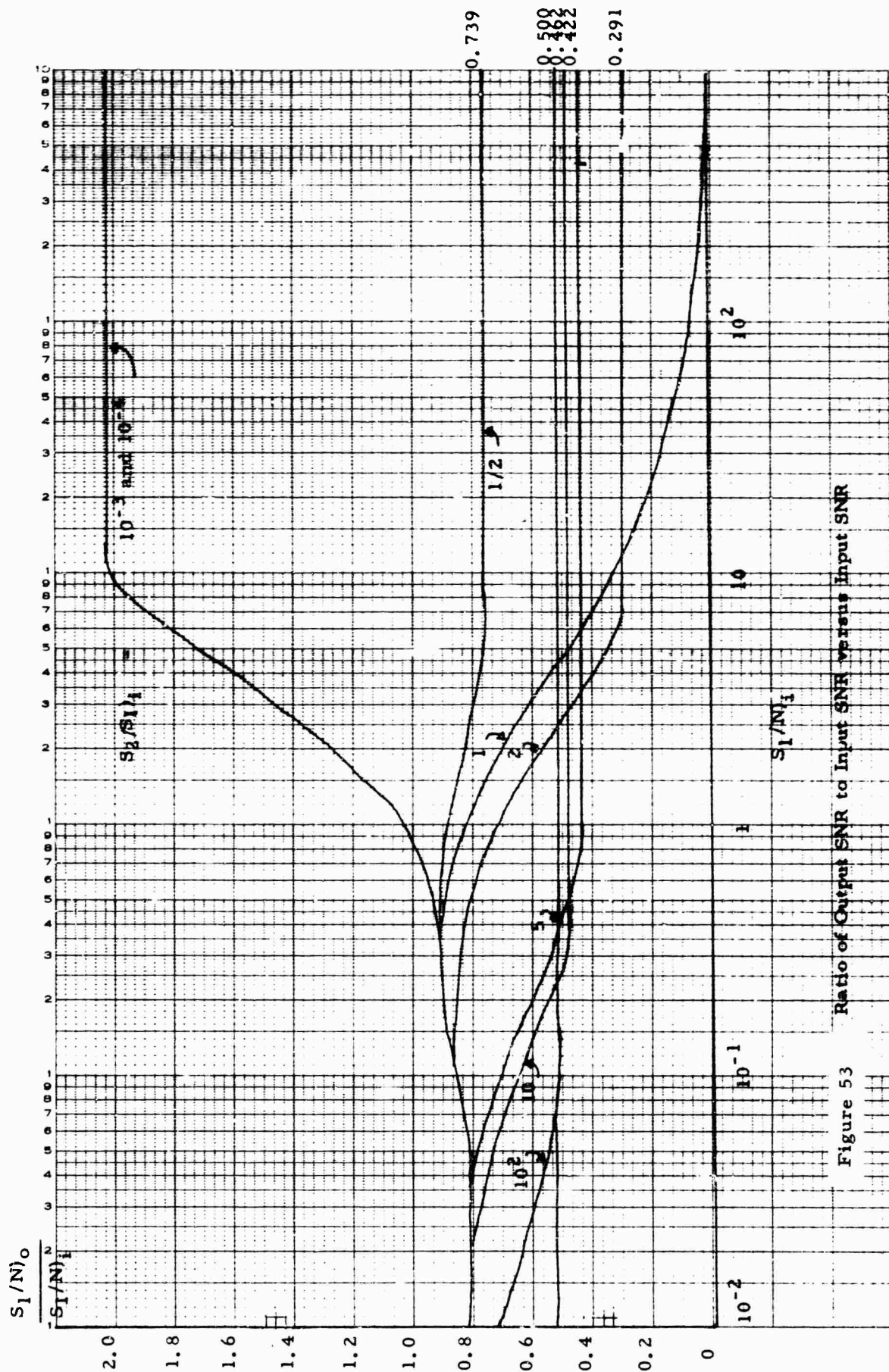


Figure 53 Ratio of Output SNR to Input SNR versus Input SNR

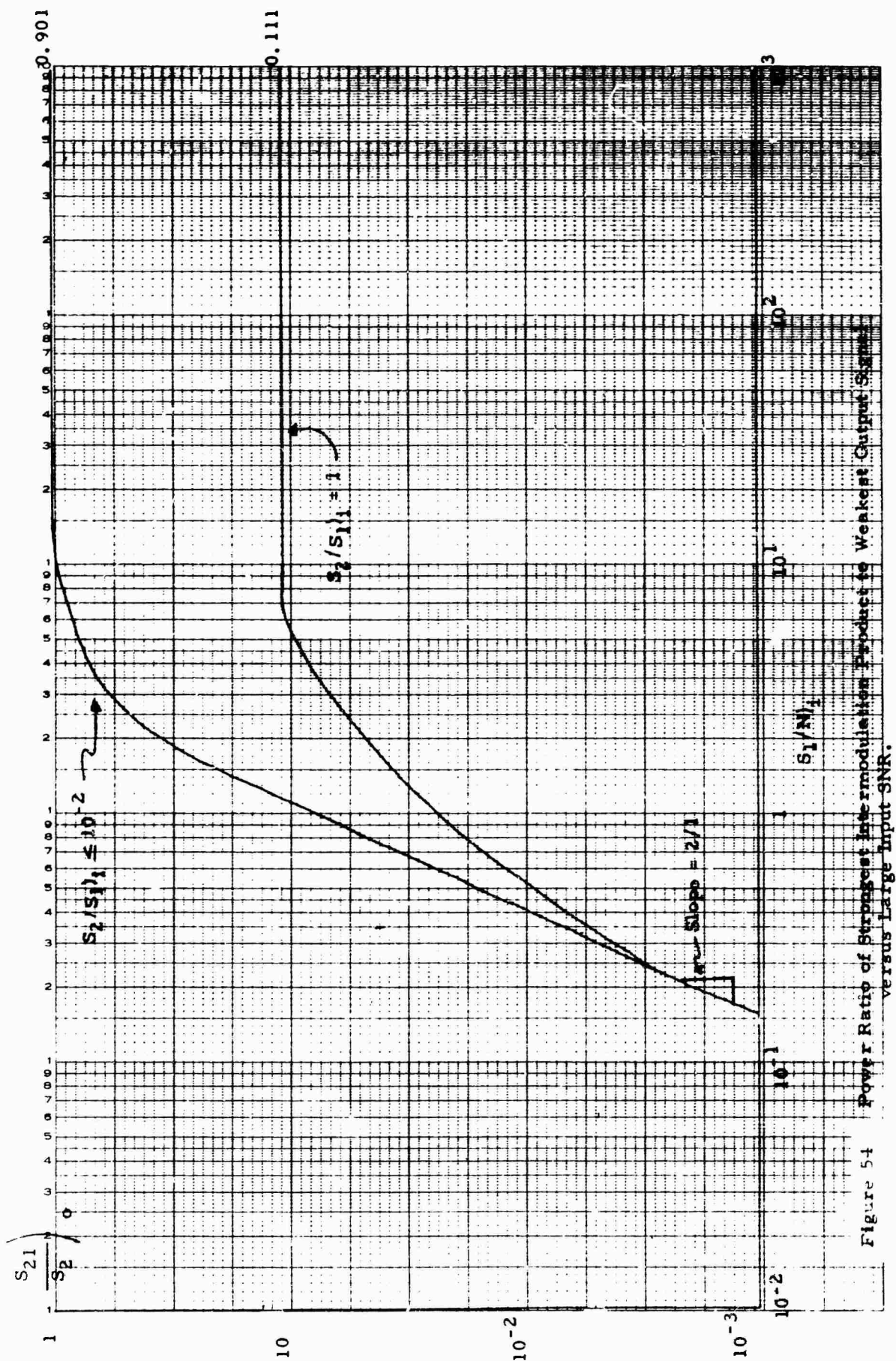


Figure 54 Power Ratio of Strongest Intermodulation Product to Weakest Output Signal versus Large Input SNR.

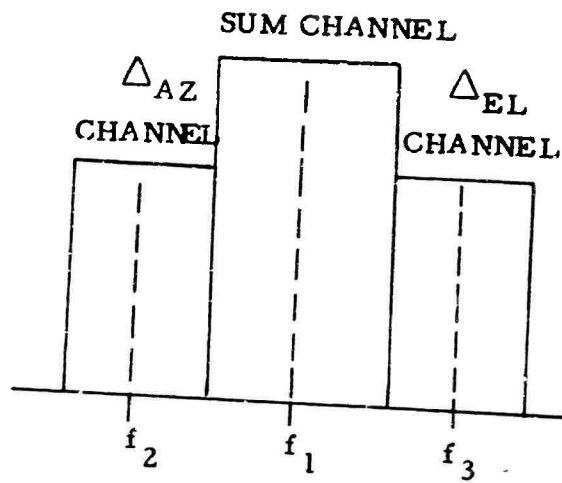


Figure 55 Illustration of Symmetrical Channel Orientation

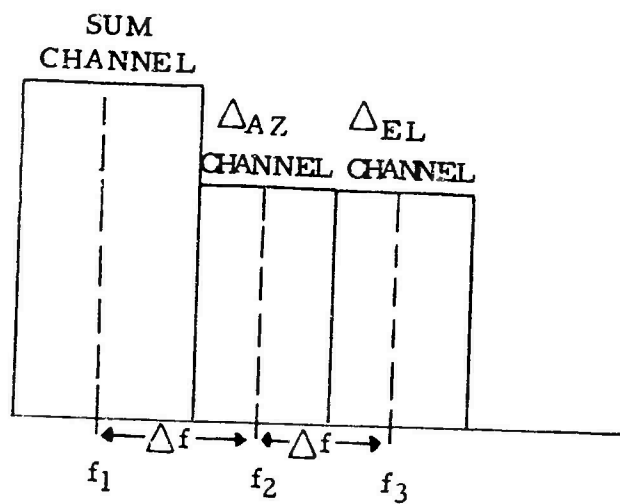


Figure 56 Illustration of Asymmetric Channel Orientation

much higher intermodulation distortion than the asymmetrical configuration of Figure 56.

Since low order intermodulation products account for the majority of the total intermodulation, channel orientation such that these products are not in-band will optimize the system performance. For equal channel spacing  $\Delta f$ , third order intermodulation will occur in-band since  $f_2 - f_1 + \Delta f$  and  $2f_2 - f_1 = f_1 + 2\Delta f = f_3$  in Figure 56. Likewise  $2f_2 - f_3 = f_3 - 2\Delta f = f_1$  results in sum channel intermodulation products. However, no low order products will fall in-band for the  $\Delta_{AZ}$  (innermost) channel. If conservation of bandwidth is not critical then the location of the  $\Delta_{EL}$  channel can be moved up in frequency  $2\Delta f$  above the  $\Delta_{AZ}$  channel and both difference channels are free of the lowest order intermodulation. Fifth order, in the form of  $3f_2 - 2f_1 = f_1 + 3\Delta f$  are now in-band in the  $\Delta_{EL}$  channel, which may not be a problem. If it is, the  $\Delta_{EL}$  channel can be moved up in frequency  $3\Delta f$  above the  $\Delta_{AZ}$  channel and the fifth order products avoided at the expense of increased bandwidth. For the case of interest here, low order intermodulation must be avoided since these undesired signals have levels approaching that of the weakest signal at the limiter output.

One possible system configuration using the SCAMP technique is shown in Figure 57. The inputs from the antenna array are supplied to the comparator. The comparator functions to provide the three outputs,  $\Sigma$ ,  $\Delta_{AZ}$ , and  $\Delta_{EL}$ . A low noise amplifier is used in the sum, or Data Translator channel to provide for low system noise temperatures and to further enhance the relative difference in signal levels into the limiter. This is desirable to provide low intermodulation levels relative to the sum signal, even though Figure 54 indicates a 9.5 dB advantage for large input SNR's if both signal levels are of equal strength. The small signal suppression is maximum under these conditions but this can be compensated for during system calibration.

Since low SNR's in the error, or small signal channels, result in noise jitter (angle fluctuation about the boresight, or mean), these SNR's are important only from the standpoint of pointing angle error. Pointing angle error is mainly a function of the sum channel SNR, and it has been shown<sup>(12)</sup> that for a sum channel SNR of 15 dB or more the rms angle error is less than one-hundredth of the antenna 3 dB beamwidth. From these considerations, only isolators are provided in the error channels before the first mixer to prevent local oscillator leakage between channels.

The FDM (Frequency Division Multiplexer) contains the oscillators, isolators, and mixers used to translate and separate in frequency the three channels. The oscillator  $f_1$  can be tunable, or replaceable, to permit extended system capability. Care must be exercised in the selection of

# DATA TRANSLATOR

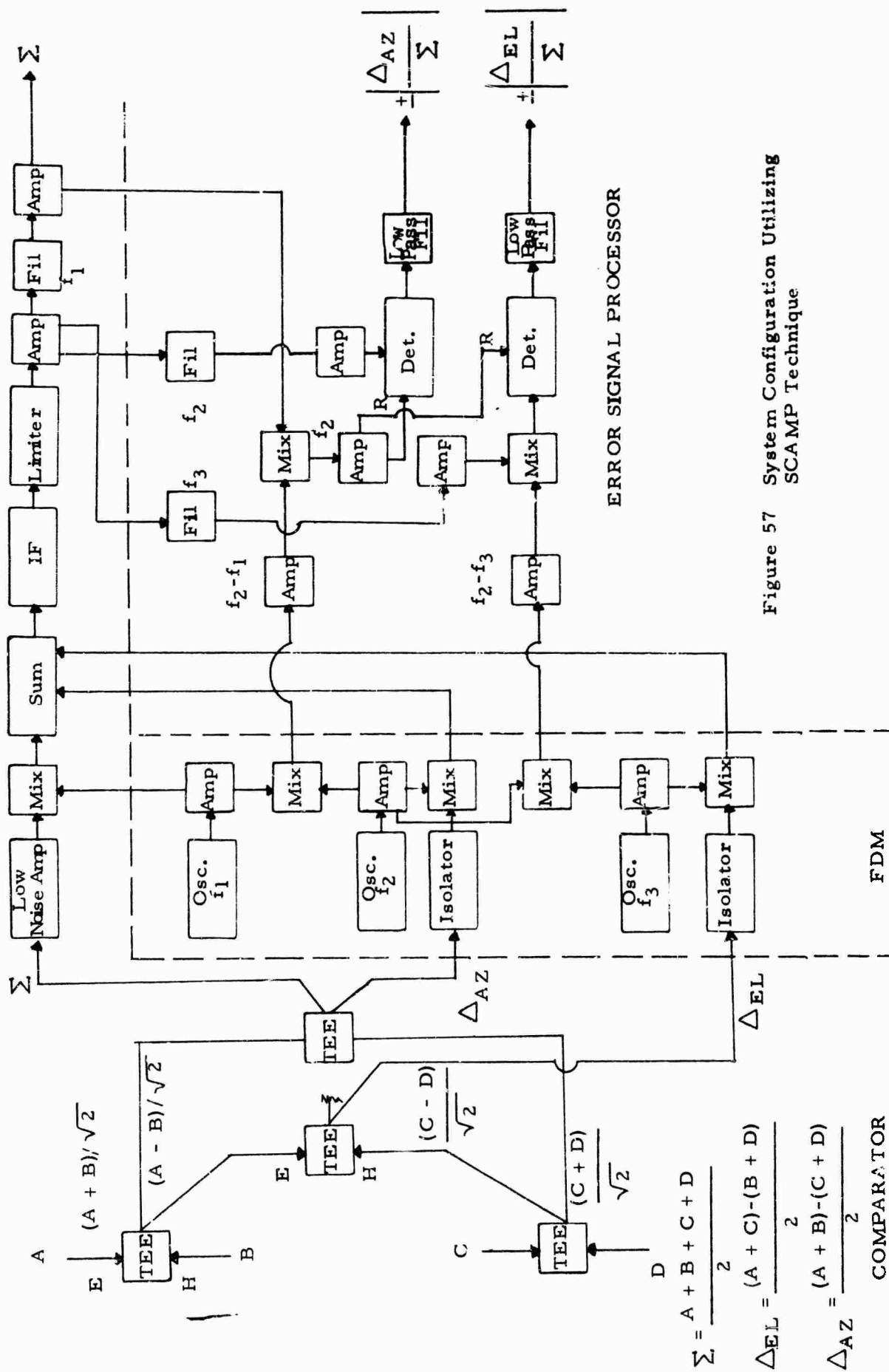


Figure 57 System Configuration Utilizing SCAMP Technique

channel orientation such that intermodulation does not degrade performance when  $f_1$  is changed (assuming no spectra overlap is introduced). The exact IF (Intermediate Frequency) is determined by spurious analysis for the most part, but is normally below 100 MHz. Circuits are less critical in this range and, also, transmission loss is minimized where long cable runs are involved.

The Error Signal Processor provides both magnitude and phase information to the servo system using the sum and difference signals and the local oscillator injection frequencies ( $f_2 - f_1$ ) and ( $f_2 - f_3$ ). The sum channel signal is translated from the center frequency  $f_1$  to  $f_2$  and used as a reference in the phase sensitive detectors for both  $\Delta_{AZ}$  and  $\Delta_{EL}$  channels. Also, the  $\Delta_{EL}$  in this case is translated to the center frequency  $f_2$  before the phase detector.

The main effect of jamming is to introduce another relatively large signal in the limiter, assuming that the signal is in-band and this signal would capture the normalization phenomenon. The system is not normally more immune to unwanted large signals than any other system(s) unless extra precautions are used prior to the limiter.

In summary, the important points of interest in SCAMP are:

- SNR degradation
- Weak signal suppression
- Intermodulation distortion
- Hardware complexity

The first three have each been considered in detail, and they present no extreme difficulty in achieving satisfactory system performance. The hardware requirements are comparable with those of the three channel monopulse techniques, and somewhat more excessive than the pseudo-monopulse case. In addition, the instantaneous normalization feature is not an advantage in the present situation. In fact, as shown in Section VIII, the normalization is worse when the SCAMP technique is used. It appears, then, that the general FDM technique is not desirable as a SCMTR, under the conditions discussed in Section II; i.e., a satellite communications terminal application.

## SECTION XII

### PSEUDO - MONOPULSE

#### 1. INTRODUCTION

Pseudo-monopulse is a hybrid technique which is neither pure TDM nor pure FDM. The term pseudo-monopulse has been previously applied to boresight scanning systems<sup>(26)</sup> in much the same context as the present usage. The basic concept then, is not novel, as may be noted from the bibliography. In fact, applications of the basic method are presently in the field in satellite communications terminals. A detailed evaluation of the technique, including design information, has not been found. The purpose of this section is to provide a compilation of basic information on pseudo-monopulse, both known and new.

The basic system block diagram is shown in Figure 58. The two error channels are combined using techniques which will be described in the next paragraph. The combined error channel (different from a conventional two channel monopulse error channel, as discussed in Section XIII) is then linearly combined with the sum channel to provide a single channel system. Performance of this method in the presence of noise is discussed in the remainder of this section and in Appendix II.

#### 2. OPTIMUM "Q-FUNCTIONS" FOR PSEUDO-MONOPULSE

This discussion is concerned with the analysis of a pseudo-monopulse tracking receiver operating in a thermal noise environment and the determination of the optimum properties of the Q functions. These Q functions for the azimuth and elevation channels are shown in the block diagram of Figure 58 where it is seen that each RF error voltage is multiplied by its respective Q function, summed together, and coupled into the sum channel to constitute the single channel pseudo-monopulse signal. This signal, corrupted by random noise, is down-converted to an IF frequency, demodulated, and multiplied by the Q functions which produce the corresponding azimuth and elevation error voltages for the servo electronics. It is noted that if the error voltages are coupled to the sum voltage with the

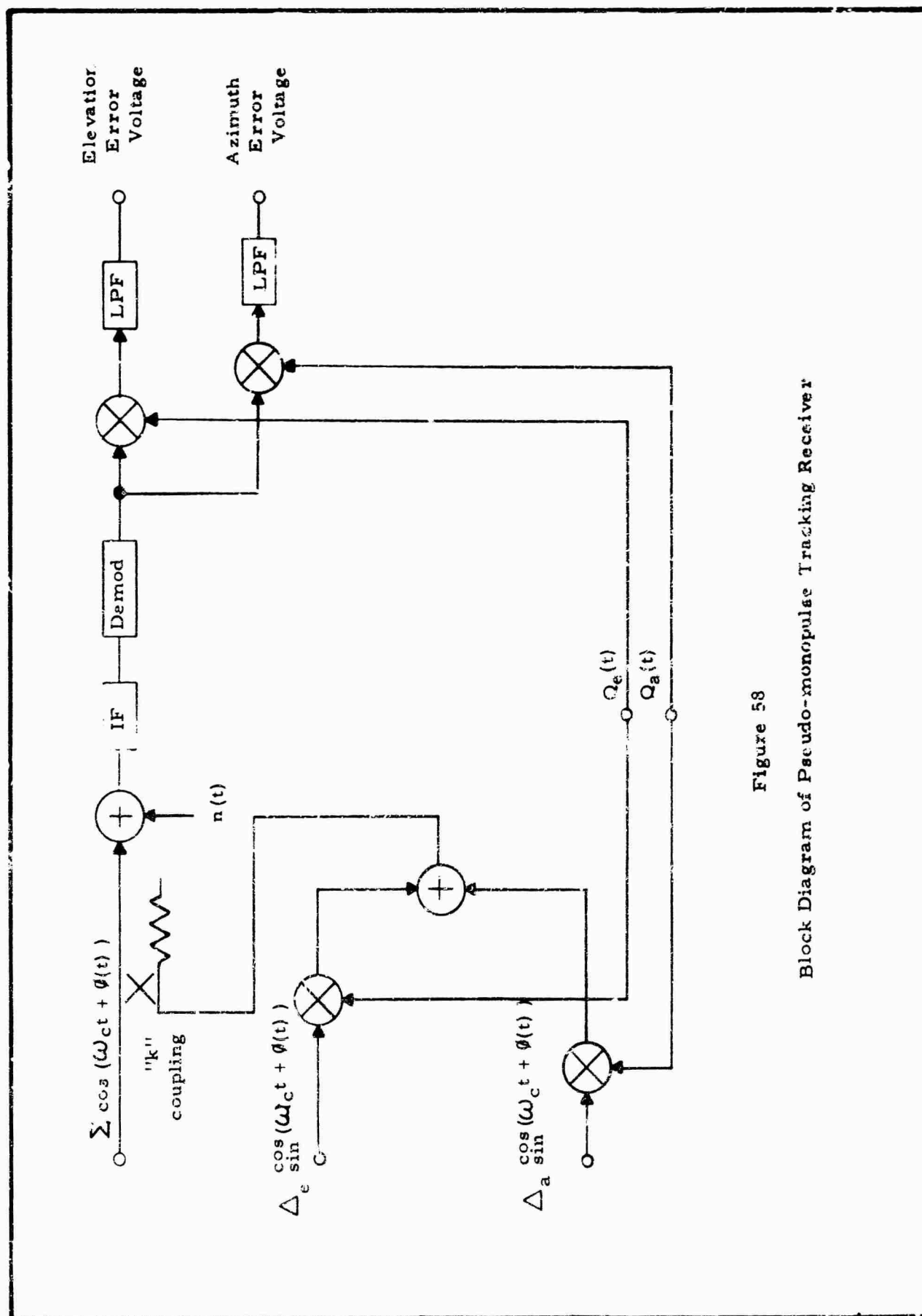


Figure 58  
Block Diagram of Pseudo-monopulse Tracking Receiver



same RF phase, an amplitude modulated signal is formed; whereas, if the sum and error channels are in RF phase quadrature, a phase-modulated signal is formed. Both these cases are considered in the following discussion. In addition, the random noise interference is shown entering the system at the single channel; however, elaboration of this assumption and the pertinence of the model is provided in a following paragraph.

The assumptions appropriate for this pseudo-monopulse model and pertinent to the following analysis are stated in this paragraph. The error signals are low pass with a bandwidth in the order of a Hz or less. The communication signals are angle modulated on the carrier (represented by  $\vartheta(t)$  in Figure 58) and are bandpass signals extending from a few hundred Hz upward. This latter assumption is generally valid and is required for the case for which the error voltages are combined in RF quadrature for a PM scheme; however, this assumption is not required for the AM scheme. The Q functions are assumed deterministic, periodic signals having a bandwidth such that spectral interference with low frequency tracking signals and the higher frequency communication signals (for the PM case) is avoided. Finally, the operations as indicated in the block diagram of Figure 58 are assumed ideal; in particular, the demodulator is assumed an ideal AM or PM detector as would be approximately the condition for above-threshold operation.

The following analysis consists of writing the expressions of the output error voltages for the system of Figure 58 and inferring the optimum properties for the Q functions. For the AM case, the IF signal can be written as:

$$e_1 = n(t) + \sqrt{1 - k^2} \sum_i \left[ 1 + \frac{k Q_e(t) \Delta_e}{\sqrt{1 - k^2} \sum_i} + \frac{k Q_a(t) \Delta_a}{\sqrt{1 - k^2} \sum_i} \right] \cos (W_c t + \phi_i) \quad (124)$$

where  $n(t)$  is the additive noise which is a sample function from a Gaussian random process having uniform spectral height over the band of interest. The output of the ideal AM demodulator for small modulation index is then given by:

$$e_2 = \frac{k Q_e(t) \Delta_e}{\sqrt{1 - k^2} \sum_i} + \frac{k Q_a(t) \Delta_a}{\sqrt{1 - k^2} \sum_i} + \frac{\chi_c(t)}{\sqrt{1 - k^2} \sum_i} \quad (125)$$

where the DC term due to the carrier is removed and where  $X_c(t)$  is the low pass, in-phase noise representation. Multiplication by  $Q_e(t)$  for the elevation error voltage prior to low pass filtering then results in,

$$e_3 = \frac{k\Delta_e Q_e^2(t)}{\sqrt{1-k^2} \Sigma} + \frac{k\Delta_a Q_e(t) Q_a(t)}{\sqrt{1-k^2} \Sigma} + \frac{X_c(t)}{\sqrt{1-k^2} \Sigma} Q_e(t) \quad (126)$$

For the PM case, the IF signal can be written as,

$$e_4 = n(t) + \sqrt{1-k^2} \cos(W_c t + \phi(t)) \quad (127)$$

$$+ \left[ (k Q_e(t) \Delta_e + k Q_a(t) \Delta_a) \right] \sin(W_c t + \phi(t))$$

and the output of the ideal PM detector assuming ideal limiting and small modulation index is thus,

$$e_5 = A \cos \left\{ W_c t + \phi(t) - \frac{k\Delta_e}{\sqrt{1-k^2} \Sigma} Q_e(t) - \frac{k\Delta_a}{\sqrt{1-k^2} \Sigma} Q_a(t) + \frac{X_s(t)}{\sqrt{1-k^2} \Sigma} \right\} \quad (128)$$

where  $X_s(t)$  is the low-pass, quadrature representation of the noise. The output of the elevation  $Q$  detector then follows as,

$$e_6 = \frac{k\Delta_e}{\sqrt{1-k^2} \Sigma} Q_e^2(t) + \frac{k\Delta_a}{\sqrt{1-k^2} \Sigma} Q_e(t) Q_a(t) + \frac{X_s(t)}{\sqrt{1-k^2} \Sigma} Q_e(t) \quad (129)$$

This expression for the PM case is thus seen to be identical to that for AM with the same properties of in-phase and quadrature noise terms -  $X_c(t)$  and  $X_s(t)$ , respectively.

The error signal,  $e_3$  or  $e_6$ , is then applied to a low pass filter or integrator such as the servo subsystem would provide and this output is desirably high signal-to-noise ratio for optimum tracking performance. The first term of  $e_3$  or  $e_6$  after filtering or integration is the desired signal and it is desired that this term be a maximum time-invariant constant,

as,

$$\frac{1}{T} \int_0^T Q_c^2(t) dt = \text{constant, maximum} \quad (130)$$

by the choice of Q functions where T is the equivalent integration time determined by the low pass filter. The second term of  $e_3$  or  $e_6$  after integration represents cross-coupling interference and it is desired that this term be approximately zero as,

$$\frac{1}{T} \int_0^T Q_e(t) Q_a(t) dt \approx 0 \quad (131)$$

The third term of  $e_3$  or  $e_6$  after filtering represents the noise which is effective in producing an angular jitter in the antenna. It can be argued that the product term  $\sum s(t) Q_1(t)$  represents convolution of the individual spectra and for  $Q_1(t)$  narrow band compared to  $\sum s(t)$  (one of the assumptions), the spectral density at low frequencies is uniform with height proportional to the integral of  $Q^2(t)$ . The conclusion is that this term is not important to the optimum Q function determination since the spectrum is not changed appreciably for different Q functions and, although the noise power increases with the energy of the Q function, the signal power increases as the square of this. Thus, Equation (130) is a sufficient constraint for both the first and third terms and Equation (131) is the constraint for the second term.

Under the assumed conditions, then, the optimum Q functions are those which are approximately orthogonal and have maximum energy for a time comparable to the integration time. It is desirable to place further restrictions on the multipliers and adder to limit the difficulties of practical realization. The intent of these restrictions is to prohibit the use of RF amplifiers or other noise-generating devices in this portion of the system.

The restriction to be placed on the scanner unit, then, is that it be "instantaneously passive". The term "instantaneously passive" means that, for a time long compared with the period of the carrier the scanner acts as a passive circuit in the conventional sense. The circuit may be time-varying, however, as long as these variations do not significantly affect the RF bandwidth. This definition allows switches, diode modulators, ferrites, motor driven elements, and other semi-passive devices to be used. The instantaneous "gain" of the device must not exceed unity, however, to be consistent with the definition.

Within the above restriction, the basic limitation on passive combiners, discussed in Appendix I, can be invoked; i.e., the total power out is limited in a three port device. In equation form,

$$Q_e^2(t) + Q_a^2(t) \leq 1 \quad (132)$$

for all  $t$ . In particular, when an equal performance requirement is placed on the two error channels, the average power out due to either error channel is one-half the input power in that channel. For example, consider the case of input powers of  $P_1$  and  $P_2$  in the azimuth and elevation error channels and noise powers  $N_1$  and  $N_2$  in the same channels. The maximum signal power out will then be,

$$\frac{1}{2} (P_1 + P_2)$$

and the noise power out will be,

$$\frac{1}{2} (N_1 + N_2)$$

under maximum signal power conditions.

Using the "instantaneously passive" argument, the output must satisfy the above conditions at any time and, therefore, must satisfy the conditions on a long term average. Note that the concepts in the "instantaneously passive" definition are consistent with the original assumptions; i.e., the  $Q$  functions have bandwidths such that spectral interference with the communications signals is avoided.

Three different sets of optimum  $Q$  functions are shown in Figure 59.

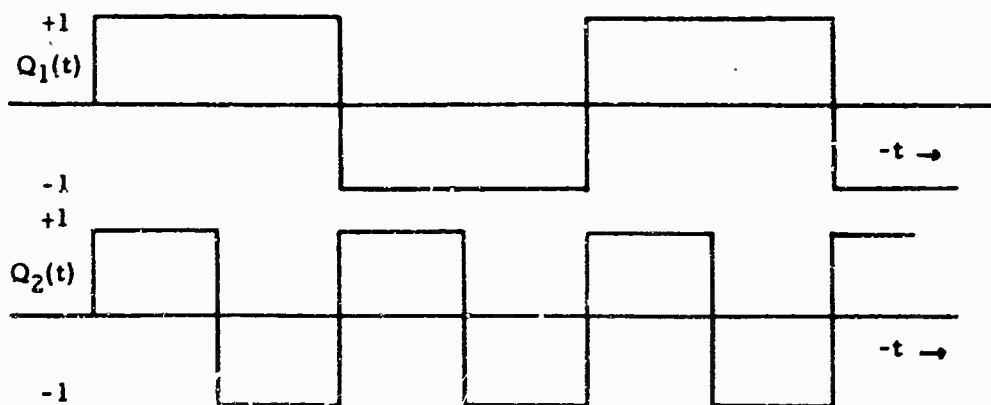


Figure 59-a

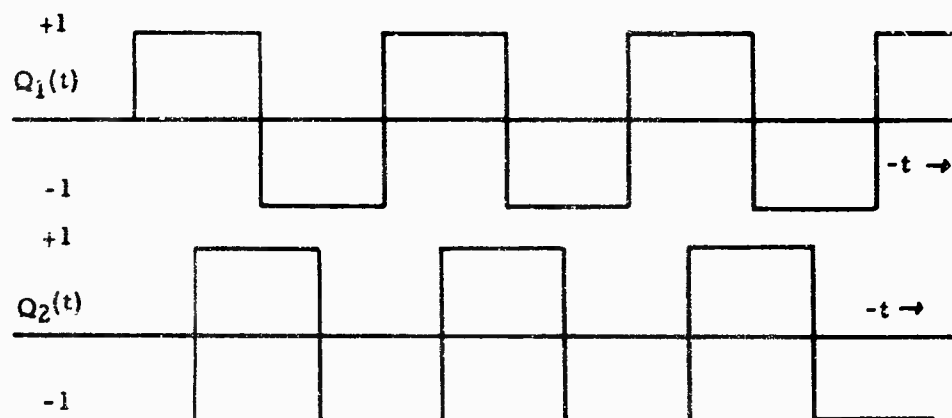


Figure 59-b

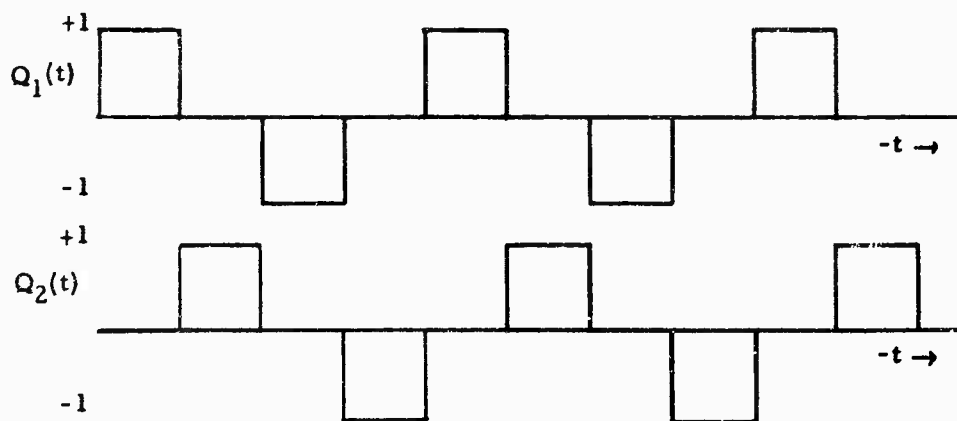


Figure 59-c

Figure 59 Q-function Examples

The first set is orthogonal due to the different frequencies of  $Q_1$  and  $Q_2$ . The sum  $Q_1^2$  plus  $Q_2^2$  is unity for all time so the maximum energy condition is satisfied. Implementation of this arrangement could be accomplished using ferrite phase shifters to obtain the phase reversals and a 3 dB coupler (reactive power divider) to sum the two signals.

The second set of signals is orthogonal because of the quadrature phase relationships. The amplitude conditions and implementation is the same as the first set.

The third set of signals is orthogonal since one of the two functions is always zero. The other function is unity, so the maximum energy condition is satisfied. Implementation could be accomplished using a phase shifting circuit to generate waveforms (as in the generation of 59(b)) followed by a switch alternately connected to the two inputs. An alternate implementation is possible using folded hybrids and latching phase shifters to accomplish the same functions.

Another optimum set of Q functions are a sine wave and a cosine wave, both with unity peak amplitude. The sine and cosine functions are orthogonal, as desired, and the total energy at any time is given by,

$$\sin^2 + \cos^2 = 1$$

therefore, the maximum energy condition is satisfied at all times. This method can be implemented using a time variable coupling device such as a rotating plate in crosspolarized waveguide; e.g., consider a circular guide driven orthogonally (in polarization) by the two error signals. A rotating quarter-wave plate in the guide, followed by a linearly polarized output port will exhibit a sinusoidal coupling as a function of the orientation of the plate. Thus, when the plate is rotated at a constant speed, the desired Q functions are generated.

One other desirable property of Q functions can be seen from equation (124). In order to maintain proper normalization, the pointing error signals should be independent of received signal strength. Normalization is normally accomplished by maintaining the sum channel at a constant level. It is desirable, then, to have the average contribution to the envelope due to the error channels equal to zero. This will prevent slow changes in normalization factor due to changes in pointing error. The desired property, then, is that the average values of both  $Q_1$  and  $Q_2$  equal zero. The Q functions illustrated all exhibit this property. Note that simpler circuits could be used if the zero average value constraint were not imposed; e.g., a simple switch cycling between the two error channels would provide

orthogonal, maximum energy signals, but additional phase shifters are required to obtain zero average value. An additional advantage occurs in the demodulation circuitry when zero average value functions are used since AC coupling can be used without the need for DC restoration.

It is of interest to examine the noise which appears at the scanner output when the input is noisy; i.e., antenna noise and line losses are appreciable. The noise power out is given by,

$$N_o = Q_1^2 N_1 + Q_2^2 N_2 \quad (133)$$

where  $N_1$  and  $N_2$  are the noise power inputs in channels 1 and 2. A case of particular interest occurs when  $N_1$  and  $N_2$  are equal power and independent. Then, under the "optimum" conditions,  $Q_1^2 + Q_2^2 = 1$ , the noise power out is constant. This result is compatible with the model used in this discussion, which verifies the original assumptions.

In summary, optimum Q functions should exhibit three basic properties:

Orthogonality	$\int Q_1(t) Q_2(t) dt = 0$
Maximum energy	$Q_1^2(t) + Q_2^2(t) = 1$ for all t
Zero Average value	$\int Q_1(t) dt = \int Q_2(t) dt = 0$

where the integrals are evaluated over a long time period. The first two requirements, and sometimes the third, will also produce an optimum two channel monopulse system, since the criteria are identical. Fortunately, optimum Q functions can be readily obtained in practice with available hardware. Selection of THE most desirable functions is generally dependent upon equipment considerations, and nearly optimum Q functions should be used. An improper choice can degrade the system significantly, so care must be taken to insure that the three basic criteria are met.

### 3. PREAMPLIFIERS IN PSEUDO-MONOPULSE RECEIVERS

The optimum usage of preamplifiers in a pseudo-monopulse system is the subject of this paragraph. It is apparent in a full monopulse system, for example, that low noise preamplifiers directly influence the signal-to-noise ratio in their respective channels. The effect in a pseudo-monopulse system is not so easily determined, since the three channels are ultimately

combined to form a single channel. Placement of preamplifiers before and/or after combining the channels causes different effective signal-to-noise ratios at the output.

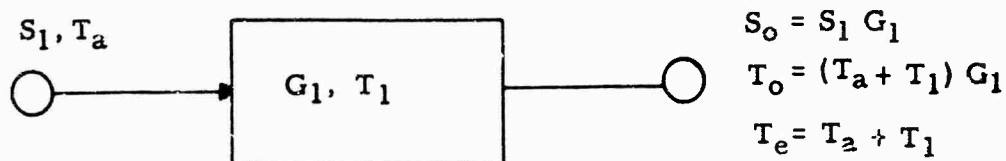
Six different circuit configurations, in addition to full monopulse for comparison, are analyzed in following paragraphs. These configurations are neither unique nor all-inclusive, but they do represent most cases of practical interest. Although this analysis does not include all possible noise sources, it can easily be extended to any desired degree of complexity. Simplifying assumptions were made to facilitate comparison of the various techniques, and they illustrate the relative values of the different configurations. These assumptions, that no excess noise is added in combiners and couplers, are very nearly achieved in practice.

The building blocks used for the systems (see Figure 60) are amplifiers, combiners, and couplers. Each amplifier is characterized by a power gain  $G$  and a noise temperature  $T$ . The inputs are the sum and difference channels from a monopulse feed-comparator system, and are described in terms of signal power  $S$  and effective antenna noise temperature  $T_a$ . Thus, the signal power out of the amplifier would be the gain times the signal power in, and the noise power out would be the gain times the sum of the source noise temperature and the amplifier noise temperature. The effective noise temperature,  $T_e$ , referred to the input terminals is the output noise temperature divided by the signal power gain from input to output. These expressions are summarized in Figure 60-a.

In pseudo-monopulse systems of most general interest, the performance required on the two error channels is identical. Under these conditions, and utilizing optimum "Q-functions" and the best possible passive combiners (see Appendix I), the combiner is characterized as shown in Figure 60-b. The signal power out due to an input signal power  $S_2$  is  $S_2/2$ . Similarly, the other channel input power is divided by 2. The output noise temperature is then one-half the sum of the input noise temperatures. Note that in the special case of equal input noise temperatures, the output noise temperature is equal to the input noise temperature on either channel.

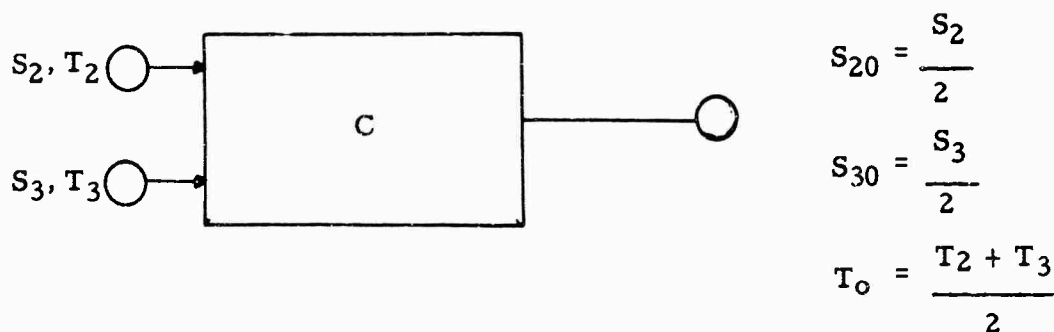
The coupler is a more general type of combiner in which the power gain to signal 1 is  $(1 - k^2)$  and the power gain to signal 2 is  $k^2$ . Thus, the output noise temperature is characterized as shown in Figure 60-c. Note that the combiner is a coupler with  $k^2 = 1/2$ . The coupler has been shown in Appendix I to be optimum in the same sense as the combiner. Thus, the building blocks are both theoretically optimum and practically realizable; e.g., the combiner could be a hybrid or magic tee and the coupler could be a directional coupler.





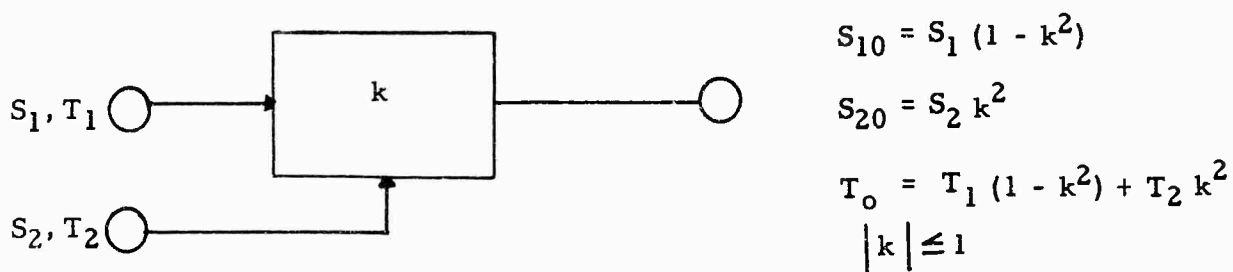
Amplifier and Input Signals

Figure 60-a



Equal Power Combiner

Figure 60-b



Coupler

Figure 1-c

Basic System Components and Properties

Figure 60

Figures 61 - 67 show the configurations being considered and the appropriate signal and noise temperature expressions. In all cases,  $S_1$  refers to the sum channel,  $S_n$  refers to the output signal  $n$ , and the effective noise temperature,  $T_{en}$ , refers to the noise temperature referenced to input channel  $n$ . Only one difference channel equation is derived since the performance of the two channels has been stipulated to be identical. In order to evaluate the various techniques, two types of amplifiers are being considered; the unit characterized by  $G_1, T_1$  would be a low noise preamplifier, whereas, the unit  $G_2, T_2$  represents a higher noise figure receiver. Thus, the number of  $G_1, T_1$  units required is a measure of the complexity of the method.

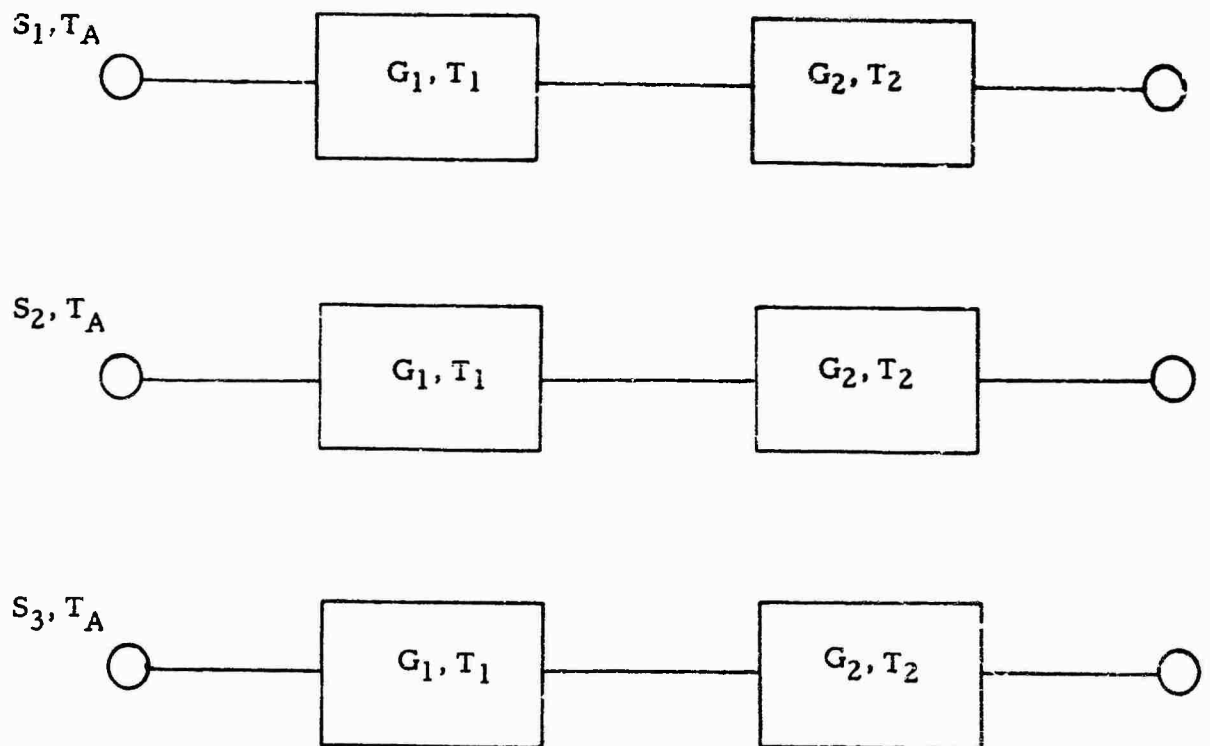
The first method shown is a full monopulse receiver with preamplifiers in each channel (see Figure 61). This case serves as a basis for comparison of performance, since all other configurations have worse signal-to-noise ratios. The performance of all three channels is identical, of course, and the effective noise temperature referred to the input terminals is, for large values of  $G_1$ , essentially determined by  $T_A$  and  $T_1$ .

The first pseudo-monopulse configuration, shown in Figure 62 uses three preamplifiers. A comparison of this technique with full monopulse shows difference in the noise characteristics determined solely by the coupling factor. Another configuration, shown in Figure 63, uses a single preamplifier following the coupler. It is interesting to note that the performance of this circuit is identical to that of the previous circuit, but two less preamplifiers are required! Thus, as long as the assumptions are valid (i.e., the combiner and coupler are nearly ideal) circuit #2 would always be preferred over circuit #1.

Figure 64 shows a configuration with three preamplifiers, but arranged differently from circuit #1. Figure 65 shows a circuit with two preamplifiers which have identical performance to the previous circuit. Thus, for the assumed ideal combiner situation, circuit #4 would always be preferred over circuit #3.

Figure 66 illustrates an alternate use of a single preamplifier. Figure 67 illustrates an alternate use of two preamplifiers. The above circuits represent all practical configurations which would provide good signal-to-noise ratios in a pseudo-monopulse system.

In order to evaluate the relative merits of these circuits, some simplifying assumptions will be made. In the event these assumptions do not fit a particular situation, the appropriate values of  $G, k$ , and  $T$ 's can be used in the general expressions in Figures 61 - 67. The comparison technique will be to examine the equivalent noise temperatures, referred



$$S_{10} = G_1 G_2 S_1$$

$$S_{20} = G_1 G_2 S_2$$

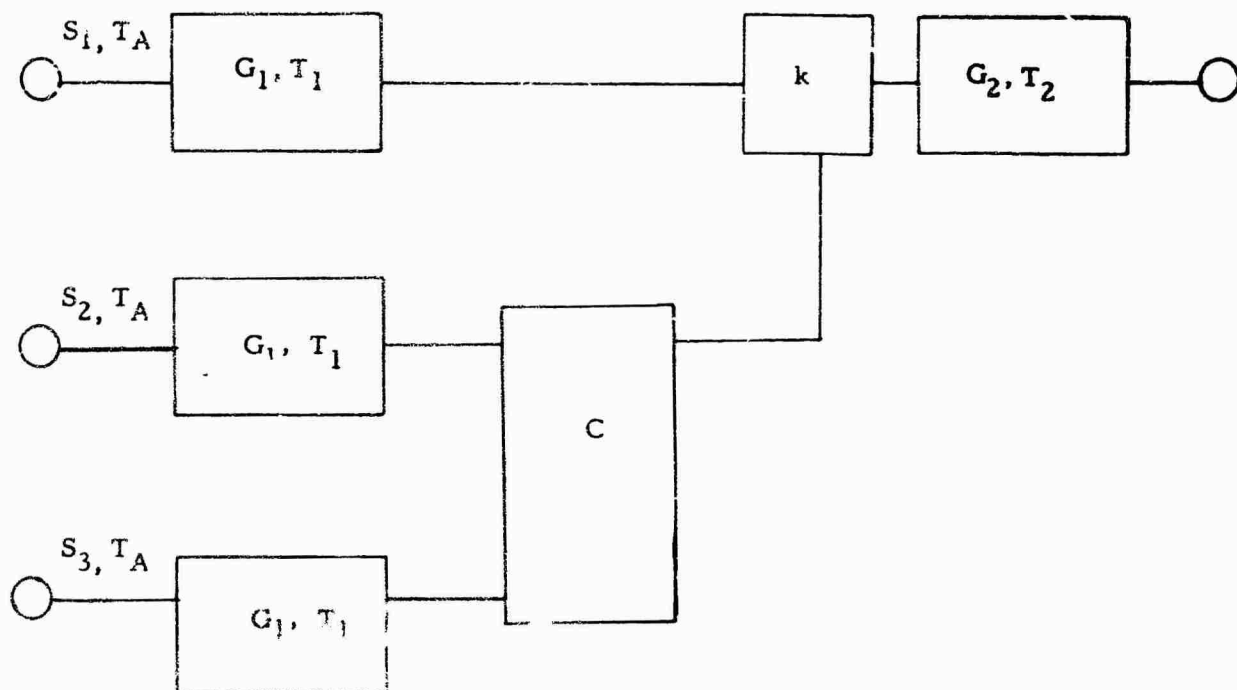
$$S_{30} = G_1 G_2 S_3$$

$$T_{10} = T_{20} = T_{30} = G_1 G_2 (T_1 + T_A) + G_2 T_2$$

$$T_{E1} = T_{E2} = T_{E3} = (T_1 + T_A) + \frac{T_2}{G_1}$$

Full Monopulse Configuration

Figure 61



$$S_{10} = S_1 G_1 G_2 (1 - k^2)$$

$$S_{20} = \frac{S_2 G_1 G_2 k^2}{2}$$

$$T_o = (T_A + T_1) G_1 G_2 + G_2 T_2$$

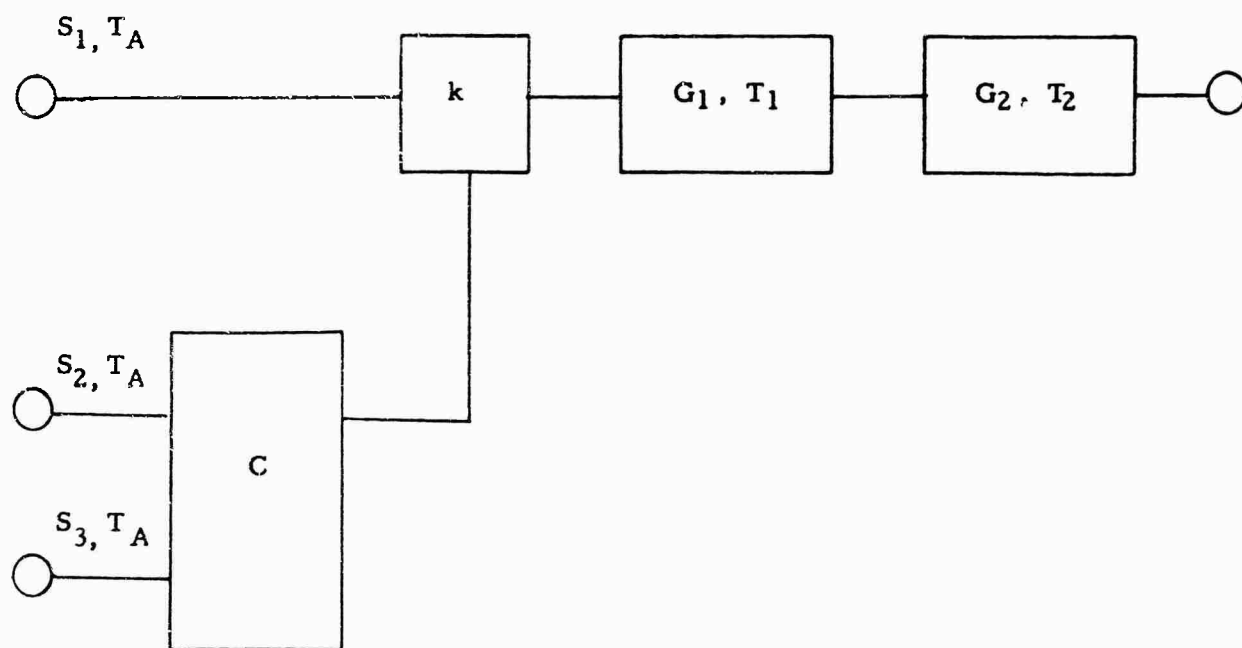
$$T_{E1} = \frac{(T_A + T_1) + T_2/G_1}{(1 - k^2)}$$

$$T_{E2} = \frac{2}{k^2} \left[ (T_A + T_1) + T_2/G_1 \right]$$

Circuit #1

Pseudo-Monopulse with Three Preamplifiers

Figure 62



$$S_{10} = S_1 G_1 G_2 (1 - k^2)$$

$$S_{20} = \frac{S_2 G_1 G_2 k^2}{2}$$

$$T_o = (T_A + T_1) G_1 G_2 + T_2 G_2$$

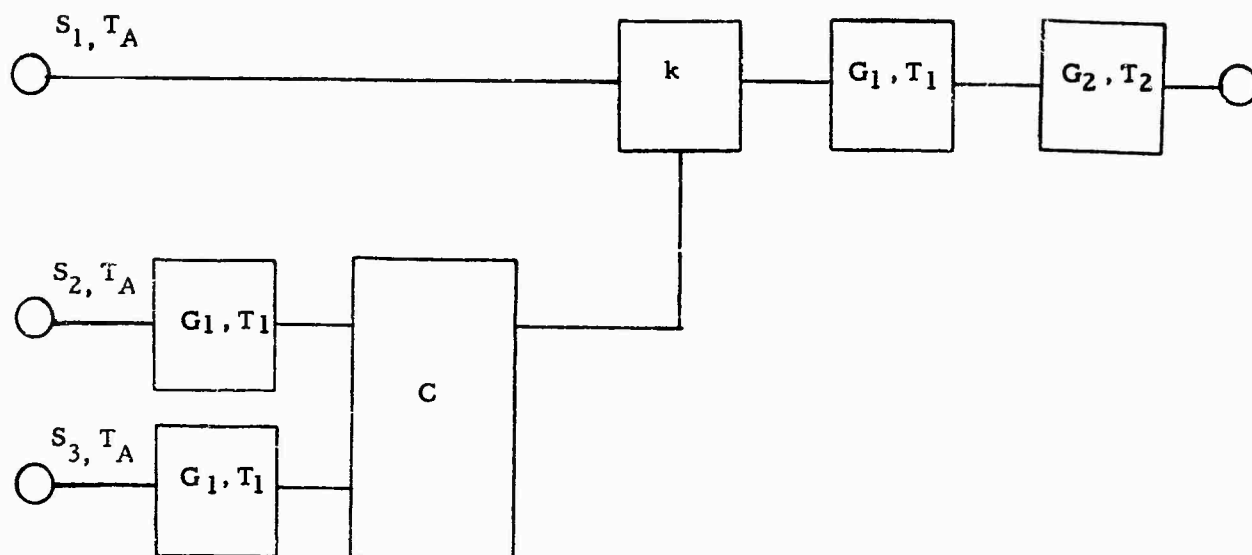
$$T_{E1} = \frac{(T_A + T_1) + T_2/G_1}{(1 - k^2)}$$

$$T_{E2} = \frac{2}{k^2} \left[ (T_A + T_1) + T_2/G_1 \right]$$

Circuit #2

Pseudo-Monopulse with One Preamplifier

Figure 63



$$S_{10} = S_1 G_1 G_2 (1 - k^2)$$

$$S_{20} = \frac{S_2 G_1^2 G_2 k^2}{2}$$

$$T_o = T_A (1 - k^2) G_1 G_2 + (T_A + T_1) k^2 G_1^2 G_2 + G_1 G_2 T_1 + G_2 T_2$$

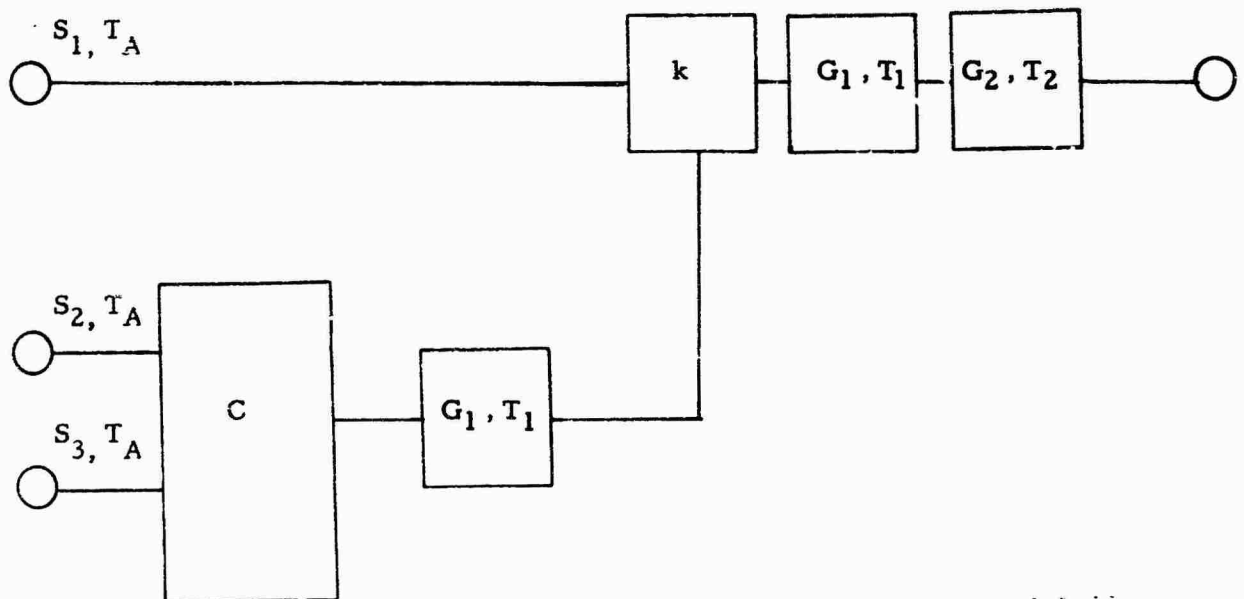
$$T_{E1} = \frac{T_A (1 - k^2) + G_1 k^2 (T_A + T_1) + T_1 + T_2/G_1}{(1 - k^2)}$$

$$T_{E2} = \frac{2}{k^2 G_1} \left[ T_A (1 - k^2) + G_1 k^2 (T_A + T_1) + T_1 + T_2/G_1 \right]$$

Circuit #3

Pseudo-Monopulse with Three Preamplifiers

Figure 64



$$S_{10} = S_1 G_1 G_2 (1 - k^2)$$

$$S_{20} = \frac{S_2 G_1^2 G_2 k^2}{2}$$

$$T_o = T_A (1 - k^2) G_1 G_2 + (T_A + T_1) k^2 G_1^2 G_2 + T_1 G_1 G_2 + T_2 G_2$$

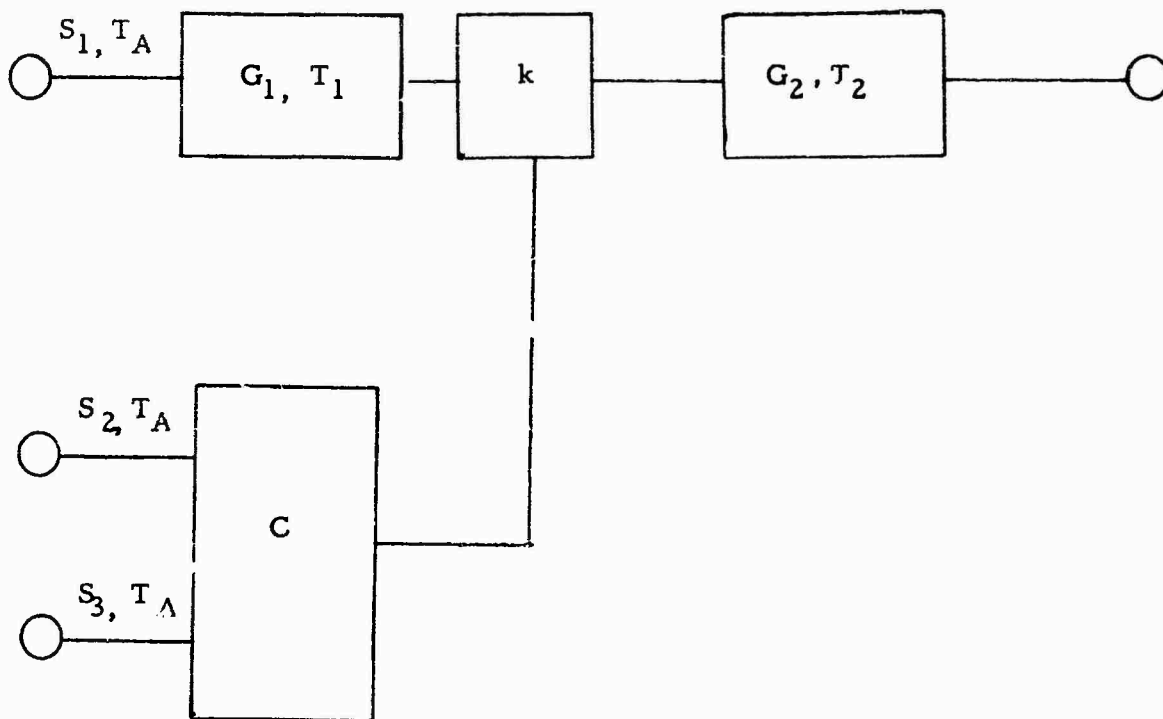
$$T_{E1} = \frac{T_A (1 - k^2) + G_1 k^2 (T_A + T_1) + T_1 + T_2 / G_1}{(1 - k^2)}$$

$$T_{E2} = \frac{2}{k^2 G_1} \left[ T_A (1 - k^2) + G_1 k^2 (T_A + T_1) + T_1 + T_2 / G_1 \right]$$

Circuit #4

Pseudo-Monopulse with Two Preamplifiers

Figure 65



$$S_{10} = S_1 G_1 G_2 (1 - k^2)$$

$$S_{20} = \frac{S_2 G_2 k^2}{2}$$

$$T_o = (T_A + T_1) G_1 G_2 (1 - k^2) + T_A k^2 G_2 + G_2 T_2$$

$$T_{E1} = (T_A + T_1) + \frac{(T_A k^2 + T_2)}{G_1 (1 - k^2)}$$

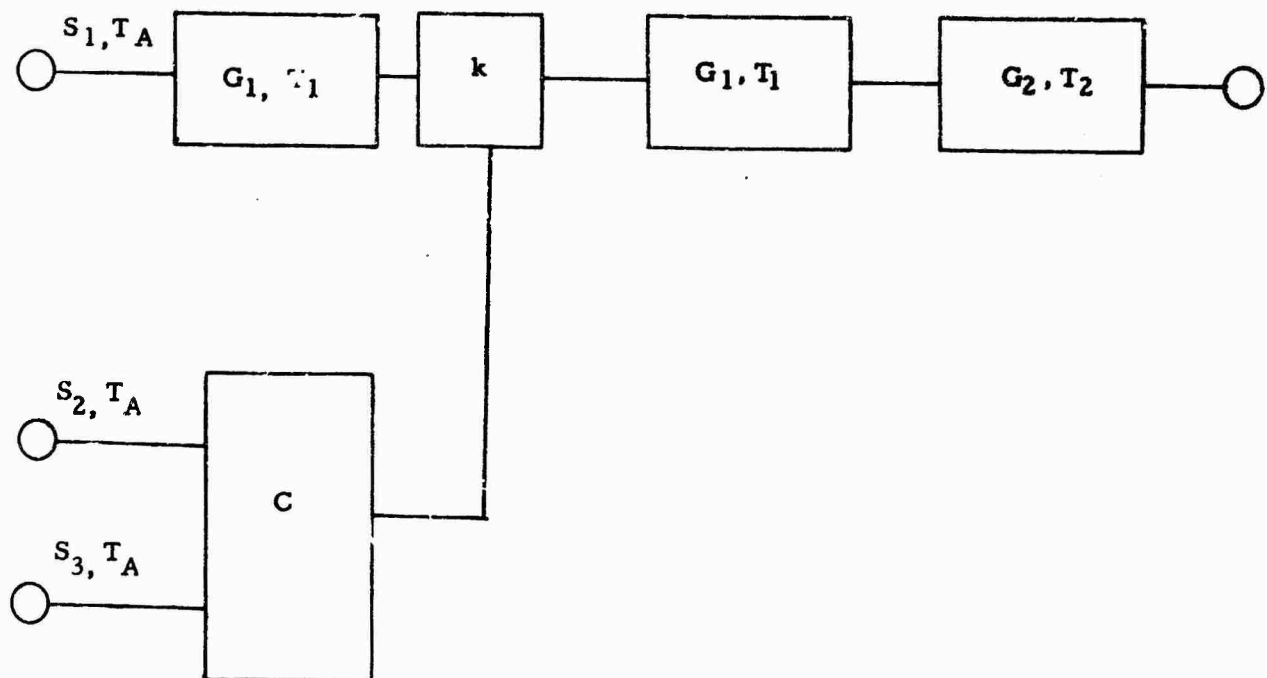
$$T_{E2} = \frac{2}{k^2} \left[ (T_A + T_1) G_1 (1 - k^2) + (T_A k^2 + T_2) \right]$$

Circuit #5

Pseudo-Monopulse with One Preamplifier

Figure 66





$$S_{10} = S_1 G_1^2 G_2 (1 - k^2)$$

$$S_{20} = \frac{S_2 k^2 G_1 G_2}{2}$$

$$T_o = (T_1 + T_A) G_1^2 G_2 (1 - k^2) + (T_A k^2 + T_1) G_1 G_2 + T_2 G_2$$

$$T_{E1} = (T_1 + T_A) + \frac{T_A k^2 + T_1 + T_2/G_1}{G_1 (1 - k^2)}$$

$$T_{E2} = \frac{2}{k^2} \left[ (T_1 + T_A) G_1 (1 - k^2) + T_A k^2 + T_1 + T_2/G_1 \right]$$

Circuit #6

Pseudo-Monopulse with Two Preamplifiers

Figure 67

ed to the appropriate input terminals, and; (1) compare the performance to full monopulse and (2) compare the difference channel performance under the conditions of equal sum channel degradation.

Consider first the comparison of circuit #2 (which is identical to circuit #1) with full monopulse. The ratio,  $\Sigma_{2F}$ , of sum channel noise temperature for circuit #2 to sum channel noise temperature in full monopulse is then,

$$\Sigma_{2F} = \frac{1}{1 - k^2} \quad (134)$$

The ratio of difference channel noise temperatures,  $\Delta_{2F}$ , is,

$$\Delta_{2F} = \frac{2}{k^2} \quad (135)$$

The sum channel performance is worse than full monopulse by a small factor (equal to the insertion loss of the coupler). The difference channel is worse than full monopulse by a relatively large factor, 3 dB plus the coupling loss of the directional coupler.

Consider next a comparison of circuit #2 and circuit #4 (which is identical with circuit #3). Equating the sum channel noise temperatures yields

$$\frac{T_A + T_1 + T_2 / G_1}{1 - k_2^2} = \frac{T_A(1 - k_4^2) + G_1 k_4^2 (T_A + T_1) + T_1 + T_2 / G_1}{1 - k_4^2} \quad (136)$$

The ratio  $\Delta_{42}$  of the circuit #4 difference channel equivalent noise temperature to that of circuit #2 is,

$$\Delta_{42} = \frac{k_2^2}{G_1 k_4^2} \left[ \frac{T_A(1 - k_4^2) + G_1 k_4^2 (T_A + T_1) + T_1 + T_2 / G_1}{T_A + T_1 + T_2 / G_1} \right] \quad (137)$$

Combining equations (136) and (137) yields,

$$\Delta_{42} = \frac{1 + \frac{T_1 + T_2/G_1}{G_1 (T_A + T_1)}}{1 + \frac{T_2}{G_1 (T_A + T_1)}} \quad (138)$$

The difference channel performance is nearly identical for the two circuits. When,

$$T_1 + T_2/G_1 \leq T_2$$

then circuit #4 will be superior to circuit #2. These conditions are likely in a well designed system, corresponding to a large ratio of  $T_2$  to  $T_1$  and/or a large gain  $G_1$ . The overall improvement is extremely small, however, and is easily outweighed by the complexity of the additional pre-amplifier required in circuit #4.

Consider next circuit #5 as compared with circuit #2. Again, equating the sum channel performance, one finds,

$$\frac{T_A + T_1 + T_2/G_1}{1 - k_2^2} = \frac{(T_A + T_1) G_1 (1 - k_5^2) + T_A k_5^2 + T_2}{G_1 (1 - k_5^2)} \quad (139)$$

The ratio of the difference channel equivalent noise temperature in circuit #5 to that in circuit #2 is,

$$\Delta_{52} = \frac{k_2^2}{k_5^2} \left[ \frac{(T_A + T_1) G_1 (1 - k_5^2) + T_A k_5^2 + T_2}{T_A + T_1 + T_2/G_1} \right] \quad (140)$$

Combining equations (139) and (140) yields,

$$\Delta_{52} = \frac{T_A + T_2}{T_A + T_1 + T_2/G_1} \quad (141)$$

Since, in most cases of interest,  $T_1$  is considerably less than  $T_2$  and  $T_2/G_1$  is less than  $T_1$ ,  $\Delta_{52}$  will be greater than unity. In the limit, when  $T_A$  is small,  $\Delta_{52}$  can become large compared to one. Thus, circuit #5 is inferior in performance to circuit #2.

Finally, consider circuit #6 which requires two preamplifiers. Equating the sum channel equivalent noise temperature to that of circuit #2 gives,

$$\frac{T_A + T_1 + T_2/G_1}{1 - k_2^2} = \frac{G_1 (1 - k_6^2) (T_1 + T_A) + T_A k_6^2 + T_1 + T_2/G_1}{G_1 (1 - k_6^2)} \quad (142)$$

The ratio of the difference channel noise temperature is,

$$\Delta_{62} = \frac{k_2^2}{k_6^2} \left[ \frac{G_1 (1 - k_6^2) (T_1 + T_A) + T_A k_6^2 + T_1 + T_2/G_1}{T_A + T_1 + T_2/G_1} \right] \quad (143)$$

Combining equations (142) and (143) yields,

$$\Delta_{62} = \frac{T_A k_6^2 + T_1 + T_2 (1/G_1 + k_6^2 - 1)}{k_6^2 (T_A + T_1 + T_2/G_1)} \quad (144)$$

Equation (144) cannot be simply interpreted without recognizing that, for circuit #6, the receiver noise contribution ( $T_2$ ) should be very small and the coupling factor,  $k_6$ , should approach unity. When the contribution from  $T_2$  can be neglected,

$$\Delta_{62} = \frac{T_A k_6^2 + T_1}{k_6^2 (T_A + T_1)} = 1 + \frac{T_1 (1 - k_2^2)}{k_6^2 (T_A + T_1)} \quad (145)$$

Thus, when effects of  $T_2$  are neglected, the performance is inferior to that of circuit #2 by a small amount. Since circuit #6 requires two preamplifiers, circuit #2 would be a preferred configuration.

In summary, the relatively simple configuration, circuit #2, which requires only one preamplifier has been shown to be equal or superior to all other pseudo-monopulse configurations. This circuit has also been compared with full monopulse, to determine the degradation due to noise. This comparison, as shown in equations (134) and (135), illustrates the tradeoff between sum channel degradation and difference channel (pointing error due to noise) accomplished, both theoretically and in practice, by simply varying the value of the coupler  $k$ . As an illustration, consider the use of a 10 dB coupler; i.e.,  $k^2 = 0.1$ . Then the sum channel degradation is,

$$= \frac{1}{1 - 0.1} = \frac{1}{0.9} \text{ or } 0.46 \text{ dB} \quad (146)$$

and the difference channel degradation is,

$$= \frac{2}{0.1} = 20 \text{ or } 13 \text{ dB} \quad (147)$$

Other values of couplers will produce less sum channel degradation and greater difference channel degradation (for smaller coupling factor) or vice-versa (for larger coupling factor). It should be noted that the comparison with full monopulse did not restrict the values of  $T$  or  $G$  in any way.

#### 4. SUMMARY

The basic properties and design requirements of pseudo-monopulse systems have been considered. Performance characteristics in the presence of noise have been utilized to determine the optimum Q functions and the most practical preamplifier configuration. A more rigorous development of the performance in the presence of noise is found in Appendix II. Although this Appendix utilizes a specific sampling (Q) function, it was shown in the preceeding sections that equivalent performance is obtained for other Q functions satisfying prescribed constraints. Also, the performance of pseudo-monopulse was compared with full monopulse, and the tradeoff between sum channel degradation and difference channel degradation was described. The tradeoff is easily accomplished in practice by changing a single component - a directional coupler. A more sophisticated method would use a variable coupling directional coupler to provide an adaptive control system; i.e., the tracking performance could be adjusted, either manually or as a function of received signal characteristics.

Precomparator and postcomparator errors were not explicitly discussed in this section, but they are important parameters in a tracking system. The precomparator errors are identical to those of full monopulse, since the pseudo-monopulse system uses a full monopulse comparator. The postcomparator errors can be maintained very low since a single channel receiver is used. Thus, only the scanner and coupler phase and amplitude characteristics will significantly affect the postcomparator errors. In this respect, the technique is generally superior to full monopulse.

One limitation to the pseudo-monopulse technique is that interference with the data channel must be avoided. This is most easily accomplished by selecting Q functions with spectra which do not overlap the signal spectrum. An additional possibility is to couple the error signals such as to create a modulation in quadrature with the basic data modulation; i.e., create AM when the data is FM and vice-versa. When interference between tracking and data signals cannot be avoided at the low end of the spectrum, it is possible to use scanning signals with higher frequency spectra than the information bandwidth. This is not generally as desirable, since hardware problems may be created and the normalization problem is somewhat enhanced.

The pseudo-monopulse technique has been shown to be generally applicable to satellite communications terminal design. The implementation is relatively simple and, in most practical cases, the degradation in performance is not appreciable. The technique is, in simplest terms,

an electronic scanning system, and as such is a modern version of mechanical lobing techniques. The versatility of the method-scanning rate, waveform, amount can be readily changed - and the simplicity of the hardware required make pseudo-monopulse a desirable technique for the purposes considered in this study.

## SECTION XIII

### AMPLITUDE AND PHASE ERRORS IN A TWO-CHANNEL PHASE MONOPULSE ANTENNA

#### 1. INTRODUCTION

In various applications, such as wideband satellite communication, the full capability of a three-channel monopulse system may not be necessary. In such cases, the single-channel monopulse is attractive because of its simplicity. The dual-channel monopulse, in which the two error channels are multiplexed into a single error channel, offers another alternative with intermediate performance and complexity characteristics.

There are two important methods of multiplexing the error signals. One method, called phase multiplexing, consists of the simple addition of the two error signals in RF phase quadrature. This addition can be performed with a magic-tee and a phase trimmer. The second method, referred to as time multiplexing, consists of switching alternately between the two error signals at some rate well in excess of the servo bandwidth necessary for proper tracking.

Both methods of multiplexing decrease the effective error channel signal-to-noise ratio by 3 dB with reference to a three-channel monopulse having the same noise figure. It is clear that with perfect time multiplexing a two-channel monopulse is affected by phase and amplitude unbalance in the same way as a three-channel monopulse. Imperfect multiplexing due to poor switch isolation or timing errors in the demultiplexer will cause crosstalk but these effects can be made small without serious design difficulty.

The phase multiplex system responds quite differently to pre-comparator and postcomparator phase and amplitude unbalance. For example, in a three-channel phase monopulse system the effect of pre-comparator amplitude unbalance is to produce a finite null depth but no boresight error results unless postcomparator phase shift is also present. With a phase multiplexed two-channel system, amplitude unbalance in one plane (elevation) causes a boresight shift in the other (azimuth), even in



the absence of postcomparator phase shift. The effect of phase and amplitude unbalances in a two-channel phase multiplexed phase monopulse are analyzed below:

## 2. ANALYSIS

Consider a four-element phase monopulse array with the phase centers lying on a square in the X-Y plane (see Figure 68). The diagonal of this square is  $2a$  long and the coordinates of the target are  $R, \psi, \gamma$ . The distance  $R_i$  from the target to a phase center with coordinates  $(x_i, y_i, 0)$  is,

$$\begin{aligned} R_i^2 &= (R \sin \psi \sin \gamma - x_i)^2 + (R \sin \psi \cos \gamma - y_i)^2 + R^2 \cos^2 \psi \\ &= R^2 + x_i^2 + y_i^2 - 2R \sin \psi (x_i \sin \gamma + y_i \cos \gamma). \end{aligned}$$

With  $R \gg x_i; R \gg y_i$

$$R_i \approx R - \sin \psi (x_i \sin \gamma + y_i \cos \gamma).$$

The phase shift from the target to the  $i^{\text{th}}$  phase center, minus the phase shift to the center of the array, is,

$$\begin{aligned} \phi_1 &= \frac{2\pi a}{\lambda} \sin \psi \cos \gamma = u, \\ \phi_2 &= \frac{2\pi a}{\lambda} \sin \psi \sin \gamma = v, \\ \phi_3 &= \frac{2\pi a}{\lambda} \sin \psi \sin \gamma = -v, \\ \phi_4 &= \frac{2\pi a}{\lambda} \sin \psi \cos \gamma = -u. \end{aligned} \tag{148}$$

Now let all elements have the same voltage gain  $g_o(u, v)$  (which depends on polarization of the target). The voltage gain of the  $i^{\text{th}}$  element, located as shown in Figure 68, can be written as (neglecting mutual coupling)

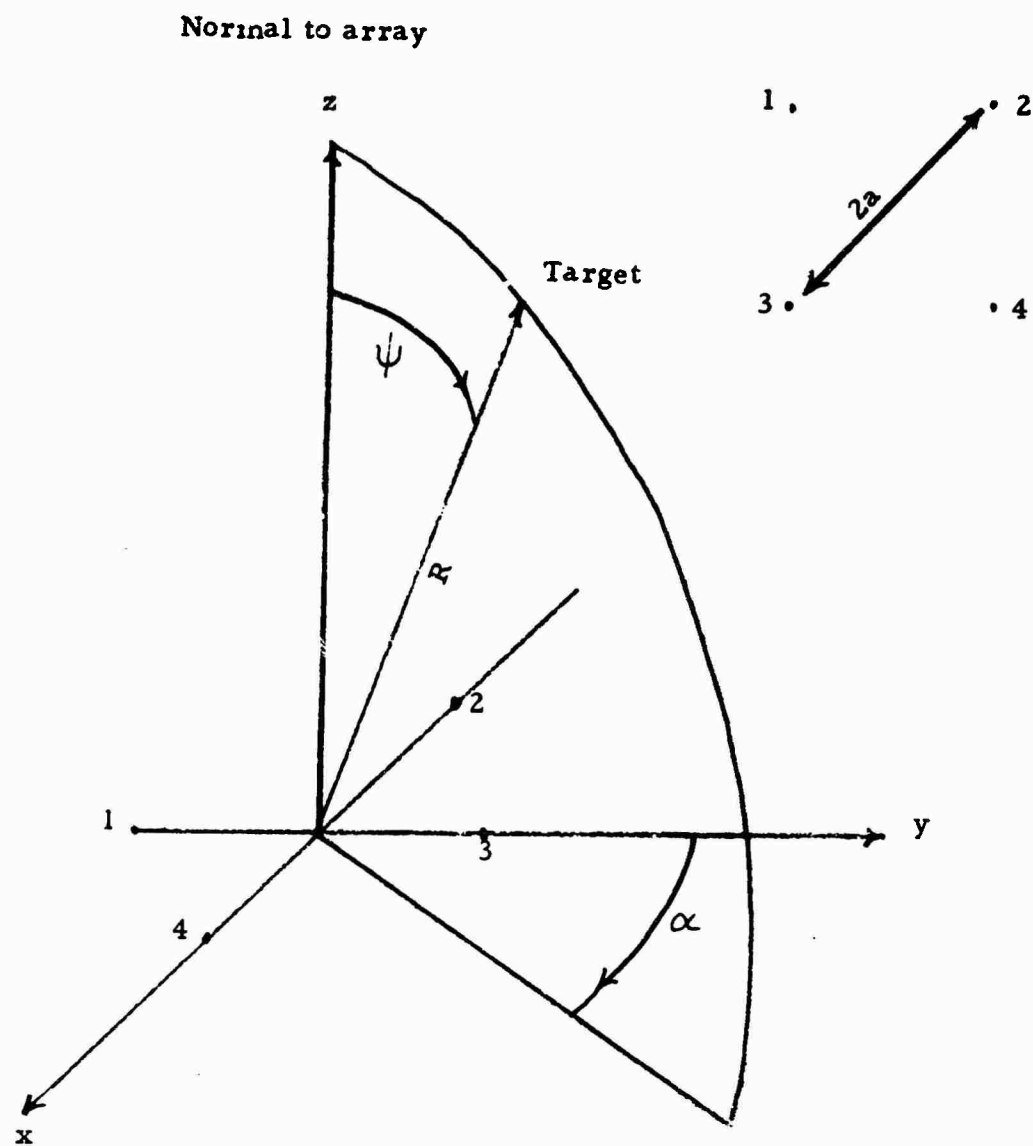


Figure 68 Coordinate System

$$\begin{aligned}
g_1(u, v) &= A_1 g_0(u, v) e^{j(u+\theta_1)} \\
g_2(u, v) &= A_2 g_0(u, v) e^{j(v+\theta_2)} \\
g_3(u, v) &= A_3 g_0(u, v) e^{-j(v-\theta_3)} \\
g_4(u, v) &= A_4 g_0(u, v) e^{-j(u-\theta_4)}
\end{aligned}
\tag{149}$$

Ideally,  $A_i = 1$  and  $\theta_i = 0$ .  $A_i \neq 1$  represents precomparator amplitude unbalance and  $\theta_i \neq 0$  represents precomparator phase unbalance.

Figure 69 shows a possible form of a two-channel monopulse comparator. Note that diametrically opposite elements are applied to the left pair of magic-tees. One might also apply 4 and 2 to the top left magic-tee, etc., but this would lead to the use of five magic-tees compared to four for the same overall operation.

With  $A_i = 1$  and  $\theta_i = 0$  the output of the error channel has a magnitude proportional to  $\sin \psi$  and a phase, with respect to the sum channel phase, equal to  $\gamma$ . To see this, substitute (149) in the comparator output signal expressions given in Figure 69. The sum signal is,

$$g_s(u, v) = g_0(u, v)(\cos u + \cos v) \tag{150}$$

and the error signal is,

$$g_e(u, v) = g_0(u, v) [j \sin u - \sin v]. \tag{151}$$

Assuming that  $u \ll 1$ ,  $v \ll 1$ , (150) and (151) can be written as,

$$g_s(u, v) = 2g_0(u, v) \tag{152}$$

$$g_e(u, v) = j \frac{2\pi a}{\lambda} \sin \psi g_0(u, v) e^{j\gamma}. \tag{153}$$

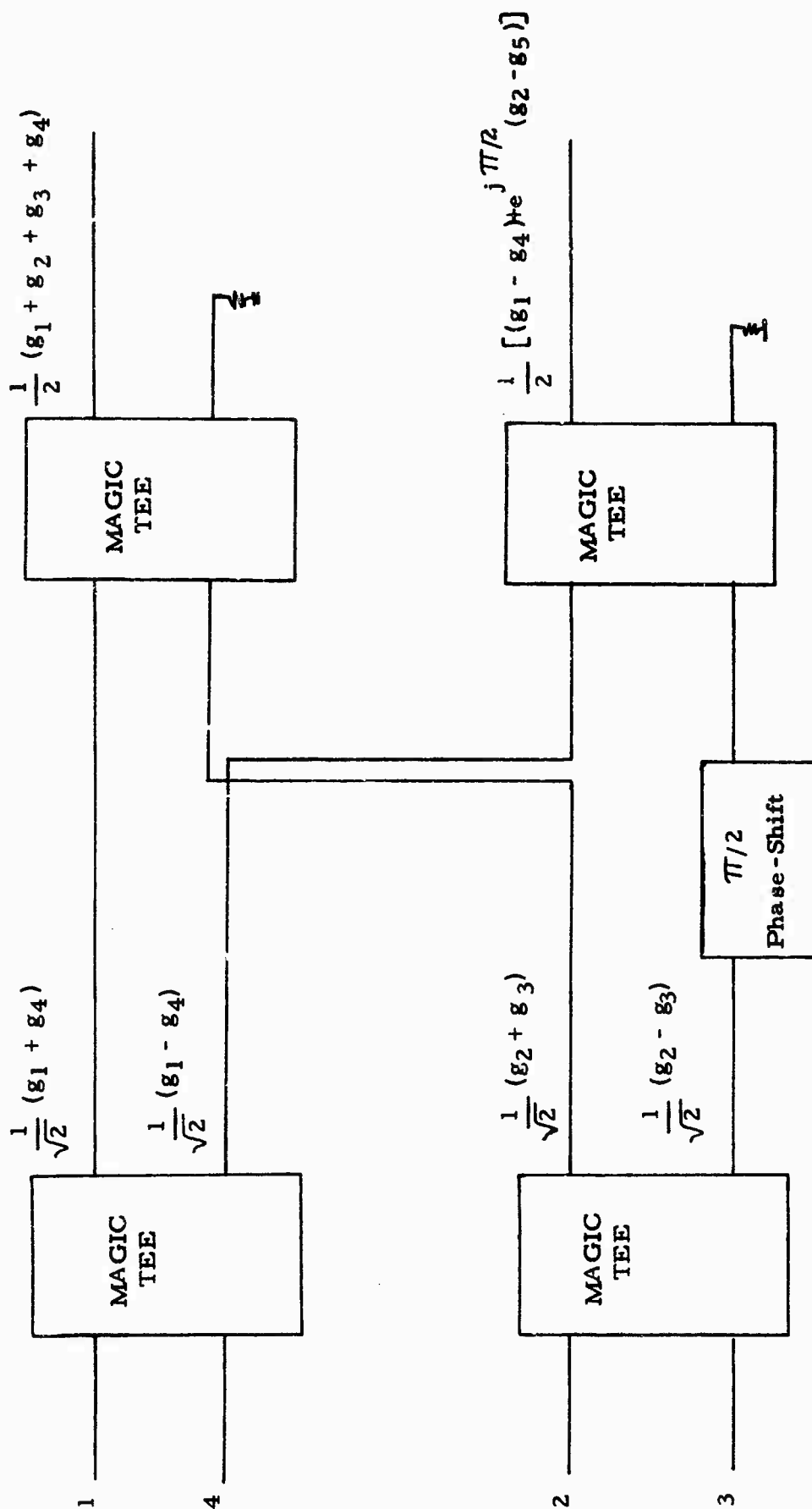


Figure 69 Two-channel Monopulse Comparator

It is clear from (153) that the effect of a postcomparator shift  $\beta$  is to change the apparent value of  $\gamma$  by the same amount  $\beta$ . This introduces crosstalk at the output of the quadrature phase detectors (demultiplexer) but there is no change in the boresight axis (direction of target for zero error channel output). Sufficient crosstalk, however, can lead to instability of the servo loop. It is also clear that a change in postcomparator gain results in an equal change in the apparent value of  $\sin \psi$ . This effect is best viewed as a change in the servo loop gain.

Now consider the error channel output when precomparator unbalances are present.

(154)

$$g_e(u, v) = \frac{g_0(u, v)}{2} \left[ A_1 e^{j(u+\theta_1)} - A_4 e^{-j(u-\theta_4)} + e^{j\pi/2} (A_2 e^{j(v+\theta_2)} - A_3 e^{-j(v-\theta_3)}) \right]$$

Boresight corresponds to the quantity in the square bracket being zero. Again, assuming  $u \ll 1$ ,  $v \ll 1$ ,  $\theta_i \ll 1$  we have, setting the real and imaginary parts equal to zero,

$$(A_1 - A_4) - A_2(v + \theta_2) - A_3(v - \theta_3) = 0 \quad (155)$$

$$A_1(u + \theta_1) + A_4(u - \theta_4) + A_2 - A_3 = 0$$

Solving these two equations for  $u$  and  $v$  gives the new boresight direction as,

$$v_b = \frac{A_1 - A_4 + A_3 \theta_3 - A_2 \theta_2}{A_2 + A_3} \approx \frac{A_1 - A_4}{2} + \frac{\theta_3 - \theta_2}{2} \quad (156)$$

$$u_b = \frac{A_3 - A_2 + A_4 \theta_4 - A_1 \theta_1}{A_1 + A_4} \approx \frac{A_3 - A_2}{2} + \frac{\theta_4 - \theta_1}{2} \quad (157)$$

The boresight error  $\psi_b$  can be obtained, with the help of (148) as,

$$\begin{aligned} \psi_b &= \sin^{-1} \frac{\sqrt{u_b^2 + v_b^2}}{(2\pi a/\lambda)} \approx \frac{\sqrt{u_b^2 + v_b^2}}{(2\pi a/\lambda)} \\ &= \frac{1}{2} \frac{1}{(2\pi a/\lambda)} \sqrt{(\Delta A_{14} + \Delta \theta_{32})^2 + (\Delta A_{32} + \Delta \theta_{41})^2}, \end{aligned} \quad (158)$$

$$\Delta A_{14} = A_1 - A_4, \text{ etc.}$$

which is the principal result of this analysis. Note that if the array elements are adjacent rectangular apertures the array is then a square of diagonal  $4a$ . The sum 3-dB beamwidth would then be in the vicinity of  $(\lambda/2 \sqrt{2} a)$  radians.

Equation (158) can be written in a number of different forms. If the gain and phase unbalance terms appearing in (158) are considered as zero mean uncorrelated random variables such that,

$$\sigma_A^2 = \text{Average} [A_1 - A_4]^2 = \text{Average} [A_3 - A_2]^2,$$

$$\sigma_\theta^2 = \text{Average} [\theta_3 - \theta_2]^2 = \text{Average} [\theta_4 - \theta_1]^2, \text{ radians.}$$

The boresight rms error can be written as,

$$\psi_b, \text{ rms} = \frac{1}{\sqrt{2}} \frac{1}{(2\pi a/\lambda)} \sqrt{\sigma_A^2 + \sigma_\theta^2}, \text{ radians} \quad (159)$$

For small gain deviations from unity we can write,

$$\begin{aligned} 20 \log \frac{A_1}{A_4} &= 20 \log \frac{1 + (A_1 - 1)}{1 + (A_4 - 1)} = 8.86 \ln \frac{1 + (A_1 - 1)}{1 + (A_4 - 1)} \\ &\approx 8.86 (A_1 - A_4) \end{aligned} \quad (160)$$

and the gain unbalance in dB is related to  $\sigma_a$  as,

$$\sigma_A, \text{ dB} = 8.86 \sigma_a.$$

Substituting in (159) gives,

$$\psi_b, \text{ rms} = \frac{1}{\sqrt{2}} \frac{1}{(2\pi a/\lambda)} \sqrt{\frac{\sigma_A^2 \text{ dB}}{(8.86)^2} + \sigma_\theta^2}, \text{ radians.}$$

Thus, it appears that a 1 dB amplitude unbalance is equivalent to  $(1/8.86)$  radians (6.5 degrees) of phase unbalance. Also, 1 dB of amplitude unbalance amounts to a boresight shift in the vicinity of  $100/(\pi \times 8.86) = 3.6\%$  of 3-dB beamwidth.

### 3. SUMMARY

Several characteristics of two-channel monopulse systems can be deduced as a result of the previous paragraphs and other sections of this report. Major system characteristics are:

- a. Two-channel monopulse processing retains the sum channel characteristics of full monopulse. The pointing errors due to thermal noise are degraded 3 dB with respect to a three channel system as a result of combining the two error signals onto a single channel.
- b. Phase multiplexing, combining the error channels in phase quadrature, can be accomplished with passive circuitry. Time multiplexing, the basic Q function multiplication described in Section XII, cannot be done without the use of microwave "switching" (e.g., a switch, modulator, phase shifter, or equivalent "semi-passive" functional operation).
- c. Time multiplexing, as used in pseudo-monopulse, exhibits an identical reaction to pre- and postcomparator errors as a three-channel system.
- d. A phase multiplexed two-channel system is sensitive to both amplitude and phase unbalance prior to the comparator. Three-channel monopulse is sensitive only to one type of unbalance; e.g., in a three-channel phase monopulse system, precomparator amplitude

unbalance is a second order effect.

e. The effects of precomparator errors in a two-channel phase multiplexed phase monopulse system can be quantitatively evaluated. For example,  $\pm 1$  dB amplitude unbalance is equivalent to about 6.5 degrees of phase unbalance, which causes a boresight shift of approximately 3.6% of the sum channel 3 dB beamwidth. It can be shown that a nearly identical boresight shift would occur in a well-designed amplitude sensing monopulse with the same pre-comparator error.

f. In a phase multiplexed two-channel monopulse system, postcomparator phase shift simulates a rotation of the antenna about its boresight axis. The rotation angle is the same as the phase error; e.g., a 90 degree postcomparator phase shift would cause an elevation error to be detected as an azimuth error.

In summary, time multiplexing requires slightly more complex hardware than phase multiplexing, but is considerably more tolerant of phase and amplitude errors.



## SECTION XIV

### CONCLUSIONS AND RECOMMENDATIONS

#### 1. CONCLUSIONS

The pseudo-monopulse technique has been shown to offer significant advantages in the design of satellite communications ground terminals. The basic system design considerations have been analyzed in detail. The effects of noise, amplitude and phase unbalance, one or more preamplifiers, and imperfect normalization have been analyzed, particularly as applied to pseudo-monopulse. The technique, basically an electronic lobing system, is not novel in itself, but the analyses and compilation of performance characteristics accomplished during this program has added to the overall knowledge of this technique. Pseudo-monopulse is particularly well suited to the satellite communications problem, since the tracking requirements are significantly less stringent than, for example, in most radar tracking systems.

A second useful technique, the Automatic Manual Simulator (AMS), is, in its simplest form, a conical scan system where the scan is generated by moving the entire reflector and feed assembly. The unique feature of this technique is that it can (generally) be added to an existing servo system with a minimum amount of additional equipment. The resultant tracking system is limited in dynamic performance, but is more than adequate for use with present communications satellites. Furthermore, when applied judiciously, the system is reliable, low cost, and it does the job. Thus, the AMS might be described as the application of a well known technique in an unusual manner to accomplish a relatively simple task in the most economical way.

The basic TDM and FDM techniques were shown to offer no significant advantages in the design of single channel tracking systems. Furthermore, the SCAMP technique, which appeared to have an advantage in normalization, is actually poorer in this respect than conventional techniques. The poorer performance is due to the wider bandwidth required in the FDM design and due to the fact that the "instantaneous" normalization capability of SCAMP cannot be efficiently utilized in the satellite communications environment. Full (three channel) monopulse was included in the study, for comparison purposes, as was some consideration of two-channel systems. The two-channel technique is highly susceptible to crosstalk and boresight shifts due to amplitude and phase unbalances. The three channel system requires more hardware, but not by a great amount, and achieves good electrical

performance. Thus, when the absolute maximum performance in both communications and tracking in the presence of noise is required, conventional three channel monopulse is recommended.

## 2. RECOMMENDATIONS

Analyses of several SCMTR techniques have been accomplished, but all of the related problems have not been solved. As is the case in any investigative program, many interesting problems are discovered for each one which is solved. There is also the possibility that potentially useful techniques have been overlooked, and these should be investigated as they come to light. The "solutions" resulting from the present study program are basically engineering compromises and are, therefore, subject to improvement as, for example, the state-of-the-art changes or system requirements are altered.

One problem of great significance in satellite communications is the "threshold" effect. Both the communications and tracking systems exhibit peculiar nonlinearities as the received signal strength is decreased. One effect, loss of normalization, was discussed in Section VIII. Since the normalization, or lack of normalization, is a function of the basic technique, the type of detector, the signal modulation parameters, the character of the noise, and the rate of change of signal strength (to mention a few parameters), a complete solution to the problem would require a large scale program. A more modest investigation under conditions most likely to occur in a satellite communications environment would be practical. For example, a program to determine the spectrum of the noise in a coherent demodulator was conceived during this program but not accomplished due to equipment limitations. Such a program is recommended, particularly when a scanning SCMTR is contemplated, since the shape of the noise spectrum would influence the selection of scan frequency. The basic threshold effect in demodulators is, of course, a long standing problem worthy of significant investigation. The tracking signal is, generally speaking, not immune to these threshold effects, particularly in a single channel receiver. Therefore, an investigation of threshold in communications demodulators and the resultant effects on the tracking signals is needed.

Some other interesting concepts which appear worthy of further investigation include:

- a) adaptive design which would be capable of making an instantaneous tradeoff between the communications channel gain and tracking sensitivity. This tradeoff could, for example be implemented in a Pseudo-Monopulse receiver by varying a single directional coupler.

- b) operation with more complex beacon signals. It is possible that the beacon signal emitted from the satellite could be designed to simplify the ground tracking receiver. Possibilities include multiple frequency and/or pulsed signals.
- c) special designs for specific satellite systems. For example, if operation with only synchronous or near synchronous satellites is required, a relatively simple combination of program track and auto track might be advantageous. Application of simple program track techniques should be investigated whenever the target motion is highly predictable and is the predominant factor in the antenna pointing error.
- d) an investigation of cross-polarization effects in monopulse systems. The degree to which cross-polarized patterns must be controlled to prevent system degradation under a variety of conditions should be examined.

In conclusion, the engineering compromises necessary to optimize a specific set of conditions have been made. It is apparent that both the conditions and the assumptions (e.g., equipment characteristics) will vary in future systems. The material in this report will hopefully be useful in future system optimizations, but it will of necessity be incomplete. A continuing investigation of the overall satellite communications system development is needed to maintain optimum subsystem designs. As a minimum, a periodic review of the relevant problems is recommended, with emphasis on changing system concepts which might allow further simplification in tracking-communications receiver designs.

## APPENDIX I

### BASIC LIMITATION ON EFFICIENCY OF PASSIVE COMBINERS

#### 1. SUMMARY

In the design of single-channel and two-channel monopulse systems, it may be necessary to add two microwave signals at the same frequency as depicted in Figure 1. For best operation in the presence of noise it is necessary that the power transfer between each source and the load be maximized.

For passive, linear, and time-invariant combiners the basic limitation on power transfer coefficients, imposed by the principle of conservation of energy is

$$T_1(\omega) + T_2(\omega) \leq 1 \quad (1)$$

where,  $T_1$  is the power delivered to the load by Source 1, with Source 2 turned off, divided by the power available from Source 1;  $T_2$  is defined in an analogous manner with Source 1 turned off. Both sources are sinusoidal at frequency  $\omega$  and maintain the same impedance in the on and off states.

Magic-tees and directional couplers have  $T_1 + T_2$  nearly equal to unity when incidental dissipation is small; such devices then may be considered optimum combiners and it is fruitless to attempt to achieve better performance by the use of more sophisticated passive time-invariant non-reciprocal networks.

If the two sources are at different frequencies conservation of energy implies

$$T_1(\omega_1) + T_2(\omega_1) \leq 1$$

$$T_1(\omega_2) + T_2(\omega_2) \leq 1$$

and perfect power transfer for both sources, i.e.,  $T_1(\omega_1) = 1$  and  $T_2(\omega_2) = 1$  is not precluded. In fact, such performance is approached by reciprocal diplexers as used in communications systems which transmit and receive on different frequencies through a common antenna.

## 2. PROOF

A three-port combiner can be characterized at a single frequency by its scattering matrix<sup>(27)</sup>

$$S = \begin{bmatrix} S_{11} & S_{12} & S_{13} \\ S_{21} & S_{22} & S_{23} \\ S_{31} & S_{32} & S_{33} \end{bmatrix}$$

The waves incident on and scattered from the combiner (see Figure 1) are related as follows

$$\begin{aligned} b_1 &= S_{11} a_1 + S_{12} a_2 + S_{13} a_3 \\ b_2 &= S_{21} a_1 + S_{22} a_2 + S_{23} a_3 \\ b_3 &= S_{31} a_1 + S_{32} a_2 + S_{33} a_3 \end{aligned} \quad (2)$$

When the load is matched it follows that  $a_3 = 0$  and (2) reduces to

$$\begin{aligned} b_1 &= S_{11} a_1 + S_{12} a_2 \\ b_2 &= S_{21} a_1 + S_{22} a_2 \\ b_3 &= S_{31} a_1 + S_{32} a_2 \end{aligned} \quad (3)$$

Further, assume that the sources at Ports 1 and 2 are matched (zero reflection coefficient). Then  $|a_1|^2$ , the power incident on Port 1, is also the power available from Source 1. With  $a_2 = 0$ ,  $b_3 = S_{31} a_1$  and the power delivered to the load is  $|S_{31}|^2 |a_1|^2$ . The power transfer coefficient  $T_1$ , defined earlier is given by

$$T_1 = |S_{31}|^2 \quad (4)$$

and, similarly,

$$T_2 = |S_{32}|^2$$

With both sources active the principle of conservation of energy is written as:

$$|b_1|^2 + |b_2|^2 + |b_3|^2 \leq |a_1|^2 + |a_2|^2 \quad (5)$$

i.e., the power leaving the combiner is at most equal to the power incident on the combiner. To prove the desired result, assume values of

$a_1$ , and  $a_2$  which will optimize the power transfer. This occurs when  $a_1$  and  $a_2$  are proportional to the complex conjugates of  $S_{31}$  and  $S_{32}$ , respectively. Selecting (arbitrarily) the constant of proportionality to normalize the total input power yields

$$a_1 = \frac{S_{31}^*}{\sqrt{|S_{31}|^2 + |S_{32}|^2}}; \quad a_2 = \frac{S_{32}^*}{\sqrt{|S_{31}|^2 + |S_{32}|^2}}, \quad (6)$$

where \* denotes the complex conjugate. With the help of (3) rewrite (5) as

$$\frac{|S_{11} S_{31}^* + S_{12} S_{32}^*|^2 + |S_{21} S_{31}^* + S_{22} S_{32}^*|^2}{|S_{31}|^2 + |S_{32}|^2} + |S_{31}|^2 + |S_{32}|^2 \leq 1 \quad (7)$$

The desired result follows directly from (7)

$$|S_{31}|^2 + |S_{32}|^2 = T_1 + T_2 \leq 1 \quad (8)$$

Further, necessary but not sufficient conditions for  $T_1 + T_2 = 1$  are

$$S_{11} S_{31}^* + S_{12} S_{32}^* = S_{21} S_{31}^* + S_{22} S_{32}^* = 0 \quad (9)$$

Equation (9) shows that if the two sources are not isolated, i. e.,

$$S_{12} \neq 0, S_{21} \neq 0, \text{ then } T_1 + T_2 = 1$$

implies that the combiner is not matched at Ports 1 and 2, i. e.,  $S_{11} \neq 0$ ,  $S_{22} \neq 0$ . It can also be shown that  $T_1 + T_2 = 1$  implies that the combiner is matched at Port 3, i. e.,  $S_{33} = 0$ .

The preceding demonstration of (1) was based on the assumption of matched load and sources. This does not detract from the generality of (1) since an arbitrary source (load) can be replaced by a matched source (load) followed by a reactive network and this network may then be regarded as part of the combiner.

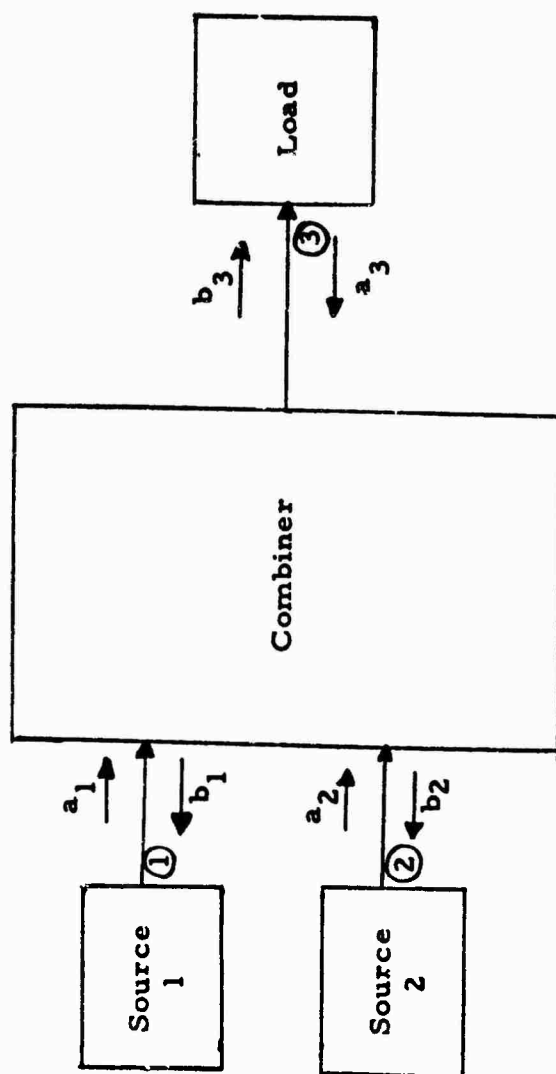


FIGURE 1 - SIGNAL COMBINER

## APPENDIX II

### PSEUDO-MONOPULSE NOISE ANALYSIS

The signal-to-noise ratio,  $S/N$ , at the output of the elevation channel in a pseudo-monopulse system is determined in this Appendix. The case of a CW signal and a small angular error are considered. It can be shown by more sophisticated techniques that the CW restriction can be lifted and the results are accurate for a frequency modulated carrier.

A block diagram of the circuit being analyzed is shown in Figure 1. The "sampling signals" being considered are sine and cosine waves. It has been shown (Section XII) that the results are essentially the same for a wide range of "Q functions" (the sampling signals) which satisfy the basic requirements set forth in Section XII. The results are also valid for lobing and conical scan systems, with suitable modification of the input definitions. In the present analysis it is assumed that equal noise power is impinging on both error channels and that the noise processes are independent.

#### 1. DEFINITION OF TERMS

Inputs:

$$y_s(t) = A s(t) + n_s(t) \quad (1)$$

$$y_{el}(t) = B s(t) + n_{el}(t)$$

$$y_{az}(t) = C s(t) + n_{az}(t)$$

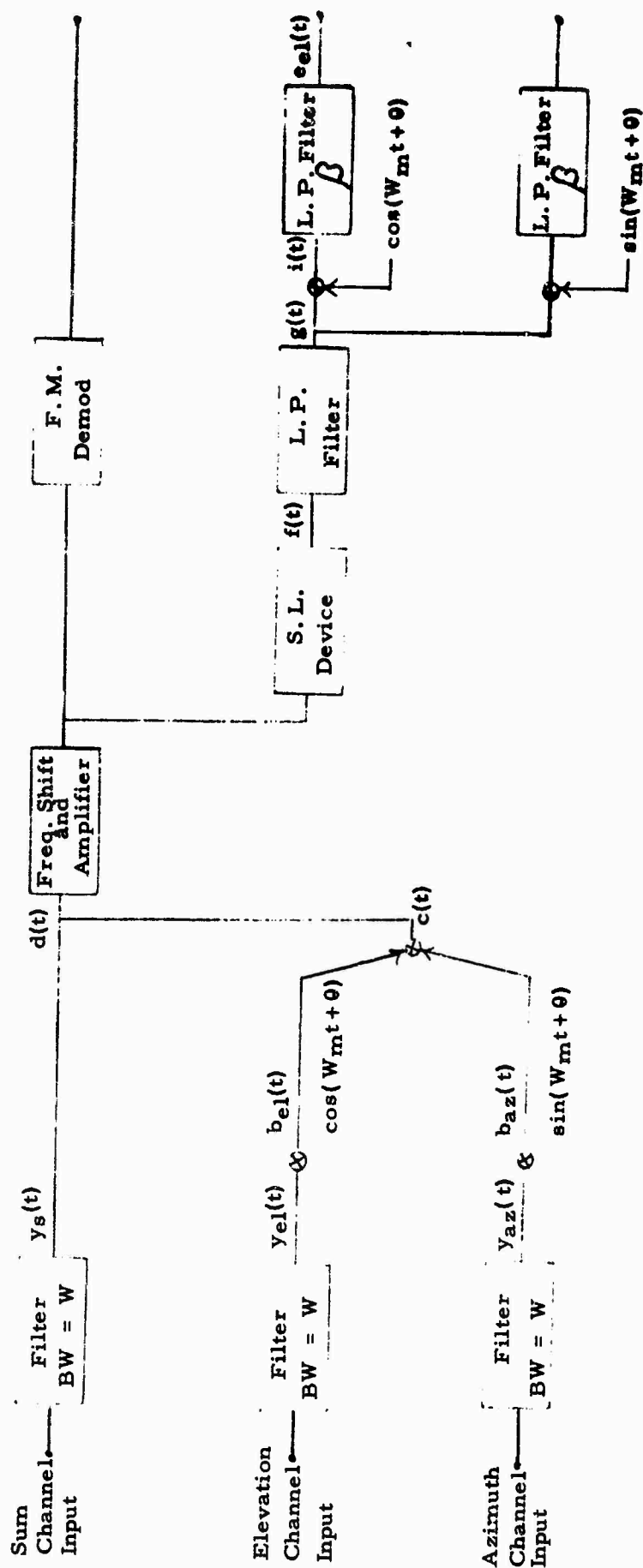
$$s(t) = \cos(W_c t)$$

Note that  $A^2/2$ ,  $B^2/2$ , and  $C^2/2$  correspond to the input Signal power on the sum, elevation, and azimuth channels, respectively.

$n_s(t)$ ,  $n_{el}(t)$ ,  $n_{az}(t)$  are sample functions from stationary gaussian random processes with zero mean.

The noise processes have the Spectra defined below:





BLOCK DIAGRAM OF PSEUDO-MONOPULSE SYSTEM

Figure 1

$$S_{n_s}(f) = (1/2)N_s \quad f_c - W/2 \leq (f) \leq f_c + W/2 \quad (2)$$

$$S_{n_{el}}(f) = (1/2)N_{er} \quad f_c - W/2 \leq (f) \leq f_c + W/2$$

$$S_{n_{az}}(f) = (1/2)N_{er} \quad f_c - W/2 \leq (f) \leq f_c + W/2$$

S will always denote a power spectral density, i. e.,

$(S_{n_s}(f) \cdot W) =$  Total noise power at the input to the sum channel.

The multiplexing waveforms are:

$$\cos(W_m t + \theta) \quad (3)$$

$$\sin(W_m t + \theta)$$

Define  $\theta$  as follows:

$\theta =$  a random variable uniformly distributed between 0 and  $2\pi$ .

## 2. DERIVATION

The first step in the derivation is to find  $e_{el}(t)$ . The spectrum of  $e_{el}(t)$  will then be determined from which the S/N ratio follows immediately.

$$b_{e1}(t) = y_{e1}(t) \cdot \cos (W_m t + \theta) \quad (4)$$

$$= \left[ B \cos W_c t + n_{e1}(t) \right] \cdot \cos (W_m t + \theta)$$

$$b_{az}(t) = y_{az}(t) \cdot \sin (W_m t + \theta) \quad (5)$$

$$= \left[ C \cos W_c t + n_{az}(t) \right] \cdot \sin (W_m t + \theta)$$

$$c(t) = b_{e1}(t) + b_{az}(t) \quad (6)$$

$$= \left[ B \cos W_c t + n_{e1}(t) \right] \cdot \cos (W_m t + \theta) \\ + \left[ C \cos W_c t + n_{az}(t) \right] \cdot \sin (W_m t + \theta)$$

$$d(t) = \sqrt{1 - k^2} y_s(t) + k c(t) \quad (7)$$

$$= \sqrt{1 - k^2} \left[ A \cos W_c t + n_s(t) \right] \\ + k \left[ B \cos W_c t + n_{e1}(t) \right] \cdot \cos (W_m t + \theta) \\ + k \left[ C \cos W_c t + n_{az}(t) \right] \cdot \sin (W_m t + \theta)$$

Put  $d(t)$  in the following form:

$$d(t) = A^1 \left[ 1 + m_1 \cos (W_m t + \theta) + m_2 \sin (W_m t + \theta) \right] \cos W_c t + n(t) \quad (8)$$

$$d(t) = \sqrt{1 - k^2} A \cos W_c t + k B \cos W_c t \cos (W_m t + \theta) \quad (9) \\ + k C \cos W_c t \sin (W_m t + \theta) + \sqrt{1 - k^2} n_s(t) \\ + k \cos (W_m t + \theta) n_{e1}(t) \\ + k \sin (W_m t + \theta) n_{az}(t)$$

$$= A \sqrt{1 - k^2} \left[ 1 + \frac{B}{A} \cdot \frac{k}{\sqrt{1 - k^2}} \cos (W_m t + \theta) + \frac{C}{A} \cdot \frac{k}{\sqrt{1 - k^2}} \sin (W_m t + \theta) \right] \cos W_c t + n(t) \quad (10)$$

$$= A^1 (1 + m_1 \cos (W_m t + \theta) + m_2 \sin (W_m t + \theta)) \cos W_c t + n(t)$$

Where

$$\begin{aligned} A^1 &= A \sqrt{1 - k^2} \\ m_1 &= \frac{B}{A} \frac{k}{\sqrt{1 - k^2}} \\ m_2 &= \frac{C}{A} \frac{k}{\sqrt{1 - k^2}} \end{aligned} \quad (11)$$

$$\begin{aligned} n(t) &= \sqrt{1 - k^2} n_s(t) + k \cos (W_m t + \theta) n_{e1}(t) \\ &\quad + k \sin (W_m t + \theta) n_{az}(t) \end{aligned}$$

Find the output of the square law device

$$\begin{aligned} f(t) &= d^2(t) \\ &= \left[ A^1 (1 + m_1 \cos (W_m t + \theta) + m_2 \sin (W_m t + \theta)) \cdot \cos W_c t + n(t) \right]^2 \end{aligned} \quad (12)$$

Write  $n(t)$  as follows:

$$n(t) = x(t) \cos W_c t + y(t) \sin W_c t \quad (13)$$

$$d(t) = \left[ A^1 (1 + m_1 \cos(W_m t + \theta) + m_2 \sin(W_m t + \theta)) + x(t) \right] \cos W_c t + y(t) \sin W_c t \quad (14)$$

$$\begin{aligned} f(t) = & \left\{ A^1 \left[ 1 + m_1 \cos(W_m t + \theta) + m_2 \sin(W_m t + \theta) \right] + x(t) \right\}^2 \cos^2 W_c t \\ & + 2y(t) \left\{ A^1 \left[ 1 + m_1 \cos(W_m t + \theta) + m_2 \sin(W_m t + \theta) \right] + x(t) \right\} \cos W_c t \sin W_c t \\ & + y^2(t) \sin^2 W_c t \end{aligned} \quad (15)$$

$$\begin{aligned} f(t) = & \left\{ A^1 \left[ 1 + m_1 \cos(W_m t + \theta) + m_2 \sin(W_m t + \theta) \right] + x(t) \right\}^2 \frac{1}{2} [1 + \cos 2 W_c t] \\ & + 2y(t) \left\{ A^1 \left[ 1 + m_1 \cos(W_m t + \theta) + m_2 \sin(W_m t + \theta) \right] + x(t) \right\} \frac{1}{2} \sin 2 W_c t \\ & + y^2(t) \frac{1}{2} [1 - \cos 2 W_c t] \end{aligned} \quad (16)$$

The output of the low pass filter is given below:

$$\begin{aligned} g(t) = & \frac{1}{2} \left\{ A^1 \left[ 1 + m_1 \cos(W_m t + \theta) + m_2 \sin(W_m t + \theta) \right] + x(t) \right\}^2 + \frac{1}{2} y^2(t) \\ = & \frac{1}{2} \left\{ A^1{}^2 \left[ 1 + m_1^2 \cos^2(W_m t + \theta) + m_2^2 \sin^2(W_m t + \theta) + 2 m_1 \cos(W_m t + \theta) \right. \right. \\ & \left. \left. + 2 m_2 \sin(W_m t + \theta) + 2 m_1 m_2 \sin(W_m t + \theta) \cos(W_m t + \theta) \right] \right. \\ & \left. + 2 A^1 x(t) \left[ 1 + m_1 \cos(W_m t + \theta) + m_2 \sin(W_m t + \theta) \right] + x^2(t) + y^2(t) \right\} \end{aligned} \quad (17)$$

$$\begin{aligned}
= & 1/2 \left\{ A^2 \left[ 1 + m_1^2/2 + m_2^2/2 \right] + x^2(t) + y^2(t) + 2 A^1 x(t) \right. \\
& + \left[ 2 A^1 m_1 x(t) + 2 m_1 A^2 \right] \cos(W_m t + \theta) \\
& + \left[ 2 A^1 m_2 x(t) + 2 m_2 A^2 \right] \sin(W_m t + \theta) \\
& + A^2 \left[ m_1^2/2 - m_2^2/2 \right] \cos 2(W_m t + \theta) \\
& \left. + A^2 m_1 m_2 \sin 2(W_m t + \theta) \right\}
\end{aligned}$$

The output of the multiplier is:

$$\begin{aligned}
i(t) &= g(t) \cos(W_m t + \theta) \quad (18) \\
= & 1/2 \left\{ \left[ A^2 (1 + m_1^2/2 + m_2^2/2) + x^2(t) + y^2(t) + 2 A^1 x(t) \right] \cos(W_m t + \theta) \right. \\
& + \left[ 2 A^1 m_1 x(t) + 2 m_1 A^2 \right] 1/2 \left[ 1 + \cos 2(W_m t + \theta) \right] \\
& + \left[ 2 A^1 m_2 x(t) + 2 m_2 A^2 \right] 1/2 \sin 2(W_m t + \theta) \\
& + A^2 \left[ m_1^2/2 - m_2^2/2 \right] 1/2 \left[ \cos 3(W_m t + \theta) + \cos(W_m t + \theta) \right] \\
& \left. + A^2 m_1 m_2 1/2 \left[ \sin 3(W_m t + \theta) + \sin(W_m t + \theta) \right] \right\}
\end{aligned}$$

Find the output of the low pass filter:

$$\begin{aligned}
e_{el}(t) &= L_p \{ i(t) \} \quad (19) \\
= & L_p 1/2 \left\{ \left[ x^2(t) + y^2(t) + 2 A^1 x(t) \right] \cos(W_m t + \theta) \right\} \\
& + 1/2 m_1 A^2 + L_p 1/2 \left\{ A^1 m_1 x(t) \cos 2(W_m t + \theta) \right\} \\
& + L_p 1/2 \left\{ A^1 m_2 x(t) \sin 2(W_m t + \theta) \right\} \\
& + 1/2 L_p \left\{ A^1 m_1 x(t) \right\}
\end{aligned}$$

The spectrum of  $e_{el}(t)$  can now be determined by performing the low pass operation on the Fourier transform of the autocorrelation function of  $e(t)$ . The autocorrelation function is:

$$R_i(\tau) = E [ i(t) i(t+\tau) ]$$

It is now convenient to use the following theorem:

If  $x$ ,  $y$  and  $z$  are uncorrelated random processes and  $p = x + y + z$

$$\text{Then } R_p(\tau) = R_{xx}(\tau) + R_{yy}(\tau) + R_{zz}(\tau)$$

Application of the above theorem yields:

$$\begin{aligned} R_i(\tau) = & 1/4 R_x^2 \cos(\tau) + 1/4 R_y^2 \cos(\tau) + A^2 R_x \cos(\tau) \\ & + 1/4 m_1^2 A^4 + 1/4 A^2 m_1^2 R_x \cos 2 \\ & + 1/4 A^2 m_2^2 R_x \sin 2 + 1/4 A^2 m_1^2 R_x \end{aligned} \quad (20)$$

$$\begin{aligned} \therefore S_i(f) = & 1/4 S_x^2 \cos(f) + 1/4 S_y^2 \cos(f) + A^2 S_x \cos(f) \\ & + 1/4 m_1^2 A^4 + 1/4 A^2 m_1^2 S_x \cos 2(f) \\ & + 1/4 A^2 m_2^2 S_x \sin 2(f) + 1/4 A^2 S_x(f) \end{aligned} \quad (21)$$

Determination of power spectra:

It must be noted at this point that since  $n_{el}(t)$  and  $n_{az}(t)$  were assumed to have the same spectrum and hence equal power, that  $n(t)$  is a stationary random process. Observe that  $n(t)$  is given by the following two expressions:

$$\begin{aligned} n(t) &= x(t) \cos W_c t + y(t) \sin W_c t \\ &= \sqrt{1 - k^2} n_g(t) + k n_{el}(t) \cos(W_m t + \theta) \\ &\quad + k n_{az}(t) \sin(W_m t + \theta) \end{aligned}$$

The spectrum of  $n(t)$  is given in Figure 2

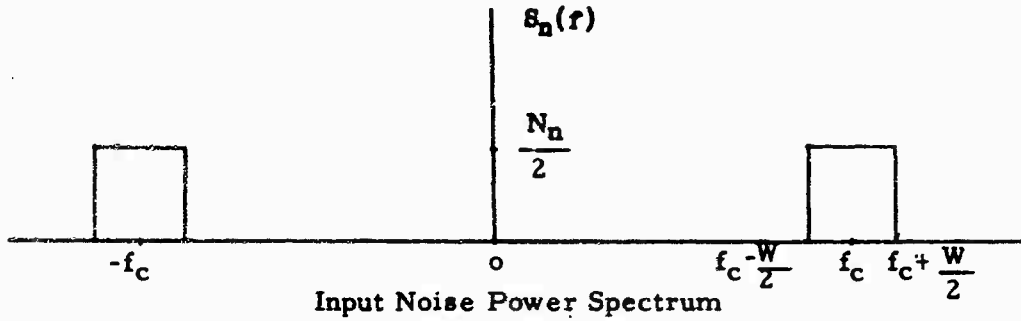


Figure 2

It can be shown that the variance of  $x(t)$  equals the variance of  $n(t)$

$$\sigma_x^2 = \sigma_n^2 \quad (22)$$

Therefore, equating power and recognizing that  $S_x(f)$  also has a flat spectrum yields:

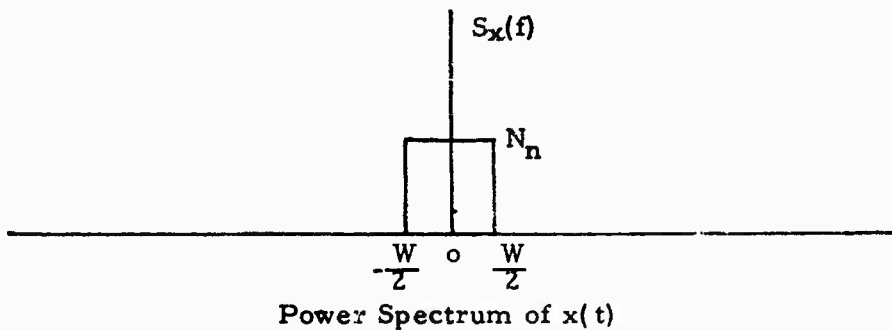


Figure 3

The value of  $N_n$  can be determined by observing that the noise is made up of three components ( $n_s(t)$ ,  $n_{e1}(t)$ , and  $n_{az}(t)$ ) and hence that:

$$\begin{aligned} R_n(\tau) &= E [n(t) n(t+\tau)] \\ &= E \left\{ \left[ \sqrt{1-k^2} n_s(t) + k n_{e1}(t) \cos(W_m t + \theta) + k \sin(W_m t + \theta) n_{az}(t) \right] \right. \\ &\quad \left[ \sqrt{1-k^2} n_s(t+\tau) + k n_{e1}(t+\tau) \cos(W_m(t+\tau) + \theta) \right. \\ &\quad \left. \left. + k n_{az}(t+\tau) \sin(W_m(t+\tau) + \theta) \right] \right\} \end{aligned} \quad (23)$$



$$\begin{aligned}
= E \left\{ \right. & (1 - k^2) n_s(t) n_s(t + \tau) \\
& + k^2 n_{el}(t) n_{el}(t + \tau) \cos(W_m t + \theta) \cos(W_m(t + \tau) + \theta) \\
& + k^2 n_{az}(t) n_{az}(t + \tau) \sin(W_m t + \theta) \sin(W_m(t + \tau) + \theta) \\
& + k \sqrt{1 - k^2} n_{el}(t) n_s(t + \tau) \cos(W_m t + \theta) \\
& + k \sqrt{1 - k^2} n_s(t + \tau) n_{az}(t) \sin(W_m t + \theta) \\
& + k \sqrt{1 - k^2} n_s(t) n_{el}(t + \tau) \cos(W_m(t + \tau) + \theta) \\
& + k^2 n_{el}(t + \tau) n_{az}(t) \sin(W_m t + \theta) \cos(W_m(t + \tau) + \theta) \\
& + k \sqrt{1 - k^2} n_s(t) n_{az}(t + \tau) \sin(W_m(t + \tau) + \theta) \\
& \left. + k^2 n_{el}(t) n_{az}(t + \tau) \cos(W_m t + \theta) \sin(W_m(t + \tau) + \theta) \right\}
\end{aligned}$$

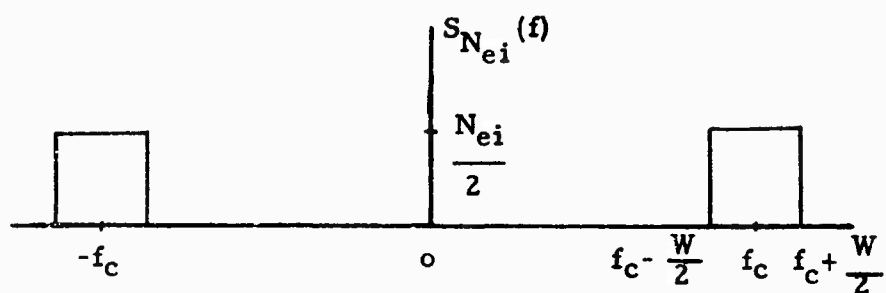
Note that  $\theta$  is a random variable uniformly distributed from 0 to  $2\pi$ . Also observe that  $n_s(t)$ , and  $n_{az}(t)$  are stationary random processes with zero mean. Hence

$$\begin{aligned}
R_n(\tau) = & (1 - k^2) R_s(\tau) + k^2 R_{nel}(\tau) R_{\cos W_m(\tau)} \\
& + k^2 R_{naz}(\tau) R_{\sin W_m(\tau)}
\end{aligned} \tag{24}$$

Thus Fourier transformation yields:

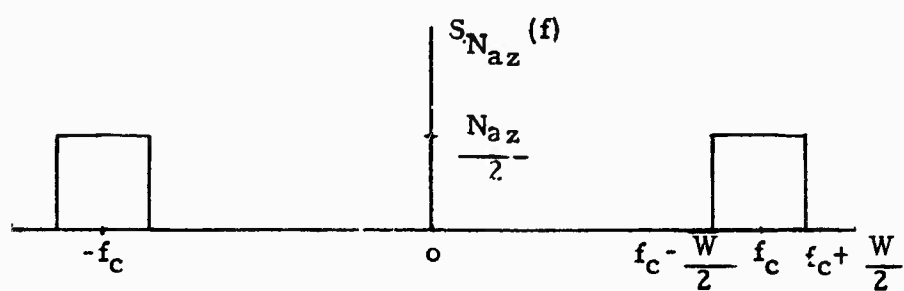
$$\begin{aligned}
\therefore S_n(f) = & (1 - k^2) S_s(f) + k^2 S_{nel}(f) * S_{\cos W_m(f)} \\
& + k^2 S_{naz}(f) * S_{\sin W_m(f)}
\end{aligned} \tag{25}$$

These component power spectra are shown in Figures 4, 5, 6, 7, and 8. It follows, then, that  $S_n(f)$  is as shown in Figure 9.



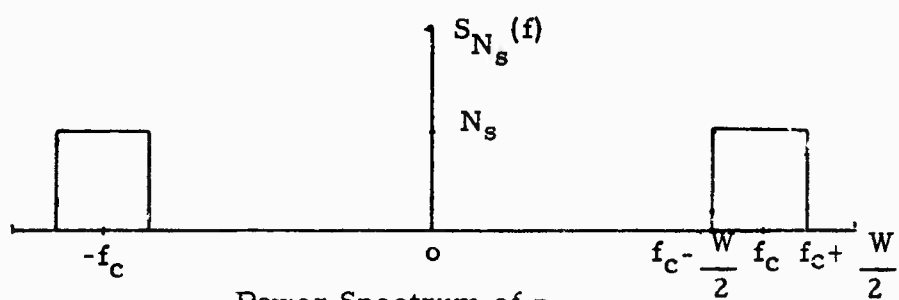
Power Spectrum of  $n_{ei}$

Figure 4



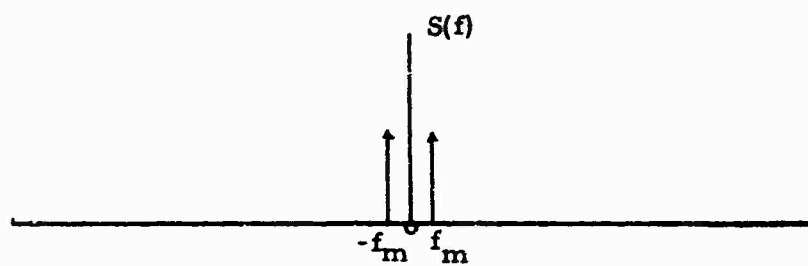
Power Spectrum of  $n_{az}$

Figure 5



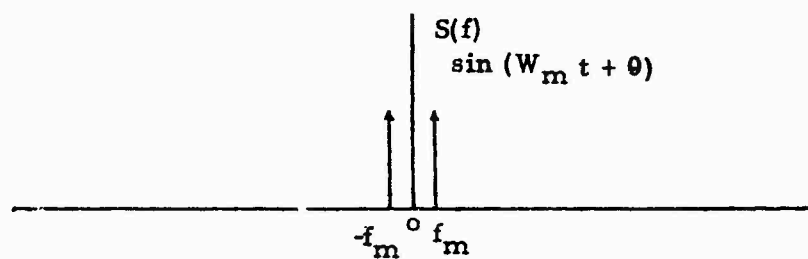
Power Spectrum of  $n_s$

Figure 6



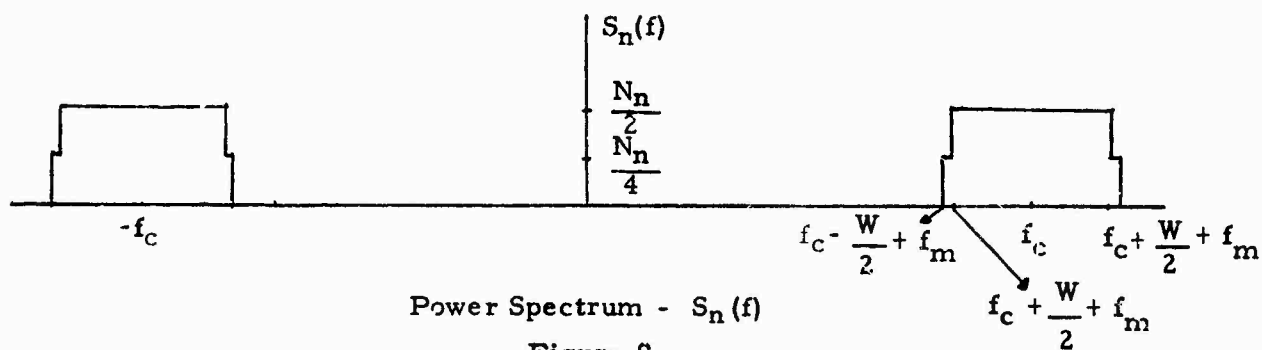
Power Spectrum of  $\cos(W_m t + \theta)$

Figure 7



Power Spectrum of  $\sin(W_m t + \theta)$

Figure 8



Power Spectrum -  $S_n(f)$

Figure 9

Where-

$$N_n = k^2 \left( \frac{N_{e1}}{2} + \frac{N_{a2}}{2} \right) + (1 - k^2) N_s \quad (26)$$

Hence  $S_x(f)$  is:

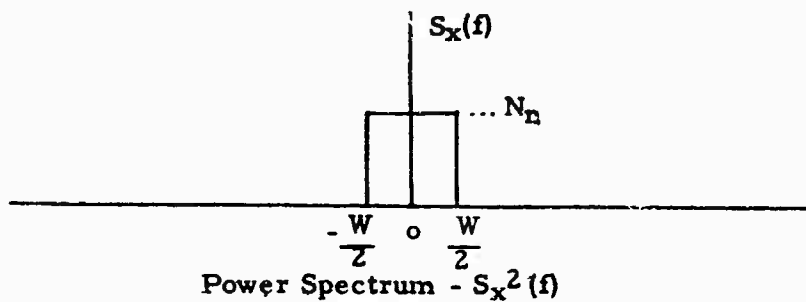


Figure 10

Find  $S_{x2}(f)$

$$S_{x2}(f) = \mathcal{F} [R_{x2}(\tau)]$$

$$R_{x2}(\tau) = E [x(t) x(t) x(t+\tau) x(t+\tau)]$$

Theorem: If  $x_1, x_2, x_3$ , and  $x_4$  are real random variables with a gaussian joint probability function and zero means, then:

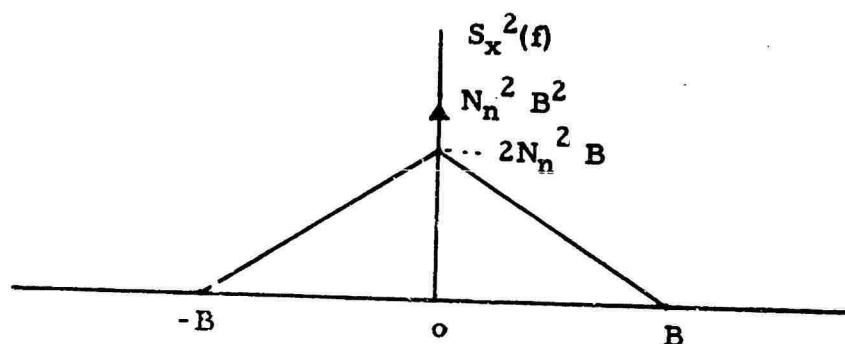
$$E [x_1 x_2 x_3 x_4] = E [x_1 x_2] E [x_3 x_4] + E [x_1 x_3] E [x_2 x_4] + E [x_1 x_4] E [x_2 x_3]$$

Application of this result yields:

$$R_{x2}(\tau) = R_x^2(0) + 2 R_x^2(\tau)$$

Hence,

$$S_{x^2}(f) = \sigma_x^4 \delta(f) + 2 S_x(f) * S_x(f) \quad (27)$$



Power Spectrum -  $S_{x^2}(f)$

Figure 11

Find  $S_{x^2 \cos(W_m t + \theta)}(f)$

$$S_{x^2 \cos(W_m t + \theta)}(f) = \mathcal{F} [R_{x^2 \cos(W_m t + \theta)}(\tau)]$$

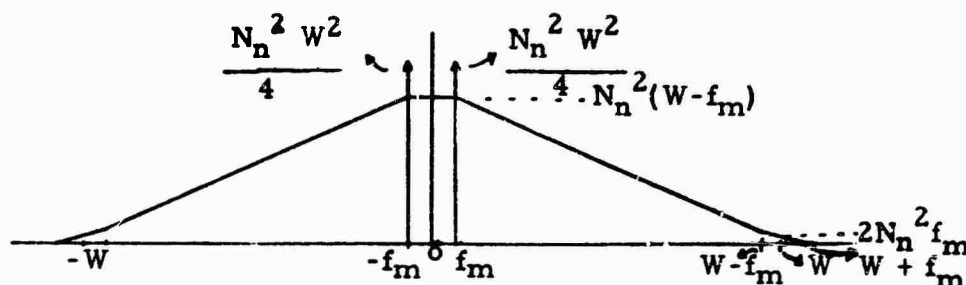
$$R_{x^2 \cos(W_m t + \theta)}(f) = E \left[ x^2(t) \cos(W_m t + \theta) x^2(t + \tau) \cos(W_m(t + \tau) + \theta) \right]$$

$$= E \left[ x^2(t) x^2(t + \tau) \right] E \left[ \cos(W_m t + \theta) \cos(W_m(t + \tau) + \theta) \right]$$

$$= R_{x^2}(\tau) \cdot R_{\cos}(\tau)$$

$$\therefore S_{x^2 \cos(W_m t + \theta)}(f) = S_{x^2}(f) * S_{\cos(W_m t + \theta)}(f) \quad (28)$$

Convolution of Figures 7 and 11 yields:



Power Spectrum

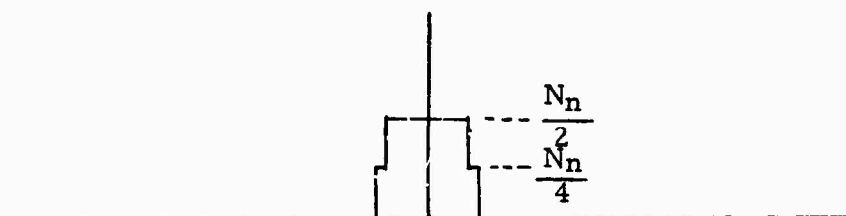
Figure 12

Find  $S_{x \cdot \cos(W_m t + \theta)}(f)$

$$S_{x \cos}(f) = \mathcal{F} [R_{x \cos}(\tau)]$$

$$\begin{aligned} R_{x \cos}(\tau) &= E [x(t) \cos(W_m t + \theta) \cdot x(t + \tau) \cos(W_m t + \tau) + \theta] \\ &= E [x(t) x(t + \tau) \cos(W_m t + \theta) \cos(W_m t + \tau) + \theta] \\ &= R_x(\tau) R_{\cos}(\tau) \end{aligned}$$

$$S_{x \cos}(f) = S_x(f) * S_{\cos}(f) \quad (29)$$



Power Spectrum

Figure 13

Observe that the powers of  $x(t)$  and  $y(t)$  are identical and that they occupy the same frequency band. Hence, the spectrum of  $y(t)$  is identical to the spectrum of  $x(t)$  which has already been determined.

Hence,

$$L_p \left[ \frac{1}{4} S_{y^2 \cos} (f) \right] = L_p \left[ \frac{1}{4} S_{x^2 \cos} (f) \right] \quad (30)$$

where  $L_p$  is the low-pass operator (represents low-pass filtering).

Find  $S_{x \cos 2}(f)$

$$S_{x \cos 2}(f) = \mathcal{F} [R_{x \cos 2}(\tau)]$$

$$\begin{aligned} R_{x \cos 2}(\tau) &= E \left[ x(t) \cos 2(W_m t + \theta) x(t + \tau) \cos 2(W_m(t + \tau) + \theta) \right] \\ &= E \left[ x(t) x(t + \tau) \right] E \left[ \cos 2(W_m t + \theta) \cos 2(W_m(t + \tau) + \theta) \right] \\ &= R_x(\tau) R_{\cos 2(W_m t + \theta)}(\tau) \end{aligned}$$

$$\therefore S_{x \cos 2}(f) = S_x(f) * S_{\cos 2}(f) \quad (31)$$

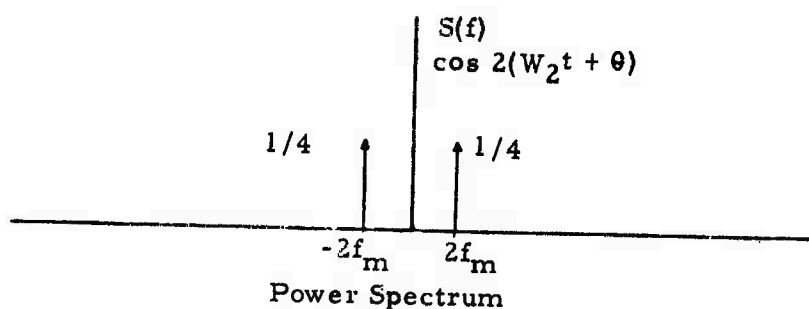
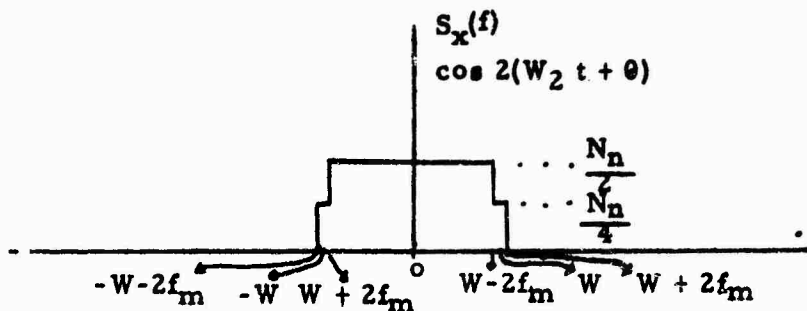


Figure 14

Application of equation 30 and Figures 10 and 14 yield:



Power Spectrum

Figure 15

Due to the fact that  $x(t)$  and  $y(t)$  have identical statistics and since sin and cos have the same power spectrum,

$S_y \sin 2(f)$  is identical to  $S_x \cos 2(f)$ .

$$S_y \sin 2(W_m t + \theta)(f) = S_x \cos 2(W_m t + \theta)(f) \quad (32)$$

The total power in  $e_{e1}(t)$  may now be determined from an inspection of equations 19, 21, 29 and 31; Figures 10, 12, 13 and 15; and the application of the low pass operation of bandwidth  $\beta$

Combining equations 19 and 21,

$$\begin{aligned} S_{e_{e1}}(f) &= L_p [S_i(f)] \\ &= L_p \left[ \frac{1}{4} S_{x^2 \cos}(f) \right] + L_p \left[ \frac{1}{4} S_{y^2 \cos}(f) \right] + L_p [A^{1^2} S_x \cos(f)] \\ &\quad + L_p \left[ \frac{1}{4} m_1^2 A^{1^4} \right] + L_p \left[ \frac{1}{4} A^{1^2} m_1^2 S_x \cos 2(f) \right] \\ &\quad + L_p \left[ \frac{1}{4} A^{1^2} m_2^2 S_x \sin 2(f) \right] + L_p \left[ \frac{1}{4} A^{1^2} m_1^2 S_x(f) \right] \end{aligned} \quad (33)$$



Now note that  $\beta \ll W - 2f_m \ll W - f_m$

Substituting:

$$\begin{aligned}
 S_{e_1}(f) = & \frac{1}{4} N_n^2 (W - f_m) 2\beta + \frac{1}{4} N_n^2 (W - f_m) 2\beta + A^2 \frac{N_n}{2} \cdot 2\beta \\
 & + \frac{1}{4} A^2 m_1^2 N_n 2\beta + \frac{1}{4} A^2 m_2^2 \frac{N_n}{2} 2\beta \\
 & + \frac{1}{4} A^2 m_1^2 \frac{N_n}{2} 2\beta + \frac{1}{4} m_1^2 A^4
 \end{aligned} \quad (34)$$

The noise power in  $e_1(t)$  is given by:

$$\begin{aligned}
 \text{Noise power in } e_1(t) = & N_n^2 (W - f_m) \beta + A^2 N_n \beta + \left( \frac{1}{4} + \frac{1}{2} \right) A^2 m_1^2 N_n \beta + \frac{1}{4} A^2 m_2^2 N_n \beta \\
 = & N_n^2 (W - f_m) \beta + A^2 N_n \beta + \frac{3}{4} A^2 m_1^2 N_n \beta + \frac{1}{4} A^2 m_2^2 N_n \beta
 \end{aligned} \quad (35)$$

The signal power is found to be:

$$\text{Signal power in } e_1(t) = \frac{A^4 m_1^2}{4} \quad (36)$$

Hence the signal to noise ratio is:

$$\left( \frac{S}{N} \right)_{\text{out}} = \frac{\frac{A^4 m_1^2}{4}}{A^2 N_n \beta + N_n^2 (W - f_m) \beta + \frac{3 A^2 m_1^2 N_n \beta}{4} + \frac{1}{4} A^2 m_2^2 N_n \beta} \quad (37)$$

It is desired to express  $\left(\frac{S}{N}\right)_{\text{out}}$  in terms of the variance of the noise at the input of the system.

Equating noise terms.

$$C_{er}^2 = N_{er} W \quad (38)$$

$$\sigma_s^2 = N_s W \quad (39)$$

$$N_n = k^2 \left( \frac{N_{el} + N_{az}}{2} \right) + (1 - k^2) N_s \quad (40)$$

$$\text{but } N_{el} = N_{az} \text{ define } N_{er} = N_{el} = N_{az}$$

$$\begin{aligned} N_n &= k^2 (N_{er}) + (1 - k^2) N_s \\ &= k^2 \frac{\sigma_{er}^2}{W} + (1 - k^2) \frac{\sigma_s^2}{W} \end{aligned}$$

where

$$\sigma_{er}^2 = \text{variance of noise into both error channels}$$

$$\sigma_s^2 = \text{variance of noise into sum channel}$$

$$\begin{aligned} \frac{S}{N}_{\text{out}} &= \frac{A^4 m_1^2}{4 N_n \beta \left[ A^2 + N_n (W - f_m) + \frac{3 A^2 m_1^2}{4} + \frac{1 A^2 m_2^2}{4} \right]} \quad (41) \\ &= \frac{A^2 m_1^2}{4 N_n \beta \left[ 1 + \frac{3}{4} m_1^2 + \frac{1}{4} m_2^2 + \frac{N_n (W - f_m)}{A^2} \right]} \end{aligned}$$

Substitute for  $A^1$ ,  $N_n$

$$\left( \frac{S}{N} \right)_{\text{out}} = \frac{A^2(1 - k^2) m_1^2}{4 \left\{ \frac{k^2 \sigma_{er}^2 + (1 - k^2) \sigma_s^2}{W} \right\} \beta} \quad (42)$$

$$1/ \left\{ 1 + \frac{3}{4} m_1^2 + \frac{1}{4} m_2^2 + \left[ \frac{k^2 \sigma_{er}^2 + (1 - k^2) \sigma_s^2}{W} \right] \frac{(W - f_m)}{A^2(1 - k^2)} \right\}$$

Note  $f_m \ll W$

Substitute for  $m_1$  and  $m_2$

$$\left( \frac{S}{N} \right)_{\text{out}} = \frac{A^2(1 - k^2) \frac{B^2}{A^2} \frac{k^2}{1 - k^2}}{4 \left[ \frac{k^2 \sigma_{er}^2 + (1 - k^2) \sigma_s^2}{W} \right] \beta} \quad (43)$$

$$1/ \left[ 1 + \frac{3}{4} \frac{B^2}{A^2} \frac{k^2}{(1 - k^2)^2} + \frac{1}{4} \frac{C^2}{A^2} \frac{k^2}{(1 - k^2)^2} + \frac{k^2 \sigma_{er}^2 + (1 - k^2) \sigma_s^2}{A^2(1 - k^2)} \right]$$

Let  $K = \frac{k^2}{1 - k^2}$

$$\left(\frac{S}{N}\right)_{\text{out}} = \frac{B^2 k^2}{4 \left[ k^2 \sigma_{er}^2 + (1-k)^2 \sigma_s^2 \right]} \frac{B}{W} \quad (44)$$

$$1/ \left[ 1 + \frac{3}{4} \frac{B^2}{A^2} K + \frac{1}{4} \frac{C^2}{A^2} K + \frac{K \sigma_{er}^2}{A^2} + \frac{\sigma_s^2}{A^2} \right]$$

The signal power at the input of the sum channel =  $\frac{A^2}{2}$

The signal power at the input of the elevation channel =  $\frac{B^2}{2}$

The signal power at the input of the azimuth channel =  $\frac{C^2}{2}$

Substitute for the above power expressions using the notation below:

Let  $\frac{A^2}{2} = P_s$  (45)

$$\frac{B^2}{2} = P_{el}$$

$$\frac{C^2}{2} = P_{az}$$

Then

$$\left( \frac{S}{N} \right)_{\text{out}} = \frac{\frac{B^2}{2} k^2}{2 \left[ k^2 \sigma_{er}^2 + (1 - k^2) \sigma_s^2 \right]} \frac{\beta}{W} \quad (46)$$

$$1/ \cdot \left[ 1 + \frac{3}{4} \frac{B^2}{A^2} \frac{K}{2} + \frac{1}{4} \frac{C^2}{2 A^2} K + K \frac{\frac{\sigma_{er}^2}{A^2}}{2} + \frac{\frac{\sigma_s^2}{A^2}}{2} \right]$$

$$= \frac{P_{el} k^2}{2 \left[ k^2 \sigma_{er}^2 + (1 - k^2) \sigma_s^2 \right]} \frac{\beta}{W} \cdot$$

$$1/ \cdot \left[ 1 + \frac{3}{4} \frac{P_{el}}{P_s} K + \frac{1}{4} \frac{P_{az}}{P_s} K + K \frac{\sigma_{er}^2}{2 P_s} + \frac{\sigma_s^2}{2 P_s} \right]$$

dividing numerator and denominator by  $1 - k^2$

$$\left( \frac{S}{N} \right)_{\text{out}} = \frac{P_{el} K}{2 \left[ K \sigma_{er}^2 + \sigma_s^2 \right]} \quad (47)$$

$$1/ \cdot \left[ 1 + \frac{3}{4} \frac{P_{el}}{P_s} K + \frac{1}{4} \frac{P_{az}}{P_s} K + \frac{\sigma_{er}^2}{2 P_s} K + \frac{\sigma_s^2}{2 P_s} \right] \cdot \frac{W}{\beta}$$

$$= \frac{\frac{P_{el}}{2}}{\left[ \sigma_{er}^2 + \frac{\sigma_s^2}{K} \right] \left[ 1 + \frac{\sigma_s^2}{2 P_s} + K \left( \frac{3}{4} \frac{P_{el}}{P_s} + \frac{1}{4} \frac{P_{az}}{P_s} + \frac{\sigma_{er}^2}{2 P_s} \right) \right]} W \beta$$

Equation 47 is the desired result. The output S/N for the elevation channel is expressed in terms of the three input signal powers, the two input noise powers (the two error channel noise powers were assumed equal), and the pre-detection and post-detection bandwidths. The coupling factor, a system design parameter, is included since it determines K. This expression reduces to commonly used approximate forms when the usual simplifying assumptions are made; e. g.,  $P_{az} = 0$ ,  $P_s \gg P_{el}$ ,  $P_s \gg \sigma^2$ ,  $\sigma_{er}^2 = \sigma_s^2$ , and  $K \ll 1$  as appropriate.

The rms pointing error due to noise can be evaluated when the appropriate relations between antenna parameters and signal functions are known. Typically, the error channel power,  $P_{el}$ , would be expressed in terms of angular error; i. e., the error channel slope. Then the pointing error is most easily evaluated by setting the output S/N to unity (i. e., let the pointing error signal equal the noise) and evaluating  $P_{el}$  using equation 47. The antenna-to-signal relationship then provides the desired pointing error in terms of  $P_{el}$ .

## APPENDIX III

### X-BAND LOW NOISE RECEIVER SURVEY

#### 1. INTRODUCTION

This appendix represents the results of a survey of the most important X-band "front end" receiver characteristics which are pertinent to the SCMTR problem. The most important types of front ends in present use have been included in this survey. They include Tunnel Diode Amplifiers, Parametric Amplifiers, Traveling Wave Tube (TWT) Amplifiers, and Diode Mixers.

#### 2. SUMMARY OF CHARACTERISTICS

Following is a tabulation (see Table III-1) of the characteristics of several types of low-noise receiving system front ends. The tabulation is the result of a survey of available devices with due consideration for theoretical limitations and the changing state-of-the-art.

A more thorough utilization of the available references will yield further details of each type of device for the interested reader. (Harvey, reference 28, gives 687 references on low noise amplification.)

With the exception of the TWT, the values given as device noise include the noise generated in the device as well as noise contributions from second stages, lossy circulators, etc. Since the TWT does not have a circulator associated with it and it is a high gain device (which makes the second stage noise contribution negligible), the value given in the table will be close to the system noise figure. The noise temperatures given for the parametric amplifiers are obtained with the narrow bandwidths.

The column titled "3 db bandwidth" gives typical values for fixed bandwidth wide-band front ends. The tunable bandwidths represent the wider of the ones available. The gain-bandwidth product is a constant for a given device for the Parametric, Tunnel Diode, and Maser Amplifiers. Thus, for a given device, the bandwidth may be increased with a corresponding decrease in gain. The exclusion of a tunable bandwidth for the TDA, TWT and Masers is due only to the fact that maximum reliable values are somewhat questionable and does not infer that the bandwidths of these devices are not tunable.

The saturation levels given are the values at which gain compression begins and is about 20 db below the maximum allowable inputs (with the exception of the Maser which acts as a limiter on input levels up to around -10 dbm).

TABLE III-1

COMPARISON OF PERTINENT CHARACTERISTICS OF  
LOW-NOISE X-BAND RECEIVER FRONT-ENDS

	Device Noise	3 db Bandwidth	Gain	Saturation Level	Size	Weight	Cost	Gain		Stability**		Phase		Stability**
								Long Term	Short Term	Short Term	Long Term	Long Term	Short Term	
Uncooled Parametric	120°K	150 Mc Tunable 500 Mc Fixed	18 db	-50 dbm	0.6'3	40#	20K	+1 db	+0.1 db	+2°	+2°		+0.2°	
Cooled Parametric	30°K	150 Mc Tunable 500 Mc Fixed	18 db	-50 dbm	12'3*	350#*	40K	+1 db	+0.1 db	+2°	+2°		+0.2°	
Tunnel Diode	5 db	500 Mc Fixed	18 db	-40 dbm	0.1'3	1#	3K	+1 db	+0.5 db	+1°	+1°		+0.1°	
TWT	4.5 db	650 Mc Fixed	20 db	-20 dbm	0.3'3	20#	6K	+0.1 db	+0.05 db	+1°	+1°		+0.1°	
Masers	10°K	500 Mc Fixed	30 db	-60 dbm	35'3	1000#	150K	+0.1 db	+0.05 db	+2°	+2°		+0.3°	
Mixers	6.0 db	500 Mc Fixed	-5 db	-15 dbm	0.1'3	1#	1K	Dependent on Local Oscillation						

\*Includes Coolers: Parametric Cooler System - 10.5 ft<sup>3</sup> and 300#.Masers Cooler System - 10.0 ft<sup>3</sup> and 700#.

\*\*Long Term Stability is over 24 hours.

Short Term Stability is over .25 hours.



The size, weight and cost columns represent typical values and sizable deviations about these will depend on such things as type of refrigerator used, environmental shielding required, etc. The cost figure may increase by several hundred percent when development is required. The phase and gain stabilities are representative of some of the best available and are applicable under normally specified environmental variations.

## APPENDIX IV

### ACQUISITION CONSIDERATIONS WITH PSEUDO-MONOPULSE TRACKING

This appendix considers the acquisition problem for a pseudo-monopulse tracking system. The general acquisition problem for a non-tracking system is first discussed to introduce the problem and to establish a basis for comparison. A somewhat detailed analysis of the performance of different generic classes of acquisition receivers may be found in reference 4. Next the particular characteristics of a pseudo-monopulse tracker in relation to acquisition are discussed and their effects on performance are analyzed.

#### 1. THE GENERAL ACQUISITION PROBLEM

The acquisition problem is that of detecting the presence of a signal emanating from a satellite in which some uncertainty exists both in the frequency of the signal and the spatial location of the emitter. If the frequency uncertainty, due to doppler shifts and oscillator instabilities, is much greater than the signal bandwidth and if the spatial uncertainty is much greater than the antenna beamwidth, then the acquisition problem may be a very important system consideration. Given a particular antenna scanning strategy, an acquisition receiver is required to detect the signal, in the presence of noise, with some confidence level while not false alarming on the noise alone. Acquisition receivers may be divided into three generic classes:

- (1) "frequency swept" in which a relatively narrow band IF is effectively swept in time over the frequency uncertainty and the detected output is compared to a threshold level.
- (2) "wide-open" in which the IF bandwidth is made equal to frequency uncertainty but appreciable post-detection filtering can be employed prior to the threshold comparison.
- (3) "multi-channel" in which several relatively narrow band IF's perform a simultaneous frequency search while still enjoying the advantage of narrow post-detection filtering prior to threshold comparison.

The performance capabilities of these three classes of receivers as well as a more detailed discussion of the acquisition problem is provided in the Appendix.

## 2. PSEUDO-MONOPULSE ACQUISITION

In this section the peculiarities of pseudo-monopulse are discussed to the extent that the acquisition is affected and different from full 3-channel monopulse. For 3-channel monopulse, it is assumed the acquisition receiver is located after the preamplifier of the sum channel. In pseudo-monopulse if the signal is taken off the sum channel prior to the directional coupler and if a comparable preamplifier is used, then the acquisition performance of 3-channel monopulse could be realized; however, this is not considered a practical solution. Next, since tracking does not occur simultaneously with acquisition, it is permissible to switch out the directional coupler and obtain acquisition performance comparable to 3-channel monopulse except for the loss incurred in the RF switch. With fairly fast, low-loss switches, this appears as an attractive possibility and should be considered in any system design. The third consideration is, if the directional coupler is left in and the acquisition receiver operates on the composite signal, then a different situation exists and some analysis is warranted.

In order to express the RF voltage in terms of an angle off boresight, a phase sensing monopulse is assumed since this is more amenable to the mathematician and is considered typically representative. In particular, for a square array and an angle off-boresight in elevation,  $\theta_e$ , the single channel IF voltage can be written in terms of the combined sum and error channel signals. For the case in which the error channel is combined in RF phase quadrature with the sum channel, the IF voltage prior to limiting can be written as,

$$e_1 = \sqrt{1 - k^2}^2 A(\theta_e) \cos(\mu_e) \cos[\omega_{ct} + \phi(t)] \\ + k Q_e(t) 2 A(\theta_e) \sin(\mu_e) \sin[\omega_{ct} + \phi(t)]$$

where  $A(\theta)$  is the antenna pattern of a single reflector,  $\phi(t)$  is the assumed angle-modulated communications information, and  $\mu_e = \pi d/\lambda \sin \theta_e$  is related to the angle off-boresight. The squared envelope for this voltage can be written as,

$$e_2 = 4 A^2(\theta_e) \cos^2(\mu_e) - k^2 4 A^2(\theta_e) [\cos^2(\mu_e) - Q_e^2(t) \sin^2(\mu_e)]$$

The first term is recognized as equivalent to that of a 3-channel monopulse or that which would occur if the directional coupler were switched out. The second term represents the change due to the pseudo-monopulse configuration and it is seen for on-boresight conditions ( $\theta_e = \mu_e = 0$ ), the loss of power is given by  $1 - k^2$  as would be expected. For angles off-boresight, the power contribution of the error channel which varies as  $Q_e^2(t)$  adds to the sum channel such that the average power increases; however, this increase is

not significant for angles off-boresight less than about the 3 db antenna beamwidth angle. Similarly, for the AM case (error channels added in RF phase coherence) the IF signal is given by,

$$e_3 = \left\{ \sqrt{1 - k^2} 2 A(\theta_e) \cos(\mu_e) + k Q_e(t) 2 A(\theta_e) \sin(\mu_e) \right\} \cdot [\cos \omega_c t + \theta(t)]$$

and the squared envelope is given by

$$e_4 = e_2 + k \sqrt{1 - k^2} 4 A^2(\theta_e) \cos(\mu_e) \sin(\mu_e) Q_e(t)$$

Thus, on-boresight the power is reduced by the same factor  $(1 - k^2)$  while for off-boresight angles, the power generally increases as before but also has the above second term which varies as  $Q_e(t)$ .

The acquisition performance for pseudo-monopulse tracking systems can be interpreted from the above equations and the acquisition analysis contained in reference 4. Basically, the receivers analyzed in reference 4 detect the energy in the IF signal over a time comparable to the sweep time for the frequency-swept receivers and over a time comparable to the servo integration time for the non-swept receivers. In any case, the acquisition performance due to the pseudo-monopulse scanner is no worse than a  $1 - k^2$  loss of signal power which for a nominal 10 db coupler is 0.46 db loss. The above equations show that for angles off-boresight as would be encountered during the antenna search mode, additional power is available for acquisition up to the above 0.46 db value. However, since the loss is small and since the communications receiver degrades by the same factor, it is not considered worthwhile to exploit this small, potential acquisition performance advantage.

## REFERENCES

1. "Study of Antenna Axis Configuration for Satellite Tracking and Continued Study of Transportable Antenna Systems," Second Quarterly Report. Prepared by General Electric for USAEMA, Fort Monmouth, New Jersey. AD-439280.
2. Wozencraft, J. M. and J. M. Jacobs, Principles of Communication Engineering. John Wiley & Sons, Inc. New York, 1965.
3. Rubin, W. L. and S. K. Kamen, "SCAMP - A Single Channel Monopulse Radar Signal Processing Technique." IRE Transactions on Military Electronics, MIL-6, April 1962.
4. Martin, A. R. and R. F. Cobb, "A Guide to Acquisition Receiver Selection and Performance." Radiation Incorporated Technical Note. To be published.
5. Wells, Sadler, Robinson and Waters, "Planar Schottky Barrier Microwave Mixers and Varactors," International Electron Device Meeting, Washington, D.C., October 1965.
6. Silver, S., Microwave Antenna Theory and Design, MIT Radiation Laboratory Series, McGraw-Hill Book Co., Inc., New York, New York, Volume 12, Chapter 6; 1949.
7. Powers, E. J., "Analysis and Synthesis of a General Class of Difference Patterns," AD-231217; July 1959.
8. Kirkpatrick, G.M., "Aperture Illumination for Radar Angle-of-Arrival Measurements," IRE Transactions on Aeronautical and Navigational Electronics, Volume AE-9, pp 20-27; September 1953.
9. Kinsey, R. R., "Monopulse Difference Slope and Gain Standards," IRE Transactions on Antennas and Propagation, Volume AP-10, pp 343-344; May 1962.
10. Cohen, W. and C. M. Steinmetz, "Amplitude and Phase-Sensing Monopulse System Parameters," Microwave Journal; Part I, Volume 2, pp 27-33, October 1959; Part II, Volume 2, pp 33-38, November 1959.

11. Pelchat, M., "Effects of Receiver and Antenna Noise in Non-Coherent Simultaneous Lobing Angle Trackers." Technical Report No. 13, Advanced Communications Group, Radiation Incorporated, Melbourne, Florida.
12. Rubin, W. L. and S. K. Kamen, "S/N Ratios in a Two-Channel Band-Pass Limiter," Proceedings of the IEEE, Volume 51, pp 389-390, February 1963.
13. Davenport, W. B., Jr., Signal-to-Noise Ratios in Band-Pass Limiters, Journal of Applied Physics, Volume 24, June 1953.
14. Jones, J. J., "Hard Limiting of Two Signals in Random Noise," IEEE Transactions on Information Theory, January 1963.
15. Feldman, C. B. and W. R. Bennett, "Bandwidth and Transmission Performance," Bell System Technical Journal, July 1949.
16. Kohlenberg, A., "Exact Interpolation of Band-Limited Functions." Journal of Applied Physics, Volume 24, No. 12, December 1953.
17. Linden, D. A., "A Discussion of Sampling Theorems." Proceedings of the IRE, July 1959.
18. Hancock, J. C., An Introduction to the Principles of Communication Theory, McGraw-Hill Book Company, New York, 1961.
19. Shannon, C. E., "Communication in the Presence of Noise." Proceedings of the IRE, January 1949.
20. Abel, J. E., George, S. F. and Sledge, O. D., "The Possibility of Cross Modulation in the SCAMP Signal Processor," Proceedings of the IEEE, Volume 53, pp 317-318; March 1965.
21. Baghdady, E. J., Communication System Theory, McGraw-Hill Book Co., Inc., New York; 1961, Chapters 4
22. Cohn, C. R., "Crosstalk Due to Finite Limiting of Frequency-Multiplexed Signals," Proceedings of the IRE, Volume 48, pp 53-59, January 1960.
23. George, S. F. and Wood, J. W., "Ideal Limiting, Part I - The Effect of Ideal Limiting on Signals and on Noise," U. S. Naval Research Laboratory Report 5683, 22 pages; October 1961.

24. Shaft, Paul D., "Limiting of Several Signals and Its Effect on Communication System Performance," IEEE Transactions on Communication Technology, Volume COM-13, Number 4, pp 504-512; December 1965.
25. Davenport & Root, Random Signals and Noise, McGraw-Hill Book Co., Inc., New York; Chapter 12.
26. Rhodes, D. R., Introduction to Monopulse, McGraw-Hill Book Co., Inc., New York; Chapter 3.
27. Altman, J. L., Microwave Circuits, Van Nostrand Co., New York, 1964, Chapter 2.
28. Harvey, A. F., Microwave Engineering, Academic Press, Inc., Ltd., Bristol, Great Britain, 1963, Chapter 17.

## BIBLIOGRAPHY

The bibliography has been divided into four general areas: Precomparator, Postcomparator, Monopulse Systems, and Related Topics. The bibliography lists references which are generally related to the single channel monopulse problem, though some references are concerned only with full monopulse.

### 1. PRECOMPARATOR COMPONENTS/TECHNIQUES

Caster, John M. and Monson, John A.: "Radar Sensors and Associated Devices." U. S. Army Electronics Laboratories Engineering Report No. DSL R-86; October 1962.

Cheston, R. C.: "Criteria for Conically Scanned Tracking Antennas." Report No. SM-992, Applied Physics Laboratory of the Johns Hopkins University; February 1961.

Delaney, W. P.: "An RF Multiple Beam-Forming Technique." IRE Transactions on Military Electronics, Volume MIL-6, pp. 179-186; April 1962.

Hannan, W.: "Optimum Feeds for All Three Modes of a Monopulse Antenna, Theory and Practice." IRE Transactions on Antennas and Propagation, Volume AP-9, pp. 444-461; September 1961.

Hansen, R. C.: Microwave Scanning Antennas. Volume I, "Apertures," New York, New York; Academic Press, 1964, Chapter 2.

Kinsey, R. R.: "Monopulse Difference Slope and Gain Standards." IRE Transactions on Antennas and Propagation, Volume AP-10, pp. 343-344; May 1962.

Kirkpatrick, G. M.: "Aperture Illuminations for Radar Angle of Arrival Measurements." IRE Transactions on Aeronautical and Navigational Electronics, Volume AE-9, pp. 20-27; September 1953.

Kirkpatrick, G. M.: "A Relationship Between Slope Functions for Array and Aperture Monopulse Antennas." IRE Transactions on Antennas and Propagation, Volume AP-10, p. 350; May 1962.



Manasse, R.: "Maximum Angular Accuracy of Tracking a Radio Star by Lobe Comparison." IRE Transactions on Antennas and Propagation, Volume AP-8, pp. 50-56; January 1960.

McLean, C. G.: A Study of the Boresight Error in the Microwave Networks of Various Monopulse Guidance Radar Systems. MSEE Thesis, USAF Institute of Technology, August 1963.

Ogg, F. C.: "Steerable Array Radars." IRE Transactions on Military Electronics, Volume MIL-6, pp. 80-94; April 1962.

Perepelkin, S. R. and Slivniak, I. M.: "Determination of Statistical Characteristics of Monopulse Radar Station Servo-System of Sum-Difference Type." Avtomatika i Telemekhanika, Volume 25, No. 7, pp. 1096-1108; July 1964.

Powers, E. J.: "Analysis and Synthesis of a General Class of Difference Patterns." ASTIA Document No. AD-231217, July 1959.

Redlien, Henry W.: "Theory of Monopulse Operation-Effects of a Defocused Antenna." Wheeler Laboratory, Inc., Report No. 495; Great Neck, N. Y.

Sciambi, A. F., Jr.: "Five-Horn Tracking Feed for Large Antennas." Presented at Large Steerable Aerial Conference, London, England, June 1965.

Stein, S.: "On Cross Coupling in Multiple-Beam Antennas." IRE Transactions on Antennas and Propagation, Volume AP-10, pp. 548-557; September 1962.

Vodolazskiy, V. I. and Terpugov, A. F.: "Optimum Antennas of Monopulse Phase Radars." NASA Information Facility Document No. N65-13895; October 1965.

Zuzolo, P. R., Jurczak, S. J. and Castrigno, J. A.: "Boresight Errors in the Near Field of a Monopulse Antenna." Paper presented at the Thirteenth Annual Symposium on USAF Antenna Research and Development at the University of Illinois, Monticello, Illinois; October 1963.

## 2. POSTCOMPARATOR COMPONENTS/TECHNIQUES

Abel, J. E., George, S. F. and Sledge, O. D.: "The Possibility of Cross Modulation in the SCAMP Signal Processor." Proceedings of the IEEE, Volume 53, pp. 317-138; March 1965.

Davenport, W. B.: "Signal-To-Noise Ratios in Band-Pass Limiters." Journal of Applied Physics, Volume 24, No. 6, pp. 720-727; June 1953.

East, T. W. R.: "The Coherent Detector with Noisy Reference Input." Physics Department of McGill University Report No. 563, 1955.

Gaarder, N. T. and Schneider, M.: "Error Analysis of a Digital Monopulse Radar." NASA Information Facility Document N65-18453; October 1965.

George, S. F. and Wood, J. W.: "Ideal Limiting - Part I - The Effect of Ideal Limiting on Signals and Noise." U. S. Naval Research Laboratories Report 5683; October 1961.

Jones, J. J.: "Hard-Limiting of Two Signals in Random Noise." IEEE Transactions on Information Theory, Volume IT-9, pp. 34-42; January 1963.

Lampard, D. G.: "The Probability Distribution for the Filtered Output of a Multiplier." IRE Transactions on Information Theory, Volume IT-5, pp. 4-11; March 1956.

Rubin, W. L. and Kamen, S. K.: "SCAMP - A Single Channel Monopulse Radar Signal Processing Technique." IRE Transactions on Military Electronics, Volume MIL-6, pp. 146-152; April 1962.

Rubin, W. L. and Kamen, S. K.: "S/N Ratios in a Two-Channel Band-Pass Limiter." Proceedings of the IEEE, Volume 51, pp. 389-390; February 1963.

Shaft, P. D.: "Limiting of Several Signals and Its Effect on Communication System Performance." IEEE Transactions on Communication Technology, Volume COM-13, No. 4, pp. 504-512; December 1965.

Tourdot, J.: "Doppler and Monopulse Tracking Receivers for the Adaptively Phased Array, Volume II - An Analysis of a Monopulse Tracking Receiver." Rome Air Development Technical Report N. RADC-TR-65-66; May 1965.

3. MONOPULSE SYSTEM TECHNIQUES

Adomian, G.: "Monopulse Radar Tracking Techniques." IEEE Transactions on Military Electronics, Volume MIL-9, pp. 293-294; October 1965.

Adomian, G.: "Summary of Angle Tracking and System Design Techniques Study." Report prepared by The Systems Development Laboratories of Hughes Aircraft Company for the Air Force under Contract AF 33(616)-3132; May 1959 (SECRET)

Adomian, G., Gofarian, A. V, Holze, D. H. and Moller, R. T.: "A Theoretical Study of the Effects of Amplitude-Modulated Jamming on Angle-Tracking Systems for Advanced Radars." Report prepared by The Systems Development Laboratories of Hughes Aircraft Company for the Air Force under Contract AF 33(616)-3132; December 1957 (SECRET)

Adomian, G., DuBois, D. F.: "Angular Tracking Noise in a Randomized Sequential Lobing System." Systems Development Laboratories, Hughes Aircraft Company Technical Memorandum 414, January 1956.

Berkowitz, Raymond S.: Modern Radar, Analysis, Evaluation, and System Design. New York, New York, John Wiley and Sons, Inc., 1965, Chapter 7.

Brennan, L. E.: "Angular Accuracy of a Phased Array Radar." IRE Transactions on Antennas and Propagation, Volume AP-9, pp. 268-275; May 1961.

Caster, J. M. and Walier, A. A.: "Significance of Target Characteristics on the Precision of Monopulse Radar." U. S. Army Electronics Laboratory Special Engineering Report DSL R-94; June 1964.

Chadwick, G. G. and Shelton, J. P.: "Two-Channel Monopulse Techniques - Theory and Practice." Record of the Conference on Military Electronics, Washington, D. C., pp. 177-181; September 1965.

Chubb, Elliott, Grindon, John R. and Venters, Donald C.: "An Instantaneous Direction Finding System." Record of the Conference on Military Electronics, Washington, D. C., pp. 169-173; September 1965.

Cohen, W. and Steinmetz, C. M.: "Amplitude and Phase-Sensing Monopulse System Parameters." Microwave Journal, Part I, Volume 2, pp. 27-33; October 1959; Part II Volume 2, pp. 33-38; November 1959.

Develet, J. A.: "Thermal Noise Errors in Simultaneous Lobing and Conical Scan Angle Tracking Systems." IRE Transactions on Space Electronics and Telemetry, Volume SET 7-7, pp. 42-51; June 1961.

Fjallbrant, Tore: "A Comparison Between the Sensitivities of Radar Monopulse and Conical-Scan Systems." Ericsson Technics, No. 2; 1963.

Franklin, Sydney B., Hilbers, Charles L., and Kosydet, Walter E.: "A Wideband Two-Channel Monopulse Technique." Record of the Conference on Military Electronics, Washington, D. C.; pp. 174-176; September 1965.

Franks, R. E. and Sundberg, V. C.: "A Comparative Study of Low-Angle Tracking System Performance." Electronic Defense Laboratories Technical Memorandum No. EDL-M541; November 1963.

Hausz, W. and Zachery, R. A.: "Phase-Amplitude Monopulse System." IRE Transactions on Military Electronics, Volume MIL-6, pp. 140-146; April 1962.

Koert, Peter; Ruttenberg, Robert M. and Rogers, Roy L.: "SHF Sequential Lobing System." U. S. Army Electronics Warfare Laboratory Technical Memorandum No. EDL-M788; May 1965.

McGinn, James W., Jr : "Thermal Noise in Amplitude Comparison Monopulse Systems." IEEE Transactions on Aerospace and Electronic Systems, Volume AES-2, No. 5, September 1966.

Moller, R. T.: "Simulation Study of the Effects of Monopulse Deception Techniques." Report prepared by The Systems Development Laboratories of Hughes Aircraft Company for the Air Force under Contract AF 33(616)-3132; May 1959.

Monson, J. A., Walier, A. A. and Clark, P. B.: "Low-Altitude Navigation and Display Techniques." U. S. Army Electronics Laboratories Quarterly Progress Report on Task No. 1E1-20601-A-219-03-06; September 1964.

Nester, W. H.: "A Study of Tracking Accuracy in Monopulse Phased Arrays." IRE Transactions on Antennas and Propagation, Volume AP-10, pp. 237-246; May 1962.

Nester, W. H.: "Introduction to Monopulse Antennas." General Electric Electronics Laboratory Technical Information Series, R63ELS-6; Syracuse, New York, 1963.

Pelchat, M. G.: "The Effects of Receiver and Antenna Noise on the Performance of a Conical-Scan Tracking System." Microwave Journal, Volume 8, pp. 37-40; February 1965.

Pelchat, M. G.: "Effects of Receiver and Antenna Noise in Non-Coherent Simultaneous Lobing Angle Trackers." Radiation Incorporated Internal Technical Report No. 13 ACG; 20 July 1964.

Pelchat, M. G.: "Relationships Between Squinted, Sum and Difference Radiation Patterns of Amplitude Monopulse Antennas with Mutual Coupling Between Feeds." To be published in IEEE Transactions on Antennas and Propagation, July 1967.

Rainal, A. J.: "Theoretical Accuracy of Monopulse Radar Receiver." IEEE Transactions on Aerospace and Electronics Systems, Volume AES-2, No. 2, pp. 234-235; March 1966.

Rainal, A. J.: "Monopulse Radars Excited by Gaussian Signals." IEEE Transactions on Aerospace and Electronic Systems, Volume AES-2, No. 3, pp. 337-345; May 1966.

Resnick, Sander: "A Note on the Angle Accuracy of a Monopulse Radar Using Logarithmic Normalization." Proceedings of the IEEE, Volume 54, No. 8, August 1966.

Rhodes, D. R.: Introduction to Monopulse. McGraw-Hill Book Co., Inc., New York, New York; 1959.

Shorenson, S.: "Angle Estimation Accuracy with a Monopulse Radar in the Search Mode." IRE Transactions on Aerospace and Navigational Electronics, Volume ANE-9, September 1962.

Simpson, Murray: "New Techniques in Three-Dimensional Radar." IRE Transactions on Military Electronics, Volume MIL-5, pp. 146-153; April 1961.

Stephenson, J. M. et al: "Design Criteria for a Large Multi-Purpose Tracking Antenna." ASTIA Document No. AD-267147, January 1961.

Urkowitz, H.: "On Detection and Estimation of Wave Fields for Surveillance." IEEE Transactions on Military Electronics, Volume MIL-9, pp. 44-56; January 1965.

"Space Communications Techniques." Rome Air Development Center Report RADC-TDR-63-111; April 1963.

"Study of Antenna Axis Configurations for Satellite Tracking and Continued Study of Transportable Antenna Systems." Second Quarterly Report. ASTIA Document No. AD-439280. Prepared by General Electric Co.

#### 4. RELATED TOPICS

Adomian, George: "Linear Stochastic Operators." Ph. D. Thesis, UCLA, August 1961.

Barton, David K.: Radar System Analysis. Englewood Cliffs, New Jersey; Prentice-Hall, Inc., 1964.

Bennett, William R. and Davey, James R.: Data Transmission. New York, New York; McGraw-Hill Book Co., Inc., 1965.

Gruenberg, Harry: "Some Optimum Properties of N Ports." IRE Transactions on Circuit Theory, Volume CT-9, No. 3, September 1961.

Korff, M., Brindley, C. M. and Lowe, M. H.: "Multiple-Target Data Handling with a Monopulse Radar." IRE Transactions on Military Electronics, Volume MIL-6, pp. 359-366; October 1962.

Schwartz, Mischa: Information Transmission, Modulation, and Noise. New York, New York; McGraw-Hill Book Co., Inc. 1959.

Shyhalla, Nick: "Experimental Feasibility Investigation of Monopulse Flight Data Measurement Techniques." Air Force System Command Technical Report No. AFF DL-TR-64-195.

Skolnik, Merrill I.: Introduction to Radar Systems. New York, New York; McGraw-Hill Book Co., Inc., 1962.

White, P. L.: "The Radar Beacon Comes Into Its Own." IRE Transactions on Military Electronics, Volume MIL-4, pp. 228-230; April 1960.

UNCLASSIFIED

Security Classification

DOCUMENT CONTROL DATA - R & D		
(Security classification of title, body of abstract and indexing annotation must be entered when the overall report is classified)		
1. ORIGINATING ACTIVITY (Corporate author)		2a. REPORT SECURITY CLASSIFICATION
Radiation Incorporated P. O. Box 37 Melbourne, Florida 32902		Unclassified
		2b. GROUP
		N/A
3. REPORT TITLE		
SINGLE CHANNEL MONOPULSE TECHNIQUES		
4. DESCRIPTIVE NOTES (Type of report and inclusive dates)		
Final Report, January 1966 to January 1967		
5. AUTHOR(S) (First name, middle initial, last name)		
Samuel B. Boor Melvin Harvey Guy M. Pelchat		
6. REPORT DATE	7a. TOTAL NO. OF PAGES	7b. NO. OF REFS
June 1967	267	28
8a. CONTRACT OR GRANT NO.		8b. ORIGINATOR'S REPORT NUMBER(S)
AF30(602)-4035		
b. PROJECT NO. 4519		
c. Task No. 451901		8d. OTHER REPORT NO(S) (Any other numbers that may be assigned this report)
d.		RADC-TR-67-143
10. DISTRIBUTION STATEMENT		
This document is subject to special export controls and each transmittal to foreign governments, foreign nationals or representatives thereto may be made only with prior approval of RADC (EMLI), GAFB, NY 13440.		
11. SUPPLEMENTARY NOTES		12. SPONSORING MILITARY ACTIVITY
Lt Eric E. Scheel Project Engineer (EMCRR) AC 315 330-3185		Rome Air Development Center (EMCRR) Griffiss Air Force Base, New York 13440
13. ABSTRACT		
<p>This report describes the results of a study and investigation to obtain a technique for processing both the communications and tracking signals in a single receiver in a satellite communications system. Various techniques were studied, with emphasis on Pseudo-Monopulse, Frequency Division Multiplexing, Time Division Multiplexing, and the Automatic Manual Simulator (AMS), a mechanical scanning method. All systems were analyzed to determine basic feasibility. Detailed analyses of the most promising techniques (Pseudo-Monopulse, AMS, FD,) were made. Major factors considered were: performance in the presence of thermal noise, errors due to phase and amplitude unbalance, normalization (dependence of pointing error on received signal strength), acquisition problems, and equipment complexity. A relative evaluation of all Single Channel Monopulse Tracking Receiver (SCMTR) techniques, including three channel monopulse for comparison, was made, and Pseudo-Monopulse was shown to offer the most advantages for the stipulated conditions. A complete Pseudo-Monopulse receiver design was accomplished and is included in this report. The AMS technique was shown to be useful when equipment simplicity is the prime goal.</p>		

DD FORM 1 NOV 65 1473

UNCLASSIFIED

Security Classification

**Security Classification**

### KEY WORDS

**LINK A**

**LINK 2**

**LINE 5**

## ROLE

५१

## ROLE

42

**ASL**

2

**Security Classification**